GEOMETRIC MODELING
OF
CUTTING TOOLS

by

PUNEET TANDON

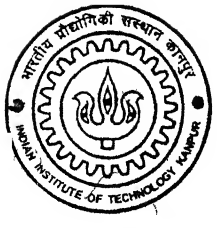

to the

DEPARTMENT OF MECHANICAL ENGINEERING
INDIAN INSTITUTE OF TECHNOLOGY, KANPUR

October, 2002

GEOMETRIC MODELING
OF
CUTTING TOOLS

A Thesis Submitted
in Partial Fulfilment of the Requirements
for the Degree of

Doctor of Philosophy

by

PUNEET TANDON

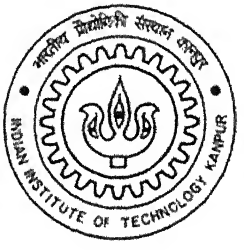

to the

DEPARTMENT OF MECHANICAL ENGINEERING
INDIAN INSTITUTE OF TECHNOLOGY, KANPUR

October, 2002

Dedicated to Almighty

CERTIFICATE

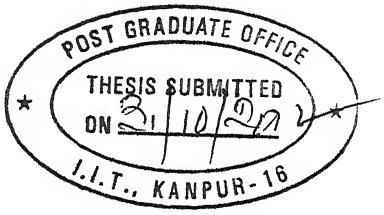

It is certified that the work contained in the thesis entitled **Geometric Modeling of Cutting Tools**, by **Puneet Tandon**, has been carried out under our supervision and that this work has not been submitted elsewhere for a degree.

Phalguni Gupta
Associate Professor
Department of CSE
Indian Institute of Technology Kanpur
Kanpur. 208 016 India

Sanjay G. Dhande
Professor
Department of ME & CSE
Indian Institute of Technology Kanpur
Kanpur. 208 016 India

October, 2002

SYNOPSIS

Geometric Modeling of Cutting Tools

A Thesis Submitted
in Partial Fulfillment of the Requirements for the Degree of
Doctor of Philosophy

by
Puneet Tandon
Roll No. 9810574

Thesis Supervisors

Dr. Sanjay G. Dhande
and
Dr. Phalguni Gupta

to the
Department of Mechanical Engineering
Indian Institute of Technology Kanpur
September, 2002

Manufacturing processes are broadly classified in three categories namely subtractive machining, additive manufacturing and metal forming processes. In subtractive machining, material is removed from the blank due to relative movement of a cutting tool over a workpiece. Additive manufacturing processes deposit material in an empty volume or layer so as to achieve the desired shape of the workpiece while metal forming processes deform plastically a given volume or sheet of material. The purpose of all these manufacturing processes is shape realization. Cutting tools hold an important position in the manufacturing world, as inspite of developments in the area of additive manufacturing and forming, subtractive machining holds the major share in the product shape and form realization. The primary motivation in this work is to outline in detail geometric models of surface patches for single-point and multi-point cutting tools and to establish a set of new three-dimensional (henceforth, referred as 3D) standards for defining the cutting tool geometries.

Geometry of the cutting tool surfaces is one of the crucial parameters affecting the quality of manufacturing processes. The geometry of the surface generated on the blank is directly dependent upon the geometry of the cutter, along with relative motion between them. This is based on the fact that the surface of the cutter in contact with workpiece and the machined surface are mutually enveloping surfaces. This forms the basis of conjugate geometry formulations, which helps in simulating machining processes.

Traditionally, the geometry of cutting tools has been defined using the principles of projective geometry. The parameters of geometry defining the cutting tools are cutting tool angles and dimensional parameters. The cutting tool angles are described by means of taking projections of the cutting tool surfaces on appropriate planes. These descriptions are two-dimensional in nature. Several standards such as ISO, ASA, DIN, BS have been established for specifying the geometry of cutting tools. The projective geometry approach is not very convenient in visualizing and understanding the geometry of the complex objects like cutting tools. It can, at best, help to identify the tool but cannot be gainfully employed for any downstream application. Till recently, this approach was considered satisfactory as the ability of designer to specify the orientation of cutting surfaces was limited to two-dimensional Cartesian coordinate frame of reference. The developments in the field of Computer Aided Geometric Design (CAGD in short) now provide a designer a more elegant approach of specifying the cutting tool surfaces as a set of biparametric surface patches. The geometric modeling of surface patches of cutting tools as a collection of biparametric surfaces would help the design, analysis and manufacturing processes of the cutting tools.

Modeling a cutting tool using geometric modeling approach provides a comprehensive 3D definition of the cutting tool. The surface patches forming the cutting tool are suitably positioned and oriented to form an unambiguous and valid surface model of the cutting tool. This surface model can be converted into a solid model and used for verification of the cutting tools using virtual or Rapid Prototyping processes. The benefits of the new paradigm include identification of defects and worn areas on the surfaces of the cutting tool using Reverse Engineering approach, generation of cutter location and orientation data for grinding and sharpening process, programming CNC tool cutter for tool manufacturing and the Finite Element based engineering analysis and simulation.

The present thesis establishes geometries of the single-point cutting tool, as well as, a range of multi-point cutting tools in terms of their surfaces. A cutting tool is

physically composed of a cutter body and one or more cutting elements or teeth placed on the surface of the body. The surfaces forming the teeth are critical in geometry and referred as functional surfaces, while the surfaces of the cutter body are non-critical in nature. The tool geometry can be defined in terms of 3D angles specifying the orientations of surface patches forming tooth of the cutter. The procedure, in general, adopted for the purpose of modeling the cutters is:

(i) Identify the critical or functional surfaces ($\Sigma_i : i \leftarrow 1\ldots$) and non-critical ($\Sigma_l : l \leftarrow 50\ldots$) surfaces of the cutting tool.

(ii) Model the surfaces giving shape to a tooth of cutter as unbounded biparametric surfaces patches.

(iii) Establish the bounds of these surface patches by evaluating the corner vertices (V_i) of the surfaces in terms of the parameters defining the surfaces. These vertices are formed due to intersections of unbounded uniparametric 3D edges of intersection ($\mathbf{e}_{ij}(s_{ij})$), which in turn are formed due to intersection of surface Σ_i with Σ_j.

(iv) Establish the orientation and position of surface patches of cutting tools in terms of new 3D rotational angles α_i, β_i and γ_i (where α_i, β_i, γ_i are the angles of rotation of surface patch i about X, Y and Z axis respectively). The 3D angles along with the dimensional parameters of the cutter, collectively, are termed as geometric parameters. These new parameters comprehensively define the cutting tool geometries in three-dimension.

(v) Derive relations among the proposed 3D tool geometry and conventional specification schemes to convert angles specified in one nomenclature to another. The set of these relations is termed as Mapping.

(vi) Model the surface patches forming the cutter body and establish suitable geometric parameters.

(vii) Identify the surface-surface intersections need to be blended or chamfered and model them as transitional surfaces.

(viii) Validate the model.

The detailed modeling of various cutting tools are elucidated in this thesis with the help of eight chapters including introduction in Chapter 1 and concluding remarks in Chapter 8. Besides the introduction to geometric modeling and cutting tools, the Chapter 1 also discusses the need and importance of the present work. This is followed by a brief discussion on the relevant available literature. This chapter also

discusses the objective of the work and the methodology adopted for establishing 3D definitions of cutting tools. Chapter 8 presents the summary of the present work along with implementation issues. It also presents the scope of further research.

The geometric modeling of the single-point cutting tool is explained in Chapter 2. The critical surfaces of a right-handed single-point turning tool, Auxiliary flank (Σ_1), Principal flank (Σ_2), Rake face (Σ_3) and Shoulder face (Σ_4), as shown in Figure 1, are modeled as unbounded biparametric planar surfaces. The nose (Σ_5) of the single-point cutting tool is modeled as oblique cone. Six rotational angles (α_1, β_1, α_2, β_2, α_3 and γ_3) define the orientation of these surface patches. Relations are developed to map proposed angles to equivalent conventional angles as detailed in ASA, ORS and NRS standards. This set of relations is known as forward mapping. Similarly, the relations to find proposed 3D angles from the given conventional angles, called as inverse mapping, are also established. These 3D angles are important from manufacturing and grinding point of view. The setting or swivel angles for grinding, θ_A, θ_B and θ_C and their relations with 3D rotational angles are developed to generate stereometric features for manufacturing and resharpening of single-point cutting tool. This chapter also highlights the technique to generate surface models of insert-based single-point cutting tools.

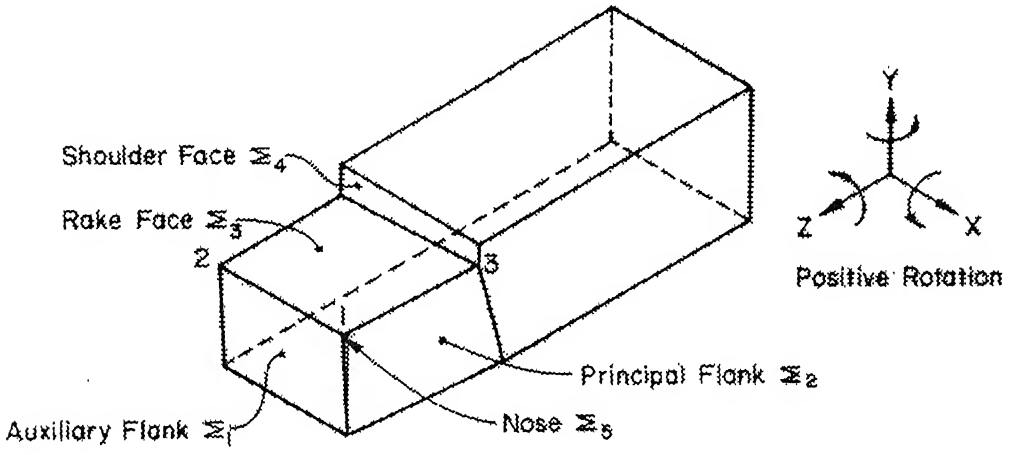

Figure 1: Wire Frame Model of Single-Point Cutting Tool

Chapters 3 to 7 of the thesis cover the modeling of multi-point cutting tools. Chapter 3 presents the technique to model Side Milling cutting tools as a set of biparametric surface patches. The work is in the direction of development of a unified representation scheme for side mills. Seven new angles (γ_1, γ_2, γ_3, α_4, β_4, γ_6, and β_7) are proposed to define the orientation of these surface patches. The comprehensive 3D definition of cutter includes geometric models of both cutting teeth and cutter

body. As all the teeth are similar in geometry, only one tooth is modeled and then it is arrayed around the periphery of the cutter body. For the purpose of modeling, a standard right hand cutter is placed in a global right handed Cartesian coordinate frame of reference (C_1) such that its axis of rotation coincide with the global Z axis and the center of the cutter lies at global origin. The tooth to be modeled is defined with respect to a local coordinate system C_2. Figure 2 presents an instantiation of the cutter and the coordinate systems C_1 and C_2. The relation between C_1 and C_2 is established based on the dimensional parameters of the cutter. A tooth of the side milling cutter comprises twelve functional surfaces ($\Sigma_i : i \leftarrow 1 \ldots 12$) (eleven for single-land side mill) and eleven to twelve transitional surfaces (σ_{ij}) depending upon the type of side milling cutter.

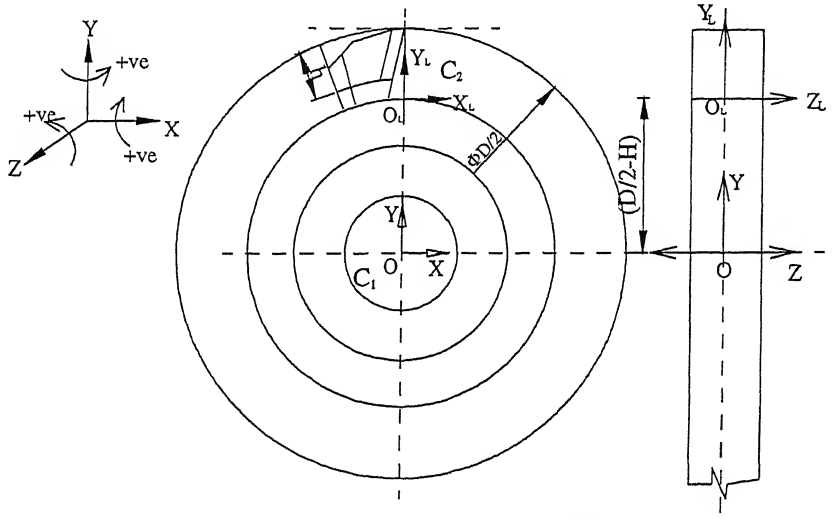

Figure 2: Coordinate systems of Side Milling Cutter

The planar surfaces of the tooth of cutter are modeled by appropriately rotating suitable XY, YZ and ZX planes, placed with their centers at the origin of C_2 about X, Y or Z axis, in terms of angles α_i, β_i and γ_i. These rotated infinite planes are then translated to place them at appropriate positions. The surface patches of the side mill are shown in Figure 3. The biparametric definitions of these surface patches are evolved in terms of parameters u_i, v_i and w_i (e.g. $\mathbf{p}_i(u_i, v_i)$), where u_i, v_i, w_i are parameters of surface i along X, Y and Z axis respectively. The parabolic surface of the cutter is modeled as a ruled surface, the boundary curves defined as Bézier curves. The relations expressing the definitions of surface patches of tooth for a straight, double-land side mill in homogenous coordinate system are derived and shown in Table 1.

Once all the surface patches are appropriately positioned and oriented, the surface

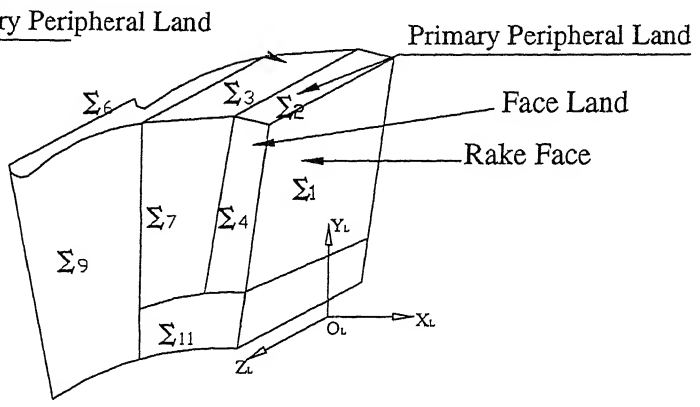

Figure 3: Surface Patches of Cutter Tooth

patches are allowed to intersect to form uniparametric unbounded edges of intersection ($\mathbf{e}_{ij}$: edge of intersection of surface patch Σ_i and Σ_j). These edges intersect among themselves to form corner or bounding vertices that define limits to the parameters of the surface patches. Once the 3D rotational angles are established, the relations to map conventional angles from them, called forward mapping, and from conventional angles to rotational angles, known as inverse mapping relations are developed.

$$
\begin{array}{lcl}
\mathbf{p}_1 & = & [-v_1 \sin\gamma_1 \quad (v_1 \cos\gamma_1 + H) \quad w_1 \quad 1] \\
\mathbf{p}_2 & = & [u_2 \cos\gamma_2 \quad (u_2 \sin\gamma_2 + H) \quad w_2 \quad 1] \\
\mathbf{p}_3 & = & [u_3 \cos\gamma_3 \quad (u_3 \sin\gamma_3 + d_{32}) \quad w_3 \quad 1] \\
\mathbf{p}_4 & = & [(u_4 \cos\beta_4 + v_4 \sin\alpha_4 \sin\beta_4) \quad v_4 \cos\alpha_4 \quad (-u_4 \sin\beta_4 + v_4 \sin\alpha_4 \cos\beta_4 + d_{43}) \quad 1] \\
\mathbf{p}_5 & = & [p_{4x} \quad p_{4y} \quad -p_{4z} \quad 1] \\
\mathbf{p}_6 & = & [u_6 \cos\gamma_6 \quad (u_6 \sin\gamma_6 + d_{62}) \quad w_6 \quad 1] \\
\mathbf{p}_7 & = & [u_7 \cos\beta_7 \quad v_7 \quad (-u_7 \sin\beta_7 + d_{73}) \quad 1] \\
\mathbf{p}_8 & = & [p_{7x} \quad p_{7y} \quad -p_{7z} \quad 1] \\
\mathbf{p}_9 & = & [u_9 \quad v_9 \quad d_{93} \quad 1] \\
\mathbf{p}_{10} & = & [u_9 \quad v_9 \quad -d_{93} \quad 1] \\
\mathbf{p}_{11} & = & [u_{11} \quad v_{11} \quad \frac{w_b}{2} \quad 1] \\
\mathbf{p}_{12} & = & [u_{11} \quad v_{11} \quad -\frac{w_b}{2} \quad 1]
\end{array}
$$

Table 1: Mathematical Definition of Surface Patches of Side Mill

The body of the cutter is supposed to be made up of eight surface patches ($\Sigma_i : i \leftarrow 50 \ldots 57$). These include surfaces forming hole for mounting arbor and keyway. For surfaces of revolution, another parameter ϕ_i replaces one of the two parameters used to define a plane. To prevent any danger to the user and damage to the cutter, some edges are modified to blending surfaces or chamfers. These are termed as transition surfaces. Blending surface that blends surface patches Σ_i and Σ_j is modeled as bicubic Bézier surface (σ_{ij}) while chamfered surface is modeled as sweep surface. Surface model of another variant of side mill, known as Half Side Mill, is also derived by

suitably modifying the proposed geometric model of the cutter.

The approach to develop geometric models of other multi-point cutting tools considered in the present work, is quite similar to one described for side milling cutters. Chapter 4 comprises modeling of Fluted Cutters. A variety of cutters that includes Slab Mills, End Mills and Drills are covered in this chapter. The chapter presents the geometric modeling methodologies of both plain and helical slab mills, end mills with different end geometries (e.g. flat, ball, conical etc.) and drills with a variety of point styles. The unified models of different types of fluted cutters are developed and their instantiations are presented. The surfaces meant for cutting operations, known as flutes, are modeled as helicoidal surfaces. For the purpose, sectional geometry of tip-to-tip profile is developed and then it is swept according to the sweeping rule, which depends on the type of the cutter under consideration. The slab mill consists of simply the flutes and two planar end surfaces, while the end mills and drills have shanks also apart from flutes and the geometric model of shank is developed separately. Further, their end geometries are also typical and have to be taken care off. The transitional surfaces of these cutters are modeled as bicubic Bézier surfaces or biparametric sweep surfaces. The relations to map 3D angles to conventional angles (forward mapping) and their reverse relations (inverse mapping) are also developed for all three types of fluted cutters.

Insert-based cutters are widely used in real practice and the development of unified representation scheme for the modeling of Inserted Face Mill is expressed in Chapter 5. An indexable insert-based cutter is made up of a cutter body and the inserts. The surfaces where an insert is placed in the cutter body form an insert seat and its profile is developed in terms of six surface patches (Σ_1 – Σ_6) placed in a local coordinate system C_2. The surfaces of the remaining cutter body, referred here as core cutter body are defined with respect to coordinate system C_1. The core cutter body is make up of twelve surface patches. The surface model of insert seat is arrayed around the core cutter body to complete the cutter body. Once the bounding edges and vertices of the cutter body are mathematically defined, the transitional surfaces are modeled as biparametric linear sweep surfaces. A range of milling inserts designated by ISO is available commercially. Geometric models of a generic square insert and a generic triangular insert are developed in terms of biparametric planar oriented surfaces. The limits of parameters are defined through intersecting edges and vertices. Certain edges that need not be sharp are graduated to transitional surfaces by modifying the continuity conditions of surfaces forming those edges. The relation between insert seat coordinate system (C_2) and the cutter body coordinate system (C_1) is defined with

the help of homogenous transformation matrix $[^2_1M]$. This helps in proper placement of insert in the cutter body. The geometry of the insert and the matrix $[^2_1M]$ are used to determine forward and inverse mapping relations. The methodology to regrind inserts, if need be, is also presented in this chapter.

Chapter 6 discusses the unified representation scheme to model Shell End Mill. The cutter teeth of this type of cutter are modeled as a combination of helicoidal and planar surfaces. A combination of nine suitably placed and oriented surfaces complete the model of a single tooth of shell end mill. The tool geometry of the shell end mill in 3D representation scheme is expressed with the aid of eight 3D angles: γ_1, γ_2, γ_3, α_6, β_6, α_7, α_9 and β_9. The geometry of the cutter body is described in terms of ten surfaces, comprising planar surfaces and surfaces of revolution only. The edges of the cutter that are not critical are converted to blends and chamfers. A set of nine transitional surfaces is identified and modeled as a combination of bicubic Bézier and sweep surfaces. The relationships between the set of conventional angles and 3D rotational angles are expressed through forward and inverse mappings.

The methodology to model geometrically gear cutting tools is taken up in Chapter 7 of the thesis. Gear Hob, the primary gear cutting tool is modeled extensively. The surface model of hob comprises six surface patches that form a single tooth, three patches making up a flute and six surface patches for the cutter body. The tool geometry of the hob is defined with the help of six 3D angles (γ_1, β_1, γ_2, γ_3, α_4, β_4). The tooth and the flute are arrayed along and about the cutter axis to complete the hob model. The unified model developed in the work, takes care of both straight flute and helical hobs. Edges of intersection of the surface patches of the hob tooth are converted into suitable transitional surfaces as per topping features of the hob and tip relief features required on the gear produced. Mapping relations between conventional and the proposed 3D angles are established to convert angles from one nomenclature to the other.

The geometric models, in terms of surface patches, of the cutting tools described in the thesis are validated by rendering them in Open Graphics Library, OGL in short, environment. By varying the input given in terms of geometric parameters, the entire family of the cutter of a type can be modeled and simulated. The models are developed keeping right hand (RH) cutting tools in mind, but left hand (LH) cutters can also be generated by suitably transforming the models of RH cutting tools. Once the 3D definitions of the cutting tools are available they can be directly utilized for down-stream applications like analysis and manufacturing of the tool. To illustrate the utility of 3D definitions of cutting tools, a few case studies on Finite

Element based Analysis, geometric assessment of tool wear and defects and CNC machining of different cutting tools are considered. Table 1.2 presents a matrix of cases considered and implemented in the present work for illustrating down-stream applications of 3D cutter models. Only one case study for each type of the cutter is presented at the end of respective chapters but others can be similarly taken up.

Cutting Tools	Grinding	CNC Machining	Geometric Assessment of Tool Wear	Finite Element Analysis
Single Point Cutting Tool	√			
Side Milling Cutter	√		√	
Fluted Cutters (Slab Mill, End Mill, Drill)				√
Insert-based Face Mill	√			√
Shell End Mill		√		
Gear Cutting Tool		√		

Table 2: Case-Studies Considered for Cutting Tools

While validating the model, the ASCII files of the cutter models are created and imported in a surface modeling environment (Surfacer) and there the surface models of the tools are created. These surface models can be easily converted to solid models in any solid modeling environment. The surface or solid models of the cutters can be post-processed for any down-stream application. For example, Figure 4 shows the comparison of the surface model developed in this work for side milling cutter with the digital data of the same physical cutter for tool wear and defects assessment on the surfaces of the cutter teeth. The distribution of stresses with the help of Finite Element Analysis on the surfaces of teeth of a slab mill, when it is in operation is shown with the help of Figure 5. Figure 6 shows once instance of in-process CNC machining operation for manufacturing a gear shaper.

Publications

(i) Tandon Puneet et.al.(2001), "Feature Based Design and Rapid Product Development of Saddletree", *International Journal of Agile Manufacturing*, Vol.4(2), pp.147-161.

(ii) Tandon Puneet, Gupta P. & Dhande S.G. (2002), "Geometric Modeling of Single Point Cutting Tool Surfaces", accepted in *International Journal of Advanced Manufacturing Technology.*

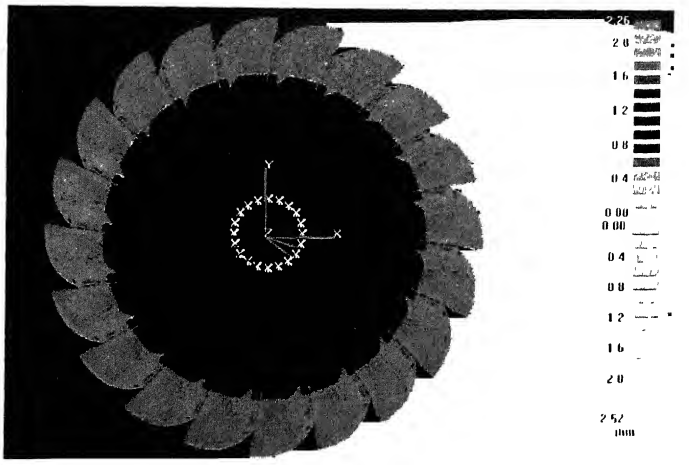

Figure 4: Surface-Point clouds comparison of the Side Mill cutter surfaces

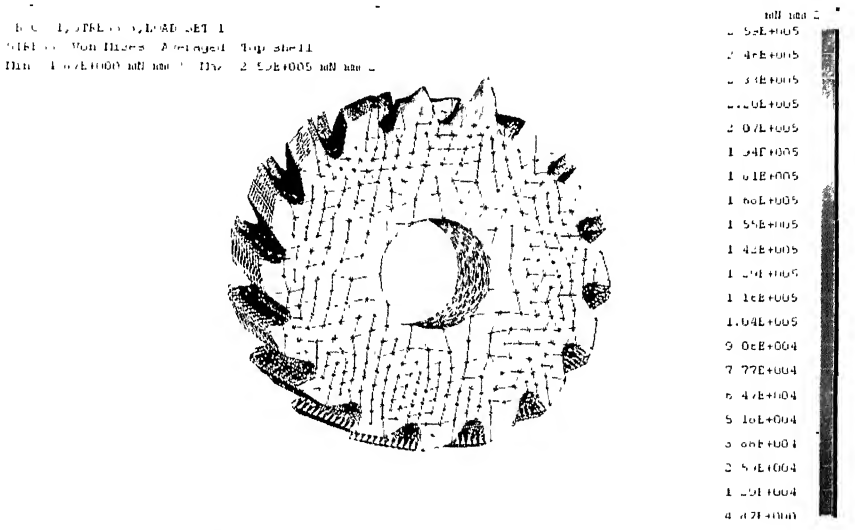

Figure 5: Stress distribution for teeth in operation in Slab Mill

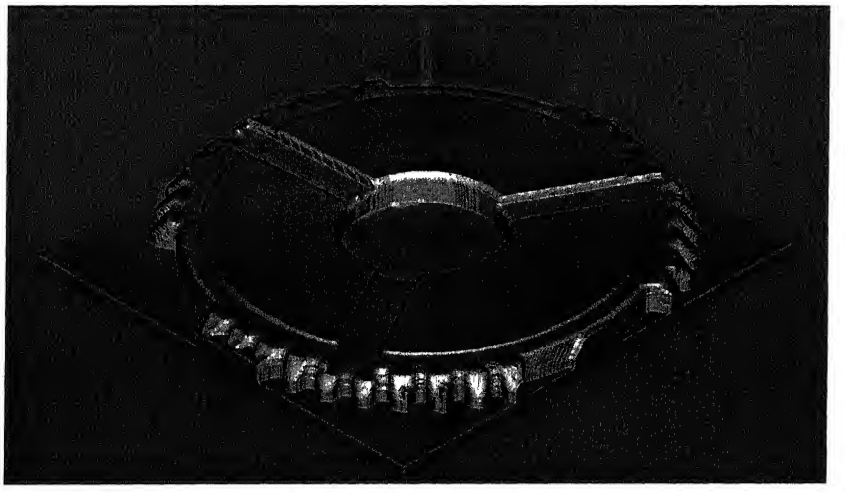

Figure 6: CNC Machining of Gear Shaper

(iii) Tandon Puneet, Gupta P. & Dhande S.G. (2002), "Geometric Modeling of Side Milling Cutting Tool Surfaces", accepted in *International Journal of Engineering Simulation.*

(iv) Tandon Puneet, Gupta P. & Dhande S.G. (2002), "Virtual Prototyping and Manufacturing of Insert-Based Single-Point Cutting Tool", accepted in the proceedings of *International Conference on e-Manufacturing* to be held at Bhopal, India.

ACKNOWLEDGMENTS

No amount of words is sufficient to express my feelings towards my thesis supervisors Professor Sanjay G. Dhande and Dr.Phalguni Gupta. It was late evening hours when I had a chance to meet Professor Dhande and that was to take his permission to register for CAED course. The impression I got on that day was everlasting and it was my pleasure to work with him for my thesis. There are a lot of aspects what one can learn from Professor Dhande and I have really got a chance to build multi-faceted personality in his company. It was a chance by which Dr.Phalguni Gupta became my thesis supervisor and it was indeed a blessing in disguise for me. He is really a gem of a person and I had learnt a lot of things in his company. I am really thankful to both of you, sirs.

A research work cannot be completed without the help of many people and I would like to take this opportunity to express my sincere gratitude towards them. I am grateful to Prof Amitabha Ghosh, Prof Kripa Shanker, Prof Prashant Kumar, Prof N.N. Kishore, Prof S.K. Chowdhury, Dr.N.V.Reddy and all others faculty members of this premier institute. I am thankful to Dr.A.D.Bhatt and Dr.P.V.M.Rao for all the help they have rendered to me for my thesis. I am also thankful to Department of Science and Technology, Government of India for sanctioning a project on the area of my work.

I had a wonderful time at IIT campus with my friends and colleagues, Rahul, Siddharth, Vikas, Sandeep, Asit, Amreesh, Saurabh, Swapnil, Ashish, Yogesh, Vinod, Jeewan, Kailash and many more. I am thankful to Siva-Eshwari, Saravana, TVK Gupta, Mukul, Anubhav, Sudhir, M.L.Jain, Yugandar, Dharmendra and Bhanu for providing me an alternate home here and all the fruitful discussions, I had with them. I am thankful to Vaibhav, Surya and Raja also during their help in my thesis preparation days. I am thankful to all my friends in and outside the IIT campus.

I am specially thankful to Mr.A.Chatterjee for whatever he has done for me. I also wish to put on records my thanks to staff of CAD-P Lab consisting of Mr.C.P.Singh, Ravindra, Surendra, Babulal, Sarju and Shailendra.

I owe a lot to my wife, Pritee and my parents for taking care of my social responsibility. They have untiringly done all what I was supposed to do during the period of my stay away from my home. I am also thankful to my in-laws for taking care of me at Kanpur and never letting me feel that I am away from my family. Last, but not the least, I am grateful to my two great sons - Pulkit and Pushkin, for understanding and loving me.

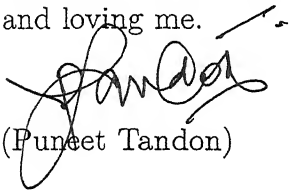

(Puneet Tandon)

Contents

List of Figures

List of Tables

Nomenclature

C_1	Coordinate system attached to the Cutter Body
C_2	Coordinate system attached to the Insert or Tooth of the Cutter
D	Diameter of Cutter
D_1	Diameter of Cutter Hub
D_c	Cutting End Diameter of End Mill/Drill
D_R	Root Circle Diameter
D_s	Mounting Shaft/Shank Diameter of End Mill/Drill
H	Height of tooth
L	Width of cutter
L_1	Reach length/length of cut of End Mill/Drill
L_2	Total/overall length of End Mill/Drill
L_3	Programming length/nominal length below chuck of End Mill/Drill
L_4	Length of cylindrical fluted shank portion of Drill
$[\frac{1}{2}\mathbf{M}]$	Homogenous transformation matrix of a vector from the coordinate system C_2 to C_1
N	Number of teeth in the cutter
N_f	Number of Flutes in a Gear Hob
P	Pitch of Helicoidal Cutters
R	Fillet Radius
$[\mathbf{R}]$	Rotation Matrix
R_g	Radius of gullet bottom
S_I	Insert thickness
S_w	Chordal thickness of cutter tooth
$[\mathbf{T}]$	Translation Matrix
V_i	Vertex 'i'
W	Width of tooth Face cutting edge/Lip length for drill
W_d	Length of Lip of drill
Z	Number of teeth per flute in a Gear Hob
a_1	Width of keyway
b_1	Depth of keyway
b_{I1}	Width of planishing surface for insert
b_{I2}	Width of surface containing auxiliary cutting edge for insert
d	Diameter of mounting hole/bore
d_c	Core diameter of End Mill/Drill
d_I	Inscribed circle diameter for equilateral and round Inserts
d_{I1}	Diameter of cylindrical hole in insert body for fixing
d_{ij}	Displacement of i^{th} plane in j^{th} direction

d_o	Pitch Diameter
d_t	Depth of tooth
$\mathbf{e}_{ij}/\mathbf{e}_{i,j}$	Edge vector formed by intersection of surface Σ_i with Σ_j
h	Height of Face Land or Length of Insert or Depth of Gear Hob tooth
h_a	Addendum of tooth of Gear Hob
l	Length/Depth of bore
l_1	Width of Primary Land
l_2	Width of Secondary Land
l_3	Width of Face Land
l_I	Length of insert
m	Thickness of body
m_I	Test dimension of the plane land for insert
$\mathbf{n}_i$	Vector normal to surface patch 'i'
p_a	Axial Pitch
p_d	Diametral Pitch
$\mathbf{p}_i(u_i, v_i)$	Position vector of any point on surface patch 'i'
$\mathbf{p}_{il}(l_i, m_i)$	Tangent vector at point $\mathbf{p}(l_i, m_i)$ on surface patch 'i' along l parameter
${}^1\mathbf{p}$	Position vector with reference to the cutter coordinate system C_1
${}^2\mathbf{p}$	Position vector with reference to the insert/tooth coordinate system C_2
$\hat{p}$	Peripheral length of one cutter tooth
r	Radius of blend
s_{ij}	Parametric variables along the edge e_{ij}
t_t	Thickness of tooth
(u, v, w)	Parametric coefficients
$\mathbf{v}_i$	Vector defining the position of vertex V_i
w_b	Width of cutter body
w_{l1}	Width of Primary Peripheral Land along the body of cutter tooth
w_{l2}	Width of Secondary Peripheral Land along the body of cutter tooth
$[x\ y\ z\ 1]_i$	Original homogenous position vector of a point on patch 'i'
Σ_i	Surface Patch 'i'
α	Relief Angle
α_A	Axial Relief Angle
α_i	Grinding angle for surface patch 'i' about the X axis
α_F	Face Relief Angle
α_{1F}	1^{st} Face clearance Angle
α_n	Normal Pressure Angle
α_P	Peripheral Relief Angle
α_{1P}	1^{st} Peripheral clearance Angle
α_{2P}	2^{nd} Peripheral clearance Angle
α_R	Radial Relief Angle
α_{1R}	Radial Clearance Angle
β	Half Point Angle for drills (2β: Point Angle)
β_i	Grinding angle for surface patch 'i' about the Y axis
γ_A	Axial rake angle
γ_i	Grinding angle for surface patch 'i' about the Z axis
γ_R	Radial rake angle
δ	Gullet or Gash Angle

δ_3	Half the difference between thickness of cutter tooth and cutter body
δ_{ij}	Distance from blend start edge to the edge $\mathbf{e}_{ij}$ of surfaces to be blended
ε	Peripheral Pitch Angle
$\theta_A, \theta_B, \theta_C$	Grinding Angles about X, Y and Z axis respectively
θ_{la}	Lip Angle
λ	Inclination/Helix/Lead angle
σ_{ij}	Blend or Transition surface between surfaces Σ_i & Σ_j along edge $\mathbf{e}_{ij}$
ϕ	Helix angle
ϕ'	Principal cutting edge angle
ϕ_e	End cutting edge angle
ϕ_F	Peripheral cutting edge angle
Ψ	Chisel Edge Angle for drills
ψ	Circumferential Pitch Angle.

Suffixes

I	Insert
i	Surface Patch or Vertex number

Chapter 1

INTRODUCTION

Geometry of cutting tools is one of the crucial parameters affecting the quality and accuracy of manufacturing processes. Traditionally, this geometry is defined by means of a set of sectional profiles, based on projective geometry approach. The advances in the field of Computer Aided Geometric Design (CAGD) have opened avenues for a designer to specify cutting tools in more elegant fashion.

This chapter develops background for the present work and discusses the need to take up this work. It presents a review of available relevant literature. Objectives of the present work along with methodology adopted to accomplish them and organization of the thesis are also discussed.

1.1 An Introduction to Geometric Modeling

Geometric modeling is the methodology of creating a mathematical or computer-based model on the description of shape [38, 40, 80]. It refers to a collection of techniques or tools used to describe mathematically the shape of an object or simulate some process. Modeling is an art of abstracting or representing a phenomenon and like it, geometric modeling provides a description of the model that is analytical, mathematical and abstract rather than descriptive. A model is convenient and economical substitute for the real object or process and it is easier to analyze a model rather than a real object. If the model is "rich", then we can safely infer the behavior of the object or process from the behavior of the model.

Geometric modeling is the key ingredient in the tasks of design conceptualization as well as design modeling and simulation in Computer Aided Design (CAD) environ-

ment. A valid geometric model is created through *definition translator* which converts the designer intent into the proper database format [125]. Down-stream applications like Computer Aided Manufacturing (CAM) and Computer Aided Engineering (CAE) analysis can be performed on CAD models with the help of *interface algorithms* that extract the required data from the model database.

In the broader sense, geometric modeling comprises parametric modeling and solid modeling. Parametric modeling includes wireframe modeling and surface modeling. Surface modeling techniques facilitate description of shape of the objects in terms of their surfaces [39, 80, 125]. Solid modeling though leads to "informationally complete" representations of three-dimensional (3D) solid objects but surface models give detailed information on free form surfaces [69, 76].

The synthesis phase of design provides flexibility of modeling complex shapes as a combination of simpler ones. Efficient description of geometry of regular and freeform shapes is an important issue in modern industry as more variety of products are being designed with free-formed or sculptured surfaces [26, 38, 122]. The purpose can be to make the products look better (aesthetics) and/or function better (functional design).

Geometric modeling methodologies have been found to be successful in specifying the geometry of complex surfaces such as impeller blades, aircrafts wings, ship hulls etc. [94]. The biparametric surface definitions such as parametric cubic spline surface, Bézier surface, B-spline surface, Coon's patch etc. provide extensive freedom to a designer for designing complex surfaces [39]. In many practical situations, a component is broken up into different surface patches and each patch is defined over a limited region. It is necessary to ensure the continuity conditions among adjacent surface patches. The overall specification of a surface model is usually governed by a set of finite parameters. These parameters, in turn, control the shape and size of each surface patch. Based on the availability of surface definitions, as well as the geometric nature of cutting tool, it has been found that the geometric modeling of a cutting tool as a collection of biparametric surfaces would help the design as well as engineering and manufacturing processes of cutting tools.

1.2 Manufacturing Processes – A Classification

Manufacturing is an activity that utilizes men, material, machine, energy and information to shape and assemble finished products with or without involving any physical and chemical changes in the material involved. The core of manufacturing operations is the process responsible for transforming the shape, size and finish of the

object [30, 46, 61]. Manufacturing processes are broadly classified in three categories, namely, (i) subtractive machining, where material is removed from the blank due to relative movement of a cutting tool over a workpiece; (ii) additive manufacturing that deposits material in an empty volume or layer so as to achieve the desired shape and (iii) forming processes that deform plastically a given volume or sheet of material. All the three categories are further subdivided into conventional and unconventional manufacturing processes. Figure 1.1 shows the different classes of manufacturing processes. The purpose of all these manufacturing processes is shape realization.

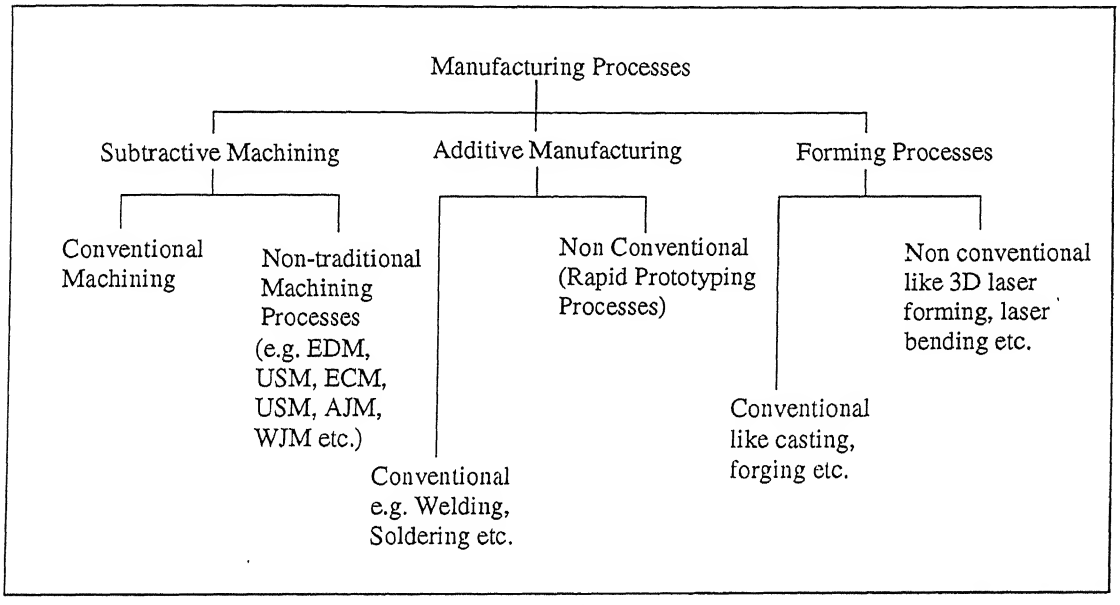

Figure 1.1: Classification of Manufacturing Processes

1.3 Introduction to Machining and Cutting Tools

In machining, the required shape and size of the object are obtained by removing the excess material from the raw workpiece. Due to this, it is also called as material removal process [19, 77, 78]. It is widely used as the finish and accuracy acquired by the parts produced by it are far better than any other process. Besides, it imparts a higher degree of geometric complexity to the work.

The cutting tool is one of the important elements in realizing the full potential out of any machining operation. It is the relative movement of the cutting tool with respect to the workpiece that produces the machined surface. The material to be removed is pressed against the hard edge(s) of the cutting tool and made to flow due to plastic deformation over the face of tool [13].

A cutting tool consists of two groups of functional parts. The first group consists of edges and surfaces responsible for actual cutting operation. These are critical elements of a cutting tool and form cutting element(s) or teeth of the cutter. The second group consists of shank, disk, cylinder etc. on which the cutting elements are established. The elements of this group form cutter body and are non-critical as they are meant to complete the geometry. The geometry of a cutting tool consist of face(s) or rake surface(s), flanks, cutting edges and the corner(s) or nose [13, 28, 87, 119]. Face is the surface of the cutting tool along which the chip flows out, while flanks are the surfaces facing the workpiece. Based on the geometry of cutting elements, a cutting tool can be single-point or multi-point cutting tool.

1.3.1 Single-Point Cutting Tools

A single-point cutting tool refers to tool for turning, planing, boring etc., that has one shank (or body) and one cutting element in the form of a cutting edge at one end [83, 109]. This cutting edge may be formed on one end of a solid piece of steel, or the cutting part of the tool may consist of an insert or tip which is held to the body of the tool by brazing, welding or mechanical means [64]. They are commonly used in lathes, shapers, planers and similar machine tools. During machining a single-point cutting tool is provided translatory motion while the job is rotated or translated.

1.3.2 Multi-Point Cutting Tools

A tool with a series of two or more cutting elements attached to a common body is known as multi-point cutting tool [83, 109]. The majority of multi-point cutting tools are provided rotary motion for shape realization as shown in Table 1.1 [13].

Operation	Motion of Cutting Tool	Motion of Workpiece
Turning	Translation	Rotation
Shaping	Translation	Intermittent Translation
Planing	Intermittent Translation	Translation
Milling	Rotation	Translation
Drilling	Rotation and Translation	Fixed
Boring	Rotation	Forward Translation
Hobbing	Rotation and Translation	Rotation
Surface Grinding	Rotation	Translation

Table 1.1: Relative Motion of Various Cutting Operations

The common machining operations associated with multi-point tools – milling, drilling, gear cutting – are introduced in the following subsections.

Milling

Milling is a subtractive shape realization process that removes material by relative motion between a workpiece and a rotating cutting tool. The cutting tool used for the purpose has multiple cutting teeth. As the cutter rotates, each tooth removes a small amount of material during each revolution from the advancing work [27, 29, 33, 44, 48].

A wide variety of operations can be performed by milling since both the workpiece and the cutter can be moved relative to one another independently or in combination. Milling consists of two motions: rotation of the cutter about its axis which is primary cutting motion, and a feed motion. In some applications, the feed is given to the workpiece while in other the workpiece is held stationary and the cutter is traversed across at a given feed rate. The feed motion is along a straight line in milling flat and cylindrical surfaces; it is rotary in milling surfaces of revolution and helical in milling helicoidal surfaces [93]. Milling operations are performed on different machines with different type of cutters. Milling cutters are bodies of revolution, rotating about their axes, with equally spaced cutting teeth on their surfaces (Figure 1.2). Applications of milling include the production of flat or contoured surfaces, slots, profile surfaces, grooves, recesses, bodies of revolution, threads, and other configurations.

Milling is one of the most universal, yet complicated machining methods. The process has more variations in the kinds of machines used, workpiece movements, and types of tooling than any other manufacturing method. Important advantages of removing material by means of milling include high stock removal rates, the capability of producing relatively smooth surface finishes, and the wide variety of cutting tools that are available. Cutting tooth of the tools can be shaped to any complex shape.

The basic process of chip formation in milling is the same as for all other metal cutting operations - a wedge-shaped cutting tool engages the workpiece to remove a layer of material in the form of a chip [13, 33]. Chip formation in milling differs from single-point metal cutting in several respects. The cutter teeth intermittently engage the workpiece and remove material, with each tooth or insert generally in the cut less than half of the total machining time per cutter revolution. The chips are relatively small in size and there are variations in chip thickness within a chip itself.

Milling cutters are made in many sizes and types for milling regular and irregular shaped surfaces on the workpiece [33, 48]. They can be classified according to:

- Construction characteristics: They may be of *solid* type, with teeth and body

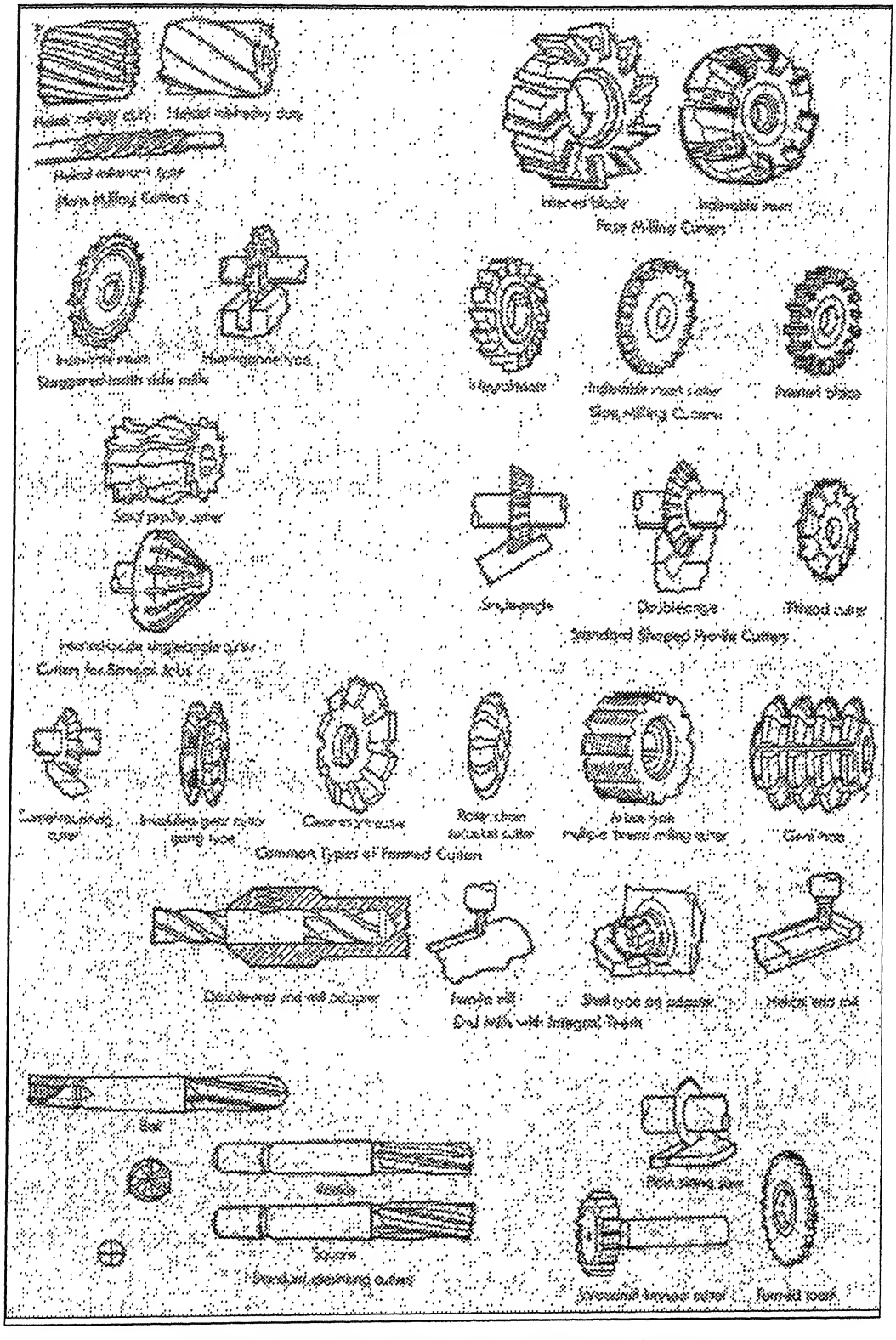

Figure 1.2: Canonical view of Milling Cutters

integral; or *carbide or cast alloy tipped solid cutters*; or *inserted-tooth* type, with removable teeth held and rigidly locked in suitable cavities in the body.

- Inclination of the teeth: The teeth may be *straight*, parallel to axis of rotation; or *helical*, at an angle known as helix angle.
- Relief of the teeth: The teeth may be *profile-relieved*, when the relief surface is comparatively simple flat or helical and the relief is obtained by grinding a narrow land back of the cutting edge; or *form-relieved*, when the relief surface is curved and the relief is obtained by grinding the faces of the teeth. A considerable large group of milling cutters have profile-sharpened teeth.
- Method of mounting: The milling cutters can be made *arbor mounted*, with a center hole for mounting on an arbor; or *shank type*; or *spindle mounted*, with the back recessed for bolting directly on the spindle nose.
- Hand of rotation and hand of helix: Milling cutters may be made for either *right* or *left hand* of rotation, and with either *right* or *left hand* helix.
- Purpose or use of the cutter: Milling cutters can be of type *T-slot cutter*, *Woodruff keyseat cutter*, *Gear or Thread milling cutter*

In the broader perspective, milling cutters fall into following two categories [27]:

- Standard Milling Cutters: These conform to dimensions approved by the international standards bodies (e.g. ISO, ASA, DIN, BS). The dimensional standards, relating chiefly to cutter diameter and width, size of center hole, width and depth of keyway, etc., have been adopted by cutter manufacturers.
- Special Milling Cutters: These are designed for work on special jobs. They may or may not have standard dimensions, and do not conform to any generally accepted standard. They are normally designed to combine several milling operations in one, and may be used for milling regular or irregular surfaces.

Drilling

The operation where the tool is rotated and fed along its axis of rotation while the workpiece remains stationary is called drilling [33, 83]. The most common type of drilling is the operation with a twist drill to generate a hole. A twist drill with a shank has two (or more) cutting edges, each responsible for removal of work material.

Gear Manufacturing

The type of gear being produced, spur, helical, bevel, etc., is usually the major factor for the choice of gear manufacturing method. In addition to this, the factors usually

considered in the final choice of the method are size of the gear, configuration of the integral sections, quantity requirements, accuracy requirements and cost [29, 33, 48]. Gear can be produced by machining, or with the use of dies. Gear production by machining can be of following types:

(i) Gear milling
(ii) Gear hobbing
(iii) Gear shaping
(iv) Shear cutting of gears
(v) Gear broaching
(vi) Bevel gear cutting

Among these, *gear hobbing* is the most popular method of gear production. it is a continuous generating process in which the tooth flanks of the constantly moving workpiece are formed by equally spaced cutting edges of the hob [33, 48]. The profile produced on the gear is a curve comprising of a number of flats, varying with the number of flutes in the hob which pass a given tooth during the generating movement. Every hob tooth, which contacts the gear along the line of action, produces one enveloping cut. Like the straight flank of the hob tooth, the individual cut is straight and in tangent plane to the involute of the tooth flank. Thus, all enveloping cuts form a polygon of tangents to the involute which on its corners form a crest and deviates from the involute curve. This deviation increases when the numbers of enveloping cuts are reduced. The conventional hob can be compared to a worm provided with flutes or gashes and with tooth profile suitably relieved behind the formed cutting edges.

1.4 Need of Geometric Modeling for Cutting Tools

Cutting tools hold an important position in the manufacturing world, as inspite of developments in the area of additive manufacturing and forming, subtractive machining holds the major share in the product shape and form realization. The geometry of the surface generated on the blank is directly dependent upon the geometry of the cutting tool surfaces along with relative motion between them. This is based on the fact that the surface of the cutter in contact with workpiece and the machined surface are mutually enveloping surfaces [62].

Design and manufacturing of cutting tools is a critical segment of any manufacturing system. Cutting tool surfaces are either planar or doubly-curved surfaces.

Traditionally, cutting tools are defined by the specification approach (ISO standards). Such definitions are complicated. Further, they are not unified and cannot be used for computer based manufacturing/grinding and engineering analysis. With recent developments in the area of conjugate geometry and availability of better definitions of curves, surfaces and solids, cutting tools can be designed and manufactured automatically, without depending on the expertise of fast vanishing experienced tool designers. Even the shapes not possible to manufacture earlier are achievable due to increased control of machine tools by CNC controllers. Thus, the stress is towards generating the accurate geometry of cutting tools. This can be achieved by geometric modeling techniques. In the present times, accurate geometric models of cutting tools are essential, as increasingly, the design and manufacturing is performed in the virtual world, called virtual prototyping and manufacturing [49, 57, 70, 84, 85, 86, 89] before actual machining is carried out.

Recent developments in the area of CAGD have led to various mathematical definitions of analytic and synthetic uniparametric curves and biparametric surfaces [39, 80, 94, 125]. These biparametric surfaces can correctly model any free formed surface. This has led to tremendous growth in the developments of CAD models of complex shaped objects. However, the area of application is still mainly confined to automobile and aerospace sectors and any work that is undertaken in the direction of developments of CAD models of cutting tools is not known. The need of geometric modeling of the cutting tools can be further stressed due to

(i) Cutting tool surfaces are complex, hence proper definitions of them are required.
(ii) Cutting tool standards need upgradation as they depend on 2D definitions.
(iii) Tool and cutter grinders are having a focused shift from manual to computer controlled.
(iv) Cutting tools are increasingly manufactured and sharpened by CNC machine tools and in CNC machines, programming is crucial, particularly of free form surfaces and not the machine tool itself. Convenience and accuracy of CNC programming improves with the CAD definition of the object.
(v) Though there exist many powerful CAD softwares today, but a cutting tool CAD software is yet to be designed.
(vi) None of the existing CAD softwares contain any cutting tool design module.
(vii) Geometric modeling enables the designer to generate centralized and integrated database. Such a database for cutting tools can convey design information for a range of downstream engineering and manufacturing applications.

(viii) A generic CAD model of the available cutting tools acts as a core model and new cutting tools can be generated by modifying its parameters and activities like rendering, simulation, analysis, manufacturing etc. can be performed using this core model.

1.5 Review of Available Literature

The prediction of cutting forces in machining along with mechanics and dynamics of cutting tools are the areas that have captured major attention of researchers in the field of manufacturing. Even in these areas also, the stress is towards milling processes and milling cutters due to their wide spread usage. With more and more components having sculptured surfaces, CNC machining is in greater demand. These surfaces are normally generated on CNC machines by end mills and this has made the researchers' focus on developing cutting force models for end milling. These models approximate the geometry of cutting tools by presenting them in two-dimensional space. The end geometry of the tool which is modeled by dividing cutting edges into infinitesimal elements is proposed by Abrari and Elbestawi [1], Li et. al. [73], Sim and Yang [98], Yang and Park [123]. Tai and Fuh [103] have modeled cutting edge as a curve of intersection of a spherical surface and a skew plane. The analytical representation of helical flute geometry is proposed by Lee and Altintaş [71], Yücesan and Altintaş [124], while cutting force prediction model is combined with models for cutter and workpiece deflection to study surface errors for end milling by Kline et. al. [67].

The work in the area of modeling the mechanics and dynamics of milling cutters is to predict factors like chip thickness, cutting force, vibration, torque, power, surface finish etc. Smith and Tlusty [100] have reviewed frequently used models of force and deflection computation for milling process and highlighted their validity, applications and limitations. A dynamic model for end milling flexible plate type structure has been reported by Altintaş et. al. [3]. A comprehensive integrated static and dynamic cutting model for ball end milling processes has been presented by Altintaş and Lee [4, 5] while Altintaş and Engin [6] have presented a model for milling with helical end mills and inserted cutters. Use of surface roughness model to analyze the effect of insert runout and variations of feed rate on surface roughness and dimensional accuracy in face milling is shown by Baek et. al. [11]. Lee et. al. [72] have designed a face milling cutter and developed a cutting model to improve its dynamic characteristics.

Another domain of interest in manufacturing research is the design of milling cutters. Vickers and Quan [114] have presented a comparison of insert-based flat end

mills and solid ball-end mills in machining low curvature surfaces. Chen and Lin [21] have developed design and manufacturing models for ball-end cutters based on envelope theory. Chen et. al. [22, 23] have presented manufacturing models to produce concave cone end milling cutters. Work on cutters other than end mills include design and manufacturing of hob for processing worm gear by Simon [99], design of cutters to manufacture helicoidal surfaces by Karunakaran and Dhande [63] and methodology of resharpening inserts by Hogarth [50]. Besides this, Oancea and Oancea [82] have studied tool profile to machine arbitrary surfaces and estimated machining errors when the tool profile is known at few discrete points and Carlsson and Stjernsoft [16] have calculated the geometrical shape of tool-work interface for rotary tools.

Simulation of milling processes is also a major area of research in manufacturing. The problem of defining the geometry of a machined surface is essentially a problem of defining the boundary of the swept volume of the cutter. Chappel [20] has presented an approach to model the metal removal process using vectors. An approach to define swept volume using envelope theory is presented by Wang and Wang [117] and using sweep differential equations is proposed by Blackmore et. al. [14]. Spence and Altintaş [101] have discussed a constructive solid geometry (CSG) based system to simulate the milling process and assist in online monitoring and control tasks. Mounayri et. al. [81] have modeled part as boundary representation (B-rep) model and tool cutting edges as cubic Bézier curves to evaluate cutter swept volume, material removed and tool-part immersion geometry. An algorithm for polygonal representation of the boundary of volume swept by the cutter using differential geometry to determine geometrically swept volumes is proposed by Glaeser and Gröller [47]. An approach to integrate solid modeling with milling process simulation and its applications in machining is shown by Spence et. al. [102]. Imani and Elbestawi [55] have developed precise B-rep model of the cutter swept volume to update part being machined for each NC block, evaluate instantaneous chip geometry and model feed marks and scallops on the machined surface. Chiu and Malkin [24] have developed simulation for creed-feed grinding operations. The virtual grinder proposed by them provides data of cutting forces, power, temperatures and surface roughness.

Geometry of the twist drills has been studied by Agullõ-Batlle et. al. [2], Armarego and Kang [7], Ehmann [34], Ekambaram and Malkin [36], Friedman et. al. [41, 42], Fujii et. al. [43], Kaldor et. al. [58, 59], Ko [68], Mizugaki et. al. [79], Sheth and Malkin [96], Tsai and Wu [111, 112, 113]. However, the work is not in the direction of development of unified representation scheme for the twist drills. These works are to evaluate the shape of drill profile for a given milling cutter or grinding wheel and

identification of geometry of milling cutter or grinding wheel used to generate a given twist drill. The former is known as direct method and the latter as inverse method. The resulting data and information have to be fed to an experienced tool engineer to manufacture or ground the twist drill. Other work on drills include drill analyses to modify its designs by Bhattacharyya et. al. [12], Ehmann et. al. [35], Shi et. al. [97], Lin et. al. [74], Ren and Ni [92] and mathematical modeling for multiflute drill designs by Wang et. al. [116], Hsieh and Lin [51].

Cutting tools like single-point cutting tools, other milling cutters and gear cutters and shapers have surprisingly not drawn much attention of researchers. The reason for this could be, the large variety of the tools that exist in practice, existence of complex surfaces that form these tools and difficulties in defining these complex, free form surfaces mathematically. To create a comprehensive geometric model that could take into account this wide variety of tool geometry is rather difficult and this could be primary reason that the researchers have not been attracted towards modeling them and the field remains largely unexplored. Recently, the work in the direction of development of geometric models for single-point cutting tools is done by Deo [31] and Rajpathak [91]. Arnold [8] has discussed the trends that drive the cutting tools development.

Recent developments in the field of geometric modeling now provide designers an elegant and precise approach of specifying the geometry of complex shaped objects (Mortenson [80], Mäntyla [76], Farin [38], Rogers and Adams [94], Choi [26], Zeid [125]). A method for modeling and machining compound surfaces using CSG has been discussed by Choi et. al. [25], while Tandon et. al. [104] have discussed the modeling and machining of complex freeform surfaces. It is found that the conjugate geometry approach can be extended to machining and together with computational models and symbolic algorithms, it can conveniently model different manufacturing processes (Dhande et. al. [32], Voruganti et. al. [115]). Some recent work in the associated areas that motivated the present work includes, a keynote paper on modeling of machining operations to stimulate the developments of models predicting quantitively the performance of machining operations by Luttervelt et. al. [75], identification of characteristics for common representation of a set of manufacturing resources [131], an approach to optimize macro-level tool geometry in machining by Kaldor and Venuvinod [60] and about orthogonal parameterization of part and tool surface for transformation of coordinate systems by Radzevitch and Goodman [90]. Research in the area of feature modeling of sculptured objects has addressed the need of unified geometric models (Au and Yuen [9, 10], Cavendish [17, 18], Hui and Yadong [52], Ka-

gan et. al. [56], Kimura [65], Kishi [66], Roller [95], Tönshoff [110], Otto [126]). The proposed approach of modeling surface patches provides unified models of single-point and a range of multi-point cutting tools.

1.6 Objective and Scope of the Present Work

The primary goal of this work is to outline in detail geometric models of surface patches for single-point and multi-point cutting tools and to establish a set of new three-dimensional (3D) standards for defining the cutting tool geometries. However, we also like to

(i) Verify the surface based definitions of cutting tools by designing and rendering them in terms of 3D geometric parameters.
(ii) Establish forward and inverse mapping relations between 3D nomenclature and conventional specification scheme(s).
(iii) Establish generic definition and to develop a geometric model of cutting tool that can be used for downstream engineering and manufacturing applications.

The scope of the present work includes:

(i) Establishment of mathematical definition of cutting tool surfaces.
(ii) Establishment of a new CAGD based, 3D standard of defining cutting tools.
(iii) Demonstration of the effectiveness of the new standard.

1.7 Methodology of Present Work

The approach adopted to accomplish the present work is by

(i) Reviewing and classifying the cutting tools on the basis of their geometric complexity and application.
(ii) Identifying critical or functional and non-critical elements of the cutting tool.
(iii) Developing appropriate mathematical biparametric definitions for unbounded functional surfaces of the cutting tool.
(iv) Defining the parameterized geometry of bounded curved surfaces by establishing the limits of parameters of the unbounded surfaces, understanding the topology of cutter and ensuring continuity conditions.
(v) Specifying the cutting tool geometry in terms of 3D rotational angles α_i, β_i and γ_i and dimensional parameters, collectively termed as geometric parameters. Angles α_i, β_i, γ_i are the angles of rotation of surface patch i about X, Y, Z axis

respectively, where positive rotation directions about the coordinate axes are counter clock wise, when looking toward the origin from a positive coordinate position on each axis.

(vi) Modeling the surface patches forming the cutter body in parametric form and establishing suitable geometric parameters.

(vii) Modeling the transitional surfaces of the surface patches. A transitional surface forms a smooth localized transition between neighboring surfaces at their edge of intersection.

(viii) Establishing relationships among the proposed 3D tool geometry and conventional specification schemes so that if angles in one nomenclature are known, they can be evaluated in the other. This operation is known as Mapping.

(ix) Validating the geometric models of right hand (RH) cutting tools by rendering them in Open Graphics Library (OGL) environment. Left hand (LH) cutters can also be generated by suitably transforming the models of RH cutting tools.

(x) Demonstrating the utility of the new convention through direct engineering applications on the proposed model.

1.8 Organization of the Work

Chapter 1 of the thesis gives an overview of the geometric modeling and manufacturing operations. It identifies the need of the present work and follows with a brief review of the available relevant literature. It concludes with the objectives and the scope of the work along with the methodology adopted to accomplish the work.

Geometric modeling of a single-point cutting tool is presented in Chapter 2. The chapter develops relations to map proposed angles to equivalent conventional angles as detailed in ASA, ORS and NRS standards and vice-versa. It is followed by the development of surface models for insert-based single-point cutting tools. It also discusses the setting or swivel angles for grinding and their relations with 3D rotational angles to generate stereometric features for manufacturing and resharpening of single-point cutting tool. The chapter considers few numerical examples for illustration.

Chapters 3 to 7 deal with multi-point cutting tools. In Chapter 3, unified geometric model along with forward and inverse mapping relations for a side milling cutting tool are developed. The approach is established with illustrations of the 3D rendered model, grinding methodology and geometric assessment of tool wear for side mill. Surface model of a variant of side mill, half-side mill, is also derived by suitably modifying its geometric model.

Chapter 4 deals with the geometric modeling of fluted cutters. The range of cutters covered in this chapter includes plain and helical slab mills, end mills with different end geometries and drills with a variety of point styles. The chapter also presents forward and inverse mappings for all three types of fluted cutters. At the end an illustration and a case study on Finite Element Analysis (FEA) of helical slab mill is presented.

Insert-based cutters are widely used in real practice and development of unified representation scheme for inserted face mill is discussed in Chapter 5. The development of geometric models for cutter body and generic square and triangular inserts is followed by establishing mapping as well as grinding methodology for inserts. The approach is validated with an example and a case study on FEA of the insert.

Chapter 6 presents the geometric modeling of shell mill. It also establishes mapping among conventional and proposed tool nomenclatures. The 3D model of shell mill is illustrated by rendering the tool and its utility highlighted by presenting a case on its CNC machining.

In Chapter 7, the geometric modeling of gear cutting tools is covered. It elucidates the surface modeling of a gear hob, forward and inverse mapping and the methodology to capture the geometry of a gear shaper in 3D space. The chapter concludes with an example on rendering of gear hob and CNC machining of gear shaper.

To summarize, a matrix of activities performed and cases for down-stream applications implemented in the present work for different types of single-point and multi-point cutting tools is given in the following table.

Cutting Tools	Geometric Modeling	Mapping	Rendering	Grinding	CNC Machining	Geometric Assessment of Wear	FEA
Single Point Cutters	√	√	√	√			
Side Mill	√	√	√	√		√	
Fluted Cutters (Slab Mill, End Mill, Drill)	√	√	√				√
Insert-based Cutters	√	√	√	√			√
Shell End Mill	√	√	√		√		
Gear Cutting Tool	√	√	√		√		

Table 1.2: Geometric Modeling of Cutting Tools: Implementation Matrix

The conclusions of this work are presented in Chapter 8. The scope of further work has also been discussed here.

Chapter 2

SINGLE POINT CUTTING TOOLS

The cutting tool is one of the important elements in realizing the full potential out of any metal cutting operation. A single-point cutting tool forms the foundation of the geometry of most of the cutting tools. The geometry of a single-point cutting tool consists of shank, rake face, flanks, cutting edges and corner [13, 29, 30, 61]. A single-point cutting tool has only one cutting point which is the meeting point of the principal cutting edge with the auxiliary cutting edge.

In this chapter, a mathematical model of the entire geometry of a single point cutting tool is formulated as a combination of planar surface patches and an oblique cone using the concept of computational geometry. This model has been developed for generating data to analyze grinding and sharpening of the cutting tool. The orientation of these planar patches is defined in a right-handed Cartesian coordinate frame of reference by six new angles, termed as rotational angles. Further, the relations between various tool angles in existing two-dimensional (2D) standards and those in the proposed three-dimensional (3D) nomenclature are established.

2.1 Geometric Modeling of Single Point Cutting Tool Surfaces

The geometry of a single point cutting tool has been proposed by various tool designing bodies [33, 119]. Some of these are:

(i) American Standards Association (ASA)

(ii) Orthogonal Rake System (ORS) or DIN/OCT-BKC/CSN

(iii) Normal Rake System (NRS) or ISO

(iv) Maximum Rake System (MRS) or BS

The basic methodology for the modeling of the tool considers the sharpening aspects as well as its manufacturing from an unmachined stock of size L×B×H where L, B and H are length, width and height of the blank. This block, shown in Figure 2.1, is bounded by six planes, numbered I-VI and is defined with respect to the parameters s_i, t_i and r_i ($i \leftarrow 1..3$). Parametric equations of these planes are:

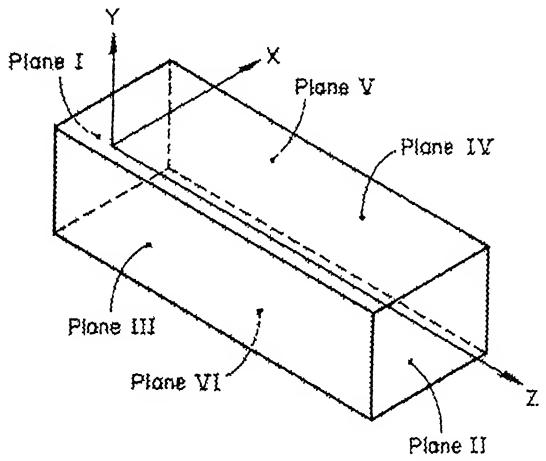

Figure 2.1: System of Planes for Tool Modeling

Plane I

$$x = s_1 \quad (-B/2 \leq s_1 \leq B/2)$$
$$y = t_1 \quad (-H/2 \leq t_1 \leq H/2)$$
$$z = 0$$

Plane II

$$x = s_1 \quad (-B/2 \leq s_1 \leq B/2)$$
$$y = t_1 \quad (-H/2 \leq t_1 \leq H/2)$$
$$z = L$$

Plane III

$$x = -B/2$$
$$y = t_2 \quad (-H/2 \leq t_2 \leq H/2)$$
$$z = r_2 \quad (\ 0 \leq r_2 \leq L\ )$$

Plane IV

$$x = B/2$$
$$y = t_2 \quad (-H/2 \leq t_2 \leq H/2)$$
$$z = r_2 \quad (\ 0 \leq r_2 \leq L\ )$$

Plane V

$$x = s_3 \quad (-B/2 \leq s_3 \leq B/2)$$
$$y = -H/2$$
$$z = r_3 \quad (\ 0 \leq r_3 \leq L\ )$$

Plane VI

$$x = s_3 \quad (-B/2 \leq s_3 \leq B/2)$$
$$y = H/2$$
$$z = r_3 \quad (\ 0 \leq r_3 \leq L\ )$$

A single point cutting tool is assumed to consist of flat planes oriented at certain specific angles to form auxiliary flank (Σ_1), principal flank (Σ_2), rake face (Σ_3) and

shoulder face (Σ_4), along with an oblique cone to model nose radius (Figure 2.2). The flank and face surfaces are defined by transforming suitable unbounded planes with their center initially coinciding with the origin, to their final orientation [31, 91, 105]. The intersections of these unbounded planes with the above six bounded, unmachined workpiece planes produces the boundaries of the single point cutting tool.

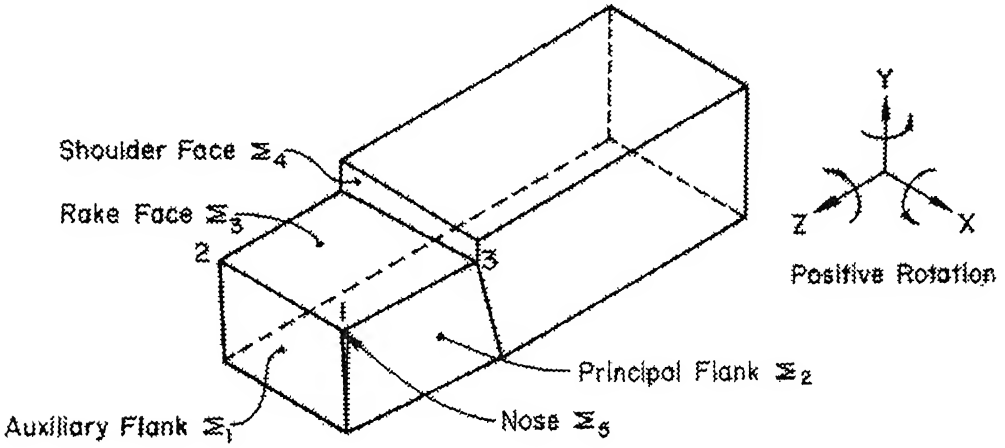

Figure 2.2: Wire Frame Model of the Tool

2.1.1 Sign Conventions

The sign convention for a single-point cutting tool is based on left hand screw theory. The clockwise rotation of the appropriate axis to meet the tool surface is taken as positive sign while the counter clockwise rotation is taken as negative [13]. For a standard right hand turning tool, if the tool rake face slopes away from the nose point in either the transverse or the longitudinal directions as per the ASA system, then the angles are taken as positive. If the face slopes towards the nose in either direction, then that angle is regarded as negative. The above concept also holds good for the ORS and the NRS systems. The clearance angles are regarded as positive if the tool recedes from the work surface when placed against it. The principal or side cutting edge angle (as the case may be) is taken as positive while the end cutting angle is taken as negative.

The sign convention for the rotational angles could be explained with respect to a standard right-hand turning tool with positive angles as per the ASA specifications placed in a right-handed coordinate frame of reference. The rake face could be positioned if an ZX plane is given a positive rotation about the Z-axis and negative rotation about the X-axis (Figure 2.2). The principal flank could be positioned to have positive clearance by rotating an XY plane about the X-axis in the positive

sense and about the Y-axis, also in positive sense, for positive principal cutting edge angle. For the auxiliary flank, the rotation of an XY plane about the X-axis would be positive while that about the Y-axis would be negative. For finding conventional angles from given rotational angles, Table 2.1 can be used as a reference. The angles denoted in this table are conventional angles, as defined by existing cutting tool standards. Further, they are described in Nomenclature too. Thereafter, all expressions are so derived that only positive angles are obtained. Three main types of tools are modeled here. These tools are categorized on the basis of sign of the rotational angles for the rake face about X-axis (α_3) and Z-axis (γ_3). These tools are H.S.S. tools having negative α_3 and positive γ_3, Brazed carbide tools having positive value of both α_3 and γ_3 and Throwaway tips tools having positive α_3 and negative γ_3.

Rotational Angles	ASA	ORS	NRS
α_1 = +ve	α'_y = +ve α'_x = +ve	α'_o = +ve	α'_n = +ve
β_1 = -ve	Φ_e = -ve	Φ_e = -ve	Φ_e = -ve
α_2 = +ve	α_y = +ve α_x = +ve	α_o = +ve	α_n = +ve
β_2 = +ve	Φ_s = +ve	Φ = +ve	Φ = +ve
γ_3 = -ve	γ_x = -ve	γ_o = -ve	γ_n = -ve
γ_3 = +ve	γ_x = +ve	γ_o = +ve	γ_n = +ve
α_3 = -ve	γ_y = +ve	λ = +ve	λ = +ve
α_3 = +ve	γ_y = -ve	λ = -ve	λ = -ve

Table 2.1: Sign Conventions for Forward Angles

2.1.2 Auxiliary Flank

To position an unbounded XY plane, represented in parametric form as $[u_1 \;\; v_1 \;\; 0 \;\; 1]$, as per the auxiliary flank (Σ_1) configuration of a right-handed tool, the plane is successively rotated about X axis through an angle α_1, about Y axis through an angle β_1 and then translated along Z axis (direction 3) by a distance d_{13}. Auxiliary flank formation is shown with the help of Figure 2.3.

If q_{ax}, q_{ay}, q_{az} represent the transformed coordinates of any point on the plane then the transformed equations of the auxiliary flank are

$$\begin{aligned} q_{ax} &= u_1 \cos\beta_1 + v_1 \sin\alpha_1 \sin\beta_1 \\ q_{ay} &= v_1 \cos\alpha_1 \\ q_{az} &= -u_1 \sin\beta_1 + v_1 \sin\alpha_1 \cos\beta_1 + d_{13} \\ & (-\infty \leq u_1, v_1 \leq \infty) \end{aligned} \tag{2.1}$$

where $d_{13} = L-(B/2-\mathrm{d}'/\tan|\beta_2|)\tan|\beta_1|-H/2\times(\sin|\alpha_1|.\sec|\beta_1|)$ (Figure 2.4).Term d′ stands for maximum permissible depth of cut. It is based on number of desired resharpenings and hence left to the discretion of tool designer.

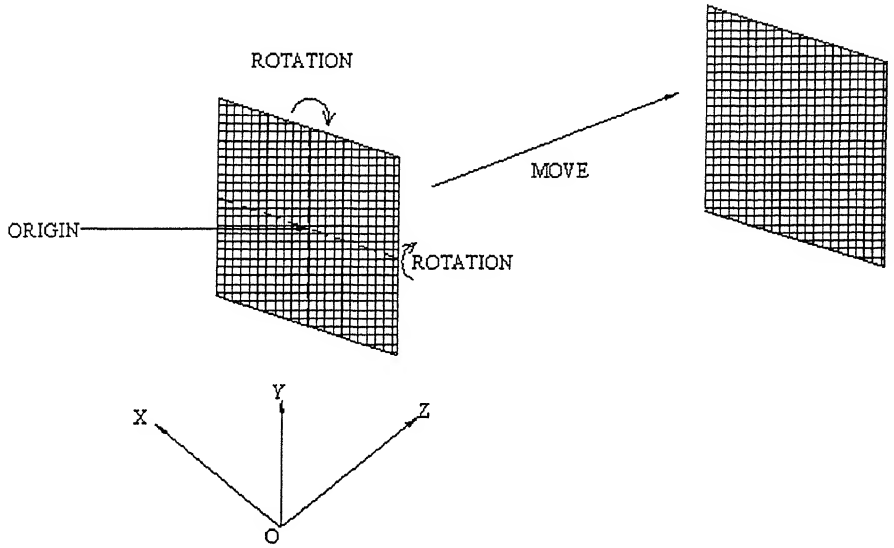

Figure 2.3: Auxiliary Flank Formation

2.1.3 Principal Flank

To position an XY plane as per the principal flank (Σ_2) orientation, the plane is rotated about X axis through an angle α_2, about Y axis through an angle β_2 and then translated along Z axis by a distance d_{23}. If q_{px}, q_{py}, q_{pz} represents the transformed coordinates of any point on Σ_2 plane then

$$\begin{aligned} q_{px} &= u_2\cos\beta_2 + v_2\sin\alpha_2\sin\beta_2 \\ q_{py} &= v_2\cos\alpha_2 \\ q_{pz} &= -u_2\sin\beta_2 + v_2\sin\alpha_2\cos\beta_2 + d_{23} \\ & (-\infty \leq u_2, v_2 \leq \infty) \end{aligned} \tag{2.2}$$

where $d_{23} = L + (B/2 - \mathrm{d}'/\tan|\beta_2|)\tan|\beta_2| - H/2 \times (\sin|\alpha_2|.\sec|\beta_2|)$ (Figure 2.4)

2.1.4 Rake Face

The rake face (Σ_3) is formulated by transforming the ZX plane ($[u_3 \;\; 0 \;\; w_3 \;\; 1]$) to place it at exact location with respect to the auxiliary and principal flanks. The operations include rotation about Z axis through an angle γ_3, about X axis through the angle α_3 and translation along Y axis through a distance d_{32} where the value of

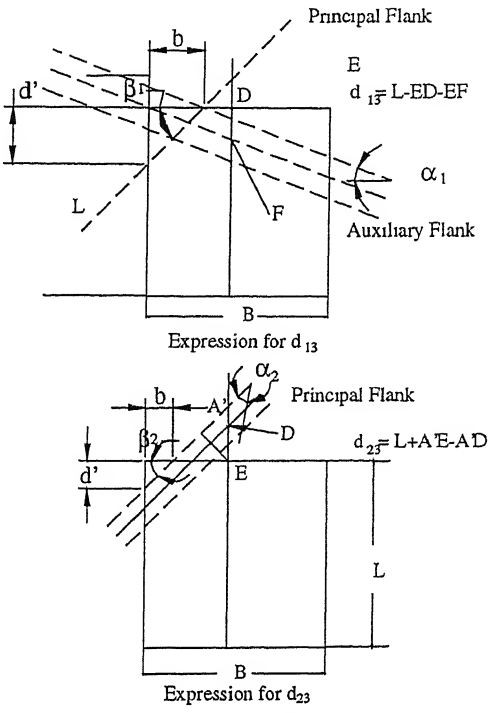

Figure 2.4: Expressions for d_{13} and d_{23}

d_{32} is evaluated, based on slope of the rake face. If the rake angle is positive, the rake face would slope away from the nose, but if the rake angle is negative, it would slope towards the nose. For the first case, it is assumed that the nose is formed at the point of intersection of the auxiliary flank and the principal flank, at a height equal to half of shank thickness ($y = H/2$). For the second case, it is assumed that the plane passes through a point $x = B/2, y = H/2 - T, z = L - \mathrm{d}'$, where T is a parameter to be determined by a suitable configuration of the rake face. If q_{rx}, q_{ry}, q_{rz} represents the transformed coordinates of any point on the plane then

$$\begin{aligned} q_{rx} &= u_3 \cos\gamma_3 \\ q_{ry} &= v_3 \sin\gamma_3 \cos\alpha_3 - w_3 \sin\alpha_3 + d_{32} \\ q_{rz} &= u_3 \sin\gamma_3 \sin\alpha_3 + w_3 \cos\alpha_3 \\ & (-\infty \leq u_3, w_3 \leq \infty) \end{aligned} \tag{2.3}$$

2.1.5 Shoulder Face

An XY plane is rotated about Y axis through an angle β_4 and translated along the Z direction through a distance d_{43}, to position it in the frame of reference as per the requirements of shoulder face (Σ_4). The values of β_4 and d_{43} are at the discretion of the designer. If q_{sx}, q_{sy}, q_{sz} represent the transformed coordinates of any point on the plane then

$$\begin{aligned} q_{sx} &= u_4 \cos\beta_1 \\ q_{sy} &= v_4 \qquad\qquad (u_4, v_4 \in [-\infty, \infty]) \\ q_{sz} &= -u_4 \sin\beta_1 + d_{43} \end{aligned} \tag{2.4}$$

2.1.6 Nose

The nose (Σ_5) is modeled as a ruled oblique cone, comprising one curved edge (directrix) and two straight lines (generators). The curved edge of the nose of the H.S.S. tool can be modeled as a rational Bézier curve with the help of three control points. Two points, one along principal cutting edge (P_0) and another along auxiliary cutting edge (P_2) are found by interpolating linearly, depending on the value of the nose radius. Third point (P_1) is obtained by ensuring C^1 continuity of the nose curve with cutting edges. Taking point of intersection of principal flank surface, auxiliary flank surface and base surface as the vertex of the cone (P^*), a ruled surface forming the oblique cone is created and shown in Figure 2.5.

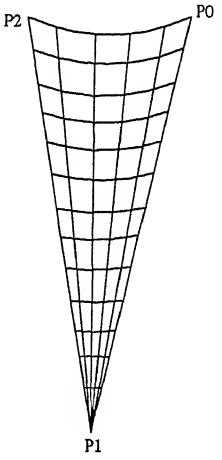

Figure 2.5: Nose Formation

The nose surface is parametrically written as:

$$q(u, v) = p(u, 0)(1 - v) + P^* v \tag{2.5}$$

where $p(u, 0)$ is the equation of the circular arc of the nose, modeled as Bézier curve.

The tool blank, after proper positioning of the planes can be looked upon as intermingling of six original planes (I–VI) and these five surface patches. The points of intersection of various surfaces and lines are evaluated. A typical H.S.S. tool can be looked upon as consisting of 13 corner points (Figure 2.2) and a surface model can be created out of it. Figure 2.6 shows the surface model of a right hand turning tool.

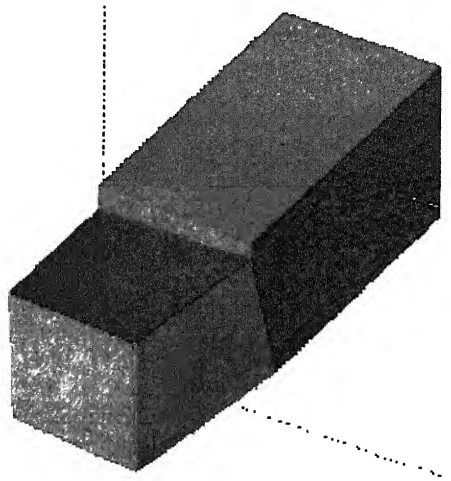

Figure 2.6: Surface Model of a Right Hand Turning Tool

2.2 Mapping

The most important data required for the grinding of the cutting tools are the angles in 3D space. If the six rotational angles are given, it is important to find the angles corresponding to the ASA, ORS and NRS nomenclatures as these angles have their own significance. The ASA angles are the projected angles and are useful for checking the conformity to the required geometry. Similarly, the ORS and the NRS angles are useful to study the mechanics of cutting [13, 33, 119]. The equations that are used to find the conventional angles for the given rotational angles are termed henceforth as forward mapping. The objective of the inverse mapping is to find the six rotational angles if the six angles corresponding to any of the conventional nomenclatures are given. It is important from the sharpening or the manufacturing point of view [31, 91].

2.2.1 Forward Mapping

In the previous section, the definitions of the five surface patches are formulated in parametric form. To find the conventional angles, normal vectors to the patches need to be found out which depend on tangent vectors at any point on the surface. Thus, if q_u and q_v are the tangents in the u and v direction respectively, then their cross product in the required order gives the normal vector to the surface in the outward direction. The normal vectors and the grinding principle help in evaluating all the angles. The signs of these calculated standard angles are as per the sign convention specified in Table 2.1.

ASA Angles

The equation of the rake face in the vector notation is

$$\vec{q_r} = q_{rx}\hat{\imath} + q_{ry}\hat{\jmath} + q_{rz}\hat{k}$$

where q_{rx}, q_{ry} and q_{rz} are given by Eq. (2.3). The tangent vectors in the u and w directions are

$$\begin{aligned} \vec{q}_{r_u} &= \cos\gamma_3\hat{\imath} + \sin\gamma_3\cos\alpha_3\hat{\jmath} + \sin\gamma_3\sin\alpha_3\hat{k} \\ \vec{q}_{r_w} &= -\sin\alpha_3\hat{\jmath} + \cos\alpha_3\hat{k} \end{aligned}$$

and the normal vector perpendicular to the rake face $\vec{n}_f$ be

$$\vec{n}_f = -\sin\gamma_3\hat{\imath} + \cos\alpha_3\cos\gamma_3\hat{\jmath} + \sin\alpha_3\cos\gamma_3\hat{k} \tag{2.6}$$

Back Rake Angle γ_y

The vector $\vec{n}_f$ is projected on the YZ plane and the projected normal vector is obtained with the help of orthographic projection matrix [94] onto X=0 plane. Then

$$\vec{n}_{f_p} = \cos\alpha_3\cos\gamma_3\hat{\jmath} + \sin\alpha_3\cos\gamma_3\hat{k}$$

The unit normal projected vector is

$$\hat{n}_{f_p} = \cos\alpha_3\hat{\jmath} + \sin\alpha_3\hat{k}$$

Taking dot product with unit vector $\hat{\jmath}$, the positive angle γ_y [33, 119] is obtained as

$$\gamma_y = \alpha_3 \tag{2.7}$$

Side Rake Angle γ_x

Projecting normal vector $\vec{n}_f$ given by Eq. (2.6) on XY plane, we get

$$\vec{n}'_{f_p} = -\sin\gamma_3\hat{\imath} + \cos\alpha_3\cos\gamma_3\hat{\jmath}$$

Finding the unit normal vector $\hat{n}_{f_p}$ from the above equation and on taking its dot product with $\hat{\jmath}$, the positive angle γ_x is obtained as

$$\gamma_x = \cos^{-1}\left[\frac{\cos\alpha_3\cos\gamma_3}{\sqrt{\sin^2\gamma_3 + \cos^2\alpha_3\cos^2\gamma_3}}\right] \tag{2.8}$$

Clearance Angles α_y and α_x

The equation for the principal flank is given by Eq. (2.2). As described for the rake face, the normal vector to the principal flank is obtained as

$$\vec{n}_p = \sin\beta_2\cos\alpha_2\hat{\imath} - \sin\alpha_2\hat{\jmath} + \cos\alpha_2\cos\beta_2\hat{k} \tag{2.9}$$

The normal vector projected on YZ plane is given by

$$\vec{n}_{p_p} = -\sin\alpha_2\hat{j} + \cos\alpha_2\cos\beta_2\hat{k}$$

If α_y is the angle made by the projected unit vector $\hat{n}_{p_p}$ with the Z-axis, then

$$\alpha_y = \cos^{-1}\left[\frac{\cos\alpha_2\cos\beta_2}{\sqrt{\sin^2\alpha_2 + \cos^2\alpha_2\cos^2\beta_2}}\right] \tag{2.10}$$

If the normal vector (Eq. (2.9)) is projected on the XY plane then

$$\vec{n}'_{p_p} = \sin\beta_2\cos\alpha_2\hat{i} - \sin\alpha_2\hat{j}$$

This vector forms an angle α_x with the X-axis, which is given by

$$\alpha_x = \cos^{-1}\left[\frac{\cos\alpha_2\sin\beta_2}{\sqrt{\sin^2\alpha_2 + \cos^2\alpha_2\sin^2\beta_2}}\right] \tag{2.11}$$

In a similar manner, the clearance angles on the auxiliary flank are obtained as

$$\alpha'_y = \cos^{-1}\left[\frac{\cos\alpha_1\cos\beta_1}{\sqrt{\sin^2\alpha_1 + \cos^2\alpha_1\cos^2\beta_1}}\right] \tag{2.12}$$

$$\alpha'_x = \cos^{-1}\left[\frac{-\cos\alpha_1\sin\beta_1}{\sqrt{\sin^2\alpha_1 + \cos^2\alpha_1\sin^2\beta_1}}\right] \tag{2.13}$$

The angles made by the principal and end cutting edges (ϕ_s and ϕ_e) are the projected angles on the base plane Π_y. These angles are measured directly from the wireframe model (Figure 2.2) by projecting the edges 1-3 and 1-2 respectively on Π_y.

ORS Angles

In DIN system, one important point to be taken care of is that although principal cutting edge lies completely in the principal flank, which is inclined at an angle β_2 with the Y axis in the top view of the tool, principal edge cutting angle is slightly different and depends on clearance angle (when $\alpha_2 \neq 0$) [13]. The positive or negative value of the inclination angle would decide whether this cutting edge angle would be greater or less than the value of β_2. Further, in ORS standard, the rake angles and clearance angles are evaluated by looking directly along respective cutting edges. Therefore, for all practical purposes, the angle of the direction of the principal cutting edge and the auxiliary cutting edge to find their clearance angles in the ORS nomenclature, can be taken as the rotational angles β_2 and β_1 respectively. This produces a difference of $\simeq 5 \times 10^{-3}$ degrees in the clearance angles which can be neglected. To show that the orthogonal clearance angle (α_o) is equal to α_2 on the principal flank if the small difference is neglected, consider the normal vector to the principal flank (Eq. (2.9)).

To find α_o, the normal vector is rotated about the Y axis through an angle $(90 - \beta_2)$ and projected on the XY plane, which gives

$$\vec{n}_p = \cos\alpha_2\hat{\imath} - \sin\alpha_2\hat{\jmath}$$

The dot product with the unit vector in the X direction gives

$$\alpha_o = \alpha_2 \tag{2.14}$$

$$\text{Similarly, } \alpha'_o = \alpha_1 \tag{2.15}$$

Similar to ASA system, the values of the principal cutting edge angle (β_2^*) and the auxiliary cutting edge angle (β_1^*) are measured directly from the geometry of the wireframe model.

Orthogonal Rake Angle γ_o and Inclination Angle λ

The normal vector to the rake face (Eq. (2.6)) when rotated by an angle $(90° - \beta_2^*)$ about the Y axis in the positive sense and projecting on the XY plane gives

$$\vec{n}_{f_p} = (-\sin\gamma_3\sin\beta_2^* + \sin\alpha_3\cos\gamma_3\cos\beta_2^*)\hat{\imath} + \cos\alpha_3\cos\gamma_3\hat{\jmath}$$

The angle γ_o is the angle made by $\vec{n}_{f_p}$ with the Y axis. Therefore, the dot product of the unit normal projected vector along the Y axis gives

$$\gamma_o = \cos^{-1}\left[\frac{\cos\alpha_3\cos\gamma_3}{\sqrt{(\cos\alpha_3\cos\gamma_3)^2 + (-\sin\gamma_3\sin\beta_2^* + \sin\alpha_3\cos\gamma_3\cos\beta_2^*)^2}}\right] \tag{2.16}$$

In a similar manner, projecting the rotated normal vector on the YZ plane and finding the positive angle with the Y axis gives the inclination angle as

$$\lambda = \cos^{-1}\left[\frac{\cos\alpha_3\cos\gamma_3}{\sqrt{(\cos\alpha_3\cos\gamma_3)^2 + (\sin\gamma_3\cos\beta_2^* + \sin\alpha_3\cos\gamma_3\sin\beta_2^*)^2}}\right] \tag{2.17}$$

and inclination angle with the auxiliary cutting edge is given by

$$\lambda_e = \cos^{-1}\left[\frac{\cos\alpha_3\cos\gamma_3}{\sqrt{(\cos\alpha_3\cos\gamma_3)^2 + (-\sin\gamma_3\cos\beta_1^* + \sin\alpha_3\cos\gamma_3\sin\beta_1^*)^2}}\right] \tag{2.18}$$

NRS Angles

In ISO specifications, the principal cutting edge angle (ϕ) and the end cutting edge angle (ϕ_e) can be found from the geometry by projecting the edges 1-3 and 1-2 on the base plane (Π_y) which are denoted as β_2^* and β_1^* respectively. The formula for finding the inclination angle remains the same as in the ORS system (Eq. (2.17)).

Existing standard tool angle relationships between the ORS and the NRS systems [13], and the above derived equations can be used to find the value of Normal Rake (γ_n) and Normal Clearance (α_n) angles which are given by

$$\gamma_n = \tan^{-1}[\tan\gamma_o \cos\lambda] \tag{2.19}$$

$$\alpha_n = \tan^{-1}\left[\frac{\tan\alpha_2}{\cos\lambda}\right] \tag{2.20}$$

The normal clearance angle on the auxiliary flank is given by

$$\alpha'_n = \tan^{-1}\left[\frac{\tan\alpha_1}{\cos\lambda_e}\right] \tag{2.21}$$

2.2.2 Inverse Mapping

The inverse problem of finding rotational angles from the standard nomenclatures is important for generating/sharpening the angles.

ASA Angles

As seen in Section 2.1, the sign convention used for the conventional angles differ from that used for the rotational angles. Hence, sign conventions specified in Table 2.1 are followed to obtain the correct signs of the rotational angles.

To find α_3 and γ_3

From Eq (2.7) we have

$$\alpha_3 = \gamma_y$$

From the expression of γ_x (Eq.(2.8))

$$\cos^2\gamma_x = \frac{\cos^2\alpha_3\cos^2\gamma_3}{[\sin^2\gamma_3 + \cos^2\alpha_3\cos^2\gamma_3]}$$

Substituting $\alpha_3 = \gamma_y$, $\cos^2\gamma_x = A$ and $\cos^2\gamma_y = B$ in the above expression, we get

$$\gamma_3 = \tan^{-1}\sqrt{\frac{(B-AB)}{A}} \tag{2.22}$$

Squaring the expressions of α_y and α_x (refer equations (2.10) and (2.11)) and substituting $\cos^2\alpha_y = C_1$, $\cos^2\alpha_x = C_2$, $\cos^2\alpha_2 = x$ and $\cos^2\beta_2 = y$, we get

$$\begin{aligned}(1-C_1)xy + C_1x - C_1 &= 0\\ (1-C_2)xy - x + C_2 &= 0\end{aligned} \tag{2.23}$$

Solution of these simultaneous equations gives the values of the angles α_2 and β_2. Similarly, substituting $\cos^2\alpha'_y = C_3$, $\cos^2\alpha'_x = C_4$, $\cos^2\alpha_1 = x'$ and $\cos^2\beta_1 = y'$ in equation (2.12) and (2.13) gives

$$\begin{aligned}(1-C_3)x'y' + C_3x' - C_3 &= 0\\ (1-C_4)x'y' - x' + C_4 &= 0\end{aligned} \tag{2.24}$$

The value of x' and y' can be used to find the angles α_1 and β_1 respectively. If the value of any one of the clearance angles is zero, no definite solution can be attained.

ORS Angles

The angle of rotation of the principal flank about the Y-axis is equivalent to the angle made by normal to the principal flank with the X-axis and is given by

$$\beta_2 = \phi - \tan^{-1}[\tan\lambda \tan\alpha_o] \tag{2.25}$$

where ϕ, principal cutting edge angle is the angle made by principal cutting edge with the X-axis in the ZX plane. Similarly, the rotational angle β_1 is given by

$$\beta_1 = \phi_e + \tan^{-1}[\tan\lambda_e \tan\alpha'_o] \tag{2.26}$$

This takes care of the negative values of angles β_1 and ϕ_e as per sign convention given in Table 2.1. The value of λ_e is found by using the following standard formula [13]:

$$\tan\lambda_e = \sin(\phi - \phi_e)\tan\gamma_o - \cos(\phi - \phi_e)\tan\lambda \tag{2.27}$$

The values of α_3 and γ_3 are found by solving equations (2.16) and (2.17) simultaneously using Newton-Raphson's technique. The two non linear equations are

$$\begin{aligned}(1-C_5^2)(\cos\alpha_3\cos\gamma_3)^2 - C_5^2(K_1\sin\alpha_3\cos\gamma_3 - K_2\sin\gamma_3)^2 &= 0\\ (1-C_6^2)(\cos\alpha_3\cos\gamma_3)^2 - C_6^2(K_2\sin\alpha_3\cos\gamma_3 + K_1\sin\gamma_3)^2 &= 0\end{aligned} \tag{2.28}$$

where $C_5 = \cos\gamma_o$, $C_6 = \cos\lambda$, $K_1 = \cos\beta_2^*$ and $K_2 = \sin\beta_2^*$. While solving these equations for the three types of tools dealt in the present work, the initial starting point is considered to be (γ_o, 0), if both inclination angle and orthogonal rake angle are positive or both negative. If one is negative and the other is positive then initial point is taken as (0, λ). It is found that for the range of angles specified in the literature [33, 119], the initial solution works well but an alteration in the initial point is required if one of the two angles specified for a tool is zero.

NRS Angles

The equations (2.20), (2.21) and (2.27) along with the relation [$\tan\gamma_n = \tan\gamma_o\cos\lambda$] are used to evaluate rotational angles α_1 and α_2, given by

$$\begin{aligned}\alpha_1 &= \tan^{-1}[\tan\alpha'_n\cos\lambda_e]\\ \alpha_2 &= \tan^{-1}[\tan\alpha_n\cos\lambda]\end{aligned} \tag{2.29}$$

The values of angle β_2 and β_1 are same as given by the equations (2.25) and (2.26). To find the rake face angles α_3 and γ_3, nonlinear equations (2.17) and (2.19) are solved to get

$$\begin{aligned}(1 - C_6^2)(\cos\alpha_3 \cos\gamma_3)^2 - C_6^2(K_2 \sin\alpha_3 \cos\gamma_3 + K_1 \sin\gamma_3)^2 &= 0 \\ C_7 - C_6 \tan\gamma_o &= 0 \end{aligned} \quad (2.30)$$

where $C_7 = \tan\gamma_n$

2.3 Geometry of Carbide Tipped Tools

Cemented carbide tips are used extensively in single-point cutting tools, where inserts are brazed or clamped to the shank. The basic design of an insert has to ensure that the tip is always in a state of compression. Also, the orientation of the tip is planned such that there is minimum loss of carbide during resharpening of the tool [13, 37].

The basic formulation for the modeling of a carbide tipped tool works out to be the same as done for the H.S.S. tool [107]. A carbide bit also has three important functional surfaces namely, auxiliary flank, principal flank and the rake face, given by equations (2.1), (2.2) and (2.3) respectively. These surfaces are given the inclination as per the design requirement. The inclination of surfaces are specified by rotational angles to model and manufacture the bit.

The carbide bit has two faces, top and bottom. The bottom face which is parallel to the top face sits in the top face of shank. This face could be modeled as an infinite plane parallel to the rake face plane. The transformed equations of the rake face are:

$$\begin{aligned} q'_{rx} &= u_4 \cos\gamma_3 - t \sin\gamma_3 \\ q'_{ry} &= v_4 \sin\gamma_3 \cos\alpha_3 + t \cos\alpha_3 \cos\gamma_3 - w_4 \sin\alpha_3 \\ q'_{rz} &= u_4 \sin\gamma_3 \sin\alpha_3 + t \cos\gamma_3 \sin\alpha_3 + w_4 \cos\alpha_3 \end{aligned} \quad (2.31)$$

where t represents the thickness of the bit. A negative value of it is used to place the plane below the top rake face, forming the bottom surface of the bit. The tool bit is placed in the seat as per the rotational angles, which are derived from conventional tool angles. The positioning of tool bit can be evaluated with the help of Figure 2.7.

From the modeling point of view, rectangular and V shaped bits are considered. The rectangular bits are defined completely using only the four planes that are already defined, but a threading bit requires an additional plane to be defined that is coincident with the YZ plane. This plane needs to be transformed on either side of the origin to obtain two vertical planes forming V shape.

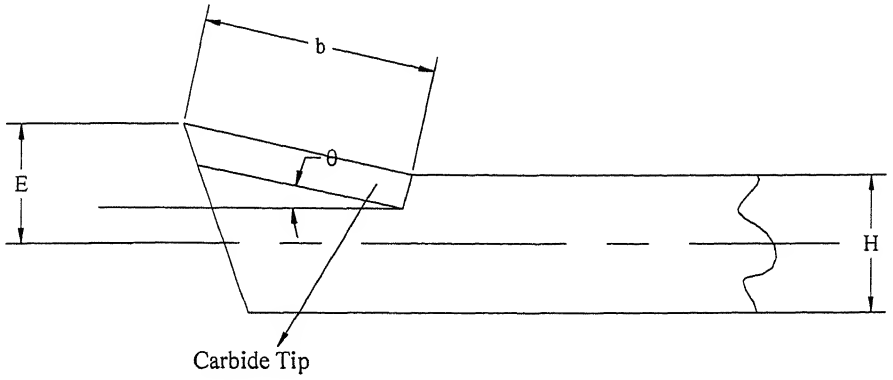

Figure 2.7: Positioning of Carbide Bit

Once the wireframe model of the carbide bit is obtained, it is oriented with the consideration that the nose tip of the tool is at higher position for positive values of the back rake angles. Negative angle would place the nose apex below the shank.

The above consideration places the bit along the Y axis in the global frame of reference. The position along the X and Z direction are determined as per the design requirements. To place the bit in the final position, apart from the translations in the X and Z directions, a rotation about the auxiliary Y-axis may also be required. Figure 2.8 shows a insert-based right hand single-point cutting tool developed on the present approach.

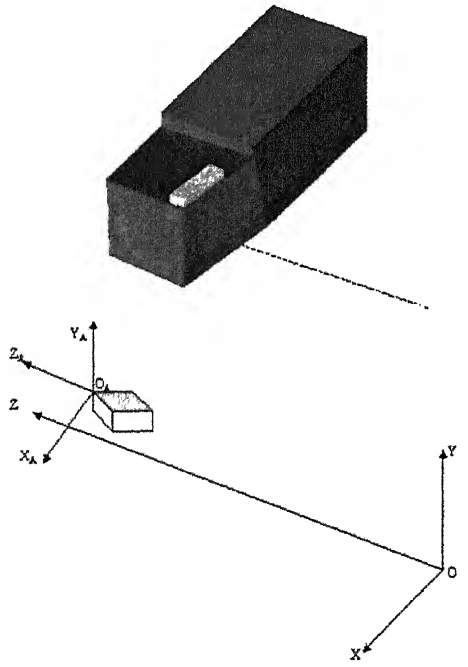

Figure 2.8: Insert-based Right Hand Single Point Cutting Tool

2.4 Grinding Methodology

The present practice of grinding a single point cutting tool is to employ the conventional technique of mounting the tool on three-swivel attachment or two-swivel worktable. The tool is then rotated about three mutually perpendicular axes, through angles defined in two-dimensional (2D) planes [87]. This practice requires experience on the part of a tool designer to find out the correct angles of rotation/swivel so as to get the appropriate geometric angles on the cutting tool. However, in most of the cases, the angles obtained on the cutting tools through this methodology are not exact and hence, corrections are needed. If the data about orientation of a cutting tool in a three-dimensional (3D) space is available then such an information can be conveniently applied for grinding of cutting tools without any need for corrections.

The surfaces of a cutting tool are grounded to impart the required stereometric features for its manufacturing and resharpening. A surface patch to be grounded has to be oriented correctly with respect to the grinding wheel. It is necessary to align the surface of the tool with the active face of the grinding wheel in order to carry out grinding in a proper manner. Let the unit vector normal to the active surface patch of the tool be $\hat{n}_1$ and to the active grinding wheel surface be $\hat{n}_2$. Then the condition of grinding is $\hat{n}_1 = \pm\hat{n}_2$.

The flanks and faces of the cutting tool can be ground using either a two-swivel tool grinder or a three-swivel universal tool grinder (Figure 2.9) [87].

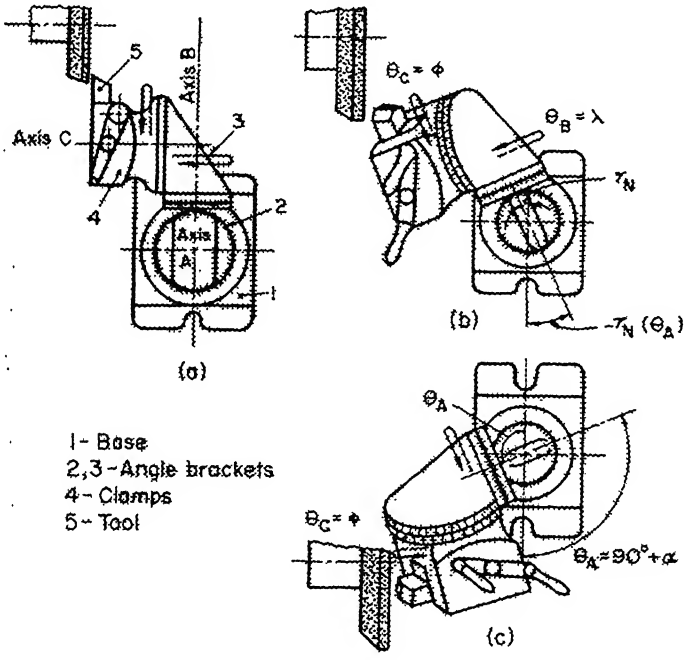

Figure 2.9: Positioning of the Tool relative to the Grinding Wheel [Refer Popov 1988]

2.4.1 Grinding of Rake Face

In the initial setup the tool is positioned such that the Z axis of the tool is perpendicular to the grinding wheel axis [87]. To satisfy the grinding principle, the tool is rotated through an angle θ''_B about Y axis followed by θ''_A about X axis (Figure 2.10a).

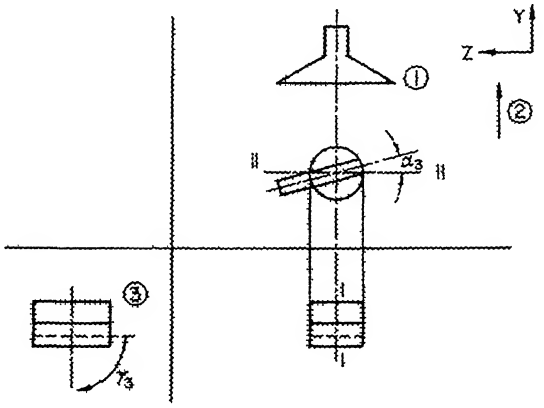

(a) Grinding of Rake Face

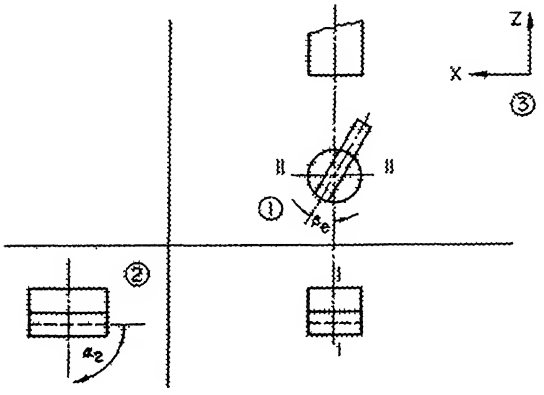

(b) Grinding of Principal Flank

Figure 2.10: Grinding of (a) Rake Face (b) Principal Flank

The grinding equation is given as $[\hat{n}_2] = \pm[\hat{n}_1][R_{y,\theta_B}][R_{x,\theta_A}]$, where normal to rake face ($\hat{n}_1$) is given by Eq.(2.6) and $\hat{n}_2 = [0 \;\; 0 \;\; 1 \;\; 1]^T$. On substituting the values we get

$$\begin{aligned} \theta''_B &= \tan^{-1}\left(\frac{\tan\gamma_3}{\sin\alpha_3}\right) \\ \theta''_A &= -\sin^{-1}\left(\frac{\cos\gamma_3}{cos\alpha_3}\right) \end{aligned} \tag{2.32}$$

2.4.2 Grinding of Principal and Auxiliary Flanks

The principal flank is described by two important tool angles, α_y and α_x. To grind principal flank a straight edge grinding wheel or the flaring cup wheel may be used [87].

Initially a cutting tool is positioned such that its Z axis is perpendicular to the axis of grinding wheel. In order to satisfy the grinding principle, the tool is successively rotated about Y axis through an angle $\theta_B$and about X axis through an angle θ_A before being fed against the grinding wheel (Figure 2.10b).

The grinding equation is given as $[\hat{n}_2] = \pm[\hat{n}_1][R_{y,\theta_B}][R_{x,\theta_A}]$ where $[R_{i,j}]$ is rotation about i-axis by an angle j and the normal to principal flank $(\hat{n}_1)$ is given by Eq.(2.9), while $\hat{n}_2 = [0 \;\; 0 \;\; 1 \;\; 1]^T$. On substituting the values we get

$$\begin{aligned} \theta_B &= -\beta_2 \\ \theta_A &= -\alpha_2 \end{aligned} \tag{2.33}$$

Similarly for grinding of the auxiliary flank, the tool is rotated by angles θ'_B & θ'_A, which are equal to $-\beta_1$ and $-\alpha_1$ respectively.

2.5 Examples

The formulae derived in the previous sections are used to perform forward and inverse mappings to validate the mapping.

ASA Angles

Starting with a set of rotational angles for the three planes of a cutting tool, the angles corresponding to the ASA nomenclature are evaluated using forward mapping and then with the inverse mapping the rotational angles are found again.

Example 1

If $\alpha_1 = 5°, \beta_1 = -15°, \alpha_2 = 5°, \beta_2 = 75°, \alpha_3 = 6°, \gamma_3 = -8°$. Using Forward Relations, ASA angles are found to be

$\gamma_y = -6°, \gamma_x = -8.045°, \alpha_y = 18.6768°, \alpha_x = 5.1754°, \alpha'_y = 5.1754°, \alpha'_x = 18.6768°$.

Performing inverse mapping for these ASA angles, the rotational angles obtained are

$\alpha_1 = 5°, \beta_1 = -15°, \alpha_2 = 5°, \beta_2 = 75°, \alpha_3 = 6°, \gamma_3 = -8°$.

Example 2

If $\alpha_1 = 5°, \beta_1 = -13.964°, \alpha_2 = 5°, \beta_2 = 74.548°, \alpha_3 = -8°, \gamma_3 = 9.905°$. Then ASA angles are

$\gamma_y = 8°, \gamma_x = 10°, \alpha_y = 18.1788°, \alpha_x = 5.1865°, \alpha'_y = 5.1515°, \alpha'_x = 19.9283°$ and using this data set and inverse relations the rotational angles obtained are

$\alpha_1 = 5°, \beta_1 = -13.964°, \alpha_2 = 5°, \beta_2 = 74.548°, \alpha_3 = -8°, \gamma_3 = 9.905°$.

ORS Angles

Here two examples, one for a carbide tipped and the other for a solid tool are taken.

Example 3

If the angles of a throw-away tip, as per the conventional nomenclature are $\lambda = -5.481°, \gamma_o = -6.633°, \alpha_o = 5°, \alpha'_o = 5°, \phi_e = -15°, \phi = 75°$, then the inverse mapping gives the rotational angles as

$\alpha_1 = 5°, \beta_1 = -15.587°, \alpha_2 = 5°, \beta_2 = 75.481°, \alpha_3 = 7°, \gamma_3 = -4.963°$.

Using these angles and the forward mapping, the ORS angles obtained are

$\lambda = -5.481°, \gamma_o = -6.633°, \alpha_o = 5°, \alpha'_o = 5°, \phi_e = -15°, \phi = 75°$.

Example 4

Let the angles of a H.S.S. tool, as per the conventional nomenclature be $\lambda = 5.149°, \gamma_o = 11.679°, \alpha_o = 5°, \alpha'_o = 5°, \phi_e = -15°, \phi = 75°$. The inverse mapping gives the rotational angles as $\alpha_1 = 5°, \beta_1 = -13.964°, \alpha_2 = 5°, \beta_2 = 74.548°, \alpha_3 = -8°, \gamma_3 = 9.905°$ and the conventional angles obtained back are $\lambda = 5.149°, \gamma_o = 11.679°, \alpha_o = 5°, \alpha'_o = 5°, \phi_e = -15°, \phi = 75°$.

NRS Angles

The two cutting tools used here to show mappings of NRS angles are the same as taken for mappings of ORS angles.

Example 5

The angles of the throw away tip, as per the conventional NRS nomenclature are $\lambda = -5.481°, \gamma_n = -6.603°, \alpha_n = 5.023°, \alpha'_n = 5.035°, \phi_e = -15°, \phi = 75°$ then the inverse mapping gives the rotational angles as

$\alpha_1 = 5°, \beta_1 = -15.587°, \alpha_2 = 5°, \beta_2 = 75.481°, \alpha_3 = 7°, \gamma_3 = -4.963°$.

Using these angles in the forward mapping, the NRS angles obtained are

$\lambda = -5.481°, \gamma_n = -6.603°, \alpha_n = 5.023°, \alpha'_n = 5.035°, \phi_e = -15°, \phi = 75°$.

Example 6

The angles of the H.S.S. tool, as per the conventional nomenclature be $\lambda = 5.149°, \gamma_n = 11.633°, \alpha_n = 5.020°, \alpha'_n = 5.103°, \phi_e = -15°, \phi = 75°$. The inverse mapping gives the rotational angles as $\alpha_1 = 5°, \beta_1 = -13.964°, \alpha_2 = 5°, \beta_2 = 74.548°, \alpha_3 = -8°, \gamma_3 = 9.905°$ and the forward mapping gives the conventional angles as $\lambda = 5.149°, \gamma_n = 11.633°, \alpha_n = 5.020°, \alpha'_n = 5.103°, \phi_e = -15°, \phi = 75°$.

Thus, we can see that, as the angles are defined in relation to the position of the edges on various surface patches of a cutting tool, the standard and mapped angles match exactly without any discrepancy.

Chapter 3

SIDE MILLING CUTTERS

Side milling process belongs to the family of milling processes that machines a plane milled surface which is generally at right angles to the cutter axis [29, 33, 48, 119]. Side milling cutters are one among the many standard milling cutters and have cutting teeth on their peripheries as well as on one or both the sides. They are profile-relieved type cutters and are made for mounting on milling machine arbor. They are normally used to mill slots, grooves and shoulders. Side mills can be made solid or insert-based. Solid side milling cutters are made by machining the required shape and number of teeth, with the specified angles grounded on the teeth. Side milling cutters may have either straight or helical teeth. They can be of right or left hand of rotation too. The various types of side mills are classified as follows [27]:

- *Side mills* are comparatively narrow cylindrical cutters with teeth on both sides as well as on the periphery. The periphery of the cutter does the actual cutting, while the face does the sizing and finishing.
- *Half-side milling cutters* are used in milling operations where only one side of the cutter is required. The length of the side teeth on half-side mills is greater than that on the standard side mill. These cutters are particularly efficient for taking heavy side milling cuts.

For the convenience in modeling, a side mill may be divided into (i) cutting teeth, and (ii) cutter body. The teeth are responsible for actual metal removal process from the stock and the body supports these cutting teeth and provides strength to the cutter to withstand dynamic cutting forces. Developing a geometric model of a side milling cutter comprises modeling of teeth and body independently. This chap-

ter presents geometric modeling of side milling cutters based on three-dimensional geometric parameters. It also discusses the methodology of modeling half-side mills.

3.1 Surface Modeling of Cutter Tooth

All the teeth of a side milling cutter are similar in geometry. In this chapter, for the purpose of modeling, only one tooth is considered and modeled in detail. Later, this cutter tooth is placed in proper position and orientation on the periphery of the cutter body as many times as the number of teeth to complete the model.

Based on the criticality of function performed by a surface patch, the surface patches forming the cutter tooth are of two types:

- critical surfaces or functional surfaces
- non-critical surfaces meant for completing the geometry

This section deals with the modeling of functional surfaces of the cutter tooth. To model a standard right-hand cutter, the tool is placed in a global right-handed Cartesian coordinate frame of reference C_1 (O-XYZ), with the axis of rotation of the cutter coinciding with Z axis and the center of the cutter lying at the origin of C_1. The geometry of the tooth is captured by modeling each functional surface individually in a local coordinate system C_2 (O_L-$X_LY_LZ_L$) (Figure 3.1). The relationship between C_1 and C_2 is established on the basis of geometric parameters of the cutter.

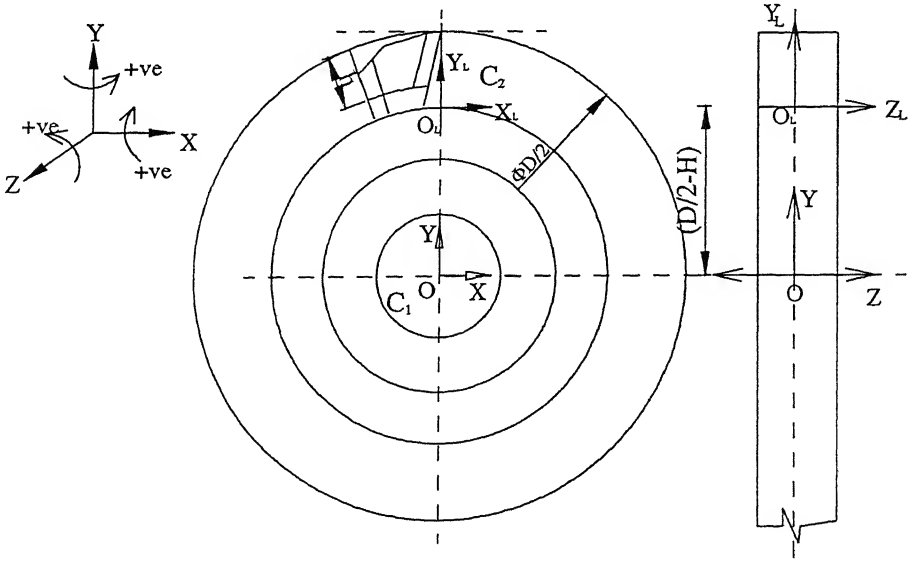

Figure 3.1: Coordinate systems of Side Milling Cutter and its Tooth

The common feature of all profile sharpened side milling cutter teeth is a narrow flat land, provided on the back (periphery) of the cutter tooth. According to the

design of their tooth, the side milling cutting tools are mainly of three types [87, 93]:

- Single-land/back or trapezoidal side milling cutter
- Double-land/back side milling cutter
- Parabolic-land/back side milling cutter

A double-land side milling cutter consists of twelve functional surfaces, as shown in Figure 3.2, while a single-land cutter consists of eleven functional surface patches. The labeling of some of these surface patches is shown in Table 3.1. A single-land cutter does not have the secondary peripheral land or minor flank (Σ_3). A parabolic-land cutter has parabolic peripheral back and can be of single-land type or double-land type [87, 93]. The geometric model of a generic double-land side milling cutter can generate all of these cutter tooth designs. Further, the geometric model of a half-side milling cutter can also be obtained from it.

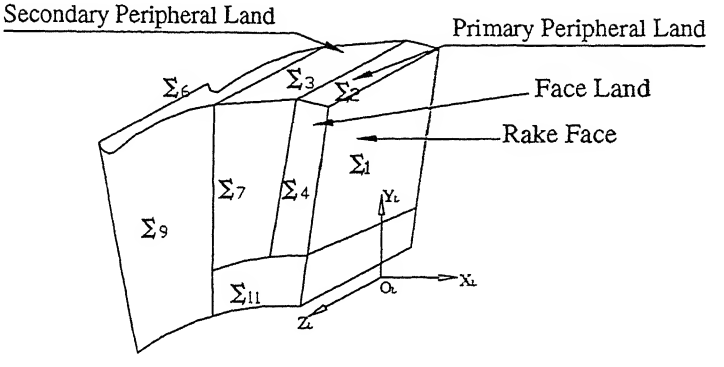

Figure 3.2: Surface Patches of Cutter Tooth

Label	Surface
Σ_1	Rake Face
Σ_2	Peripheral Land
Σ_3	Secondary Peripheral Land or Minor Flank
Σ_4, Σ_5	Face Land
Σ_6	Tertiary Peripheral Land
Σ_7, Σ_8	Secondary Face Land
Σ_9, Σ_{10}	Chip Clearance Face

Table 3.1: Surfaces of a Side Mill Tooth

The surface patches, other than the parabolic land, of the cutter tooth are defined by transforming suitable unbounded two-dimensional planes with their center initially coinciding with the origin in C_2 to their final orientation [106]. A vertex on the surface Σ_i is given by $\mathbf{p}_i(u_i, v_i) = [\, p_{ix} \;\; p_{iy} \;\; p_{iz} \;\; 1] = [\, x_i(u_i, v_i) \;\; y_i(u_i, v_i) \;\; z_i(u_i, v_i) \;\; 1]$. An

infinite XY plane is given by $\mathbf{p}(u_i, v_i) = [u_i \;\; v_i \;\; 0 \;\; 1]$, where $-\infty \leq (u_i, v_i) \leq \infty$. Similarly, YZ and ZX infinite planes can be defined by $\mathbf{p}(v_i, w_i) = [0 \;\; v_i \;\; w_i \;\; 1]$ and $\mathbf{p}(u_i, w_i) = [u_i \;\; 0 \;\; w_i \;\; 1]$ respectively $(-\infty \leq (u_i, v_i, w_i) \leq \infty)$.

3.1.1 Rake Face

Rake face (Σ_1) is formed by rotating YZ plane about Z axis by an angle γ_1 ($[\mathbf{R}_{z,\gamma_1}]$), followed by displacement along Y axis ($[\mathbf{T}_{y,d_{12}}]$) by amount $d_{12} = H$, where H is the height of the cutter tooth (Figure 3.3). Position vector of any point on the transformed surface patch Σ_1 can be found as

$$\begin{aligned} \mathbf{p}_1(v_1, w_1) &= \mathbf{p}(v_1, w_1).[\mathbf{R}_{z,\gamma_1}].[\mathbf{T}_{y,d_{12}}] \\ &= [0 \; v_1 \; w_1 \; 1] \begin{bmatrix} \cos\gamma_1 & \sin\gamma_1 & 0 & 0 \\ -\sin\gamma_1 & \cos\gamma_1 & 0 & 0 \\ 0 & 0 & 1 & 0 \\ 0 & d_{12} & 0 & 1 \end{bmatrix} \\ &= [-v_1 \sin\gamma_1 \quad (v_1 \cos\gamma_1 + H) \quad w_1 \quad 1] \end{aligned} \tag{3.1}$$

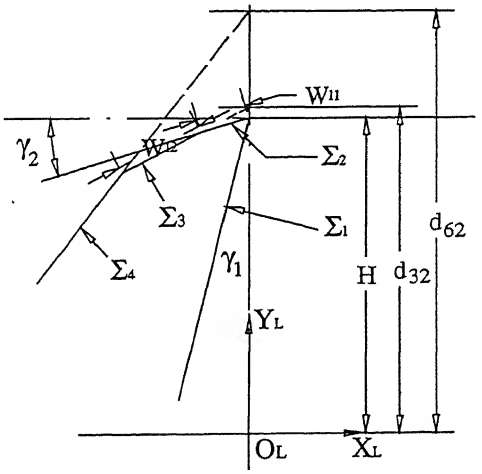

Figure 3.3: Orientation and Positioning of Cutter Tooth Surfaces in C_2

3.1.2 Peripheral Land

This is formed by rotating ZX plane about Z axis by an angle γ_2 ($[\mathbf{R}_{z,\gamma_2}]$), followed by translation along Y axis by amount $d_{22} = H$ ($[\mathbf{T}_{y,d_{22}}]$) (Figure 3.3). Therefore, peripheral land Σ_2 is mathematically defined by

$$\begin{aligned} \mathbf{p}_2(u_2, w_2) &= \mathbf{p}(u_2, w_2).[\mathbf{R}_{z,\gamma_2}].[\mathbf{T}_{y,d_{22}}] \\ &= [u_2 \cos\gamma_2 \quad (u_2 \sin\gamma_2 + H) \quad w_2 \quad 1] \end{aligned} \tag{3.2}$$

3.1.3 Secondary Peripheral Land

If a ZX plane is rotated about Z axis by an angle γ_3 ($[\mathbf{R}_{z,\gamma_3}]$) and then translated by a distance d_{32} along Y axis ($[\mathbf{T}_{y,d_{32}}]$), then it forms secondary peripheral land or minor flank (Σ_3) (Figure 3.3), where $d_{32} = (H + w_{l1}\cos\gamma_2\tan\gamma_3 - w_{l1}\sin\gamma_2)$. Terms w_{l1} and w_{l2} are for the width of primary peripheral land and secondary peripheral land along the body of cutter respectively. Mathematically Σ_3 is defined by

$$\mathbf{p}_3(u_3, w_3) = [u_3\cos\gamma_3 \quad (u_3\sin\gamma_3 + d_{32}) \quad w_3 \quad 1] \tag{3.3}$$

3.1.4 Face Lands

Face Land Σ_4 is formed by rotating XY plane successively about X axis by an angle α_4 ($[\mathbf{R}_{x,\alpha_4}]$) and about Y axis by an angle β_4 ($[\mathbf{R}_{y,\beta_4}]$), followed by translation along Z axis by amount d_{43} ($[\mathbf{T}_{z,d_{43}}]$), as shown in Figure 3.4, where d_{43} is given by

$$d_{43} = \frac{W}{2} - \frac{H\tan\alpha_4}{\cos\beta_4}$$

The term W stands for the width of the cutter. This helps to define face land Σ_4 as

$$\begin{aligned}
\mathbf{p}_4(u_4, v_4) &= \mathbf{p}(u_4, v_4).[\mathbf{R}_{x,\alpha_4}].[\mathbf{R}_{y,\beta_4}].[\mathbf{T}_{z,d_{43}}] \\
&= [\,p_{4x} \quad p_{4y} \quad p_{4z} \quad 1], \text{ where} \\
p_{4x} &= u_4\cos\beta_4 + v_4\sin\alpha_4\sin\beta_4 \\
p_{4y} &= v_4\cos\alpha_4 \\
p_{4z} &= -u_4\sin\beta_4 + v_4\sin\alpha_4\cos\beta_4 + d_{43}
\end{aligned} \tag{3.4}$$

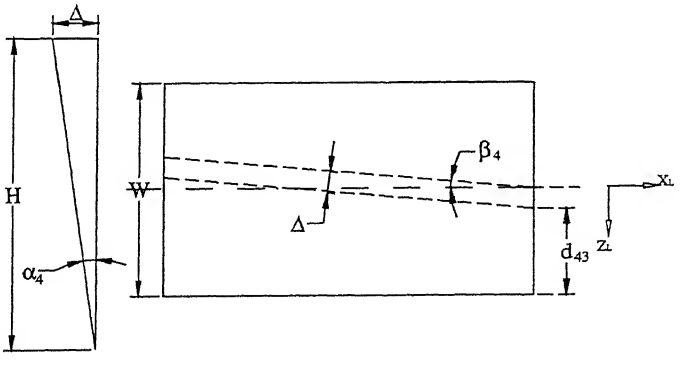

Figure 3.4: Orientation and Positioning of Face Land

Another face land Σ_5 is formed as a mirror image of Σ_4 about X_LY_L plane. It is defined by taking reflection of Σ_4 about Z_L=0 plane by

$$\mathbf{p}_5(u_5, v_5) = [\,p_{4x} \quad p_{4y} \quad -p_{4z} \quad 1] \tag{3.5}$$

3.1.5 Tertiary Peripheral Land

This is formed by rotating a ZX plane about Z axis by an angle γ_6 ($[\mathbf{R}_{z,\gamma_6}]$), followed by translation by d_{62} along Y axis ($[\mathbf{T}_{y,d_{62}}]$), as shown in Figure 3.5. Displacement d_{62} depends upon whether the value of only w_{l1} or both w_{l1} and w_{l2} are known to the tool designer and accordingly it is expressed by either of the following two relations.

$$d_{62} = \begin{cases} (\frac{D}{2} - d_1)(\cos(\frac{2\pi}{N} + \phi) + \sin(\frac{2\pi}{N} + \phi)\tan\gamma_6) - (\frac{D}{2} - H) & \text{(if } w_{l1} \text{ known) or} \\ H + (w_{l1}\cos\gamma_2 + w_{l2}\cos\gamma_3)\tan\gamma_6 - (w_{l1}\sin\gamma_2 + w_{l2}\sin\gamma_3) & (w_{l1},\ w_{l2}\text{: known}) \end{cases}$$

$$\phi = \sin^{-1}[\frac{D}{D - 2d_1}\sin|\gamma_1|] - |\gamma_1|$$

where d_1 is the radial distance between peripheral cutting edge and the edge of intersection of tertiary land and rake face, as shown in Figure 3.5. This helps to express mathematically $\mathbf{p}_6$ as

$$\mathbf{p}_6(u_6, w_6) = [u_6\cos\gamma_6 \quad (u_6\sin\gamma_6 + d_{62}) \quad w_6 \quad 1] \tag{3.6}$$

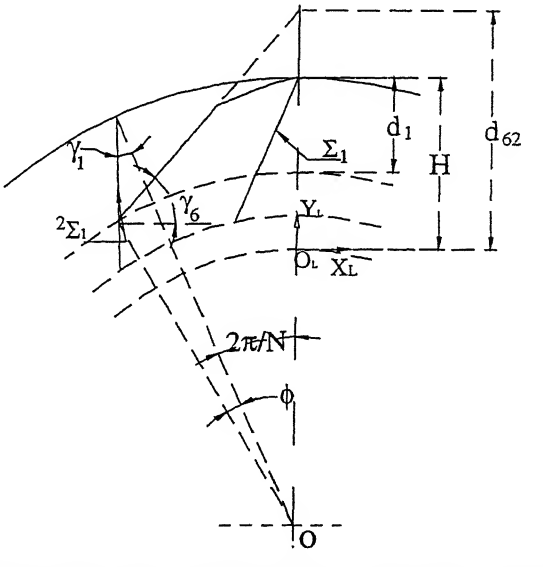

Figure 3.5: Orientation and Positioning of Tertiary Peripheral Land

3.1.6 Secondary Face Lands

Secondary face land (Σ_7) is formed by rotating XY plane about Y axis by an angle β_7 ($[\mathbf{R}_{y,\beta_7}]$), followed by translation along Z axis by a distance of d_{73} ($[\mathbf{T}_{z,d_{73}}]$), where d_{73} is given by $d_{73} = \frac{W}{2} - \delta_1 + w_f\cos\beta_4(\tan\beta_4 - \tan\beta_7)$, and δ_1 is the distance as shown in Figure 3.6. The equation for Σ_7 is given by

$$\mathbf{p}_7(u_7, v_7) = [u_7\cos\beta_7 \quad v_7 \quad (-u_7\sin\beta_7 + d_{73}) \quad 1] \tag{3.7}$$

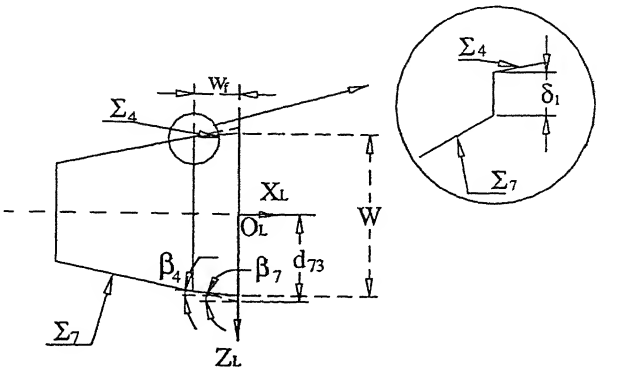

Figure 3.6: Orientation and Positioning of Secondary Face Land

Secondary face land Σ_8 is the mirror image of Σ_7 about X_LY_L plane and is given by

$$\mathbf{p}_8(u_8, v_8) = [p_{7x} \quad p_{7y} \quad -p_{7z} \quad 1] \tag{3.8}$$

3.1.7 Chip Clearance Faces

Chip clearance face Σ_9 is formed by translating an XY plane along Z axis by a distance d_{93} ($[\mathbf{T}_{z,d_{93}}]$), where d_{93} is given by $d_{93} = \frac{W_b}{2} - \delta_2$. Thus, Σ_9 is expressed as

$$\mathbf{p}_9(u_9, v_9) = [u_9 \quad v_9 \quad d_{93} \quad 1] \tag{3.9}$$

Chip Clearance Face Σ_{10} is the reflection of Σ_9 about X_LY_L plane and is defined by

$$\mathbf{p}_{10} = [u_9 \quad v_9 \quad -d_{93} \quad 1] \tag{3.10}$$

3.1.8 Surface Patches Σ_{11} and Σ_{12}

The surface Patch Σ_{11} is formed by displacing XY plane along Z axis by a distance $d_{11,3} = \frac{W_b}{2}$ ($[\mathbf{T}_{z,d_{11,3}}]$), while the surface formed by reflecting Σ_{11} about X_LY_L plane is Σ_{12}. This helps to define Σ_{11} and Σ_{12} as

$$\begin{aligned} \mathbf{p}_{11}(u_{11}, v_{11}) &= [u_{11} \quad v_{11} \quad \frac{w_b}{2} \quad 1] \\ \mathbf{p}_{12}(u_{11}, v_{11}) &= [u_{11} \quad v_{11} \quad -\frac{w_b}{2} \quad 1] \end{aligned} \tag{3.11}$$

3.1.9 Parabolic Tertiary Peripheral Land

In the case of parabolic-land side milling cutters, the tertiary peripheral land Σ_6 is parabolic in geometry, instead of flat plane. Tertiary peripheral land for parabolic-land cutters (Σ_6^p) is modeled as a biquadratic Bézier patch. Two of the four Bézier boundary curves are meant to model parabolic arcs and other two curves model straight edges along Z axis. The quadratic parabolic curves are parallel to XY plane

and lie on the planes z= $\pm(\frac{w_b}{2} - \delta_2)$ (given by the intersection of the bounding planes Σ_9 and Σ_{10} with Σ_6^p). Three points Q_0, Q_1, Q_2 require to model the quadratic Bézier curve(s) can be found with the help of equations of surfaces and the Figure 3.7.

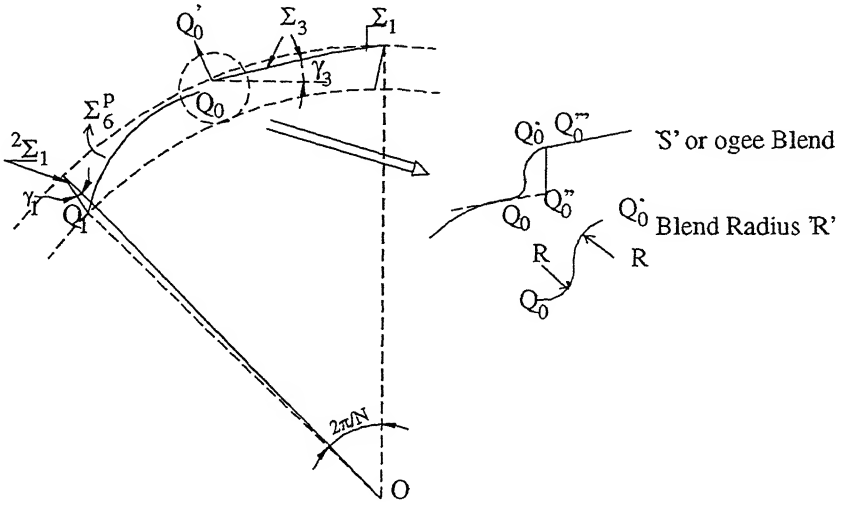

Figure 3.7: Orientation and Positioning of Parabolic Tertiary Peripheral Land

Position vectors required to define vertices Q_0 and Q_1 are

$$\mathbf{q_0} = [-(w_{l1}\cos\gamma_2 + w_{l2}\cos\gamma_3) \quad \{H - (w_{l1}\sin\gamma_2 + w_{l2}\sin\gamma_3)\} \quad Q_{0z} \quad 1] \quad (3.12)$$

$$\mathbf{q_1} = [\ \{-(\frac{D}{2} - d_1)\sin\frac{2\pi}{N} + d_1\tan\gamma_1\cos\frac{2\pi}{N}\} \quad \{(\frac{D}{2} - d_1)\cos\frac{2\pi}{N} - (\frac{D}{2} - H) + d_1\tan\gamma_1\sin\frac{2\pi}{N}\} \quad Q_{1z} \quad 1\ ] \quad (3.13)$$

The Z components of Q_0 and Q_1 are equal to $(\frac{w_b}{2} - \delta_2)$. The second quadratic curve $Q_0'Q_1'$ is the mirror image of the curve Q_0Q_1 about X_LY_L plane. These two quadratic curves along with straight edges Q_0Q_0' and Q_1Q_1' complete the patch Σ_6^p. Third vertex of the parabolic arc Q_2 is obtained by simultaneous solution of following two equations

$$l\cos\gamma_6 + m\cos\gamma_3 = n_1$$
$$l\sin\gamma_6 + m\sin\gamma_3 = n_2$$

where $l = |\mathbf{q_2} - \mathbf{q_1}|$, $m = |\mathbf{q_2} - \mathbf{q_0}|$, $n_1 = Q_{1x} - Q_{0x}$ and $n_2 = Q_{1y} - Q_{0y}$.

Two other variants of parabolic-land cutters are used in industry, namely:

(i) *Single Land Cutter*: In the case of single-land parabolic cutter, secondary peripheral land (Σ_3) is not there i.e. $w_{l2} = 0$.

(ii) *Cutter with Ogee Blend*: If the blending between surfaces Σ_3 and Σ_6^p is 'S' in shape it is known as ogee blend. It is modeled as cubic Bézier curve with control points as shown in Figure 3.7.

3.2 Mapping

The process to convert the angles given in one nomenclature to define the geometry of a side milling cutter to angles in another nomenclature is known as mapping. When the three-dimensional (3D) rotational angles, proposed in this work, to define the tool geometry of a side mill are converted to angles proposed by conventional nomenclatures (ISO, ASA, DIN, BS), based on projective geometry approach, the mapping is called forward mapping. On the contrary, when angles as defined in existing standards are mapped to equivalent 3D rotational angles, the procedure is called inverse mapping. The conventional angles are shown in Figure 3.8. The procedure of their formation is summarized in Mapping Guide Table (Table 3.2). Table 3.3 shows the sign convention adopted for the purpose of mapping.

Conventional Angles	Formed by Plane	About the Plane	Projected on the Plane
Radial Rake Angle, γ_R	Σ_1	$Y_L Z_L$	$X_L Y_L$
End Cutting Edge Angle, ϕ_e	Σ_4	$X_L Y_L$	$Y_L Z_L$
Face Relief Angle, α_F	Σ_4	$X_L Y_L$	$Z_L X_L$
First Face Clearance Angle, α_{1F}	Σ_7	$X_L Y_L$	$Z_L X_L$
Peripheral Relief Angle, α_P	Σ_2	$Z_L X_L$	$X_L Y_L$
First Peripheral Clearance Angle, α_{1P}	Σ_3	$Z_L X_L$	$X_L Y_L$
Second Peripheral Clearance Angle, α_{2P}	Σ_6	$Z_L X_L$	$X_L Y_L$

Table 3.2: Mapping Guide Table

Rotational Angles	Conventional Angles
γ_1 = -ve	γ_R = +ve
γ_1 = +ve	γ_R = -ve
α_4 = +ve	ϕ_e = +ve
α_4 = -ve	ϕ_e = -ve
β_4 = -ve	α_F = +ve
β_4 = +ve	α_F = -ve
β_7 = -ve	α_{1F} = +ve
β_7 = +ve	α_{1F} = -ve
γ_2 = +ve	α_P = +ve
γ_3 = +ve	α_{1P} = +ve
γ_6 = +ve	α_{2P} = +ve

Table 3.3: Sign Conventions for Cutting Tool Angles

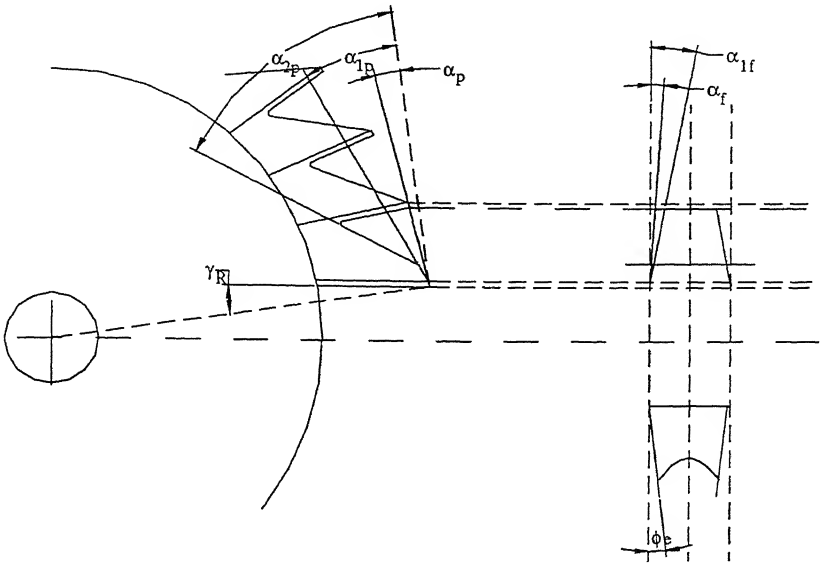

Figure 3.8: Tool Angles of a Side Mill as proposed by Conventional Nomenclatures

3.2.1 Forward Mapping

A set of relations given by existing tool standards in terms of proposed 3D rotational angles constitute forward mapping. This subsection presents such relations.

3.2.1.1 Radial Rake Angle (γ_R)

Radial rake angle (γ_R) is formed by rake face (Σ_1) with Y_LZ_L plane and viewed when projected on X_LY_L plane in C_2, as discussed in Mapping Guide Table (Table 3.2). From the definition of Σ_1, position vector of any point on it is given by Eq. (3.1) as

$$\mathbf{p}_1(v_1, w_1)=[-v_1 \sin\gamma_1 \quad (v_1 \cos\gamma_1 + H) \quad w_1 \quad 1]$$

The tangents along v and w parametric directions are

$$\begin{aligned} \mathbf{p}_{1v}(v_1, w_1) &= -\sin\gamma_1\hat{\imath} + \cos\gamma_1\hat{\jmath} \\ \mathbf{p}_{1w}(v_1, w_1) &= \hat{\hat{k}} \end{aligned}$$

The vector normal to Σ_1 ($\mathbf{n}_1$) is given by $\mathbf{p}_{1v}(v_1, w_1) \times \mathbf{p}_{1w}(v_1, w_1) = \cos\gamma_1\hat{\imath} + \sin\gamma_1\hat{\jmath}$
Projecting $\mathbf{n}_1$ on X_LY_L plane, the projected normal vector is $\mathbf{n}_{1p}$=$\cos\gamma_1\hat{\imath} + \sin\gamma_1\hat{\jmath}$.
Unit projected normal vector to Σ_1 is $\hat{\mathbf{n}}_{1p} = \frac{\mathbf{n}_{1p}}{|\mathbf{n}_{1p}|} = \cos\gamma_1 i + \sin\gamma_1 j$
To find angle formed by rake face Σ_1 with Y_LZ_L plane in X_LY_L plane (γ_R), scalar product of $\mathbf{n}_{1p}$ with $\hat{\imath}$ (unit vector normal to Y_LZ_L plane) is taken, which gives

$$\begin{aligned} \cos\gamma_R &= \cos\gamma_1 \text{ i.e.} \\ \gamma_R &= \gamma_1 \end{aligned}$$

The sign of γ_R is taken as per the Table 3.3. Ifγ_1 is negative then γ_R is positive and vice-versa. This gives

$$\gamma_R = -\gamma_1.$$

3.2.1.2 Face Cutting Edge Angle (ϕ_e) & Face Relief Angle (α_F)

These angles are formed by face land Σ_4 with X_LY_L plane and viewed on projection to Y_LZ_L and Z_LX_L planes respectively in C_2. Σ_4 is defined by Eq. (3.4) as

$\mathbf{p}_4(u_4, v_4)=(u_4 \cos\beta_4+v_4 \sin\alpha_4 \sin\beta_4)\hat{\imath}+v_4 \cos\alpha_4\hat{\jmath}+(-u_4 \sin\beta_4+v_4 \sin\alpha_4 \cos\beta_4+d_{43})\hat{k}$

The tangents along u and v directions are given by

$$\begin{aligned}\mathbf{p}_{4u}(u_4, v_4) &= \cos\beta_4\hat{\imath} - \sin\beta_4\hat{k}\\ \mathbf{p}_{4v}(u_4, v_4) &= \sin\alpha_4 \sin\beta_4\hat{\imath} + \cos\alpha_4\hat{\jmath} + \sin\alpha_4 \cos\beta_4\hat{k}\end{aligned}$$

The vector normal to Σ_4 is given by $\mathbf{n}_4 = \cos\alpha_4 \sin\beta_4\hat{\imath} - \sin\alpha_4\hat{\jmath} + \cos\alpha_4 \cos\beta_4\hat{k}$
Projection of $\mathbf{n}_4$ on Y_LZ_L (x=0) plane is $(-\sin\alpha_4\hat{\jmath} + \cos\alpha_4 \cos\beta_4\hat{k})$ and
unit projected normal vector on Y_LZ_L plane is $\mathbf{n}_{4p}=\dfrac{-\sin\alpha_4\hat{\jmath}+\cos\alpha_4 \cos\beta_4\hat{k}}{\sqrt{\sin^2\alpha_4+\cos^2\alpha_4 \cos^2\beta_4}}$.
As Σ_4 makes the face cutting edge angle ϕ_e with X_LY_L plane in the Y_LZ_L plane, therefore, scalar product of $\mathbf{n}_{4p}$ with $\hat{k}$ (unit vector along Z axis) gives (ϕ_e) as

$$\phi_e = \cos^{-1}\Big[\frac{\cos\alpha_4 \cos\beta_4}{\sqrt{\sin^2\alpha_4+\cos^2\alpha_4 \cos^2\beta_4}}\Big]$$

From Table 3.3, angles α_4 & ϕ_e have the same signs.
Projection of $\mathbf{n}_4$ on Z_LX_L (y=0) plane is $(\cos\alpha_4 \sin\beta_4\hat{\imath} + \cos\alpha_4 \cos\beta_4\hat{k})$ and
unit projected normal vector on Z_LX_L plane is $\mathbf{n}'_{4p}$=$\sin\beta_4\hat{\imath} + \cos\beta_4\hat{k}$.
Dot product of $\mathbf{n}'_{4p}$ with $\hat{k}$ (Z axis) gives the Face Relief Angle (α_F) as:

$$\alpha_F = \beta_4$$

The signs of β_4 & α_F are opposite i.e. when β_4 is negative, α_F will be positive and vice-versa. Therefore, $\alpha_F = -\beta_4$

3.2.1.3 First Face Clearance Angle (α_{1F})

This angle is formed by secondary face land (Σ_7) with X_LY_L plane and viewed on projection to Z_LX_L plane. The equation of Σ_7 is given by Eq. (3.7) as

$$\mathbf{p}_7(u_7, v_7)=u_7 \cos\beta_7\hat{\imath} + v_7\hat{\jmath} + (-u_7 \sin\beta_7 + d_{73})\hat{k}$$

The tangents along u and v directions are

$$\begin{aligned}\mathbf{p}_{7u}(u_7, v_7) &= \cos\beta_7\hat{\imath} - \sin\beta_7\hat{k}\\ \mathbf{p}_{7v}(u_7, v_7) &= \hat{\jmath}\end{aligned}$$

The vector normal to Σ_7 is $\mathbf{n}_7 = \sin\beta_7\hat{\imath} + \cos\beta_7\hat{k}$
Unit projected normal vector on Z_LX_L plane is $\hat{\mathbf{n}}_{7p}$=$\sin\beta_7\hat{\imath} + \cos\beta_7\hat{k}$
Dot product of $\hat{\mathbf{n}}_{7p}$ with $\hat{k}$ gives the First Face Clearance Angle (α_{1F}) as

$$\alpha_{1\mathbf{F}} = \beta_7$$

As the signs of β_7 & α_{1F} are opposite. Therefore,

$$\alpha_{1\mathbf{F}} = -\beta_7$$

3.2.1.4 Peripheral Relief Angle (α_P)

Peripheral relief angle (α_P) is formed by peripheral land (Σ_2) with Z_LX_L plane on X_LY_L plane. The equation of Σ_2 is given by Eq. (3.2) as

$$\mathbf{p}_2(u_2, w_2)=u_2\cos\gamma_2\hat{\imath} + (u_2\sin\gamma_2 + H)\hat{\jmath} + w_2\hat{k}$$

The tangents along u & w directions are given by

$$\mathbf{p}_{2u}(u_2, w_2) = \cos\gamma_2\hat{\imath} + \sin\gamma_2\hat{\jmath}$$
$$\mathbf{p}_{2w}(u_2, w_2) = \hat{k}$$

and the vector normal to Σ_2 is $\mathbf{n}_2 = \sin\gamma_2\hat{\imath} - \cos\gamma_2\hat{\jmath}$
The unit projected normal vector on X_LY_L plane is $\hat{\mathbf{n}}_{2p}$=$\sin\gamma_2\hat{\imath} - \cos\gamma_2\hat{\jmath}$
As Σ_2 makes peripheral relief angle with Z_LX_L plane, therefore, dot product of $\hat{\mathbf{n}}_{2p}$ with $\hat{\jmath}$ gives

$$\alpha_{\mathbf{P}} = -\gamma_2$$

From sign convention table, as γ_2 is positive, therefore, α_P will also be positive or

$$\alpha_{\mathbf{P}} = \gamma_2$$

3.2.1.5 First Peripheral Clearance Angle (α_{1P})

Angle α_{1P} is formed by secondary peripheral land (Σ_3) with Z_LX_L plane and viewed on projection to X_LY_L plane. From the equation of Σ_3 (Eq. (3.3)

$$\mathbf{p}_3(u_3, w_3)=(u_3\cos\gamma_3 - w_{l1}\cos\gamma_2)\hat{\imath} + (u_3\sin\gamma_3 - w_{l1}\sin\gamma_2 + H)\hat{\jmath} + w_3\hat{k}$$

The tangents along u and w directions and normal to Σ_3 are

$$\mathbf{p}_{3u} = \cos\gamma_3\hat{\imath} + \sin\gamma_3\hat{\jmath}$$
$$\mathbf{p}_{3w} = \hat{k}$$
$$\mathbf{n}_3 = \sin\gamma_3\hat{\imath} - \cos\gamma_3\hat{\jmath}$$

The unit projected normal vector on X_LY_L plane is $\mathbf{n}_{3p}$=$\sin\gamma_3\hat{\imath} - \cos\gamma_3\hat{\jmath}$
Dot product of $\hat{\mathbf{n}}_{3p}$ with $\hat{\jmath}$ gives First Peripheral Clearance Angle (α_{1P}) by

$$\alpha_{1\mathbf{P}} = -\gamma_3$$

From the sign convention table, if γ_3 is positive, then α_{1P} is also positive. Therefore,

$$\alpha_{1\mathbf{P}} = \gamma_3$$

3.2.1.6 Second Peripheral Clearance Angle (α_{2P})

This angle is formed by tertiary peripheral land (Σ_6) with Z_LX_L plane and viewed on projection to X_LY_L plane. The equation to Σ_6 is given by Eq. (3.6) as

$$\mathbf{p}_6(u_6, w_6)=u_6 \cos\gamma_6\hat{\imath} + (u_6 \sin\gamma_6 + d_{62})\hat{\jmath} + w_6\hat{k}$$

The tangents and normal to Σ_6 are

$$\begin{aligned} \mathbf{p}_{6u} &= \cos\gamma_6\hat{\imath} + \sin\gamma_6\hat{\jmath} \\ \mathbf{p}_{6w} &= \hat{k} \\ \mathbf{n}_6 &= \sin\gamma_6\hat{\imath} - \cos\gamma_6\hat{\jmath} \end{aligned}$$

Projection of $\mathbf{n}_6$ on X_LY_L plane gives unit projected normal vector $\hat{\mathbf{n}}_{6p}=\sin\gamma_6\hat{\imath}-\cos\gamma_6\hat{\jmath}$
Scalar product of $\hat{\mathbf{n}}_{6p}$ with $\hat{\jmath}$ gives Second Peripheral Clearance Angle (α_{2P}) by

$$\alpha_{2\mathbf{P}} = -\gamma_6$$

From the sign convention table, as γ_6 is positive, α_{2P} will also be positive, therefore

$$\alpha_{2\mathbf{P}} = \gamma_6$$

3.2.2 Inverse Mapping

From forward relations and sign conventions table, most of the 3D rotational angles in terms of conventional two-dimensional angles are obtained and shown in Table 3.4.

Rotational Angles		Conventional Angles
γ_1	=	$-\gamma_R$
β_4	=	$-\alpha_F$
β_7	=	$-\alpha_{1F}$
γ_2	=	α_P
γ_3	=	α_{1P}
γ_6	=	α_{2P}

Table 3.4: Inverse Mapping Relations for Side Mill

The equation of Face Cutting edge Angle (ϕ_e) is given by

$$\phi_e = \cos^{-1}\Big[\frac{\cos\alpha_4\cos\beta_4}{\sqrt{\sin^2\alpha_4+\cos^2\alpha_4\cos^2\beta_4}}\Big]$$

Squaring the above equation and putting $\beta_4 = -\alpha_F$ in it gives

$$\cos^2\phi_e=\frac{\cos^2\alpha_4\cos^2\alpha_F}{\sin^2\alpha_4+\cos^2\alpha_4\cos^2\alpha_F}$$

Putting $\cos^2\phi_e=k_1$ and $\cos^2\alpha_F=k_2$ in the above equation leads to

$$\alpha_4 = \tan^{-1}\left[\sqrt{\left(\frac{k_2-k_1.k_2}{k_1}\right)}\right]$$

3.3 Modeling of Cutter Body

Cutter body is the portion on which the teeth of the cutter are cut. Cutter body governs the global geometric properties of the cutter and takes care of strength and stability considerations of the cutter. The surface patches forming the cutter body model can be classified into two categories, namely:

- Surface patches forming the body of the side milling cutting tool.
- Transitional surface patches on the body of the cutting tool, responsible for completing the geometry of the side milling cutting tool.

In this section, the methodology to create geometric models of surface patches forming the body of the side milling cutting tool is described. The body of a side mill is considered to be made up of eight surface patches, labeled as $\Sigma_{50}, \ldots, \Sigma_{57}$, and shown in Figure 3.9. These surface patches are either planar or cylindrical in geometry. Cylindrical surface patches are modeled as surface of revolution.

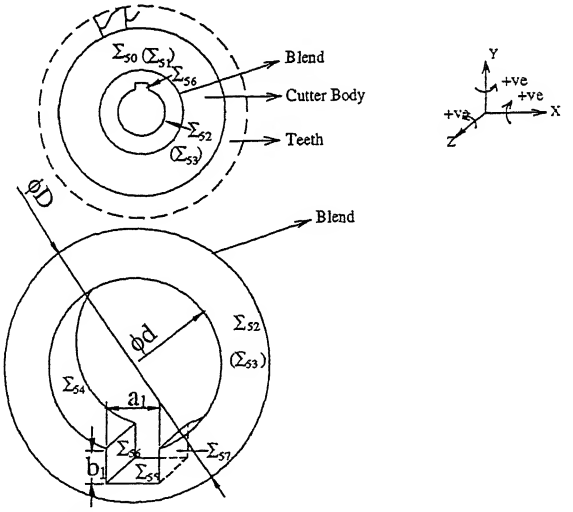

Figure 3.9: Side Milling Cutter Body Model

Surface Patch Σ_{50} is formed by displacing XY plane along Z axis by a distance $\frac{w_b}{2}$. The mathematical definition of Σ_{50} is given by

$$\mathbf{p}_{50} = [\, u_{50} \quad v_{50} \quad \frac{w_b}{2} \quad 1], \text{ with } u_{50}, v_{50} \in [-\infty, +\infty]$$

Surface Patch Σ_{51} is the reflection of Σ_{50} about XY plane and given by

$$\mathbf{p}_{51} = [\, u_{51} \quad v_{51} \quad \frac{-w_b}{2} \quad 1] \; (u_{51}, v_{51} \in [-\infty, +\infty])$$

Surface Σ_{52} is formed by displacing an XY plane along Z axis by $\frac{W}{2}$. Therefore,

$$\mathbf{p}_{52} = [\, u_{52} \quad v_{52} \quad \frac{W}{2} \quad 1], \; (u_{52}, v_{52} \in [-\infty, +\infty])$$

Surface Patch Σ_{53} is the mirror plane of Σ_{52} about XY plane.

Surface Patch Σ_{54} is the surface forming the bore/mounting hole of the cutter. It is in contact with cutter arbor. Σ_{54} is formed as a surface of revolution, when a straight edge lying in ZX plane and given by $[\frac{d}{2} \;\; 0 \;\; w_{54} \;\; 1]$ is rotated about Z axis by an angle v_{54}. Therefore,

$$\mathbf{p}_{54} = [\tfrac{d}{2}\cos v_{54} \quad \tfrac{d}{2}\sin v_{54} \quad w_{54} \quad 1], \text{ with } v_{54} \in [0, 2\pi] \text{ and } w_{54} \in [\tfrac{-W}{2}, \tfrac{W}{2}]$$

Surface Patch Σ_{55} is formed by displacing a ZX plane along Y axis by a distance $(\frac{d}{2}+b_1)$. This helps to define Σ_{55} by

$$\mathbf{p}_{55} = [\, u_{55} \quad (\tfrac{d}{2}+b_1) \quad w_{55} \quad 1], \text{ with } -a_1 \leq u_{55} \leq a_1 \;\&\; \tfrac{-W}{2} \leq w_{55} \leq \tfrac{W}{2}$$

Surface Patch Σ_{56} is $Y_L Z_L$ plane displaced along X axis by $(\frac{a_1}{2})$ and defined by

$$\mathbf{p}_{56} = [\, \tfrac{a_1}{2} \quad v_{56} \quad w_{56} \quad 1], \text{ with } \tfrac{d}{2} \leq v_{56} \leq (\tfrac{d}{2} + b_1) \;\&\; \tfrac{W}{2} \leq w_{56} \leq \tfrac{W}{2}$$

Surface Patch Σ_{57} is formed by taking reflection of Σ_{56} about YZ plane.

3.4 Modeling of Transitional Surfaces

A transitional surface σ_{ij} is formed by blending two surface patches Σ_i and Σ_j to form a smooth localized transition between neighboring surfaces at their edge of intersection. When the surfaces to be blended are identified, the edge to be blended $\mathbf{e}_{ij}$ (Appendix A.1) and the vertices forming the edge of intersection V_i and V_j along with vertices in the neighborhood V_{i-1}, V_{j-1}, V_{i+1} & V_{j+1} are evaluated (Appendix A.2). The blending surface is modeled as a bicubic Bézier patch [26]. The v parametric curves modeling the blend (P_{kj}; k=constant, $j \leftarrow 0 \ldots 3$) are considered to be circular arcs of radius 'r' and are modeled as cubic Bézier curves with control points P_{kj}, while the u parametric curves are straight edges and modeled as cubic Bézier curves with control points P_{ik}, ($i \leftarrow 0 \ldots 3$, k=constant). This is shown in Figure 3.10.

To model a circular arc as cubic Bézier curve, unit vectors $\hat{a}$ and $\hat{b}$ along V_iV_{i-1} and V_iV_{i+1} on Σ_i and Σ_j respectively, are found. The half corner angle is given by

$$\phi = \frac{1}{2}\cos^{-1}(\hat{a}.\hat{b}) \tag{3.14}$$

The distance between blend start point to the point of intersection of two surfaces Σ_i and Σ_j to be blended depends on radius of blend r and is given by

$$\delta_{ij} = \frac{r}{\tan\phi} \tag{3.15}$$

The control points of the Bézier curve modeling the circular boundary curve then are

$\mathbf{p}_{00} = \mathbf{v}_i + \delta_{ij}\hat{a}$, $\mathbf{p}_{03} = \mathbf{v}_i + \delta_{ij}\hat{b}$, $\mathbf{p}_{01} = \mathbf{p}_{00} - \Delta\hat{a}$ and $\mathbf{p}_{02} = \mathbf{p}_{03} - \Delta\hat{b}$, where

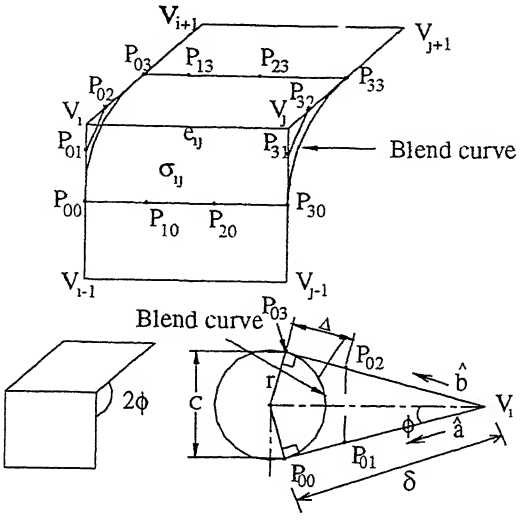

Figure 3.10: Modeling of Transitional Surfaces of a Side Mill Tooth

$$\Delta = \frac{2C}{3(1+\sin\phi)}, \text{ with } C = |\mathbf{p}_{03} - \mathbf{p}_{00}|.$$

Similarly, the control points of other boundary curve, $P_{30}P_{31}P_{32}P_{33}$ can be found.

The control points of the other parametric boundary curve geometrically forming a straight edge, are P_{00}, P_{10}, P_{20} and P_{30}, where P_{00} and P_{30} are given as above and the other two can be found out using the following relation.

$$\mathbf{p}_{10} = \frac{2\mathbf{p}_{00} + \mathbf{p}_{30}}{3} \quad \mathbf{p}_{20} = \frac{\mathbf{p}_{00} + 2\mathbf{p}_{30}}{3}$$

On the same lines control points P_{03}, P_{13}, P_{23} and P_{33} forming the other bounding straight edge can be located.

3.4.1 Transitional Surfaces on Cutter Tooth

On a side milling cutter tooth, except the surfaces intersecting to form the cutting edges, all the edges are blended. This leads to eleven blending surfaces on the tooth of a side mill. These blending surfaces are labeled as $\sigma_{i,j}$ based on the intersection of cutter tool surfaces Σ_i with Σ_j. The modeling of the geometry of these blending surfaces is discussed in this subsection.

Blending surface σ_{47} is the surface blending primary and secondary face lands, Σ_4 and Σ_7. The vertices of intersection are V_5 and V_9 and the intersecting edge is $\mathbf{e}_{47}$, given in Appendix A.1. The circular bounding curves of the blend surface are in $Z_L X_L$ plane. The two unit vectors $\hat{a}$ and $\hat{b}$ depend on vertices V_5 and V_{11} and given by $\hat{k}$ and $\frac{\mathbf{v}_{11} - \mathbf{v}_5'}{|\mathbf{v}_{11} - \mathbf{v}_5'|}$ respectively, where $V_5' = V_5|_{z=V_{5z}-\delta_1}$. This provides δ_{47}, the distance between blend start point and the point of intersection of two surfaces, as $= |\mathbf{v}_5' - \mathbf{v}_5|$.

The radius of blend r_{47} is given as per the Eq. (3.15) by $r_{47} = \delta_{47} \tan\phi$. The blend σ_{47} is shown in Figure 3.11. The different control points forming the bicubic Bézier blending surface σ_{47} are

$$\mathbf{p}_{00} = \mathbf{v}_5,\ \mathbf{p}_{03} = \mathbf{v}_5' + \delta_1.\hat{b},\ \mathbf{p}_{01} = [V_{5x}\ \ V_{5y}\ \ (V_{5z} - \Delta)\ \ 1],\ \mathbf{p}_{02} = \mathbf{p}_{03} - \Delta\hat{b},$$
$$\mathbf{p}_{30} = \mathbf{v}_9,\ \mathbf{p}_{33} = \mathbf{v}_9' + \delta_1.\hat{b},\ \ \mathbf{p}_{31} = [V_{9x}\ \ V_{9y}\ \ (V_{9z} - \Delta)\ \ 1],\ \text{and}\ \ \mathbf{p}_{32} = \mathbf{p}_{33} - \Delta\hat{b}$$

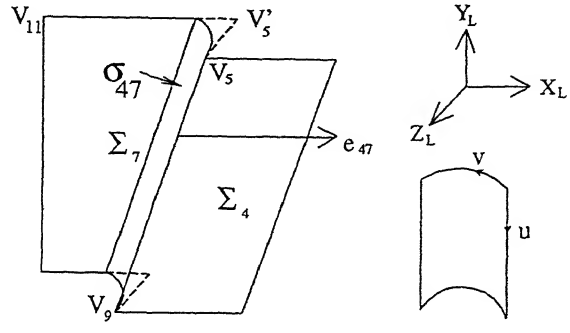

Figure 3.11: Geometric Model of Transitional Surface σ_{47}

Blending surface σ_{79} blends the surface patches Σ_7 and Σ_9 at their intersection edge $\mathbf{e}_{79}$ (Appendix A.1). The two vertices of intersection are V_{11} and V_{13}. The distance between Σ_7 and Σ_9 in Z_L direction is δ_{79} and the blending radius is r_{79}. The two unit vectors required to form the circular blending curve are $\hat{a} = \hat{k}$ and $\hat{b} = -\hat{i}$ respectively, which gives half angle ϕ as 45°, shown in Figure 3.12.

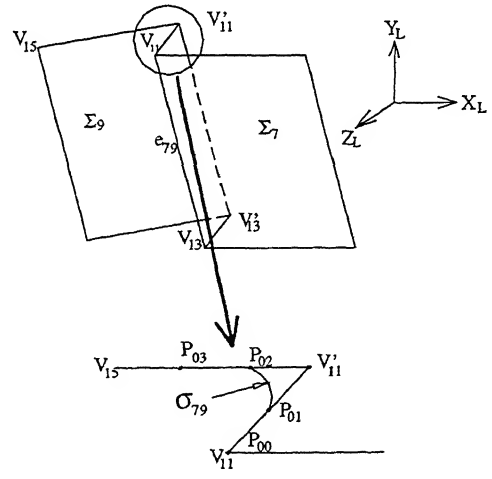

Figure 3.12: Geometric Model of Transitional Surface σ_{79}

The control points shaping the bicubic blending surface σ_{79} are

$$\mathbf{p}_{00} = \mathbf{v}_{11},\ \mathbf{p}_{03} = [(V_{11x} - \delta_2)\ \ V_{11y}\ \ (V_{11z} - \delta_2)\ \ 1],\ \mathbf{p}_{01} = [V_{11x}\ \ V_{11y}\ \ (V_{11z} - \Delta)\ \ 1],$$
$$\mathbf{p}_{02} = [(V_{11x} - \delta_2 + \Delta)\ \ V_{11y}\ \ (V_{11z} - \delta_2)\ \ 1],\ \mathbf{p}_{30} = \mathbf{v}_{13},$$
$$\mathbf{p}_{33} = [(V_{13x} - \delta_2)\ \ V_{13y}\ \ (V_{13z} - \delta_2)\ \ 1],\ \mathbf{p}_{31} = [V_{13x}\ \ V_{13y}\ \ (V_{13z} - \Delta)\ \ 1],$$
$$\mathbf{p}_{32} = [(V_{13x} - \delta_2 + \Delta)\ \ V_{13y}\ \ (V_{13z} - \delta_2)\ \ 1]$$

Blending surface $\sigma_{9,1}$ blends the edge of intersection of chip clearance face Σ_9 with rake face of second tooth ${}^2\Sigma_1$ and the vertices of intersection are V_{15} and V_{21} as shown in Figure 3.13. The two unit vectors $\hat{a}$ and $\hat{b}$ in this case are $\hat{i}$ and $\hat{k}$ respectively and the half angle is 45°. The control vertices of the blend surface responsible for forming the bicubic Bézier patch are

$$\mathbf{p}_{00} = \mathbf{v}_{15} + \delta_{9,1}\hat{a},\ \mathbf{p}_{03} = \mathbf{v}_{15} + \delta_{9,1}\hat{b},\ \mathbf{p}_{30} = \mathbf{v}_{21} + \delta_{9,1}\hat{a},\ \text{and}\ \mathbf{p}_{33} = \mathbf{v}_{21} + \delta_{9,1}\hat{b}.$$

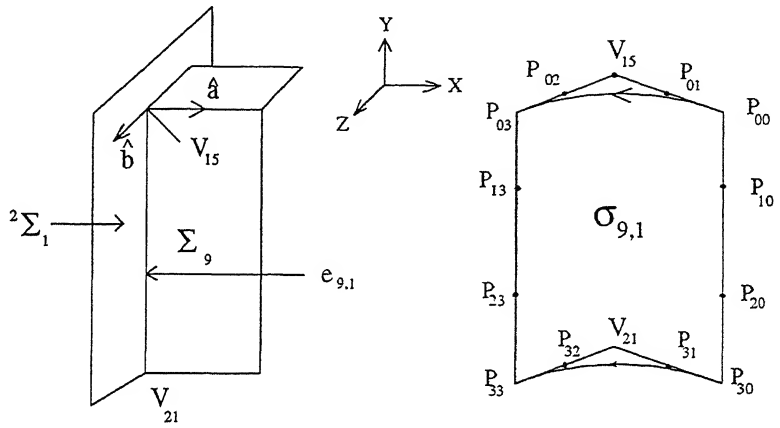

Figure 3.13: Geometric Model of Transitional Surface $\sigma_{9,1}$

The other control points on the Bézier patch $P_{01}, P_{02}, P_{31}, P_{32}, P_{10}, P_{20}, P_{13}$ and P_{23} can be located as per the approach discussed in Section 3.4.

Blending surface $\sigma_{4/7,11}$ is formed at the intersection of cutter surfaces Σ_4 and Σ_{11} at edge $\mathbf{e}_{4,11}$ and surface patches Σ_7 and Σ_{11} at edge $\mathbf{e}_{7,11}$ (Figure 3.14). The intersecting vertices are V_7 and V_{13}. The position vector of the shadow vertices V_7' i.e. projection of V_7 on Σ_{11} and V_{13}' (projection of V_{13} on Σ_{11}) are given by

$$V_7' = [\ h\tan\gamma_1 \quad (H-h) \quad \tfrac{w_b}{2} \quad 1\ ] \text{ and } V_{13}' = [\ V_{13_x} \quad V_{13_x} \quad \tfrac{w_b}{2} \quad 1\ ]$$

V_{13}' is geometrically positioned by rotating V_7' about Z axis by an angle κ, given by

$$\kappa = \tan^{-1}\left[\frac{-V_{11_x}}{\frac{d}{2} + V_{11_y}}\right]$$

Unit vectors responsible for creating circular blends at the vertex V_7' are (Figure 3.14)

$$\hat{a} = \sin\gamma_1.\hat{i} - \cos\gamma_1.\hat{j},\ \text{and}\ \hat{b} = \hat{k}$$

and at vertex V_{13}' are

$$\hat{a}' = \sin\kappa.\hat{i} - \cos\kappa.\hat{j},\ \text{and}\ \hat{b}' = \hat{k}$$

The distance between blend start point and the point of intersection of surfaces Σ_4 (Σ_7) and Σ_{11} is equal to radius of blend $r_{4/7,11}$ as per the Eq. 3.15. The corner vertices forming the bicubic blending surface are

$\mathbf{p}_{00} = \mathbf{v}'_7 + r_{4,7,11}\hat{a}$, $\mathbf{p}_{03} = \mathbf{v}'_7 + r_{4,7,11}\hat{b}$, $\mathbf{p}_{30} = \mathbf{v}'_{13} + r'_{4,7,11}\hat{a}'$ and $\mathbf{p}_{33} = \mathbf{v}'_{13} + r'_{4,7,11}\hat{b}'$

The other control points falling on the circular blend curve $P_{01}, P_{02}, P_{31}, P_{32}$ are evaluated as per Section 3.4. The u parametric curves forming the boundaries of the blend surface patch are circular curves and are defined on the similar lines. The two unit vectors in the tangent directions are

$$\mathbf{a}'' = -\cos\kappa_1.\hat{i} - \sin\kappa_1.\hat{j} \quad \text{and} \quad \mathbf{b}'' = \cos\kappa_2.\hat{i} + \sin\kappa_2.\hat{j}$$

where $\kappa_1 = \left[\sin^{-1}\left(\frac{D}{D-2h}\sin|\gamma_1|\right) - |\gamma_1|\right]$ and $\kappa_2 = \frac{4\pi}{3n}$

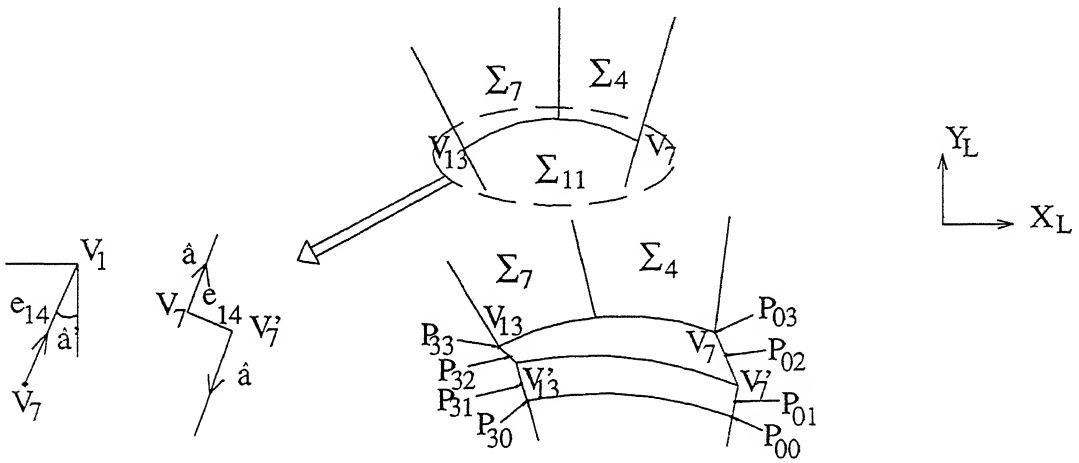

Figure 3.14: Geometric Model of Transitional Surface $\sigma_{4/7,11}$

Blending surface $\sigma_{9,0}$ is the surface between cutter tooth surface Σ_9 and cutter body. The vertices of intersection are V_{13} and V_{19}. The projection of V_{13} on the Σ_{11} and Σ_9 planes are the two shadow vertices labeled as V'_{13} and V''_{13} respectively (Figure 3.15). The unit vectors $\hat{a}$ and $\hat{b}$ at the end points of the circular arcs are given as $\hat{k}$ and $-\sin\kappa_2.\hat{a} + \cos\kappa_2.\hat{j}$ respectively, where $\kappa_2 = \frac{4\pi}{3n}$. The corner vertices of bounding circular arc $P_{00}P_{03}$ are $\mathbf{p}_{00} = \mathbf{v}_{19}$ and $\mathbf{p}_{03} = \mathbf{v}''_{13}$, where $V''_{13} = V_{13_z}|_{z=(\frac{w_b}{2}-\delta_2)}$.

The second bounding circular arc of the blend $P_{30}P_{33}$ is positioned by rotating first boundary curve $P_{00}P_{03}$ by an angle ψ about global Z axis, where $\psi = \frac{2\pi}{3n} + \eta_1$, with $\eta_1 = \left[\sin^{-1}\left(\frac{D}{D-2H}\sin|\gamma_1|\right) - |\gamma_1|\right]$.

The other parametric boundary curves $P_{00}P_{30}$ and $P_{03}P_{33}$ of $\sigma_{9,0}$ are also modeled as Bézier circular arcs, instead of straight edges and the unit vectors required to shape the two u-parameter based boundary curves are respectively given by

$$\hat{a}' = -\cos\frac{4\pi}{3n}.\hat{i} - \sin\frac{4\pi}{3n}.\hat{j}, \quad \hat{b}' = \cos(\psi + \frac{4\pi}{3n}).\hat{i} + \sin(\psi + \frac{4\pi}{3n}).\hat{j},$$
$$\hat{a}'' = -\cos\frac{4\pi}{3n}.\hat{i} - \sin\frac{4\pi}{3n}.\hat{j}, \quad \hat{b}'' = \cos(\psi' + \frac{4\pi}{3n}).\hat{i} + \sin(\psi' + \frac{4\pi}{3n}).\hat{j}$$

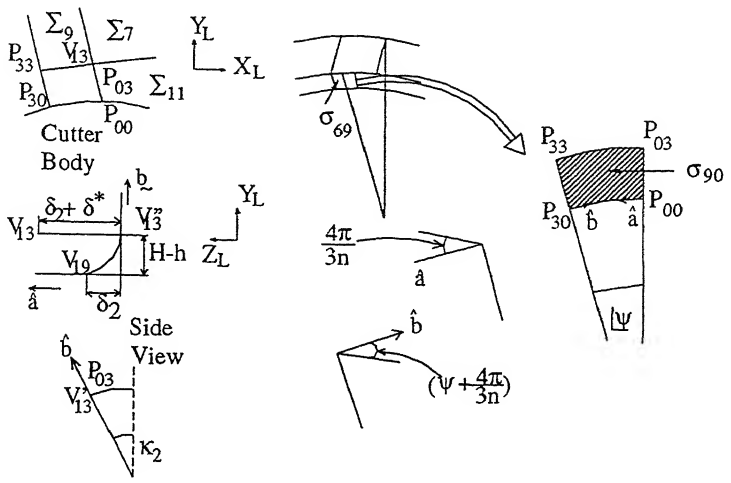

Figure 3.15: Geometric Model of Transitional Surface $\sigma_{9,0}$

where $\psi' = \frac{2\pi}{3n} + \kappa_1$. The other control vertices (P_{ij}) required to complete the bicubic Bézier blending surface patch $\sigma_{9,0}$ can be located as discussed in Section 3.4.

Blending surface $\sigma_{6,1}$ blends the edge $e_{6,1}$ formed due the intersection of surfaces Σ_6 and ${}^2\Sigma_1$. The end vertices of intersecting edge are V_{15} and V_{16}. Unit vector along the surface ${}^2\Sigma_1$ at V_{15} is $\hat{a} = -\sin\gamma_1\hat{i} + \cos\gamma_1\hat{j}$ and along the surface Σ_6 at V_{15} is $\hat{b} = \cos\gamma_6\hat{i} + \sin\gamma_6\hat{j}$. Radius of blend $r_{6,1}$ is designers' prerogative and value of the distance from blend start point to V_{15}, $\delta_{6,1}$, depends upon it. The corner vertices of the bicubic blend surface patch $\sigma_{6,1}$ are:

$$\mathbf{p}_{00} = \mathbf{v}_{15} + \delta_{6,1}.\hat{a},\ \mathbf{p}_{03} = \mathbf{v}_{15} + \delta_{6,1}.\hat{b},\ \mathbf{p}_{30} = \mathbf{v}_{16} + \delta_{6,1}.\hat{a},\ \mathbf{p}_{33} = \mathbf{v}_{16} + \delta_{6,1}.\hat{b}$$

Other control points of the surface patch can be found as per the approach described in Section 3.4 earlier.

Blending surface σ_{58} is the mirror image of blend surface σ_{47} about X_LY_L plane and can be defined accordingly. Similarly, blend $\sigma_{8,10}$ is formed by taking reflection of σ_{79} about X_LY_L plane, $\sigma_{10,1}$ is the mirror image of blending surface $\sigma_{9,1}$ aboutX_LY_L plane, while transitional surfaces $\sigma_{5/8,12}$ and $\sigma_{10,0}$ are the mirror images of the blending surfaces $\sigma_{4/7,11}$ and $\sigma_{9,0}$ respectively about X_LY_L plane.

3.4.2 Transitional Surfaces on Cutter Body

Two types of transitional surfaces, blends and chamfers, are created on the body of a side mill. A generic side mill consists of two blending and eight chamfer body transitional surfaces. These transitional surfaces are modeled with the help of Figure 3.9.

The body blending surface $\sigma_{\mathbf{b02}}$ blends planes Σ_{50} and Σ_{52} and is modeled as a surface of revolution by rotating a circular arc in YZ plane about Z axis. The circular

arc is modeled as a cubic Bézier curve and is defined with the help of control points P_{00}, P_{01}, P_{02} and P_{03}. The radius of blend is the designers' prerogative and labeled here as r_{02}. The base point of intersection (V_{b02}) shown in Figure 3.16 is given by $\mathbf{V}_{b02} = [0 \ \frac{D_1}{2} \ \frac{w_b}{2} \ 1]$. The unit vectors at V_{b02}, tangent to the curve along the directions $V_{b02}P_{00}$ and $V_{b02}P_{03}$ are $\hat{a} = \hat{k}$ and $\hat{b} = \hat{j}$ respectively, which gives the distance between blend start point and the intersection point δ_{b02} as equal to r_{b02} as half point angle is $\phi = \frac{1}{2}\cos^{-1}(\hat{a}\hat{b}) = 45°$.

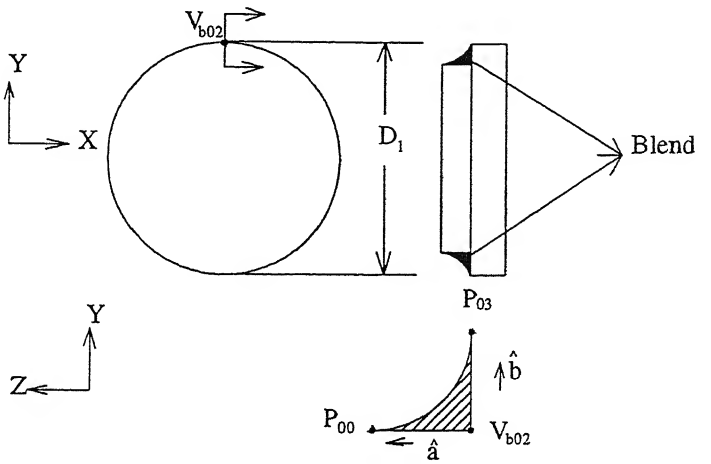

Figure 3.16: Transitional Surfaces of Cutter Body

The control points of the Bézier curve are

$$\mathbf{p}_{00} = \mathbf{v}_{b02} + \delta_{b02}.\hat{a}, \ \mathbf{p}_{03} = \mathbf{v}_{b02} + \delta_{b02}.\hat{b}, \ \mathbf{p}_{01} = \mathbf{p}_{00} - \Delta.\hat{a}, \ \mathbf{p}_{02} = \mathbf{p}_{00} - \Delta.\hat{b}$$

where $C = |\mathbf{p}_{03} - \mathbf{p}_{00}|$ and $\Delta = \frac{2C}{3\sin\phi}$. The resultant Bézier curve is expressed by $\mathbf{r}(u)$ [80, 125]. Blending surface σ_{b02}, thus, satisfies the relation

$$\mathbf{p}_{b02}(u,v) = [\ -r_y(u)\sin v \quad r_y(u)\cos v \quad r_z(u) \quad 1\ ]$$

where $0 \leq u \leq 1 \ \ \& \ \ 0 \leq v \leq 2\pi$.

The blending surface $\sigma_{\mathbf{b13}}$ blends surfaces Σ_{51} and Σ_{53} and is the reflection of blending surface $\sigma_{\mathbf{b02}}$ about XY plane.

The transitional surface $\sigma_{\mathbf{b24}}$ is considered to be a 45° chamfer at the edge of intersection of surfaces Σ_{52} and Σ_{54}. The chamfer is modeled as a rotational sweep surface. An edge passing through the point of intersection $V_{b24} = [0 \ \frac{d}{2} \ \frac{W}{2} \ 1]$ on YZ plane and inclined at 45° is swept by an angle v ($\phi \leq v \leq 2\pi - \phi$) ($\phi = \sin^{-1}\left[\frac{a_1}{d}\right]$) to form σ_{b24}. The edge can be defined in terms of parameter u ($0 \leq u \leq 1$).

The chamfered surface $\sigma_{\mathbf{b25}}$ is modeled as a linear sweep surface. It smoothens the edge formed due to intersection of cutter surfaces Σ_{52} and Σ_{55}. A straight u parametric

edge ($u \in [0,1]$) passing through the point of intersection $V_{b25} = [0 \ (\frac{d}{2}+H) \ \frac{W}{2} \ 1]$ on YZ plane is swept along X axis varying parameter v ($-\frac{a_1}{2} \leq v \leq \frac{a_1}{2}$) to form σ_{b25}.

The chamfer $\sigma_{\mathbf{b26}}$ at the edge of intersection of cutter body surfaces Σ_{52} and Σ_{56} is a linear sweep surface. This is modeled by sweeping along Y axis a straight edge passing through the point of intersection $V_{b26} = [\frac{a_1}{2} \ (\frac{d}{2}(1-\cos\phi) \ \frac{W}{2} \ 1]$ in terms of a parameter varying from 0 to H.

The other five chamfer surfaces on the cutter tool body are labeled as $\sigma_{\mathbf{b27}}$, $\sigma_{\mathbf{b34}}$, $\sigma_{\mathbf{b35}}$, $\sigma_{\mathbf{b36}}$ and $\sigma_{\mathbf{b37}}$. Chamfer σ_{b27} is formed by taking reflection of σ_{b26} about YZ plane while σ_{b34}, σ_{b35}, σ_{b36} and σ_{b37} are formed by reflecting σ_{b24}, σ_{b25}, σ_{b26} and σ_{b27} about XY plane respectively.

3.5 Grinding of Side Mill

Side milling cutter is a profile sharpened cutter. In the case of side mills, peripheral lands and clearance surfaces are grounded for sharpening and resharpening. Peripheral lands and clearance surfaces are practically grounded by either cup face of a grinding wheel or periphery of a straight wheel, as shown in Figure 3.17 [13, 87].

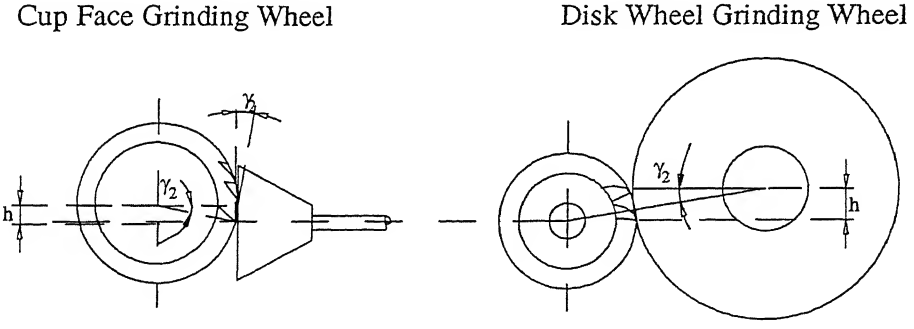

Figure 3.17: Grinding of Peripheral Lands of Side Milling Cutters

For the purpose of grinding, the tool can be attached to three-axis universal swivel table or any three-dimensional (3D) attachment can be used instead. The setting of the grinding wheel for the purpose of grinding of primary peripheral land shown in Figure 3.17, in terms of cutter parameters and 3D rotational angles are

- For cup face grinding wheel, $h = \frac{D}{2}\sin\gamma_2$
- For disk wheel grinding wheel, $h = \frac{D_w}{2}\sin\gamma_2$

where D is diameter of cutter and D_w is the diameter of the grinding wheel. The tool is rotated about Z axis by an angle θ_c, where

$$\theta_c = \sin^{-1}\left[\frac{2h}{D}\right] = \gamma_2$$

3.6 Half Side Mill

Half side mill is a type of side milling cutter, which contains teeth on one side and the periphery of the cutter only. As it machines jobs from one side only, therefore, the teeth cut on its periphery are helical to withstand cutting forces. In the case of a helical cutter, the rake face is at a helix angle λ with respect to axis of the cutter. The geometric model of a half side mill is similar to that of helical side mill. In the case of helical side mills, and hence half side mills, among all the surfaces forming the tool only the rake face Σ_1 is modeled in a different style then the approach discussed in Section 3.1. Rest of the surface patches of the tooth, as well as, the body of the helical (or half) side mill will be modeled similarly. The modeling of rake face for the helical/half side mill is discussed in this section.

Rake Face of Helical/Half Side Mill

To model rake face (Σ_1^H) as shown in Figure 3.18, a YZ plane is given two successive rotations, firstly about Z axis by an angle γ_1 [$\mathbf{R}_{z,\gamma_1}$] and then about Y axis by an angle β_1 [$\mathbf{R}_{y,\beta_1}$]. This is followed by translation along Y axis by an amount d_{12} [$\mathbf{T}_{y,d_{12}}$]. This gives the mathematical definition of Σ_1^H as

$$\begin{aligned} p_{1x}^H &= -v_1 \sin\gamma_1 \cos\beta_1 + w_1 \sin\beta_1 \\ p_{1y}^H &= v_1 \cos\gamma_1 + d_{12} \\ p_{1z}^H &= v_1 \sin\gamma_1 \sin\beta_1 + w_1 \cos\beta_1 \end{aligned} \tag{3.16}$$

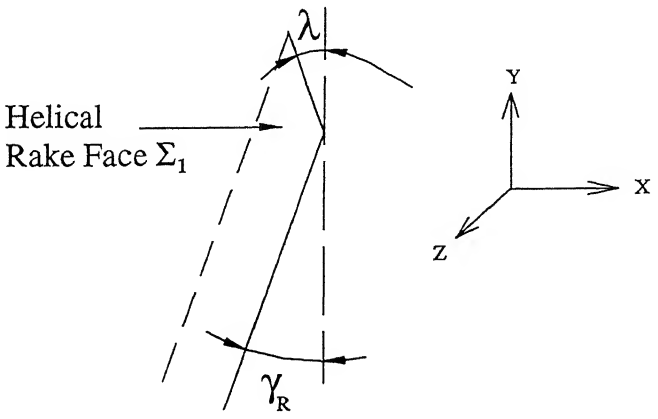

Figure 3.18: Rake Face of Helical/Half Side Mill

Due to change in the representation of rake face, the definitions of edges, formed due to intersection of a surface with Σ_1^H and that of vertices formed due to intersection of edges, will change accordingly.

3.7 Example

This section presents an illustration of a side milling cutter, modeled in terms of 3D geometric parameters to validate the model. The cutter rendered here is referred in $ANSI/ASME\ B94.19-1985$ standards [83] and labeled as $8'' \times \frac{5}{8}'' \times 1\frac{1}{4}''$ side mill. The input parameters of the side mill are presented in Table 3.5. The resultant side mill is rendered in OpenGL environment [127, 132, 120, 121] and shown in Figure 3.19.

Input Data for Side Mill	
Dimensional Parameters	Value (in inches)
Cutter Diameter(D)	8
Width of Cutter(W)	$\frac{5}{8}$
Diameter of Bore(d)	$1\frac{1}{4}$
Number of Teeth(N)	24
Other Dimensional Parameters	Value (in mm)
Height of Tooth(H)	30
Height of Face Land(h)	23
Width of Primary Peripheral Land(w_{l1})	2
Width of Secondary Peripheral Land(w_{l2})	15
Rotational Angles	Value (in degrees)
γ_1	-5.0
γ_2	3.0
γ_3	25.0
α_4	0.5
β_4	-3.0
γ_6	60.0
β_7	-7.0

Table 3.5: Geometric Parameters of Side Milling Cutting Tool

3.8 Case Study

This chapter develops comprehensive 3D models of side milling cutters on the basis of 3D geometric parameters. A 3D model offers a lot of utility and can be subjected to a variety of down-stream applications. This section presents one such application of

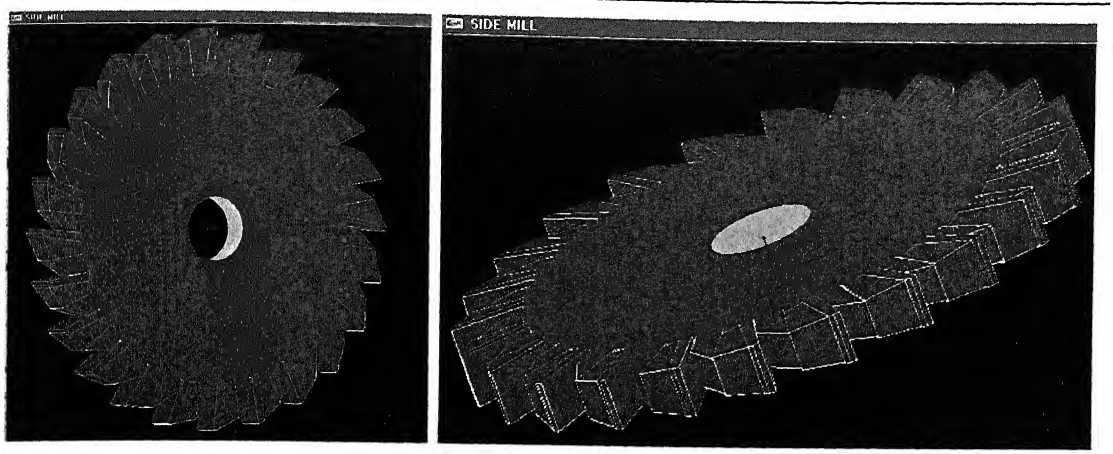

Figure 3.19: Rendering of Side Milling Cutting Tools

geometric assessment of tool wear. The case study confirms the immense advantages offered by the availability of geometric models of cutting tools. The case study identifies the geometric wear of the cutting tools. The case presented here helps further in establishing the approach adopted in this work for geometric modeling of cutting tools. For the purpose of identification of tool wear, a parabolic-land side mill is reverse engineered with the help of a tactile scanner, FARO arm (a robotic arm with six degrees of freedom), available at CAD Project Laboratory (CAD-P Lab), I.I.T. Kanpur. A surface-based model of the same tool is created with the proposed approach. This surface model is imported to a surface modeling environment, Surfacer, and compared with the point-cloud obtained earlier for surface-cloud difference. The results are shown with the help of Figure 3.20. Similar exercise can be carried out for a worn or used tool to geometrically locate the worn areas on a cutting tool.

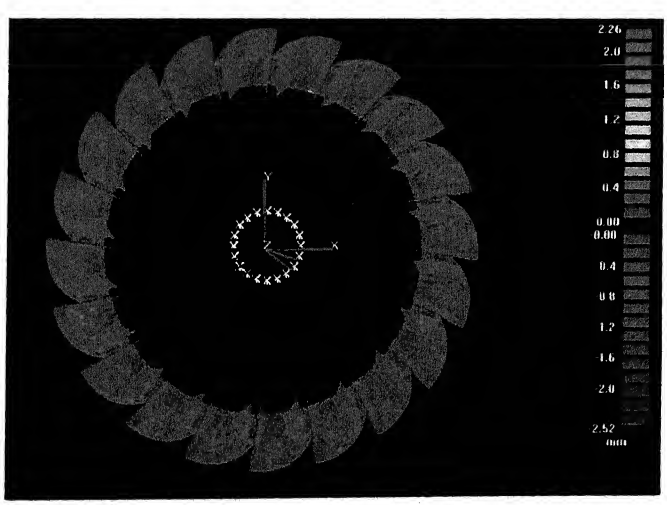

Figure 3.20: Surface-Point clouds comparison of the Side Mill cutter surfaces

Chapter 4

FLUTED CUTTERS

A wide range of cutters used in practice are fluted in geometry. Fluted cutters are cylindrical cutters with cutting teeth on the circumferential surface and cylindrical grooves along the axis of the cutter for chip removal [29, 30, 33, 61]. These cutters are modeled by sweeping the sectional profile of the cutter along the perpendicular direction. The sweep can be linear or helical depending upon the type of the cutter. Among various types of standard cutters, the cutters that are classified and modeled as fluted cutters, in this work, are

- Slab milling cutters
- End mills
- Drills

The geometric modeling of these three types of fluted cutters are discussed in the subsequent sections.

4.1 Slab Milling Cutters

The other common names of slab milling cutters are plain milling cutters and peripheral milling cutters. These are meant for peripheral cutting and used to produce flat surfaces parallel to the axis of the spindle. They are made in a wide variety of diameters and widths. The cutting edges can be straight or helical and are on the circumference only. There are no cutting edges on the sides of the cutters. Based on the type of cutting edges, the slab mills are of two types: (a) Straight tooth cutters and (b) Helical mills. The plain milling cutters with width less than 20 mm generally

have straight teeth (parallel to the axis of the cutter) and others have the helical teeth [27, 33]. The helix angle varies in the range 15° to 25° for the cutters with width less than 50 mm and in the range 25° to 45° for others. The former types of cutters are used for light duty applications, while the latter are used for heavy applications. Slab mills with higher helix angles are called plain helical mills.

4.1.1 Surface Modeling of Slab Milling Cutter Tooth

The cutting tooth of a slab mill is made up of five surface patches, labeled Σ_1 to Σ_5 and is shown in Figure 4.1. The cutter tooth is geometrically modeled as a sweep surface. To construct a mathematical model of the sweep surface, a generic composite curve perpendicular to the axis and a sweeping rule is required [66]. When the sweeping is linear (parallel sweeping) i.e. cross-section curve in XY plane is extruded along Z axis, the straight tooth cutter is formed and when the sweep operation is a combination of rotational and parallel sweep about the Z axis, then the resultant surface is helicoidal surface and the cutter is helical slab mill.

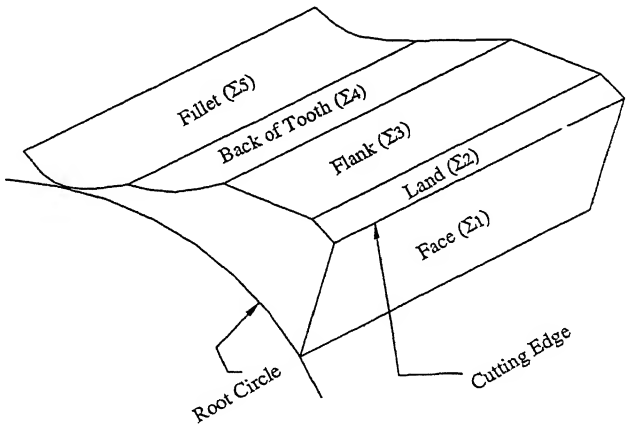

Figure 4.1: Surface Patches of Slab Mill Tooth

The composite curve in XY plane ($V_1V_2V_3V_4V_5V_6V_7$), which is to be swept to generate the cutter tooth surfaces is shown in Figure 4.2. The composite curve is a tip-to-tip curve on outer circle diameter of the cutter, with the rake face of N^{th} tooth (V_0V_1) excluded and that of $(N+1)^{th}$ tooth (V_6V_7) included for modeling convenience.

The composite sectional curve is made up of five segments, with V_1V_2, V_2V_3, V_3V_4 and V_6V_7 as straight lines and segment $V_4V_5V_6$ as a circular arc of fillet radius R, with center of the arc at vertex c_1. The homogenous coordinates of these vertices may be evaluated with the help of Figure 4.2 in terms of dimensional parameters and three-dimensional (3D) rotational angles. Let D, D_R and l_1 be cutter diameter, root circle

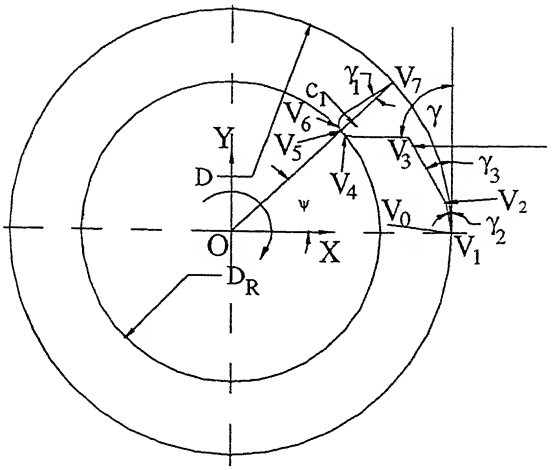

Figure 4.2: Sectional Curve of a Slab Mill Tooth

diameter and length of land respectively and α_i, β_i, γ_i be the angles of rotation of surface patch i about X, Y, Z axis respectively. Then the position vectors of vertices V_1 to V_7 are satisfied by the following relations.

$$\mathbf{v}_1 = [\ \frac{D}{2} \quad 0 \quad 0 \quad 1\ ]$$

$$\mathbf{v}_2 = [\ (\frac{D}{2} - l_1 \sin\gamma_2) \quad l_1 \cos\gamma_2 \quad 0 \quad 1\ ]$$

$$\mathbf{v}_3 = [\ \left\{\frac{\tan\gamma_3 \tan\gamma_4(V_{4y} - V_{2y}) + \tan\gamma_3 V_{4x} - \tan\gamma_4 V_{2x}}{(\tan\gamma_3 - \tan\gamma_4)}\right\} \left\{\frac{(V_{2x} - V_{4x}) + \tan\gamma_3 V_{2y} - \tan\gamma_4 V_{4y}}{(\tan\gamma_3 - \tan\gamma_4)}\right\} \quad 0 \quad 1\ ]$$

$$\mathbf{v}_4 = [\ \{c_{1x} - R\sin(90° - \gamma_4)\} \quad \{c_{1y} - R\cos(90° - \gamma_4)\} \quad 0 \quad 1\ ]$$

$$\mathbf{c}_1 = [\ (\frac{D_R}{2} + R)\cos\psi' \quad (\frac{D_R}{2} + R)\sin\psi' \quad 0 \quad 1\ ]$$

$$\mathbf{v}_5 = [\ \frac{D_R}{2}\cos\psi' \quad \frac{D_R}{2}\sin\psi' \quad 0 \quad 1\ ]$$

$$\mathbf{v}_6 = [\ \left\{\frac{D}{2}\cos\psi - \left(\frac{\frac{D-D_R}{2} - R}{\cos\gamma_1} + R\tan\gamma_1\right)\cos(\psi + \gamma_1)\right\} \left\{\frac{D}{2}\sin\psi - \left(\frac{\frac{D-D_R}{2} - R}{\cos\gamma_1} + R\tan\gamma_1\right)\sin(\psi + \gamma_1)\right\} \quad 0 \quad 1\ ]$$

$$\mathbf{v}_7 = [\ \frac{D}{2}\cos\psi \quad \frac{D}{2}\sin\psi \quad 0 \quad 1\ ]$$

$$\mathbf{v}_0 = [\ \left\{\frac{D}{2} - \left(\frac{\frac{D-D_R}{2} - R}{\cos\gamma_1} + R\tan\gamma_1\right)\cos\gamma_1\right\} \left\{-\left(\frac{\frac{D-D_R}{2} - R}{\cos\gamma_1} + R\tan\gamma_1\right)\sin\gamma_1\right\} \quad 0 \quad 1\ ]$$

where $\psi' = \psi - \delta$ and δ is obtained by solving the equation

$$\sin\delta + \cos\delta \tan\gamma_1 = \frac{\frac{R}{\cos\gamma_1} + \frac{D}{2}\tan\gamma_1}{\frac{D_R}{2} + R}$$

4.1.1.1 Parametric Representation of Section Curve

The cross-section curve V_0V_7 is composed of five parametric curve segments defined in terms of parameter s, namely $\mathbf{p}_1(s)$, $\mathbf{p}_2(s)$, $\mathbf{p}_3(s)$, $\mathbf{p}_4(s)$ and $\mathbf{p}_5(s)$. The curve segments $\mathbf{p}_1(s)$, $\mathbf{p}_2(s)$, $\mathbf{p}_3(s)$ and $\mathbf{p}_5(s)$ are straight lines between vertices V_1V_2, V_2V_3, V_3V_4 and V_6V_7 respectively, while the curve $\mathbf{p}_4(s)$ is a circular arc of radius R. The equation of $\mathbf{p}_1(s)$ is evolved as

$$\mathbf{p}_1(s) = V_1 + s(V_2 - V_1), \text{ where } 0 \leq s \leq 1$$

Substituting the relations for the x, y and z coordinates of V_1 and V_2, the homogenous equation of $\mathbf{p}_1(s)$ becomes

$$\mathbf{p}_1(s) = [(\frac{D}{2} - sl_1\sin\gamma_2) \quad sl_1\cos\gamma_2 \quad 0 \quad 1] \text{ where } 0 \leq s \leq 1$$

Similarly, other curve segments are given parametrically by

$$\begin{aligned}
\mathbf{p}_2(s) &= [\{\frac{D}{2} - l_1\sin\gamma_2 + s(V_{3x} - \frac{D}{2} + l_1\sin\gamma_2)\} \quad \{l_1\cos\gamma_2 + s(V_{3y} - l_1\cos\gamma_2)\} \quad 0 \quad 1] \\
\mathbf{p}_3(s) &= [\{V_{3x} + s(V_{4x} - V_{3x})\} \quad \{V_{3y} + s(V_{4y} - V_{3y})\} \quad 0 \quad 1] \\
\mathbf{p}_4(s) &= [(c_{1x} + R\cos\kappa) \quad (c_{1y} - R\sin\kappa) \quad 0 \quad 1] \\
\mathbf{p}_5(s) &= [\{V_{6x} + s(V_{7x} - V_{6x})\} \quad \{V_{6y} + s(V_{7y} - V_{6y})\} \quad 0 \quad 1]
\end{aligned}$$

where $\kappa_1 \leq \kappa \leq \kappa_2$, with $\kappa_1 = \pi - \gamma_4$ and $\kappa_2 = 2\pi - \phi_1$.
The angle ϕ_1 is given by $\phi_1 = \tan^{-1}\left[\frac{V_{6y} - c_{1y}}{V_{6x} - c_{1x}}\right]$ and satisfies the value of κ_2 by the following conditional relation

$$\begin{aligned}
&\text{If } \phi_1 \geq 0, \text{ then } \phi_1 = \phi_1 \\
&\qquad\qquad \text{else } \phi_1 = \pi + \phi_1
\end{aligned}$$

4.1.1.2 Cutter Tooth Surface Patches

There are seven surface patches of the plain milling cutter tooth as shown in Figure 4.1 and they are labeled as shown in Table 4.1. The left and right end surface patches are the surfaces on the ends of the cutter, perpendicular to the axis of the cutter rotation. The left end surface patch rotates in clockwise direction about cutter axis during cutting while the right end surface patch moves counterclockwise during cutting.

Label	Surface
Σ_1	Face
Σ_2	Land
Σ_3	Flank
Σ_4	Back of Tooth
Σ_5	Fillet
Σ_6	Left Hand Surface Patch
Σ_7	Right Hand Surface Patch

Table 4.1: Surfaces of a Slab Mill Tooth

Let ϕ be the parameter for rotation angle about cutter (Z) axis and t the parameter for linear sweep along Z axis and $[\mathbf{T}_s]$ the transformation matrix meant for sweeping operation. Then, the surface patches Σ_1 to Σ_5 are sweep surfaces and are parametrically formed as $\mathbf{p}(s,\phi)$or $\mathbf{p}(s,t) = \mathbf{p}(s).[\mathbf{T}_s]$, where s is the parameter of section curve in XY profile and $\mathbf{p}(s)$ is the equation for curve segments defined earlier. For straight tooth cutter, $[\mathbf{T}_s]$ leads to parallel sweep and is given by the matrix

$$\begin{bmatrix} 1 & 0 & 0 & 0 \\ 0 & 1 & 0 & 0 \\ 0 & 0 & 1 & 0 \\ 0 & 0 & \frac{L}{2}(1-2t) & 0 \end{bmatrix}, \text{ with } 0 \leq t \leq 1$$

At $t = 0$, left end surface patch of the cutter is obtained while at $t = 1$, one gets right end surface patch of the cutter.

For helical milling cutter tooth, Σ_1 to Σ_5 are helicoidal surfaces and $[\mathbf{T}_s]$ is responsible for combined rotational and linear sweep. If ϕ is the rotational angle and P the pitch of the helical cutter, then the transformation matrix $[\mathbf{T}_s]$ is given by

$$\begin{bmatrix} \cos\phi & \sin\phi & 0 & 0 \\ -\sin\phi & \cos\phi & 0 & 0 \\ 0 & 0 & 1 & 0 \\ 0 & 0 & -\frac{P\phi}{2\pi} & 0 \end{bmatrix} \left(-\frac{\pi L}{P} \leq \phi \leq \frac{\pi L}{P}\right)$$

At ϕ_{min}, left end surface patch of the cutter is obtained while right end surface patch of the cutter is obtained at ϕ_{max}.

The sweeping operation $\mathbf{p}_1(s).[\mathbf{T}_s]$ models Land (Σ_2). Flank (Σ_3) is obtained by using relation $\mathbf{p}_2(s).[\mathbf{T}_s]$, while back of the tooth (Σ_4) and fillet (Σ_5) are modeled by performing the operations $\mathbf{p}_3(s).[\mathbf{T}_s]$ and $\mathbf{p}_4(s).[\mathbf{T}_s]$ respectively. The operation $\mathbf{p}_5(s).[\mathbf{T}_s]$ leads to face of the 2^{nd} tooth, represented as ${}^2\Sigma_1$.

The two end surfaces i.e. Σ_6 and Σ_7 are modeled as bounded circular (XY) planes, positioned at z $= +L/2$ and z$= -L/2$ respectively. They may be defined by

$$\mathbf{p}_6(u_6, v_6) = [u_6 \cos v_6 \quad u_6 \sin v_6 \quad \frac{L}{2} \quad 1] \text{ and}$$
$$\mathbf{p}_7(u_7, v_7) = [u_7 \cos v_7 \quad u_7 \sin v_7 \quad -\frac{L}{2} \quad 1]$$

where $\frac{D_R}{2} \leq u_6, u_7 \leq \frac{D}{2}$, $-\frac{\pi L}{P} \leq v_6 \leq (\frac{-\pi L}{P} + \psi)$ and $\frac{\pi L}{P} \leq v_7 \leq (\frac{\pi L}{P} + \psi)$.

4.1.2 Modeling of Slab Mill Cutter Body

The body of the slab mill is composed of six surface patches. These surface patches are (i) Left body end surface (Σ_{50}), (ii) Right body end surface (Σ_{51}), (iii) Bore surface (Σ_{52}) and (iv) Three surface patches (Σ_{53}, Σ_{54} and Σ_{55}) making the keyway. These surface patches are shown in Figure 4.3.

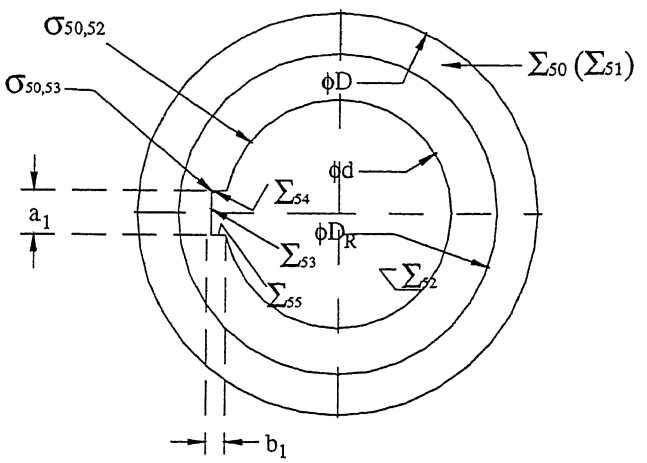

Figure 4.3: Modeling of Slab Mill Cutter Body

Surface patches Σ_{50} and Σ_{51} are part of the same transformed infinite XY planes, as are Σ_6 and Σ_7. Surface patch Σ_{50} is formed by positioning XY plane (z=0 plane) at z=$L/2$. It can be defined with $\mathbf{p}_{50}(u_{50}, v_{50}) = [u_{50} \quad v_{50} \quad \frac{L}{2} \quad 1]$ for $-\infty \leq u_{50}, v_{50} \leq 1$. It can be also defined as a bounded circular surface given by
$\mathbf{p}_{50}(u_{50}, v_{50}) = [u_{50} \cos v_{50} \quad u_{50} \sin v_{50} \quad \frac{L}{2} \quad 1]$ for $\frac{d}{2} \leq u_{50} \leq \frac{D_R}{2}$ and $0 \leq v_{50} \leq 2\pi$

Similarly, Σ_{51} is geometrically modeled by positioning an XY plane at z=$-\frac{L}{2}$. This gives the vector equation of the plane Σ_{51} as $\mathbf{p}_{51}(u_{51}, v_{51}) = [u_{51} \quad v_{51} \quad -\frac{L}{2} \quad 1]$ $(-\infty \leq u_{50}, v_{50} \leq 1)$. The bounded circular surface patch Σ_{51} may be defined by $\mathbf{p}_{51}(u_{51}, v_{51}) = [u_{51} \cos v_{51} \quad u_{51} \sin v_{51} \quad -\frac{L}{2} \quad 1]$, where $\frac{d}{2} \leq u_{51} \leq \frac{D_R}{2}$ and $0 \leq v_{51} \leq 2\pi$

The bore of the plain milling cutter is of diameter d and length L, varying from z=$\frac{-L}{2}$ to $\frac{+L}{2}$, as shown in Figure 4.3. The cylindrical bore surface may be mathematically expressed as below
$\mathbf{p}_{52}(v_{52}, w_{52}) = [\frac{d}{2} \cos v_{52} \quad \frac{d}{2} \sin v_{51} \quad \frac{L}{2}(1 - 2w_{52}) \quad 1]$ $(0 \leq v_{52} \leq 2\pi$ and $0 \leq w_{52} \leq 1)$

The keyway plane Σ_{53} is formed by translating a YZ plane to x=$-(\frac{d}{2}+b_1)$ and is expressed as

$\mathbf{p}_{53}(v_{53}, w_{53}) = [-(\frac{d}{2}+b_1) \quad \frac{a_1}{2}(1-2v_{53}) \quad \frac{L}{2}(1-2w_{53}) \quad 1]$, where $0 \leq v_{53}, w_{53} \leq 1$ and a_1 and b_1 are the width and depth of keyway respectively.

The side walls of keyway Σ_{54} and Σ_{55} and formed by positioning ZX planes at y=$\frac{a_1}{2}$ and y=-$\frac{a_1}{2}$ respectively. Thus, the equations of Σ_{54} and Σ_{55} are:

$\mathbf{p}_{54}(u_{54}, w_{54}) = [-(\frac{d}{2}+u_{54}b_1) \quad \frac{a_1}{2} \quad \frac{L}{2}(1-2w_{54}) \quad 1]$ and

$\mathbf{p}_{55}(u_{55}, w_{55}) = [-(\frac{d}{2}+u_{55}b_1) \quad -\frac{a_1}{2} \quad \frac{L}{2}(1-2w_{55}) \quad 1]$ where $0 \leq u_{54}, w_{54}, u_{55}, w_{55} \leq 1$

4.1.3 Modeling of Blending Surfaces

All the edges of intersection on a slab mill tooth are sharp and act as cutting edges. Hence, there are no blending surfaces on the cutter tooth. On the other hand, the cutter body has eight transitional surfaces in the form of chamfers. Let the chamfer between surface patch Σ_i and Σ_j be $\sigma_{i,j}$, where $i = 50, 51$ and $j = 52, 53, 54, 55$. Some of these chamfers are shown in Figure 4.3.

Chamfer $\sigma_{50,52}$ is modeled as a surface of revolution. A straight edge of unit width on ZX plane and inclined at 45° (for 45° chamfer) is revolved to form $\sigma_{50.52}$. The coordinates of the ends of this straight edge are $(\frac{d}{2}, 0, (\frac{L}{2} - 0.707))$ and $((\frac{d}{2} + 0.707), 0, \frac{L}{2})$. This gives the parametric equation of the straight line in terms of parameter u as $[(\frac{d}{2} + 0.707u) \quad 0 \quad \{\frac{L}{2} - 0.707(1-u)\} \quad 1]$, with $0 \leq u \leq 1$. When this edge is rotated about the cutter (Z) axis, it forms $\sigma_{50,52}$, expressed by

$$\mathbf{p}_{50,52}(u, \theta) = [(\frac{d}{2} + 0.707u)\cos\theta \quad (\frac{d}{2} + 0.707u)\sin\theta \quad \{\frac{L}{2} - 0.707(1-u)\} \quad 1] \quad (4.1)$$

where $0 \leq u \leq 1$ and $0 \leq \theta \leq 2\pi$ with the chamfer $\sigma_{50,52}$ non existent when $\theta \in (\pi - \sin^{-1}(\frac{a_1}{d}), \pi + \sin^{-1}(\frac{a_1}{d}))$ due to formation of keyway.

Chamfered surface $\sigma_{50,53}$ is formed by linearly sweeping a straight edge of unit width on ZX plane, inclined at 45° along Y axis. The coordinates of the two ends of this straight edge are $(-(\frac{d}{2} + b_1), 0, (\frac{L}{2} - 0.707))$ and $(-(\frac{d}{2} + b_1 + 0.707), 0, \frac{L}{2})$. The parametric equation of the straight line joining these ends in terms of parameter u becomes $[-(\frac{d}{2} + b_1 + 0.707u) \quad 0 \quad \{\frac{L}{2} - 0.707(1-u)\} \quad 1]$ $(0 \leq u \leq 1)$. This edge is swept along Y axis in terms of parameter v and forms $\sigma_{50,53}$, where

$$\mathbf{p}_{50,53}(u, v) = [-(\frac{d}{2} + b_1 + 0.707u) \quad -\{\frac{a_1}{2}(1-2v)\} \quad \{\frac{L}{2} - 0.707(1-u)\} \quad 1]$$

where $0 \leq u, v \leq 1$

Chamfer $\sigma_{50,54}$ is also a sweep surface formed by linearly sweeping a straight edge of unit width on YZ plane, inclined at 45° along X axis. The parametric equation of

the straight edge is $[0 \quad (\frac{a_1}{2} + 0.707v) \quad \{\frac{L}{2} - 0.707(1-v)\} \quad 1]$, for $0 \leq v \leq 1$. Thus the swept surface is

$$\mathbf{p}_{50.54}(u,v) = [-(\tfrac{d}{2} + b_1 u) \quad (\tfrac{a_1}{2} + 0.707v) \quad \{\tfrac{L}{2} - 0.707(1-v)\} \quad 1] \ (0 \leq u, v \leq 1)$$

Chamfer $\sigma_{50,55}$ is also a sweep surface and can be given by reflecting the surface $\sigma_{50,54}$ about ZX plane. Thus, $\sigma_{50,55}$ can be mathematically defined by

$$\mathbf{p}_{50,55}(u,v) = [-(\tfrac{d}{2} + b_1 u) \quad -(\tfrac{a_1}{2} + 0.707v) \quad \{\tfrac{L}{2} - 0.707(1-v)\} \quad 1] \ (0 \leq u, v \leq 1)$$

Chamfers $\sigma_{51,52}$, $\sigma_{51,53}$, $\sigma_{51,54}$, $\sigma_{51,55}$ are the reflections of the chamfers $\sigma_{50,52}$, $\sigma_{50,53}$, $\sigma_{50,54}$, $\sigma_{50,55}$ respectively about XY plane and thus can be represented accordingly.

4.1.4 Mapping

The process of conversion of tool angles given in one nomenclature to other is known as mapping. When the three-dimensional (3D) rotational angles developed in this work defining the geometry of slab milling cutters are converted to conventional two-dimensional (2D) nomenclatures based on projective geometry approach, the mapping is called forward mapping. On the contrary, when angles defined as per existing standards are mapped to proposed rotational angles, the process is called inverse mapping. The development of conventional angles formed by projecting the surface patches of the plain milling cutter tooth are shown in Mapping Guide Table (Table 4.2). The sign convention adopted for the purpose of mapping is given in Table 4.3. The convention angles are shown in Figure 4.4 [29, 33].

Conventional Angles	Formed by Plane	About the Plane	Projected on Plane
γ_R	Σ_1	ZX	XY
α_P	Σ_2	YZ	XY
α_{1P}	Σ_3	YZ	XY
α_{2P}	Σ_4	YZ	XY
Gash Angle δ	$\Sigma_1 \& {}^N\Sigma_4$ †	–	XY
Lip Angle θ_{la}	$\Sigma_1 \& \Sigma_2$	–	XY

Table 4.2: Mapping Guide Table for Slab Mill
(†: Between Σ_1 of 1^{st} tooth and Σ_4 of N^{th} (last) tooth ${}^N\Sigma_4$)

4.1.4.1 Forward Mapping

This subsubsection presents forward mapping so as to evaluate the values of conventional 2D angles if 3D rotational angles are known.

Rotational Angles	Conventional Angles
γ_1 = -ve	Radial Rake Angle, γ_R = +ve
γ_2 = +ve	Relief Angle, α_P = +ve
γ_3 = +ve	1^{st} Clearance Angle, α_{1P} = +ve
γ_4 = +ve	2^{nd} Clearance Angle, α_{2P} = +ve

Table 4.3: Sign Convention for the Angles of Slab Mill

Radial Rake Angle (γ_R)

This angle γ_R is formed by face Σ_1 with ZX plane and viewed on projection to XY plane. The mathematical equation of Σ_1 is given with the help of Section 4.1.1.2 as

$$\begin{aligned}\mathbf{p}_1(s,\phi) &= \mathbf{p}_5(s)_{|\psi=0}.[\mathbf{T}_s] \\ &= [\{\frac{D}{2} - A\cos\gamma_1(1-s)\} \quad \{-A\sin\gamma_1(1-s)\} \quad 0 \quad 1].[\mathbf{T}_s] \end{aligned} \tag{4.2}$$

where $A = \left\{\frac{\frac{D-D_R}{2}-R}{\cos\gamma_1} + R\tan\gamma_1\right\}$ and $[\mathbf{T}_s]$ is the sweeping matrix defined earlier in the same section. The tangents to Σ_1, $(\frac{\partial \mathbf{p}_1}{\partial s}, \frac{\partial \mathbf{p}_1}{\partial \phi})$, are

$$\begin{aligned}\mathbf{p}_{1s}(s,\phi) &= [A(\cos\gamma_1\cos\phi - \sin\gamma_1\sin\phi)]\hat{\imath} + [A(\cos\gamma_1\sin\phi + \sin\gamma_1\cos\phi)]\hat{\jmath} \\ \mathbf{p}_{1\phi}(s,\phi) &= [-\{\frac{D}{2} - A\cos\gamma_1(1-s)\}\sin\phi - \{-A\sin\gamma_1(1-s)\}\cos\phi]\hat{\imath} + \\ &\quad [\{\frac{D}{2} - A\cos\gamma_1(1-s)\}\cos\phi - \{-A\sin\gamma_1(1-s)\}\sin\phi]\hat{\jmath} - \frac{P}{2\pi}\hat{k} \end{aligned} \tag{4.3}$$

The cross product of these tangents gives normal to the surface Σ_1 by

$$\mathbf{n}_1 = -\frac{PA}{2\pi}\sin(\gamma_1+\phi)\hat{\imath} + \frac{PA}{2\pi}\cos(\gamma_1+\phi)\hat{\jmath} + \frac{DA}{2}\{\cos(\gamma_1+\phi) + \sin(\gamma_1+\phi) + A^2(s-1)\}\hat{k}$$

To find radial rake angle γ_R, $\mathbf{n}_1$ is projected on XY plane. The unit projected normal vector is $\hat{n}_{1p} = -\sin(\gamma_1+\phi)\hat{\imath} + \cos(\gamma_1+\phi)\hat{\jmath}$.

Radial rake angle is found by taking dot product of $\hat{n}_{1p}$ with unit vector $\hat{\jmath}$ as it is similar to the angle between normal to Σ_1 projected on XY plane and Y axis. Therefore, $\cos\gamma_R = cos(\gamma_1+\phi)$

For straight tooth cutter, angle ϕ is zero, while for helical cutters, γ_R is evaluated on z=0 plane, where again value of angle ϕ is equal to zero°. This gives

$$\gamma_R = \gamma_1 \tag{4.4}$$

Note from sign convention table (Table 4.3), angles γ_1, γ_R are having opposite signs.

Relief Angle (α_P)

Relief Angle (α_P) is formed by Land Σ_2 about YZ plane when projected on XY plane. The land Σ_2 is geometrically expressed by

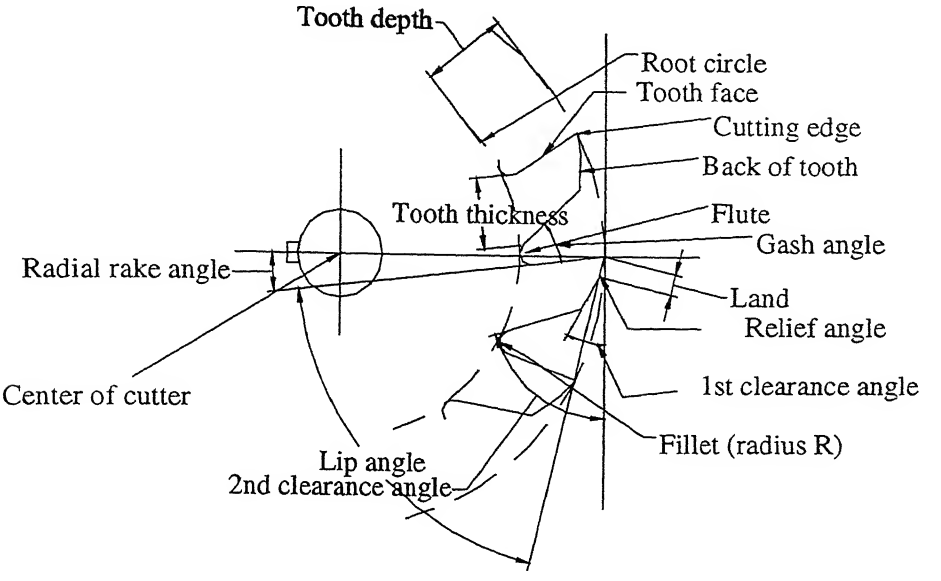

Figure 4.4: Conventional Tool Geometry for Slab Mill

$$\begin{aligned}\mathbf{p}_2(s,\phi) &= \mathbf{p}_1(s).[\mathbf{T}_s] \\ &= [\{(\frac{D}{2}-sl_1\sin\gamma_2)\cos\phi - sl_1\cos\gamma_2\sin\phi\} \\ &\quad \{(\frac{D}{2}-sl_1\sin\gamma_2)\sin\phi + sl_1\cos\gamma_2\cos\phi\} \quad (-\frac{P\phi}{2\pi}) \quad 1]\end{aligned} \tag{4.5}$$

The tangents $(\frac{\partial \mathbf{p}_2}{\partial s}, \frac{\partial \mathbf{p}_2}{\partial \phi})$ to Σ_2 are

$$\begin{aligned}\mathbf{p}_{2s}(s,\phi) &= (-l_1\sin\gamma_2\cos\phi - l_1\cos\gamma_2\sin\phi))\hat{\imath} + (-l_1\sin\gamma_2\sin\phi + l_1\cos\gamma_2\cos\phi)]\hat{\jmath} \\ \mathbf{p}_{2\phi}(s,\phi) &= [-(\frac{D}{2}-sl_1\sin\gamma_2)\sin\phi - sl_1\cos\gamma_2\cos\phi]\hat{\imath} + \\ &\quad [(\frac{D}{2}-sl_1\sin\gamma_2)\cos\phi - sl_1\cos\gamma_2\sin\phi]\hat{\jmath} - \frac{P}{2\pi}\hat{k}\end{aligned} \tag{4.6}$$

and the normal is

$$\mathbf{n}_2 = \frac{Pl_1}{2\pi}\cos(\gamma_2+\phi)\hat{\imath} - \frac{Pl_1}{2\pi}\sin(\gamma_2+\phi)\hat{\jmath} + \frac{Dl_1}{2}\sin\gamma_2 + sl_1{}^2)\}\hat{k}$$

This normal when projected on XY plane gives following unit projected normal vector

$$\hat{n}_{2p} = (\sin\gamma_2\sin\phi - \cos\gamma_2\cos\phi)\hat{\imath} - (\sin\gamma_2\cos\phi + \cos\gamma_2\sin\phi)\hat{\jmath}$$

Relief angle α_P is given as an angle between Σ_2 and YZ plane, which is equivalent to the angle between unit projected normal $\hat{n}_{2p}$ and unit normal to YZ plane i.e. unit vector $\hat{\imath}$. Scalar product of $\hat{n}_{2p}$ and $\hat{\imath}$ gives α_P, which is expressed by the relation $\cos\alpha_P = -\cos(\gamma_2+\phi)$. As ϕ is zero for straight tooth cutters and for helical cutters at z=0 plane, it makes the equation

$$\alpha_P = \gamma_2 \tag{4.7}$$

From sign convention table, α_P is positive when angle γ_2 is positive.

First Clearance Angle (α_{1P})

Surface patch Σ_3 (Flank) of cutter tooth forms first clearance angle (α_{1P}) with YZ plane on projection to the XY plane. As per the methodology of formation of cutter tooth surfaces discussed earlier, the flank can be expressed by

$$\begin{aligned}\mathbf{p}_3(s,\phi) &= \mathbf{p}_2(s).[\mathbf{T}_s] \\ &= [\{(A+sC)\cos\phi-(B+sD)\sin\phi\} \ \{(A+sC)\sin\phi+(B+sD)\cos\phi\} \ -\frac{P\phi}{2\pi} \ 1]\end{aligned} \tag{4.8}$$

where $A = (\frac{D}{2} - l_1 \sin\gamma_2)$, $B = l_1 \cos\gamma_2$, $C = V_{3x} - A$ and $D = V_{3y} - B$
The tangents to Σ_3 are

$$\mathbf{p}_{3s}(s,\phi) = (C\cos\phi - D\sin\phi)\hat{\imath} + (C\sin\phi + D\cos\phi)\hat{\jmath} \tag{4.9}$$

$$\mathbf{p}_{3\phi}(s,\phi) = [-(A+sC)\sin\phi-(B+sD)\cos\phi]\hat{\imath}+[(A+sC)\cos\phi-(B+sD)\sin\phi]\hat{\jmath}-\frac{P}{2\pi}\hat{k}$$

and the vector normal to the flank is

$$\mathbf{n}_3 = -\tfrac{P}{2\pi}(C\sin\phi+D\cos\phi)\hat{\imath}+\tfrac{P}{2\pi}(C\cos\phi-D\sin\phi)]\hat{\jmath}+\{AC+BD+s(C^2+D^2)\}\hat{k}$$

This normal after projection to XY plane and dividing by the magnitude of the projected normal vector gives unit projected normal vector $\hat{n}_{3p}$ as

$$\hat{n}_{3p} = \frac{(C\sin\phi + D\cos\phi)\hat{\imath} + (C\cos\phi - D\sin\phi)\hat{\jmath}}{\sqrt{C^2+D^2}}$$

Scalar product of $\hat{n}_{3p}$ with $\hat{\imath}$ gives α_{1P} as

$$\cos\alpha_{1P} = \left[\frac{(C\sin\phi + D\cos\phi)}{\sqrt{C^2+D^2}}\right]$$

For straight tooth cutters, ϕ is zero and for helical cutters angles are evaluated on z=0 plane, where angle ϕ is equal to zero. On solving this gives

$$\alpha_{1P} = \gamma_3 \tag{4.10}$$

Second Clearance Angle (α_{2P})

This angle α_{2P} is formed by the surface patch Σ_4 (back of the cutter) of cutter tooth. The angle in projective geometry approach is the angle between Σ_4 with YZ plane on projection to the XY plane, where Σ_4 is

$$\begin{aligned}\mathbf{p}_4(s,\phi) &= \mathbf{p}_3(s).[\mathbf{T}_s] \\ &= [\{(V_{3x}+s(V_{4x}-V_{3x}))\cos\phi-(V_{3y}+s(V_{4y}-V_{3y}))\sin\phi\} \\ &\quad \{(V_{3x}+s(V_{4x}-V_{3x}))\sin\phi-(V_{3y}+s(V_{4y}-V_{3y}))\cos\phi\} \ -\frac{P\phi}{2\pi} \ 1]\end{aligned} \tag{4.11}$$

The tangents to this surface Σ_4 are

$$\mathbf{p}_{4s}(s,\phi) = \{(V_{4x}-V_{3x})\cos\phi-(V_{4y}-V_{3y})\sin\phi\}\hat{\imath}+\{(V_{4x}-V_{3x}))\sin\phi+(V_{4y}-V_{3y}))\cos\phi\}\hat{\jmath}$$

$$\mathbf{p}_{4\phi}(s,\phi) = [-\{V_{3x}+s(V_{4x}-V_{3x})\}\sin\phi-\{V_{3y}+s(V_{4y}-V_{3y})\}\cos\phi]\hat{\imath}+$$

$$[\{V_{3x}+s(V_{4x}-V_{3x})\}\cos\phi-\{V_{3y}+s(V_{4y}-V_{3y})\}\sin\phi]\hat{\jmath}-\frac{P}{2\pi}\hat{k} \qquad (4.12)$$

As for both straight tooth cutter and helical cutters, the angles are evaluated at z=0 plane, where ϕ is equal to zero. Therefore, tangents to Σ_4 at $\phi = 0$ are given by

$$\mathbf{p}_{4s}(s,\phi)_{|\phi=0} = (V_{4x}-V_{3x})\hat{\imath}+(V_{4y}-V_{3y})\hat{\jmath}$$

$$\mathbf{p}_{4\phi}(s,\phi)_{|\phi=0} = -\{V_{3y}+s(V_{4y}-V_{3y})\}\hat{\imath}+\{V_{3x}+s(V_{4x}-V_{3x})\}\hat{\jmath}-\frac{P}{2\pi}\hat{k}$$

With these tangent vectors, the vector normal to the surface Σ_4 can be evaluated and unit normal vector projected on XY plane is given by

$$\hat{n}_{4p_{|\phi=0}} = \frac{-(V_{4y}-V_{3y})\hat{\imath}+(V_{4x}-V_{3x})\hat{\jmath}}{\sqrt{(V_{4y}-V_{3y})^2+(V_{4x}-V_{3x})^2}}$$

On solution the angle formed by $\hat{n}_{4p_{|\phi=0}}$ with the unit vector along X axis ($\hat{\imath}$) is

$$\alpha_{2P} = \gamma_4 \qquad (4.13)$$

From sign convention, angles α_{2P}, γ_4 are having similar signs.

Gash Angle (δ)

Gash angle is the angle of fillet i.e. the angle formed by the back of N^{th} tooth with face of $(N+1)^{th}$ tooth. From the Figure 4.4, gash angle can be found to be $\delta = 90° - \gamma_R - \alpha_{2P} + \psi$.
Knowing the relations of conventional angles γ_R and α_{2P} from above, gash angle can be put in terms of rotational angles as

$$\delta = 90° + \gamma_1 - \gamma_4 + \frac{2\pi}{N} \qquad (4.14)$$

where N is the number of teeth of the cutter.

Lip Angle (θ_{la})

Lip angle is the angle formed by the cutter tooth solid side at the cutting edge (cutting point, in terms of projective geometry nomenclature). From the figure of cutting tool angles Figure 4.4, lip angle is given by $\theta_{la} = 90° - \gamma_R - \alpha_P$
In terms of rotational angles, the lip angle is, thus, given by

$$\theta_{la} = 90° + \gamma_1 - \gamma_2 \qquad (4.15)$$

4.1.4.2 Inverse Mapping

The relations that help to evaluate proposed 3D rotational angles, if the angles in conventional 2D nomenclatures are known, constitute inverse mapping. These relations are presented here. The forward mapping relations derived above is summarized in Table 4.4 and based on it the values of 3D rotational angles can be inferred in the form of the inverse mapping as presented in Table 4.5.

Conventional Angles		Rotational Angles
Radial Rake Angle, $\pm\gamma_R$	=	$\mp\gamma_1$
Relief Angle, α_P	=	γ_2
1^{st} Clearance Angle, α_{1P}	=	γ_3
2^{nd} Clearance Angle, α_{2P}	=	γ_4

Table 4.4: Forward Mapping Relations for Slab Mill

Rotational Angles		Conventional Angles
γ_1	=	$-\gamma_R$
γ_2	=	α_P
γ_3	=	α_{1P}
γ_4	=	α_{2P}

Table 4.5: Inverse Mapping Relations for Slab Mill

4.2 End Milling Cutters

End milling cutters are multiple teeth cutters with cutting surfaces both on the end face and the circumferential surface of the cutter [29, 30, 33, 61]. The teeth can be straight or helical. End mills combine the abilities of end cutting, peripheral cutting and face milling into one tool. The end mills have a straight or tapered shank for mounting and driving. Used vertically, the end mill can plunge cut a counter bore or face mill a slot equal in width to the cutting diameter of the tool. When used horizontally in a peripheral milling operation, the end mill's flute length limits the width of the cut. End mills can be used for various operations like facing, slotting, profiling, die sinking, engraving etc. End mills can be classified according to

(i) Configuration of end profile — Flat, Chamfer, Radius, Ball, Taper, Bull Nose end mills and their combinations.

(ii) Shank type — Straight shank and Brown & Sharpe or Morse Taper shank

(iii) Mounting type — Cylindrical, cylindrical threaded, cylindrical power chuck. Weldon and Weldon threaded

In the present work, a generic flat end mill is modeled as it can be generalize other types of end mills. Other end profiles of the end mills can be subsequently developed based on the additional parameter required for them. For example, for radius end mill, the value of radius is the additional parameter required to model it apart from the parameters required to model flat end mill [27].

4.2.1 Surface Modeling of Flat End Milling Cutter Tooth

The geometry of flat end mill projected on two-dimensional planes is shown in Figure 4.5. The geometry of an end mill may consist of two classes, namely

- Geometry of fluted shank
- End surface geometry

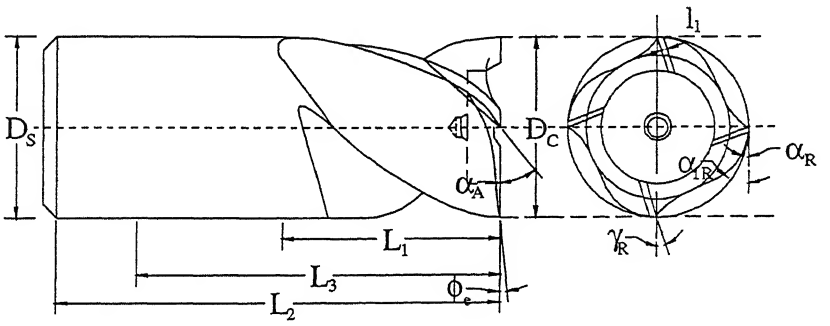

Figure 4.5: Two-Dimensional Projected Geometry of End Mill

The geometry of fluted shank consist of circumferential surface patches formed by sweeping profile of a section, perpendicular to the axis of the cutter. The end geometry depends on the configuration of the end profile. A single tooth of the end milling cutter is modeled with the help of nine surface patches, labeled Σ_1 to Σ_9. Table 4.6 lists the surface patches of a tooth of the flat end mill. The schematic figure of the tooth of the right hand, right helix flat end mill is shown with the help of Figure 4.6 [48].

4.2.1.1 Geometry of Fluted Shank

Surfaces Σ_1 to Σ_6 are the surface patches on the fluted shank. These surfaces are formed as helicoidal surfaces. Helicoidal surfaces are formed when a composite curve

Symbol	Surface Patch Name	Code	Surface Patch Name
Σ_1	Face	Σ_6	Fillet
Σ_2	Peripheral Land	Σ_7	Face Land
Σ_3	Heel or Secondary Land	Σ_8	Minor Flank
Σ_4	Blending surface	Σ_9	Rake Face Extension
Σ_5	Back of Tooth		

Table 4.6: Surface Patches of End Mill

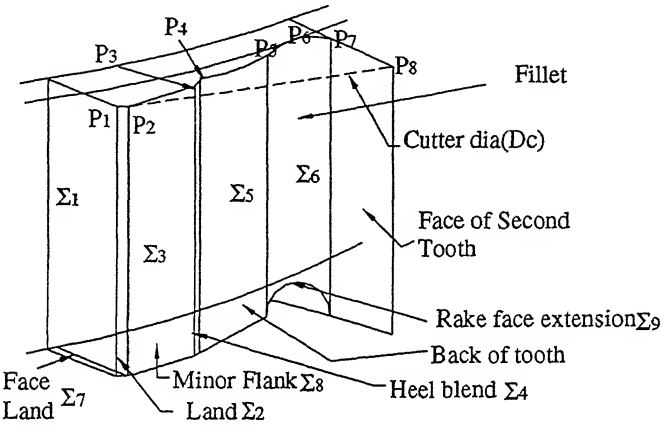

Figure 4.6: Surface Modeling of an End Mill Tooth

in XY plane is swept with a sweeping rule, composed of combined rotational and parallel sweep. The curve is rotated about Z axis and linearly advanced along negative Z axis to form the fluted shank. The composite section curve ($V_1 \ldots V_8$) profile at the cutting end is composed of six segments and is shown in Figure 4.7.

Segments V_1V_2, V_2V_3 and V_7V_8 of the composite curve are straight lines, while segments V_3V_4, V_4V_5 and $V_5V_6V_7$ are circular arcs of radii r_2, r_3 and R respectively. The sectional geometry of fluted shank is mathematically evolved and presented below.

Sectional Geometry of Fluted Shank

The composite profile of the sectional geometry of the fluted shank is described with the help of six cross-sectional segments. Out of these six, three segments correspond to the three land widths, namely peripheral land, heel and face, and are straight lines in two-dimensional projective plane. The other three segments are circular arcs in geometry and correspond to fillet, back of cutting tooth and blending surface. The circular arcs are meant to provide smooth surfaces, primarily for easy and convenient chip disposal.

To model the cross-sectional profile in two-dimensional plane, the input parameters are (i) widths of lands i.e. peripheral land, heel or secondary land and face given

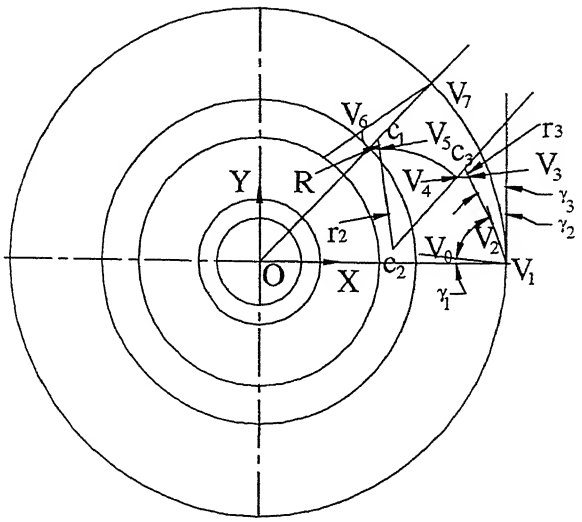

Figure 4.7: Composite Section Curve for an End Mill Tooth

by l_1, l_2 and l_3 respectively, (ii) angles obtained to form face (γ_1), land (γ_2) and heel (γ_3) about Z axis, (iii) radii of fillet (R), back of tooth (r_2) and blending surface (r_3), (iv) diameter of cutting end of end mill (D_c) and (v) number of flutes (N). Besides, the length and angle of chord represented by l_4 and γ_4 respectively, joining the end vertices V_3 and V_4 of blending surface are also known.

When the end mill is placed in a global coordinate system C_1, with origin coinciding with the center of the circle representing the end mill cross-section, the position vectors of end vertices of different sections of the composite profile curve and center points of the three circular arcs (c_1, c_2, c_3) are satisfied by the following relations

$$\mathbf{v}_1 = [\tfrac{D_c}{2} \quad 0 \quad 0 \quad 1]$$

$$\mathbf{v}_2 = [(\tfrac{D_c}{2} - l_1 \sin\gamma_2) \quad l_1 \cos\gamma_2 \quad 0 \quad 1]$$

$$\mathbf{v}_3 = [\{\tfrac{D_c}{2} - (l_1 \sin\gamma_2 + l_2 \sin\gamma_3)\} \quad (l_1 \cos\gamma_2 + l_2 \cos\gamma_3) \quad 0 \quad 1]$$

$$\mathbf{v}_4 = [\{\tfrac{D_c}{2} - (l_1 \sin\gamma_2 + l_2 \sin\gamma_3 + l_4 \sin\gamma_4)\} \quad (l_1 \cos\gamma_2 + l_2 \cos\gamma_3 + l_4 \sin\gamma_4) \quad 0 \quad 1]$$

$$\mathbf{v}_5 = [\{\tfrac{D_c}{2} \cos\psi - l_3 \cos(\psi + \gamma_1) + R(\sin(\psi + \gamma_1) + \cos\theta_1)\} \quad \{\tfrac{D_c}{2} \sin\psi - l_3 \sin(\psi + \gamma_1) - R(\cos(\psi + \gamma_1) + \sin\theta_1)\} \quad 0 \quad 1]$$

$$\mathbf{v}_6 = [\{\tfrac{D_c}{2} \cos\psi - l_3 \cos(\psi + \gamma_1)\} \quad \{\tfrac{D_c}{2} \sin\psi - l_3 \sin(\psi + \gamma_1)\} \quad 0 \quad 1]$$

$$\mathbf{v}_7 = [\tfrac{D_c}{2} \cos\psi \quad \tfrac{D_c}{2} \sin\psi \quad 0 \quad 1]$$

$$\mathbf{c}_1 = [\{\tfrac{D_c}{2} \cos\psi - l_3 \cos(\psi + \gamma_1) + R \sin(\psi + \gamma_1)\} \quad \{\tfrac{D_c}{2} \sin\psi - l_3 \sin(\psi + \gamma_1) - R \cos(\psi + \gamma_1)\} \quad 0 \quad 1]$$

$$\mathbf{c}_2 = [\{\tfrac{D_c}{2} - (l_1 \sin\gamma_2 + l_2 \sin\gamma_3 + l_4 \sin\gamma_4) - r_2 \cos\theta\} \quad \{(l_1 \cos\gamma_2 + l_2 \cos\gamma_3 + l_4 \sin\gamma_4) - r_2 \sin\theta\} \quad 0 \quad 1]$$

$$\mathbf{c}_3 = [\{\tfrac{D_c}{2} - (l_1 \sin\gamma_2 + l_2 \sin\gamma_3) - r_3 \sin(\gamma_4 - \phi)\} \quad \{l_1 \cos\gamma_2 + l_2 \cos\gamma_3 + r_3 \cos(\gamma_4 - \phi) \quad 0 \quad 1]$$

where $\psi = \frac{2\pi}{N}$, $\phi = \cos^{-1}(\frac{l_4}{2r_3})$, $\theta = \tan^{-1}\left(\frac{c_{3y}-V_{4y}}{c_{3x}-V_{4x}}\right)$ and $\theta_1 = \tan^{-1}\left(\frac{c_{1y}-c_{2y}}{c_{1x}-c_{2x}}\right)$, with the condition that

If $\theta_1 < 0$, then $\theta_1 = \pi + \theta_1$

else $\theta_1 = \theta_1$

Sweeping Rules

The fluted section of an end mill can have right helix or left helix. If the flute's spiral have a clockwise contour when looked along the cutter axis from either end, then it is a right helix else helix is left [33, 29]. For a right helix cutter, the cross-section curve rotates by an angle $+\phi$ about Z axis in right hand sense. Three different sweeping rules can be formulated for the fluted shank and the end profile portions of the cutter based on the helical path traversed by the sectional profile. These rules are for

(i) Cylindrical Helical Path
(ii) Conical Helical Path
(iii) Hemispherical Helical Path

Cylindrical Helical Path – The path when the composite profile curve is swept helically along a cylinder is known as cylindrical helical path. For a helical cutter let ϕ be the parameter denoting the angular movement, P the pitch of the helix, D_c the cylindrical cutter diameter and L_1 the length of the cutter, then the mathematical definition of the helix is

$$\begin{aligned} x &= \frac{D_c}{2}\cos\phi \\ y &= \frac{D_c}{2}\sin\phi \\ z &= \frac{P\phi}{2\pi} \end{aligned} \tag{4.16}$$

$$\text{where } 0 \leq \phi \leq \frac{2\pi}{P}.L_1$$

Conical Helical Path – The helical path along a frustum of cone of cutting end diameter D_c and shank side diameter D_s is defined by

$$\begin{aligned} x &= \frac{D}{2}\cos\phi \\ y &= \frac{D}{2}\sin\phi \\ z &= \frac{P\phi}{2\pi} \end{aligned} \tag{4.17}$$

$$\text{where } D = D_c + \frac{(D_s - D_c)z}{L_1} \text{ and } 0 \leq \phi \leq \frac{2\pi}{P}.L_1$$

This is valid for both types of frustum of cones i.e. when $D_c < D_s$ and when $D_c > D_s$.

Hemispherical Helical Path – The helical path along the hemispherical object of diameter D_c is given by the following mathematical definition.

$$\begin{aligned} x &= \frac{D}{2}\cos\psi\cos\phi \\ y &= \frac{D}{2}\cos\psi\sin\phi \\ z &= \frac{D_c}{2}(1-\sin\psi) \end{aligned} \tag{4.18}$$

$$\text{where } 0 \leq \phi \leq \frac{\pi D_c}{P} \text{ and } 0 \leq \psi \leq \frac{\pi}{2}$$

Here, ϕ is the angle about Z axis and ψ is the angle with XY plane. The following equation gives the relation between the angles ψ and ϕ.

$$\psi = \sin^{-1}\left[1 - \frac{P\phi}{D_c\pi}\right]$$

4.2.1.2 End Surface Geometry

The end geometry of a fluted end mill depends upon the end mill profile configuration. For example, in the case of the flat end mill, the end consist of three planes and one blending surface. The planes are (i) Face Land Σ_7, (ii) Minor Flank Σ_8 and (iii) rake face extension Σ_9, whereas the blending surface blends surface patch Σ_8 of the first tooth with surface Σ_9 of the second tooth of the end mill (labeled as ${}^2\Sigma_9$). Modeling of end surface patches in the case of the flat end mill is described below.

End Surface Geometry of Flat End Mill

Face Land (Σ_7)

Face land is formed when an XY plane given by $[u_7 \quad v_7 \quad 0 \quad 1]$ is transformed in the following sequence

(i) Rotation by an angle α_7 about X axis $[R_{x,\alpha_7}]$

(ii) Rotation by angle γ_1 about Z axis $[R_{z,\gamma_1}]$

Therefore, equation of the surface Σ_7 is

$$\begin{aligned} \mathbf{p}_7(u_7, v_7) &= [u_7 \quad v_7 \quad 0 \quad 1].[R_{x,\alpha_7}].[R_{z,\gamma_1}] \\ &= [(u_7\cos\gamma_1 - v_7\cos\alpha_7\sin\gamma_1) \quad (u_7\sin\gamma_1 + v_7\cos\alpha_7\cos\gamma_1) \quad v_7\sin\alpha_7 \quad 1] \end{aligned} \tag{4.19}$$

Minor Flank (Σ_8)

This surface is formed when an XY plane is transformed as follows:

(i) Rotation by an angle α_8 about X axis $[R_{x,\alpha_8}]$

(ii) Rotation by angle γ_1 about Z axis $[R_{z,\gamma_1}]$

(iii) Translation by a distance d_{82} along Y axis and d_{83} along Z direction $[\mathbf{T}_{yz}]$

where $d_{82} = l_1 \cos\gamma_2$ and $d_{83} = l_1 \cos\gamma_2 \sin\alpha_7$. The surface Σ_8 may be developed as

$$\begin{aligned}\mathbf{p}_8(u_8, v_8) &= [u_8 \quad v_8 \quad 0 \quad 1].[R_{x,\alpha_8}].[R_{z,\gamma_1}].[\mathbf{T}_{yz}] \\ &= [(u_8\cos\gamma_1 - v_8\cos\alpha_8\sin\gamma_1) \quad (u_8\sin\gamma_1 + v_8\cos\alpha_8\cos\gamma_1 + d_{82}) \quad (v_8\sin\alpha_8 + d_{83} \quad 1]\end{aligned} \tag{4.20}$$

Rake Face Extension (Σ_9)

An ZX plane, ($[u_9 \quad 0 \quad w_9 \quad 1]$), forms rake face extension Σ_9 when transformed as

(i) Rotation by an angle α_9 about X axis $[R_{x,\alpha_9}]$

(ii) Rotation by an angle γ_1 about Z axis $[R_{z,\gamma_1}]$

where, helix angle $\lambda = \tan^{-1}\left(\frac{P}{\pi D_c}\right)$, $\alpha_9 = 90° - \lambda^*$ and $\lambda^* = \lambda + (15° - 25°)$but $\leq 90°$. The surface Σ_9 then can be defined by

$$\begin{aligned}\mathbf{p}_9(u_9, w_9) &= [u_9 \quad 0 \quad w_9 \quad 1].[R_{x,\alpha_9}].[R_{z,\gamma_1}] \\ &= [(u_9\cos\gamma_1 - w_9\sin\alpha_9\sin\gamma_1) \quad (u_9\sin\gamma_1 + w_9\sin\alpha_9\cos\gamma_1) \quad (w_9\cos\alpha_9) \quad 1]\end{aligned} \tag{4.21}$$

4.2.1.3 Ball End Mill Cutter

Similar to flat end mills, the geometry of ball end mills can also be subdivided into geometry of fluted shank and end portion geometry. The fluted shank geometry is similar for all types of end mills but the end geometry differs. In the case of ball end mill, the end geometry is also fluted in nature. For end portion of the ball end mill, each flute lies on the surface of the hemisphere, and is ground with a constant helix lead [87, 93]. The radius of the ball in XY planes reduces along the cutter axis towards cutting end, as the tip of the hemisphere lies in contact with work surface. Due to this, the local helix angle varies along the cutting flute.

The diameter of the cross section of the hemispherical ball is a function of z, which varies from 0 at the tip of the ball part to D_c at the meeting of ball and shank boundary. The radius of cross-section at any instance z, is $r(z) = \sqrt{(D_c z - z^2)}$, where $z = \frac{P\phi}{2\pi}$ and $0 \leq \phi \leq \frac{\pi D_c}{P}$. The ratio by which the cross-section is reduced while going towards the tip of the ball end mill is $ratio = \frac{2r(z)}{D_c}$

Conical End Milling Cutter

In the case of conical end mills, similar to ball end mills, the end portion is fluted. To obtain the fluted end geometry, the radius of cross-section $r(z)$ for conical end portion satisfies the relation $r(z) = \frac{D_c z}{2h}$, where h is the height of the conical end.

4.2.1.4 Modeling of Fluted Surfaces of End Mill

As discussed earlier, the cross-section profile of an end mill consists of three parametric linear edges and three parametric circular edges, namely, $\mathbf{p}_1(s)$ to $\mathbf{p}_6(s)$. Edges $\mathbf{p}_1(s)$, $\mathbf{p}_2(s)$ and $\mathbf{p}_6(s)$ are straight edges and $\mathbf{p}_3(s)$, $\mathbf{p}_4(s)$ and $\mathbf{p}_5(s)$ are circular in two-dimensional space. The generic definition of the sectional profile in XY plane in terms of parameter s may be represented by

$$\mathbf{p}_i(s) = [\mathbf{f}_{i1}(s) \quad \mathbf{f}_{i2}(s) \quad 0 \quad 1]$$

The fluted surface is obtained by combined rotational and parallel sweeping. The profile is rotated about the Z axis and advanced simultaneously along the Z axis. The helix angle remains constant on the cylindrical shank. The helicoidal surface for fluted shank is parametrically described by

$$\mathbf{p}(s, \phi) = \mathbf{p}(s).[\mathbf{T}_s] \text{ where}$$

$$\mathbf{T}_s = \begin{bmatrix} \cos\phi & \sin\phi & 0 & 0 \\ -\sin\phi & \cos\phi & 0 & 0 \\ 0 & 0 & 1 & 0 \\ 0 & 0 & \frac{P\phi}{2\pi} & 1 \end{bmatrix} \text{ for } 0 \leq \phi \leq \frac{2\pi L}{P}$$

In the above equation, L is the length of fluted shank. It may be equal to reach length L_1 for flat end mills and to $(L_1 - \frac{D_c}{2})$ for ball end mills.

4.2.2 Modeling of Cutter Body and Blending Surfaces

The cutter body of end mill consists of a shank, which may be modeled as a combination of two surface patches. These surface patches are (i) cylindrical surface of revolution Σ_{50} and (ii) planar end surface Σ_{51}. The cylindrical surface of shank may be parametrically defined by

$$\mathbf{p}_{50}(w, \phi) = [\frac{D'}{2}\cos\phi \quad \frac{D'}{2}\sin\phi \quad \{L_1 + w(L_2 - L_1)\} \quad 1] \tag{4.22}$$

for $0 \leq \phi \leq 2\pi$, $0 \leq w \leq 1$. The term L_2 stands for overall length of end mill and diameter D' may be given by

$$D' = \begin{cases} \frac{D_s}{2}, & \text{for straight shank} \\ \frac{D_c}{2} + w\frac{D_s - D_c}{2}, & \text{for tapered shank} \end{cases}$$

The planar end surface forming the end opposite to cutting end is parametrically modeled as

$$\mathbf{p}_{51}(u,v) = [u \quad v \quad L_2 \quad 1] \text{ for } -\infty \leq u, v \leq \infty \tag{4.23}$$

The only blending surface on the body of the cutter is a unit width, 45° chamfer between body surface patches Σ_{50} and Σ_{51}. The chamfer $\sigma_{50,51}$ is modeled as a surface of revolution. The coordinates of the two end points of the edge that is revolved about Z axis to form the chamfer are $((\frac{D_s}{2} - 0.707), 0, L_2))$ and $(\frac{D_s}{2}, 0, (L_2 - 0.707))$. These end points lead to an edge $[\{\frac{D_s}{2} - 0.707(1-u)\} \quad 0 \quad (L_2 - 0.707u) \quad 1]$ $(-\infty \leq u \leq \infty)$. Thus, the chamfer is given by

$$\sigma_{50,51}(u,\theta) = [\{\frac{D_s}{2} - 0.707(1-u)\}\cos\theta \quad \{\frac{D_s}{2} - 0.707(1-u)\}\sin\theta \quad (L_2 - 0.707u) \quad 1] \tag{4.24}$$

for $0 \leq u \leq 1$ and $0 \leq \theta \leq 2\pi$

4.2.3 Mapping

In this subsection, sets of relations that map proposed 3D rotational angles to conventional angles and vice versa are developed. The former is called forward mapping while the latter is known as inverse mapping. The sign convention of the rotational and the conventional angles is given in Table 4.7. The conventional angles are formed by projecting the surface patches of the end mill and traditional tool geometry can be referred from [27, 29, 33, 48]. Mapping guide table (Table 4.8) shows the methodology of formation of conventional angles.

Rotational Angles	Conventional Angles
γ_1 = −ve	Radial Rake Angle, γ_R = +ve
γ_2 = +ve	Relief Angle, α_R = +ve
γ_3 = +ve	First Clearance Angle, α_{1R} = +ve
	End Cutting Edge Angle, ϕ_e = +ve
	Axial Relief Angle, α_A = +ve

Table 4.7: Sign Convention for the Angles of End Mill

4.2.3.1 Forward Mapping

This subsubsection presents conventional angles in terms of proposed three-dimensional rotational angles.

Conventional Angles	Formed by	About the Plane	Plane of Projection
γ_R	Σ_1	ZX	XY
α_R	Σ_2	YZ	XY
α_{1R}	Σ_3	YZ	XY
ϕ_e	Σ_7	XY	ZX
α_A	Σ_7	XY	YZ

Table 4.8: Mapping Guide Table for End Mill

Radial Rake Angle (γ_R)

Rake face Σ_1 forms radial rake angle (γ_R) with ZX plane. This angle is expressed when projected to XY plane. The plane Σ_1 is formed by the edge (e_{01}) joining vertex V_0 to V_1, when swept by transformation matrix $[\mathbf{T}_s]$, defined earlier. In terms of homogenous coordinates the vertex V_0 is expressed by

$V_0 = [(\frac{D_c}{2} - l_3\cos\gamma_1) \quad -l_3\sin\gamma_1 \quad 0 \quad 1]$ and the edge $\mathbf{e}_{01}$ by

$$\mathbf{e}_{01} = [\{\tfrac{D_c}{2} - l_3\cos\gamma_1(1-s)\} \quad -l_3\sin\gamma_1(1-s) \quad 0 \quad 1]$$

The mathematical equation of Σ_1 is given by

$$\begin{aligned}\mathbf{p}_1(s,\phi) &= \mathbf{e}_{01}.[\mathbf{T}_s] \\ &= [\{(\frac{D_c}{2} - l_3\cos\gamma_1(1-s))\cos\phi + l_3\sin\gamma_1(1-s)\sin\phi\} \\ &\quad \{(\frac{D_c}{2} - l_3\cos\gamma_1(1-s))\sin\phi - l_3\sin\gamma_1(1-s)\cos\phi\} \quad \frac{P\phi}{2\pi} \quad 1]\end{aligned} \tag{4.25}$$

The tangent vectors to rake face Σ_1 are found by differentiating above equation with respect to parameters s and ϕ. Therefore tangents $\frac{\partial \mathbf{p}_1}{\partial s}, \frac{\partial \mathbf{p}_1}{\partial \phi}$ are

$$\begin{aligned}\mathbf{p}_{1s}(s,\phi) &= l_3\cos(\gamma_1+\phi)\hat{\imath} + l_3\sin(\gamma_1+\phi)\hat{\jmath} \\ \mathbf{p}_{1\phi}(s,\phi) &= [-\{\frac{D}{2} - l_3\cos\gamma_1(1-s)\}\sin\phi + l_3\sin\gamma_1(1-s)\cos\phi]\hat{\imath} + \\ &\quad [\{\frac{D}{2} - l_3\cos\gamma_1(1-s)\}\cos\phi + l_3\sin\gamma_1(1-s)\sin\phi]\hat{\jmath} + \frac{P}{2\pi}\hat{k}\end{aligned} \tag{4.26}$$

which leads to the following relation for the vector normal to the surface Σ_1

$$\mathbf{n}_1 = \tfrac{Pl_3}{2\pi}\sin(\gamma_1+\phi)\hat{\imath} - \tfrac{Pl_3}{2\pi}\cos(\gamma_1+\phi)\hat{\jmath} + [\tfrac{D_c}{2}l_3\cos\gamma_1 - l_3^2(1-s)\}\hat{k}$$

To find radial rake angle γ_R, $\mathbf{n}_1$ is projected on XY plane ($\mathbf{n}_{1p}$) and unit projected normal vector ($\hat{n}_{1p}$) is evaluated as

$\hat{n}_{1p} = \mathbf{n}_{1p}/|\mathbf{n}_{1p}| = \sin(\gamma_1+\phi)\hat{\imath} - \cos(\gamma_1+\phi)\hat{\jmath}$

Radial rake angle is found by taking scalar product of $\hat{n}_{1p}$ with unit vector $\hat{\jmath}$, as this is similar to the angle between normal to face Σ_1, projected on XY plane and Y axis. Therefore, $\cos\gamma_R = -cos(\gamma_1+\phi)$. At $z=0$ plane, $\phi = 0$, therefore

$$\gamma_R = -\gamma_1 \tag{4.27}$$

From sign convention table, angles γ_R, γ_1 are of opposite signs.

Radial Relief Angle (α_R)

Radial relief Angle (α_R) is formed by Land Σ_2 about YZ plane when projected on XY plane. The land Σ_2 can be geometrically expressed with

$$\begin{aligned}\mathbf{p}_2(s,\phi) &= [\{(\frac{D_c}{2}-sl_1\sin\gamma_2)\cos\phi - sl_1\cos\gamma_2\sin\phi\} \\ &\quad \{(\frac{D_c}{2}-sl_1\sin\gamma_2)\sin\phi + sl_1\cos\gamma_2\cos\phi\} \quad \frac{P\phi}{2\pi} \quad 1]\end{aligned} \tag{4.28}$$

The tangents to Σ_2 at any arbitrary point are

$$\begin{aligned}\mathbf{p}_{2s}(s,\phi) &= \{-l_1\sin(\gamma_2+\phi)\}\hat{\imath} + l_1\cos(\gamma_2+\phi)\hat{\jmath} \\ \mathbf{p}_{2\phi}(s,\phi) &= [(\frac{D_c}{2}-sl_1\sin\gamma_2)\sin\phi - sl_1\cos\gamma_2\cos\phi]\hat{\imath} + \\ &\quad [(\frac{D_c}{2}-sl_1\sin\gamma_2)\cos\phi - sl_1\cos\gamma_2\sin\phi]\hat{\jmath} - \frac{P}{2\pi}\hat{k}\end{aligned} \tag{4.29}$$

The normal to surface Σ_2 projected on XY plane $\mathbf{n}_{2p}$ is

$$\mathbf{n}_{2p} = \tfrac{Pl_1}{2\pi}\cos(\gamma_2+\phi)\hat{\imath} + \tfrac{Pl_1}{2\pi}\sin(\gamma_2+\phi)\hat{\jmath}$$

and the unit projected normal vector is

$$\hat{n}_{2p} = \cos(\gamma_2+\phi)\hat{\imath} + \sin(\gamma_2+\phi)\hat{\jmath}$$

Angle of surface Σ_2 with YZ plane is similar to the angle of $\hat{n}_{2p}$ with unit vector $\hat{\imath}$. Therefore, taking scalar product of $\hat{n}_{2p}$ and $\hat{\imath}$, one gets $\cos\alpha_R = \cos(\gamma_2+\phi)$. At $z=0$ plane, ϕ is zero, which gives

$$\alpha_R = \gamma_2 \tag{4.30}$$

From sign convention table, angles α_R, γ_2 are having same signs.

Radial Clearance Angle (α_{1R})

Radial clearance angle is formed by surface patch Σ_3 (flank) of cutter tooth with YZ plane on projection to the XY plane, where flank Σ_3 satisfies the relation

$\mathbf{p}_3(s,\phi) = \mathbf{p}_2(s).[\mathbf{T}_s]$ or

$$\begin{aligned}\mathbf{p}_3(s,\phi) = [\{(\frac{D_c}{2} - l_1\sin\gamma_2 - sl_2\sin\gamma_3)\cos\phi - (l_1\cos\gamma_2 + sl_2\cos\gamma_3)\sin\phi\} \\ \{(\frac{D_c}{2} - l_1\sin\gamma_2 - sl_2\sin\gamma_3)\sin\phi + (l_1\cos\gamma_2 + sl_2\cos\gamma_3)\cos\phi\} \quad \frac{P\phi}{2\pi} \quad 1]\end{aligned} \tag{4.31}$$

The tangents to Σ_3 at any arbitrary point are

$$\begin{aligned}\mathbf{p}_{3s}(s,\phi) &= -l_2\sin(\gamma_3+\phi)\hat{\imath} + l_2\cos(\gamma_3+\phi)\hat{\jmath} \\ \mathbf{p}_{3\phi}(s,\phi) &= \{-(\tfrac{D_c}{2} - l_1\sin\gamma_2 - sl_2\sin\gamma_3)\sin\phi - (l_1\cos\gamma_2 + sl_2\cos\gamma_3)\cos\phi\}\hat{\imath} \\ &\quad + \{(\tfrac{D_c}{2} - l_1\sin\gamma_2 - sl_2\sin\gamma_3)\cos\phi - (l_1\cos\gamma_2 + sl_2\cos\gamma_3)\sin\phi\}\hat{\jmath} + \tfrac{P\phi}{2\pi}\hat{k}\end{aligned}$$

and the normal is

$$\mathbf{n}_3 = \tfrac{Pl_2}{2\pi}\cos(\gamma_3+\phi)\hat{\imath} + \tfrac{Pl_2}{2\pi}\sin(\gamma_3+\phi)\hat{\jmath} + \{-\tfrac{D_c}{2}l_2\sin\gamma_3 + l_1l_2\cos(\gamma_3-\gamma_2) + sl_2^2\}\hat{k}$$

This normal on projection to XY plane and leads to the following unit normal vector projected on XY plane

$$\hat{n}_{3p} = \cos(\gamma_3+\phi)\hat{\imath}+\sin(\gamma_3+\phi)\hat{\jmath}$$

Radial clearance angle is similar to the angle formed by $\hat{n}_{3p}$ with unit vector normal to YZ plane. Scalar product of $\hat{n}_{3p}$ with $\hat{\imath}$ gives

$$\cos\alpha_{1R} = \cos(\gamma_3 + \phi)$$

At $z = 0$ plane, $\phi = 0$, therefore

$$\alpha_{1R} = \gamma_3 \tag{4.32}$$

Axial Relief Angle (α_A)

Axial relief Angle (α_A) is formed by surface Σ_7, which satisfies the relation

$$\mathbf{p}_7(u_7, v_7)=[(u_7\cos\gamma_1-v_7\cos\alpha_7\sin\gamma_1) \quad (u_7\sin\gamma_1+v_7\cos\alpha_7\cos\gamma_1) \quad v_7\sin\alpha_7 \quad 1] \tag{4.33}$$

The tangents and normal to this surface are

$$\begin{aligned}
\mathbf{p}_{7u}(u_7, v_7) &= \cos\gamma_1\hat{\imath}+\sin\gamma_1\hat{\jmath} \\
\mathbf{p}_{7v}(u_7, v_7) &= -\cos\alpha_7\sin\gamma_1\hat{\imath} + \cos\alpha_7\cos\gamma_1\hat{\jmath} + \sin\alpha_7\hat{k} \\
\mathbf{n}_7 &= \sin\gamma_1\sin\alpha_7\hat{\imath} - \cos\gamma_1\sin\alpha_7\hat{\jmath} + \cos\alpha_7\hat{k}
\end{aligned}$$

The projection of this normal vector on YZ plane is $\mathbf{n}_{7p} = -\cos\gamma_1\sin\alpha_7\hat{\jmath} + \cos\alpha_7\hat{k}$ and the unit vector normal to Σ_7 and projected on YZ plane, $\hat{n}_{7p}$, is defined by

$$\hat{n}_{7p} = \frac{-\cos\gamma_1\sin\alpha_7\hat{\jmath} + \cos\alpha_7\hat{k}}{\sqrt{\cos^2\gamma_1\sin^2\alpha_7 + \cos^2\alpha_7}}$$

Scalar product of $\hat{n}_{7p}$ with unit vector $\hat{k}$ gives an angle which is equivalent to α_A, where

$$\alpha_A = \cos^{-1}\left[\frac{\cos\alpha_7}{\sqrt{\cos^2\gamma_1\sin^2\alpha_7 + \cos^2\alpha_7}}\right] \tag{4.34}$$

End Cutting Edge Angle (ϕ_e)

End cutting edge angle is formed by the surface patch Σ_7 with XY plane and is measured when projected on ZX plane. This angle is equivalent to the angle between the unit vectors normal to Σ_7 and to XY plane, when projected on ZX plane. End cutting edge angle is computed mathematically by finding the scalar product of unit normal vector projected on ZX plane and unit vector $\hat{k}$. Normal to Σ_7 ($\mathbf{n}_7$) is given above and its projection on ZX plane is given by $\mathbf{n}'_{7p} = \sin\gamma_1\hat{\imath} + \cos\alpha_7\hat{k}$ and unit projected normal vector by

$$\hat{n}'_{7p} = \frac{\sin\gamma_1 \sin\alpha_7 \hat{i} + \cos\alpha_7 \hat{k}}{\sqrt{\sin^2\gamma_1 \sin^2\alpha_7 + \cos^2\alpha_7}}$$

This helps to put ϕ_e in terms of rotational angles as

$$\phi_e = \cos^{-1}\left[\frac{\cos\alpha_7}{\sqrt{\sin^2\gamma_1 \sin^2\alpha_7 + \cos^2\alpha_7}}\right] \tag{4.35}$$

4.2.3.2 Inverse Mapping

Inverse mapping constitute a set of relations, which maps the given conventional 2D angles in terms of proposed 3D angles. Once the inverse mapping relations and conventional angles are available, it is very convenient to find the rotational angles. The forward mapping relations for end mills are summarized in Table 4.9.

Conventional Angles		Rotational Angles
Radial Rake Angle, $\pm\gamma_R$	=	$\mp\gamma_1$
Radial Relief Angle, α_R	=	γ_2
Radial Clearance Angle, α_{1R}	=	γ_3
Axial Relief Angle, α_A	=	$\cos^{-1}\left[\frac{\cos\alpha_7}{\sqrt{\cos^2\gamma_1 \sin^2\alpha_7 + \cos^2\alpha_7}}\right]$
End Cutting Edge Angle, ϕ_e	=	$\cos^{-1}\left[\frac{\cos\alpha_7}{\sqrt{\sin^2\gamma_1 \sin^2\alpha_7 + \cos^2\alpha_7}}\right]$

Table 4.9: Forward Mapping Relations for End Mill

Solving these forward mapping relations establishes inverse mapping that help to evaluate the 3D rotational angles if tool angles specified by conventional nomenclatures are known. Table 4.10 presents the inverse mapping for end mills.

Rotational Angles	Conventional Angles	
γ_1	=	$-\gamma_R$
γ_2	=	α_R
γ_3	=	α_{1R}
α_7	=	$\cos^{-1}\left[\frac{\cos\alpha_A . \cos\phi_e}{\sqrt{\cos^2\alpha_A + \cos^2\phi_e - \cos^2\alpha_A . \cos^2\phi_e}}\right]$

Table 4.10: Inverse Mapping Relations for End Mill

4.3 Twist Drills

Drills are rotary cutting tools used for the production of holes [29, 33]. The drills have one or more cutting lips and one or more helical or straight flutes for the passage of chips and cutting fluids. They are available in wide variety of types and geometries. The most common of them is helically fluted twist drills with different shank and tip geometries. Drills are widely classified on the basis of [77]

- Type — Different drill types include solid drill, carbide drill and insert-based drill
- Shank Configuration — Drills can have straight shank or taper shank. The diameter of the shank may be the same or different than the body of the drill.
- Length — Stub drill, regular length drill and longer flute drill
- Helix Angle — Twist drill, low helix, high helix and straight flute drill
- Number of Flutes — Single-flute drill, Two-flute drill and three or four flute (core) drill
- Hand of Cut — Right-hand cut and left-hand cut drill
- Profiles
- Applications
- Drill Material

In the present work, a two-flute, right-cut, straight shank type of solid twist drill is modeled. This is the drill most commonly used for originating holes.

4.3.1 Surface Modeling of Twist Drill body

Geometrically a drill may be considered to be made of (i) drill body and (ii) shank [33, 78]. Drill body is the portion responsible for material removal and the part by which it is held and driven in a drilling machine is shank. For the convenience of modeling, the geometry of the drill body may further be fragmented into (i) flute geometry and (ii) end geometry. The flute is the cutting portion of the drill extending from shank to the outer corners of the cutting edges. The end of the drill is the portion that facilitates entry of the drill into the workpiece material body and is an extension of the drill body. The conventional two-dimensional projected geometry of a twist drill is shown in Figure 4.8.

The geometry of the fluted shank of a twist drill is formed by sweeping helically a cross-section of the drill. The section is perpendicular to the axis of the drill. The parameters of sweeping are determined by the pitch (P) and the length of cylindrical

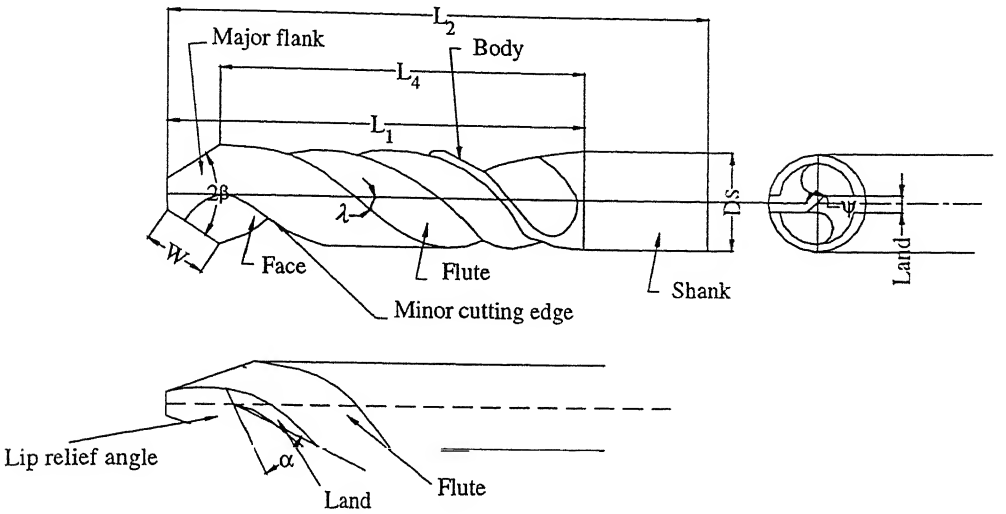

Figure 4.8: Two-Dimensional Projected Geometry of Twist Drill

fluted shank portion of drill (L_4) the drill body. The fluted surface of a two-flute drill is made up of three surface patches, namely, Σ_1 to Σ_3. Table 4.11 lists the surface patches of a twist drill flute. The end geometry of the twist drill is dependent on the configuration of the end profile.

Symbol	Surface Patch Name
Σ_1	Face
Σ_2	Land
Σ_3	Flank

Table 4.11: Twist Drill Body Surface Patches

4.3.1.1 Sectional Geometry

The sectional geometry of the fluted shank comprises a composite curve. The composite curve formed by joining vertices V_1 to V_4 is supposed to be made of three curve segments, V_1V_2, V_2V_3 and V_3V_4, where segment V_1V_2 is a straight line and forms Land when swept helically. The other two curve segments are circular in geometry and on sweeping form flank and face respectively. Figure 4.9 shows the composite section curve of the twist drill body. The geometry of sectional curve depends on various dimensional parameters like width of the land (l_1), radii of the flank (r_1) and the face (r_2), angle subtended by flank about Z axis (θ_1) and angle of inclination of the land about Z axis (γ_2) and diameter of cutting end of drill (D_c).

When the center of drill cross-section coincides with the global origin (O) in coordinate system C_1, position vectors of end vertices of different curve sections and

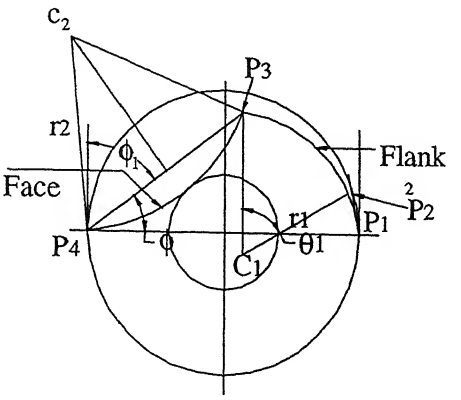

Figure 4.9: Composite Section Curve for a Twist Drill

center points of the two circular arcs (c_1, c_3) are represented as

$\mathbf{v}_1 = [\frac{D_c}{2} \quad 0 \quad 0 \quad 1]$

$\mathbf{v}_2 = [(\frac{D_c}{2} - l_1 \sin\gamma_2) \quad l_1 \cos\gamma_2 \quad 0 \quad 1]$

$\mathbf{v}_3 = [\{\frac{D_c}{2} - l_1 \sin\gamma_2 - r_1 \cos\gamma_2 + r_1 \cos(\gamma_2 + \theta_1)\} \quad \{l_1 \cos\gamma_2 - r_1 \sin\gamma_2 + r_1 \sin(\gamma_2 + \theta_1)\} \quad 0 \quad 1]$

$\mathbf{v}_4 = [-\frac{D_c}{2} \quad 0 \quad 0 \quad 1]$

$\mathbf{c}_1 = [(\frac{D_c}{2} - l_1 \sin\gamma_2 - r_1 \cos\gamma_2) \quad (l_1 \cos\gamma_2 - r_1 \sin\gamma_2) \quad 0 \quad 1]$

$\mathbf{c}_2 = [\{-\frac{D_c}{2} + r_2 \cos(\phi_1 + \phi_2)\} \quad r_2 \sin(\phi_1 + \phi_2) \quad 0 \quad 1]$

where $\phi_1 = \cos^{-1}(\frac{\sqrt{(V_{3x} - V_{4xy})^2 + (V_{3y} - V_{4y})^2}}{2r_2})$ and $\phi_2 = \tan^{-1}(\frac{V_{3y} - V_{4y}}{V_{3x} - V_{4x}})$.

4.3.1.2 Flute Geometry

The flute geometry is obtained when the sectional curve is rotated by an angle ϕ about Z axis around a cylinder of diameter D_c and translated along Z axis and forms helicoidal surfaces Σ_1 to Σ_3. The sweep matrix is

$$[\mathbf{T}_s] = \begin{bmatrix} \cos\phi & \sin\phi & 0 & 0 \\ -\sin\phi & \cos\phi & 0 & 0 \\ 0 & 0 & 1 & 0 \\ 0 & 0 & \frac{P\phi}{2\pi} & 1 \end{bmatrix} \text{ where } 0 \leq \phi \leq \frac{2\pi L_4}{P}$$

The helicoidal surfaces Σ_1 to Σ_3 are formed on the basis of following sweep rule.

$$\text{Face}, \Sigma_1 = \mathbf{p}_3(s).[\mathbf{T}]$$

$$\text{Land}, \Sigma_2 = \mathbf{p}_1(s).[\mathbf{T}]$$

$$\text{Flank}, \Sigma_3 = \mathbf{p}_2(s).[\mathbf{T}]$$

where $\mathbf{p}_i(s)$ is the curve vector having end points V_i and V_{i+1}.

4.3.1.3 End Geometry

The drill end is made of as many surface patches as the number of flutes. For a two-flute drill, two surface patches form the drill end. They are labeled as Σ_4 and Σ_5

and both are known as lip relief surfaces. The major cutting edges of the drill called lips, are formed by the intersection of the helical surface of a flute with the lip relief surface. For efficient cutting, lips should be straight, equal in length and symmetrical with the axis of the drill [19, 28]. The edge at the end of the drill called chisel edge is formed due to intersection of the lip relief surfaces. The lip relief surface can be a part of the surface of (i) plane, (ii) cylinder, (iii) cone and (iv) helicoid. Drill end of these types are shown in Figure 4.10.

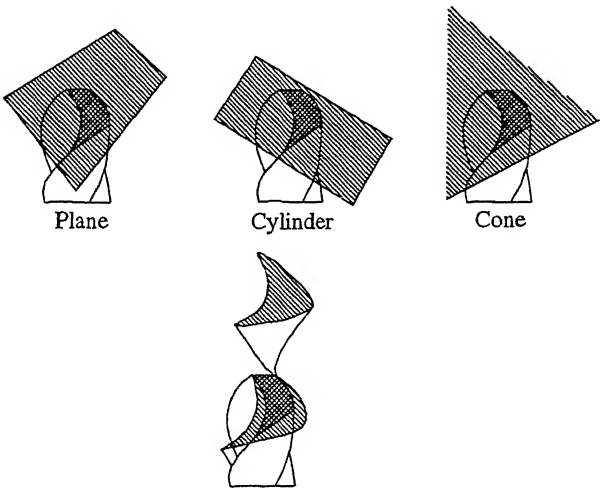

Figure 4.10: Various Types of Drill End

The two common types of drill ends (i) conical and (ii) planar are discussed in this subsubsection.

Conical End Geometry

For a conical end, the flank (Σ_3) is in contact with lip relief surface (Σ_4) at the end of fluted shank (z=0 plane) and the contact is in the form of a circular arc of diameter D_c. Surface Σ_4 is a segment of a cone of half angle δ. The apex of the cone is placed at a distance H from drill axis. The detailed schematic diagram of the conical end is shown in Figure 4.11.

Lip Relief Surface (Σ_4)

Surface Σ_4 is formed as a surface of revolution by rotating edge AB as shown in Figure 4.11 about the axis AA_1. The edge AB ($\mathbf{e}_{ab}(s)$) lies in ZX plane and is parametrically defined in terms of parameter s by

$$[\{-\frac{D_c}{2} + s(H + \frac{D_c}{2})\} \quad 0 \quad \frac{s(H + D_c/2)}{\tan\beta_0} \quad 1] \quad \text{for } 0 \leq s \leq 1$$

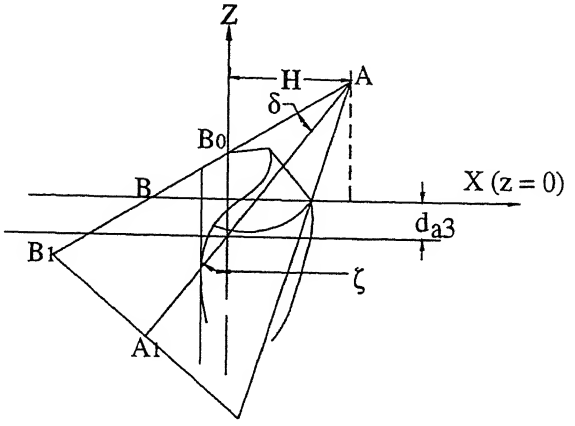

Figure 4.11: Conical Drill End

Surface Σ_4 satisfies the relation $\mathbf{p}_4(s,\phi) = \mathbf{e}_{ab}(s).[\mathbf{R}_{AA_1}]$, where $[\mathbf{R}_{AA_1}]$ is concatenated rotation matrix about axis AA_1 and is given by

$$[R_{AA_1}] = [\mathbf{T}_{z,d_{a3}}].[R_{Y,\zeta}].[R_{Z,\phi}].[R_{Y,\zeta}]^{-1}.[\mathbf{T}_{z,d_{a3}}]^{-1}$$

Matrix $[\mathbf{T}_{z,d_{a3}}]$ is the translation matrix meant for displacing axis AA_1 in the Z direction by a distance $d_{a3} = \frac{H}{\tan\zeta} - \frac{H + d_c/2}{\tan\beta_0}$ to make the axis AA_1 pass through the origin, while $[R_{Y,\zeta}]$ and $[R_{Z,\phi}]$ are the rotation matrix about Y and Z axes respectively. Angle β_0, the angle of drill positioning, is measured from the drill axis and is influenced by point angle 2β required for the drill cutting end. Angle β_0 is somewhat less than the angle β and can be found approximately from the Table 4.12 as given in [87].

Relief Angle α (degrees)	Point Angle 2β (degrees)						
	60	70	90	118	140	160	180
	Angle β_0 (degrees)						
6	30	35	45	59	70	79	86
12	30	35	45	58	68	76	80
18	30	35	44	57	66	71	74
24	30	35	44	56	62	66	68

Table 4.12: Approximate values of Drill Axis Angles

Angle ζ is given by the relation $\zeta = \beta_0 - \delta$ and the parametric equation of the surface Σ_4 is given by the following relations.

$$\begin{aligned}
\mathbf{p}_{4X}(s,\phi) &= A(\cos^2\zeta\cos\phi + \sin^2\zeta) + B(\cos\zeta\sin\zeta\cos\phi - \cos\zeta\sin\zeta) \\
\mathbf{p}_{4Y}(s,\phi) &= A\cos\zeta\sin\phi + B\sin\zeta\sin\phi \\
\mathbf{p}_{4Z}(s,\phi) &= A(\cos\zeta\sin\zeta\cos\phi - \cos\zeta\sin\zeta) + B(\sin^2\zeta\cos\phi + \cos^2\zeta) - d_{a3}
\end{aligned} \tag{4.36}$$

where $A = \{-\frac{D_c}{2} + s(H + \frac{D_c}{2})\}$ and $B = \{\frac{s(H+\frac{D_c}{2})}{\tan\beta_0} + d_{a3}\}$

Second Lip Relief Surface (Σ_5)

The other lip relief surface is formed by rotating Σ_4 about Z axis by an angle of 180°. For N-fluted drill, surface patches Σ_5 to Σ_{3+N} can be formed by rotating the surface patch Σ_4 about Z axis by angles $(\frac{2\pi m}{N})°$ respectively, where $m \leftarrow 1 \ldots N$.

Planar End Geometry

The lip relief surface of a twist drill can also be formed as a plane or a combination of planes. The end geometry of the drill can be composed of single-plane per flute, two-plane per fluter or three planes per flute as discussed in [87]. End geometry of single plane per flute is employed commonly for drills below 3 mm diameter. Each lip relief surface for a N-fluted drill is formed as a single plane. For drill more than 3 mm diameter, end geometry consist of two planes per flute, one of these planes form land of the drill (Σ_4) and the other forms lip (Σ_5). For a N-fluted drill, there will be 2n planes at the cutting end of the drill (Σ_4 to Σ_{3+2n}).

For double-angle point drills, as shown in Figure 4.12. the end geometry is a combination of three planes per flute. One of these planes form land (Σ_4) and the other two form lip relief surfaces (Σ_5 and Σ_6). The edge of intersection of Σ_5 and Σ_6 passes through the drill axis and forms with the main lip an angle δ_0. The chisel edge is composed of two inclined edges with the center farthest from the z=0 plane. This enhances the drill operation at the beginning of cutting and improves the accuracy of drilling.

The plane forming land or lip is modeled as an infinite XY plane inclined at an angle β_i about Y axis, γ_i about Z axis and translated along Z axis by a distance that depends on lip length W and is equal to $-W \sin\gamma_i$.

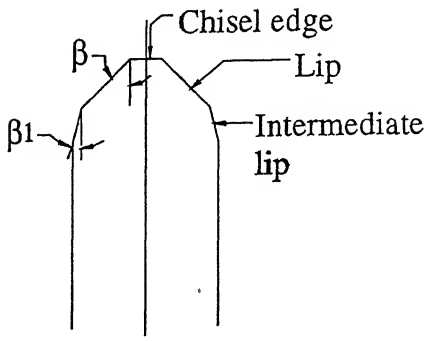

Figure 4.12: Double Angle Point Drill

4.3.2 Modeling of Shank

Drill body is composed of a shank that may be straight or tapered in geometry. Both types of shanks can be modeled as surfaces of revolution. For straight shank, an edge $\mathbf{e}(s)$ of length equal to specified shank length is revolved about Z axis by an angle 2π. The edge lies on the ZX plane at a distance $x = \frac{D_s}{2}$. The neck may also be modeled as a cylindrical surface of revolution. The tang and back end of the drill may be modeled as planar surfaces.

4.3.3 Mapping

This section establishes relations between conventional two-dimensional (2D) angles and rotational three-dimensional (3D) angles. The methodology of formation of conventional angles by the different surface patches constituting drill is shown in Mapping Guide Table (Table 4.13). The angles of twist drills as specified by conventional nomenclatures are shown in Figure 4.8.

Conventional Angles	Formed by	About the Plane	Plane of Projection
Half Point Angle, β	Σ_4	YZ	ZX
Chisel Edge Angle, ψ	Σ_4	ZX	XY
Relief Angle, α	Σ_4	XY	YZ
Helix Angle, λ	Σ_1	YZ	ZX
Peripheral Relief Angle, α_P	Σ_2	YZ	XY

Table 4.13: Mapping Guide Table for Drill

4.3.3.1 Forward Mapping

Lip relief surface (Σ_4) is formed by rotating an XY plane $[u_4 \quad v_4 \quad 0 \quad 1]$ by an angle β_4 about Y axis, followed by an angle γ_4 about Z axis, and then translating it by a distance $-W\sin\gamma_4$ about Z axis. According to the sign convention adopted in the present work, all three rotation angles γ_2, β_4 and γ_4 are positive and so are all the conventional 2D angles of the drill.

The mathematical definition of the Σ_4 may evolved as

$$\begin{aligned}\mathbf{p}_4(u_4, v_4) &= [u_4 \quad v_4 \quad 0 \quad 1].[R_{Y,\beta_4}].[R_{Z,\gamma_4}].[\mathbf{T}_{Z,d_{43}}] \\ &= [(u_4\cos\beta_4\cos\gamma_4 - v_4\sin\gamma_4) \quad (u_4\cos\beta_4\sin\gamma_4 + v_4\cos\gamma_4) \quad (-u_4\sin\beta_4 + d_{43}) \quad 1]\end{aligned}$$

The tangents to $\mathbf{p}_4$ along u_4 and v_4 directions are

$$\mathbf{p}_{4u}(u_4, v_4) = \cos\beta_4 \cos\gamma_4 \hat{\imath} + \cos\beta_4 \sin\gamma_4 \hat{\jmath} - \sin\beta_4 \hat{k}$$
$$\mathbf{p}_{4v}(u_4, v_4) = -\sin\gamma_4 \hat{\imath} + \cos\gamma_4 \hat{\jmath}$$

and normal to Σ_4 is $\mathbf{n}_4 = \sin\beta_4 \cos\gamma_4 \hat{\imath} + \sin\beta_4 \sin\gamma_4 \hat{\jmath} + \cos\beta_4 \hat{k}$

Half Point Angle (β)

The methodology of formation of half point angle β is shown in Table 4.13. To find β normal to Σ_4 shown above is projected on ZX plane and angle between unit vector of this projected normal vector and unit vector, normal to YZ plane ($\hat{\imath}$) is evaluated. Normal vector projected on ZX plane is given by $\mathbf{n}_{4p} = \sin\beta_4 \cos\gamma_4 \hat{\imath} + \cos\beta_4 \hat{k}$ and unit projected normal vector is given by $\hat{n}_{4p} = \mathbf{n}_{4p}/|\mathbf{n}_{4p}|$ Scalar product of $\hat{n}_{4p}$ and $\hat{\imath}$ gives the half point angle β as

$$\beta = \cos^{-1}\left[\frac{\sin\beta_4 \cos\gamma_4}{\sqrt{\sin^2\beta_4 \cos^2\gamma_4 + \cos^2\beta_4}}\right] \tag{4.37}$$

Chisel Edge Angle (ψ)

Chisel edge angle (ψ) is evaluated by projecting the angle between Σ_4 and ZX plane on XY plane. The normal to the surface Σ_4 on projection to XY plane is
$\mathbf{n}'_{4p} = \sin\beta_4 \cos\gamma_4 \hat{\imath} + \sin\beta_4 \sin\gamma_4 \hat{\jmath}$
The unit projected normal, then, is $\hat{n}'_{4p} = \cos\gamma_4 \hat{\imath} + \sin\gamma_4 \hat{\imath}$
The scalar product of $\hat{n}'_{4p}$ and unit vector $\hat{\jmath}$ leads to the chisel edge angle, as

$$\psi = 90° - \gamma_4 \tag{4.38}$$

Relief Angle (α)

The relation for the relief angle is established by projecting $\mathbf{n}_4$ on YZ plane, which can be given by $\mathbf{n}''_{4p} = \sin\beta_4 \sin\gamma_4 \hat{\jmath} + \cos\beta_4 \hat{k}$
Relief angle α is the angle between $\mathbf{n}''_{4p}$ and unit vector $\hat{k}$ and given by

$$\alpha = \cos^{-1}\left[\frac{\cos\beta_4}{\sqrt{\sin^2\beta_4 \sin^2\gamma_4 + \cos^2\beta_4}}\right] \tag{4.39}$$

Helix Angle (λ)

Helix angle (λ) is formed by Σ_1 and may be satisfied by the relation

$$\lambda = \tan^{-1}\left[\frac{P}{\pi D_c}\right] \tag{4.40}$$

Peripheral Relief Angle (α_p)

Peripheral relief angle is formed by the surface patch Σ_2 with XY plane which is formed by helically sweeping parametric edge formed by joining vertices V_1 and V_2. The edge is expressed by $\mathbf{e}_{14} = [(\frac{D_c}{2} - sl_1 \sin\gamma_2) \quad sl_1 \cos\gamma_2 \quad 0 \quad 1]$. The surface patch Σ_2 formed by sweeping $\mathbf{e}_{14}$, may be defined with the following relation

$\mathbf{p}_2(s,\phi) = [(e_{14x}\cos\phi - e_{14y}\sin\phi\} \quad (e_{14x}\sin\phi + e_{14y}\cos\phi) \quad \frac{P\phi}{2\pi} \quad 1]$

The tangents to surface patch at an arbitrary vertex are

$\mathbf{p}_{2s}(s,\phi) = -l_1\sin(\gamma_2+\phi)\hat{\imath} + l_1\cos(\gamma_2+\phi)\hat{\jmath}$

$\mathbf{p}_{2\phi}(s,\phi) = (-e_{14x}\sin\phi - e_{14y}\cos\phi)\hat{\imath} + (e_{14x}\cos\phi - e_{14y}\sin\phi)\hat{\jmath} + \frac{P}{2\pi}\hat{k}$

The vector normal to surface patch Σ_2 is

$\mathbf{n}_2 = \frac{Pl_1}{2\pi}\cos(\gamma_2+\phi)\hat{\imath} + \frac{Pl_1}{2\pi}\sin(\gamma_2+\phi)\hat{\jmath} + (\frac{D_c}{2}l_1\sin\gamma_2 - sl_1{}^2)\hat{k}$

This normal when projected on XY plane leads to an unit normal projected vector expressed by $\hat{n}_{2p} = \cos(\gamma_2+\phi)\hat{\imath} + \sin(\gamma_2+\phi)\hat{\jmath}$

Scalar product of $\hat{n}_{2p}$ with unit vector $\hat{\imath}$ gives $\cos\alpha_p = \cos(\gamma_2+\phi)$. At $z = 0$ plane, $\phi = 0$ and this leads to the mapping relation

$$\alpha_p = \gamma_2 \tag{4.41}$$

4.3.3.2 Inverse Mapping

This section presents the relations to map the known conventional 2D angles to unknown 3D angles. From the forward mapping, the relations for half point angle, chisel edge angle, relief angle and peripheral relief angle are given by Eq. (4.37), (4.38), (4.39) and (4.41) respectively. Using these equations the inverse relations for angles γ_4 and γ_2 are

$$\gamma_4 = 90^\circ - \psi \tag{4.42}$$

$$\gamma_2 = \alpha_p \tag{4.43}$$

Solving the Eq. (4.37), one gets

$$\beta_4 = \tan^{-1}\left[\frac{1}{\tan\beta\sin\psi}\right] \tag{4.44}$$

4.4 Example

This section presents an example on geometric modeling of a helical slab mill on the basis of 3D geometric parameters. The 3D parameters used to construct the model of slab mill is referred in *ANSI/ASME B*94.19 – 1985 standards [83]. The geometric parameters of the cutter used for rendering, to validate the approach of modeling of

cutters in terms of 3D parameters is presented in Table 4.14 [133, 134]. The resultant cutter is rendered in OpenGL environment [127, 132, 120, 121] and shown with the help of Figure 4.13.

Input Data for Slab Mill	
Dimensional Parameters	Value (mm)
Cutter Diameter(D)	80.0
Length of cutter(L)	120.0
Bore Diameter(d)	25.0
Root Diameter(D_R)	68.0
Number of Teeths(N)	16.0
Other Dimensional Parameters	Value (in mm)
Pitch(P)	1500.0
Length of Land(h)	15.0
Fillet Radius(R)	2.0
Rotational Angles	Value (in degrees)
γ_1	-10.0
γ_2	4.0
γ_3	18.0
γ_4	60.0

Table 4.14: Geometric Parameters of Helical Slab Mill

Figure 4.13: Rendering of a Helical Slab Mill

4.5 Case Study

This chapter illustrates the development of comprehensive 3D models of slab mills, end mills and drills. The input to the models are 3D geometric parameters. The models, thus, developed can be imported into any surface or solid modeling environment

and subjected to a wide range of down-stream applications. This section presents an exercise on finite element based engineering analysis (FEA) on the 3D model of the helical slab milling cutter. This case study highlights the advantages and utilities unfolded, once a comprehensive 3D definition of the cutter is available. The purpose here is not to present any detailed analysis of slab mill during machining. The 3D CAD model of slab mill is imported through ASCII file format in one of the commercial CAD/Analysis software and a wide range of analysis (e.g. static, dynamic, impact, fatigue, thermal etc.) for stress, wear, deflection etc. can be performed on it using the tools of the software. The present case study models the static and impact analysis carried out on the teeth of slab mill using I-DEAS [53].

In this example a solid helical slab mill of nominal diameter 80 mm (Figure 4.13) and machining a low alloy steel workpiece is assumed for the purpose of analysis. The slab mill is subjected to static and impact analysis. It is assumed that during machining two teeth are actually involved in cutting operation at a time and this is taken as the basis of loading of teeth as shown with the help of Figure 4.14. The load considered on each tooth is 140 MPa. The maximum load considered is based on the fact that the stresses developed in the slab mill should not exceed yield stress of the cutter material. The load is distributed on the two teeth based on the angles formed by the tooth from the bottom most point [13]. The angle formed by the first tooth is taken to be 5° and as the slab mill has 16 teeth, the angle formed by the second tooth is 27.5°. The ratio of tangential load to the radial load on the first tooth for this data comes out to be 7 : 3 and for the second tooth the ratio is 9.8 : 0.2. If the exact load on the cutter is known, which in turn depend upon the machine tool, then the distribution of load can be varied and simulated to simultaneously optimize the depth of cut and maximum number of teeth in operation.

The impact analysis can be useful for high speed machining applications. One can evaluate the maximum velocity at which cutter can move before hitting the workpiece. The cutter moving at 40,000 rpm is subjected to a impact time of 0.001 seconds. The damping ratio is taken to be 6% [53]. The fracture strength of the material is 50 MPa [15]. First four mode shapes of the slab mill are shown in Figure 4.15 and the stress and displacement distribution at one of the corners of the major cutting edge of slab mill is shown in Figure 4.16. When impact occurs at the major cutting edge of the slab mill, it is found through stress distribution at various points of the tooth of the cutter that the vulnerable edge is the edge of the fillet at root diameter (formed by vertex V_5). This can be attributed to cantilever effect.

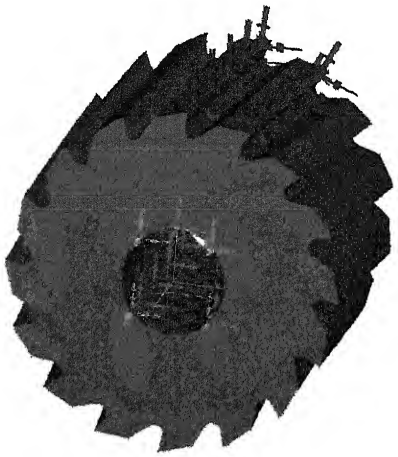

Figure 4.14: Loading of Slab Mill Teeth during machining

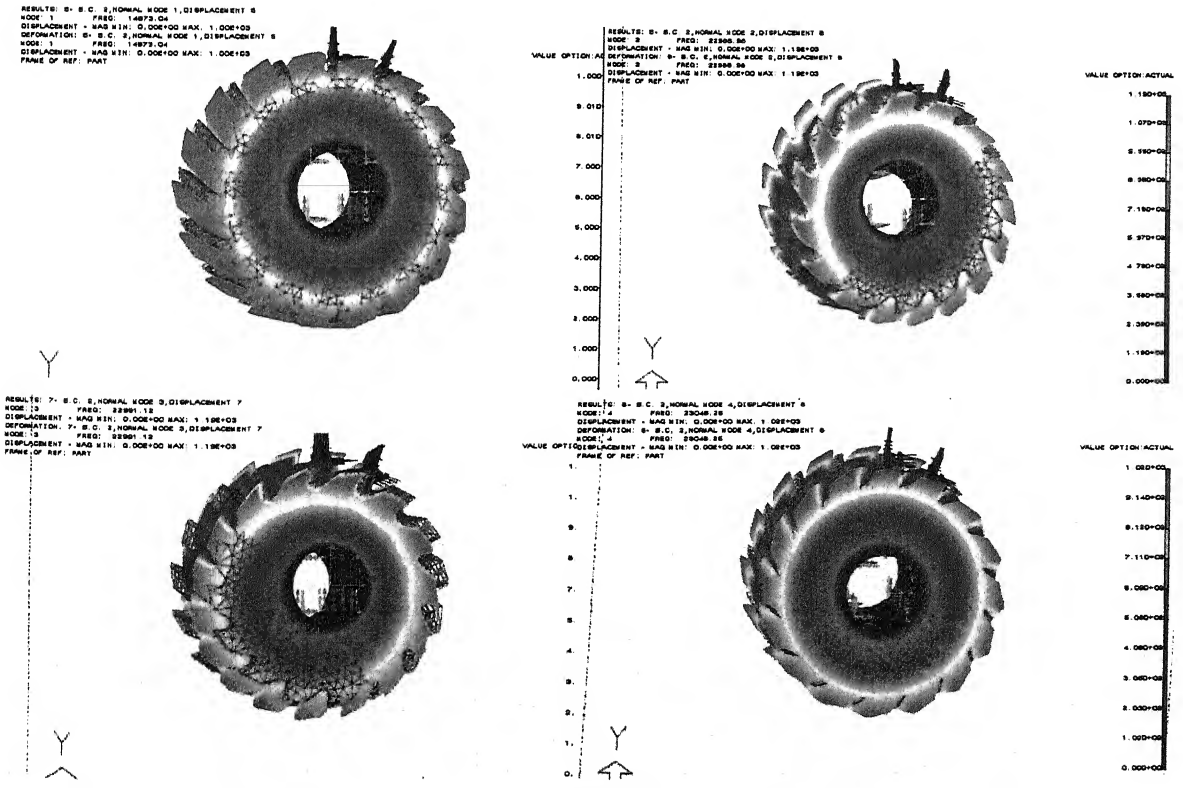

Figure 4.15: First Four Mode Shapes of Slab Mill

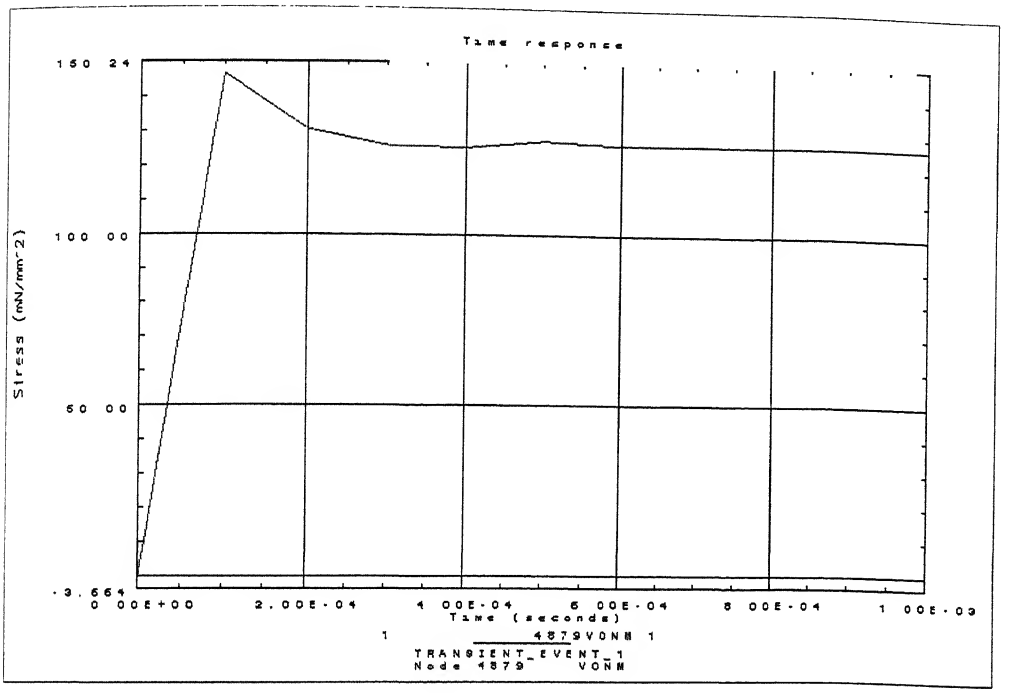

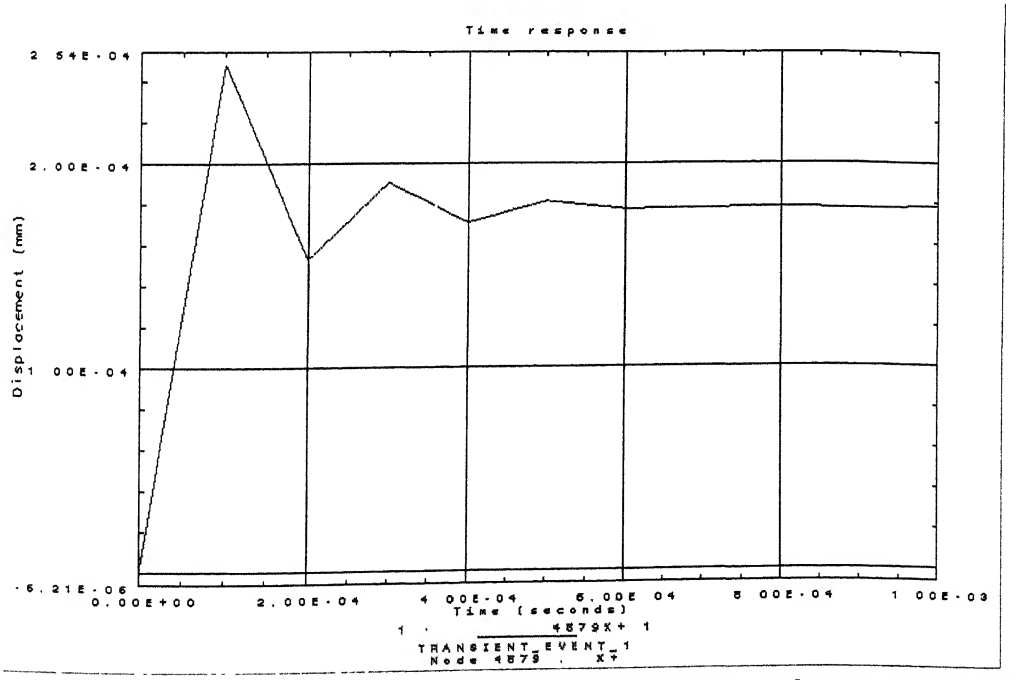

Figure 4.16: Stress and Displacement Distribution at the tip of Slab Mill

Chapter 5

INSERT-BASED CUTTERS

Many machining operations are performed with the cutters that use a small cutting insert, normally made of materials like carbide or ceramic. These inserts are generally mechanically locked to the cutter body with the help of wedges and clamps or brazed to it. These cutters are made with a cylindrical body of low-cost steel and grooves or slots are cut into the body for inserting the cutter teeth or blades. The major advantage of insert based cutters is that body of the cutter need not be replaced when the insert wears out. The insert has one or more cutting edges located at various corners and often on both sides of the inserts, or around the circumference in case of round inserts. When they become dull, they are repositioned to allow new cutting edges to take charge of cutting operation [13, 27, 29, 33, 48, 64, 77, 78, 44, 119].

The inserts may be available in wide variety of cutting materials and geometries. On the basis of geometry, inserts of various types and shapes are available. These include equilateral and equiangular inserts (square, hexagonal, pentagonal, triangular and octagonal), equilateral but not equiangular inserts (rhombic and trigon), non-equilateral but equiangular inserts (rectangular), non-equilateral and non-equiangular inserts (parallelogram) and round inserts. Further, these inserts may have holes of different shapes for fixing and chip breakers. Besides, there may be inserts with wiper edges for finishing operations [37, 128, 108, 133, 134, 135].

A variety of inserted cutters are used in milling operations. They may range from face milling cutters with one layer of inserts to multi-layered indexed cutters. The shape and distribution of inserts may significantly vary depending on the manufacturer and application. This chapter deals with indexable insert-based milling cutters and develops the geometric model for insert-based face mill. Face milling cutter is

preferred as it has no parallel among the solid cutters. An insert-based milling cutter is made up of (i) cutter body, (ii) inserts and (iii) spares and accessories that include axial support, wiper axial support, wedges for axial support and insert and wedge screws. This type of cutter is one of the most commonly used one and employs modular construction system which provides different types of cutters for different applications just by changing the insert, axial supports and clamping wedges that reduces the inventory cost drastically.

5.1 Surface Modeling of Body of Face Mill

The body of a insert-based milling cutter is considered to be made of two categories of surface patches, which are

(i) Surface patches constituting insert seat

(ii) Surface patches constituting core cutter body

For a general insert-based face milling cutter, the surface patches forming the insert seat are six in number, labeled Σ_1 to Σ_6, while there are twelve surface patches that form the core cutter body (Σ_{50} to Σ_{61}). Figure 5.1 and Figure 5.2 show the schematic two-dimensional layout of the face mill and surface patches forming the body of the cutter respectively. The surface patches comprising insert seat are geometrically modeled in a local coordinate system C_2, while those of core cutter body are modeled placing them in the global coordinate system C_1.

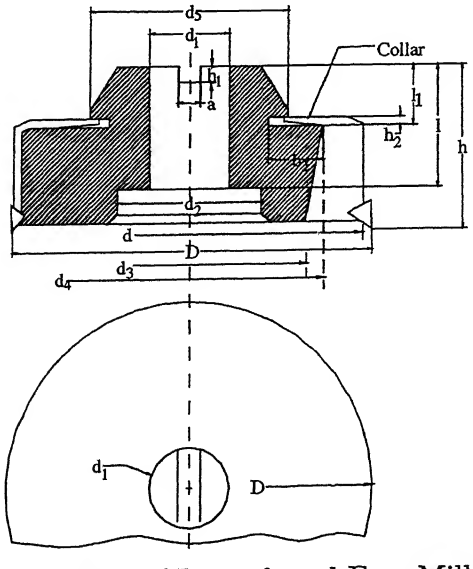

Figure 5.1: Projective View of Insert-based Face Milling Cutter

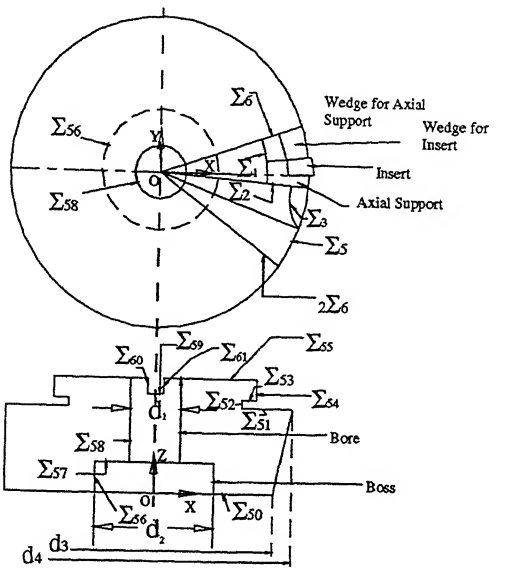

Figure 5.2: Surface Patches of the body of Inserted Face Mill

5.1.1 Geometric Modeling of Insert Seat Surface Patches

An insert seat is a cavity created in the cutter body to locate insert with the help of axial support and wedges. A group of six cutter body surfaces as shown in Figure 5.3 makes up a single insert seat. For a cutter having N inserts, the total number of surface patches becomes $6n$.

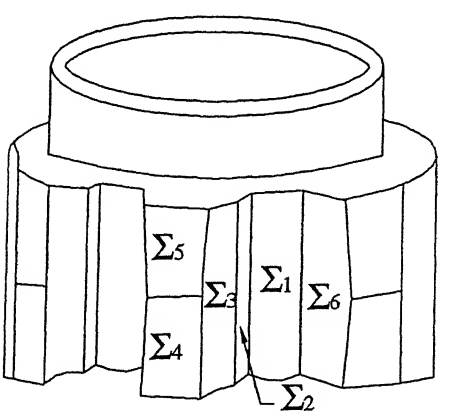

Figure 5.3: Surface Patches of the Insert Seat in Insert-based Face Mill

5.1.1.1 Seat for Axial Support and Wedge Σ_1

This is a conical surface patch and labeled as Σ_1. The axial support and wedge for axial support rests against it. The diameter of the cone is d_3 at the bottom and d_4 at the top, with height $(h-l_1)$, as shown in Figure 5.1 and Figure 5.2. The conical surface is modeled as a surface of revolution by rotating a straight edge by an angle θ. Let s_1 be the parameter along the edge and θ_s and θ_e are the starting and ending

angles of revolution, then parametric equation for surface patch Σ_1 may be presented as

$$\mathbf{p}_1(s_1,\theta) = [\{\frac{d_3}{2}+s_1\frac{d_4-d_3}{2}\}\cos\theta_1 \quad \{\frac{d_3}{2}+s_1\frac{d_4-d_3}{2}\}\sin\theta_1 \quad s_1(h-l_1) \quad 1] \quad (5.1)$$

where $\theta_s \leq \theta \leq \theta_e$ and $0 \leq s_1 \leq 1$. For a general design of a face mill, $\theta \approx 0.4\psi$, with $\theta_s \approx -0.0667\psi$ and $\theta_e \approx 0.3333\psi$ ($\psi = \frac{2\pi}{N}$, for N = number of inserts)

5.1.1.2 Side Rest for Axial Support Σ_2

This surface is a planar side surface of the insert seat and make the axial support rests on it (Figure 5.2). To model Σ_2, a ZX plane is rotated about Z axis by an angle γ_2 ($[R_{Z,\gamma_2}]$) ($\gamma_2 \approx -0.667\psi$ for general design) in clockwise direction. Thus, Σ_2 may be defined as

$$\begin{aligned}\mathbf{p}_2(u_2,w_2) &= [u_2 \quad 0 \quad w_2 \quad 1].[R_{Z,\gamma_2}] \\ &\quad [u_2\cos\gamma_2 \quad u_2\sin\gamma_2 \quad w_2 \quad 1]\end{aligned} \quad (5.2)$$

5.1.1.3 Cavity for Chip Disposal Σ_3

Surface Patch Σ_3 forms a cavity on the cutter body meant for chip disposal. This is formed as a cylindrical surface of radius R_1 and height $(h-l_1)$. The axis of the cylindrical surface is taken as perpendicular to XY plane and it is positioned at a distance of δ_1 from global Z axis making an angle of γ_2 with ZX plane. Surface patch Σ_3 is modeled by performing the following transformations in order.

(i) Revolve a straight vertical edge given by $[R_1 \quad 0 \quad w_3(h-l_1) \quad 1]$ $(0 \leq w_3 \leq 1)$ in counter-clockwise sense by an angle θ_3 $(\pi \leq \theta_3 \leq \pi+\zeta_2)$, with the axis of the surface of revolution passing through the origin. The angle for which the edge is revolved to form the cylindrical surface is evaluated and is given by ζ_2.

(ii) Rotate the resultant surface of revolution by an angle θ_3' $(= \gamma_2)$ about Z axis.

(iii) Translate the resultant surface on XY plane such that the axis of the cylindrical surface is now at a distance δ_1 from the Z axis.

The resultant surface of revolution Σ_3 becomes

$$\mathbf{p}_3(w_3,\theta_3) = [\{R_1\cos(\theta_3+\theta_3')+\delta_1\cos\theta_3'\} \quad \{R_1\sin(\theta_3+\theta_3')+\delta_1\sin\theta_3'\} \quad w_3(h-l_1) \quad 1] \quad (5.3)$$

The distance δ_1 is designers' prerogative and may be approximated to $(\frac{d}{2}+0.25R_1)$.

5.1.1.4 Surface Patch Σ_4

It is a planar surface and connects Σ_3 with side surface wall of the next insert seat against which wedges rest ${}^2\Sigma_6$. This surface is modeled by transforming suitably an infinite ZX plane $[u_4 \quad 0 \quad w_4 \quad 1]$ $(-\infty \leq u_4, w_4 \leq \infty)$. The transformations executed are

(i) rotation by an angle α_4 in counter-clockwise direction about X axis $[R_{X,\alpha_4}]$
(ii) rotating by γ_4 in counter-clockwise direction about Z axis $[R_{Z,\gamma_4}]$
(iii) translation by $R\sin\gamma_4$ along X axis and $-R\cos\gamma_4$ along Y axis $[T_{XY}]$

The resultant surface Σ_4 is thus evolved as

$$\begin{aligned}\mathbf{p}_4(u_4, w_4) \;=\; & [\{u_4\cos\gamma_4 + w_4\sin\alpha_4\sin\gamma_4 + R\sin\gamma_4\} \\ & \{u_4\sin\gamma_4 - w_4\sin\alpha_4\cos\gamma_4 - R\cos\gamma_4\} \quad w_4\cos\alpha_4 \quad 1] \end{aligned} \tag{5.4}$$

5.1.1.5 Surface Patch Σ_5

This surface is also a planar surface and together with surface Σ_4 completes the surface model in between cavity for chip disposal and the side surface of the seat for wedges of next insert, as shown in Figure 5.3. It is modeled by performing following transformations on a ZX plane $[u_5 \quad 0 \quad w_5 \quad 1]$ $(-\infty \leq u_5, w_5 \leq \infty)$:

(i) rotation by an angle α_5 about X axis in clockwise direction $[R_{X,\alpha_5}]$
(ii) rotating by γ_5 about Z axis in counter-clockwise direction $[R_{Z,\gamma_5}]$
(iii) translation by $R\sin\gamma_5$ along X axis and $-R\cos\gamma_5$ along Y axis $[T'_{XY}]$

The resultant surface Σ_5 is becomes

$$\begin{aligned}\mathbf{p}_5(u_5, w_5) \;=\; & [\{u_5\cos\gamma_5 + w_5\sin\alpha_5\sin\gamma_5 + R\sin\gamma_5\} \quad \{u_5\sin\gamma_5 - w_5\sin\alpha_5\cos\gamma_5 \\ & -R\cos\gamma_5\} \quad \{w_5\cos\alpha_5 + (h - l_1)\} \quad 1] \end{aligned} \tag{5.5}$$

5.1.1.6 Side Surface of the Seat for Wedges Σ_6

Surface patch Σ_6 is a flat plane formed by rotating a ZX plane by an angle γ_6 about Z axis in clockwise direction and can be expressed by the relation

$$\mathbf{p}_6(u_6, w_6) = [u_6\cos\gamma_6 \quad u_6\sin\gamma_6 \quad w_6 \quad 1] \tag{5.6}$$

where $-\infty \leq u_6, w_6 \leq \infty$ and for a general design of face mill, $\gamma_6 = 0.333\psi$

5.1.2 Modeling of Surface Patches of Core Cutter Body

The surface patches that joins all the insert seats and completes the body of face mill are identified as surface patches of core cutter body. For a face mill body, these are twelve in number and they are shown explicitly in Figure 5.2. The modeling of their geometry is shown herewith.

Surface Patch Σ_{50}

This type of planar surface lies at the cutting end side of face mill and closes the surface model of all the insert seats at that end. Σ_{50} is parallel to the workpiece surface to be machined and separated by it by the projection of the insert. The mathematical definition of the surface Σ_{50} can be given by

$$\mathbf{p}_{50}(u_{50}, v_{50}) = [u_{50} \quad v_{50} \quad 0 \quad 1], \text{ for } -\infty \leq u_{50}, v_{50} \leq \infty$$

Surface Patch Σ_{51}

Surface patch Σ_{51} like Σ_{50} is also a planar surface and closes the surface model of the insert seats at opposite to cutter end. It is the bottom surface of collar, where axial supports rest. It is formed by translating an infinite XY plane along Z axis by a distance $(h - l_1)$. The equation of Σ_{51} is

$$\mathbf{p}_{51}(u_{51}, v_{51}) = [u_{51} \quad v_{51} \quad (h - l_1) \quad 1], \text{ where } -\infty \leq u_{51}, v_{51} \leq \infty$$

Surface Patch Σ_{52}

This is the cylindrical side wall of the collar, which supports the axial support for the insert. It is formed as a surface of revolution by rotating a straight edge formed by joining vertices, given by the coordinates $(\frac{d_4}{2} - b_2, 0, h - l_1)$ and $(\frac{d_4}{2} - b_2, 0, h - l_1 + h_2)$. The parametric equation of the edge to be rotated in terms of parameter w_{52} is $[(\frac{d_4}{2} - b_2) \quad 0 \quad w_{52}(h - l_1 + h_2) \quad 1]$ and that of the surface patch Σ_{52} is

$$\mathbf{p}_{52}(w_{52}, \theta_{52}) = [(\tfrac{d_4}{2} - b_2)\cos\theta_{52} \quad (\tfrac{d_4}{2} - b_2)\sin\theta_{52} \quad \{(h - l_1) + w_{52}h_2\} \quad 1]$$
$$\text{where } 0 \leq w_{52} \leq 1 \text{ and } 0 \leq \theta_{52} \leq 2\pi$$

Surface Patch Σ_{53}

This is formed by positioning an XY plane at $z = (h - l_1 + h_2)$ and is expressed with

$$\mathbf{p}_{53}(u_{53}, v_{53}) = [u_{53} \quad v_{53} \quad (h - l_1 + h_2) \quad 1], \text{ where } -\infty \leq u_{53}, v_{53} \leq \infty$$

Surface Patch Σ_{54}

A cylindrical surface of diameter d_5 and height $(l - h_1)$ forming the portion above the collar of the cutter body is named as Σ_{54}. It may be expressed by

$$\mathbf{p}_{54}(w_{54}, \theta_{54}) = [\tfrac{d_5}{2}\cos\theta_{54} \quad \tfrac{d_5}{2}\sin\theta_{54} \quad \{(h - l_1 + h_2) + w_{54}(l_1 - h_2)\} \quad 1]$$
$$\text{for } 0 \leq w_{54} \leq 1 \text{ and } 0 \leq \theta_{54} \leq 2\pi$$

Surface Patches Σ_{55}, Σ_{57} and Σ_{59}

As shown in Figure 5.2, surface Σ_{55} is the top surface of the face mill, opposite to cutting end, Σ_{57} is the top surface of the boss and Σ_{59} is the bottom surface of the keyway. These are all planar surfaces and modeled by placing an infinite XY plane at $z = h$, $(h - l)$ and $(h - h_1)$ respectively. Following relations express them parametrically for $(-\infty \leq u_{55}, v_{55}, u_{57}, v_{57}, u_{59}, v_{59} \leq \infty)$.

$$\begin{aligned}
\mathbf{p}_{55}(u_{55}, v_{55}) &= [u_{55} \quad v_{55} \quad h \quad 1] \\
\mathbf{p}_{57}(u_{57}, v_{57}) &= [u_{57} \quad v_{57} \quad (h-l) \quad 1] \\
\mathbf{p}_{59}(u_{59}, v_{59}) &= [u_{59} \quad v_{59} \quad (h-h_1) \quad 1]
\end{aligned}$$

Surface Patches Σ_{56} and Σ_{58}

Figure 5.2 shows that surfaces Σ_{56} and Σ_{58} are both cylindrical surfaces, whereas former represents surface of boss and later that of bore. Both are modeled as surfaces of revolution. Boss is of diameter d_2 and height $(h-l)$, ranging from $z = 0$ to $(h-l)$ planes, while the bore is of diameter d_1 and height l, varying from $z = (h - l)$ to h. They may be mathematically expressed as

$$\begin{aligned}
\mathbf{p}_{56}(w_{56}, \theta_{56}) &= [\frac{d_2}{2}\cos\theta_{56} \quad \frac{d_2}{2}\sin\theta_{56} \quad w_{56}(h-l)\} \quad 1] \\
\mathbf{p}_{58}(w_{58}, \theta_{58}) &= [\frac{d_1}{2}\cos\theta_{58} \quad \frac{d_1}{2}\sin\theta_{58} \quad \{(h-l)+w_{58}l\} \quad 1]
\end{aligned}$$

where $0 \leq w_{56}, w_{58} \leq 1$ and $0 \leq \theta_{56}, \theta_{58} \leq 2\pi$

Surface Patches Σ_{60} and Σ_{61}

Surfaces Σ_{60} and Σ_{61} form the two side walls of the keyway. They are planar surfaces and modeled by placing YZ planes at $x = -\frac{a}{2}$ and $x = \frac{a}{2}$ distances respectively

$$\begin{aligned}
\mathbf{p}_{60}(v_{60}, w_{60}) &= [-\frac{a}{2} \quad v_{60} \quad w_{60} \quad 1] \\
\mathbf{p}_{61}(v_{61}, w_{61}) &= [\frac{a}{2} \quad v_{61} \quad w_{61} \quad 1]
\end{aligned}$$

for $-\infty \leq v_{60}, w_{60}, v_{61}, w_{61} \leq \infty$

5.2 Blending Surfaces of Face Mill Cutter Body

An intersection of two surface patches leads to a sharp edge. In the case of body of a face mill, most of the sharp edges do not play any functional role except those defining insert seat surfaces for proper clamping of insert. The sharp edges on the body of the

cutter are further not desired so as to prevent injury to the worker and avoid damage to cutter. For a face mill body, eight transitional surface patches are identified, shown in Figure 5.4, which blend the sharp edges. These transitional surfaces can be in the form of surface of revolutions or chamfers, as listed below

(A) Blending surfaces as surface of revolution:
  (i) Blending surface between Σ_1 and Σ_{51} – $\sigma_{1,51}$
  (ii) Blending surface between Σ_5 and Σ_{51} – $\sigma_{5,51}$
  (iii) Blending surface between Σ_{54} and Σ_{55} – σ_{b45}
  (iv) Blending surface between Σ_{55} and Σ_{58} – σ_{b58}
  (v) Blending surface between Σ_{50} and Σ_{56} – σ_{b06}
  (vi) Blending surface between Σ_{57} and Σ_{58} – σ_{b78}

(B) Blending surfaces in the shape of a planar chamfered surface
  (i) Blending surface between Σ_{55} and Σ_{60} – $\sigma_{b5,10}$
  (ii) Blending surface between Σ_{55} and Σ_{61} – $\sigma_{b5,11}$

Blending surfaces A–(i) and A–(ii) are the blending surfaces for the insert seat, while rest of them are for the core cutter body.

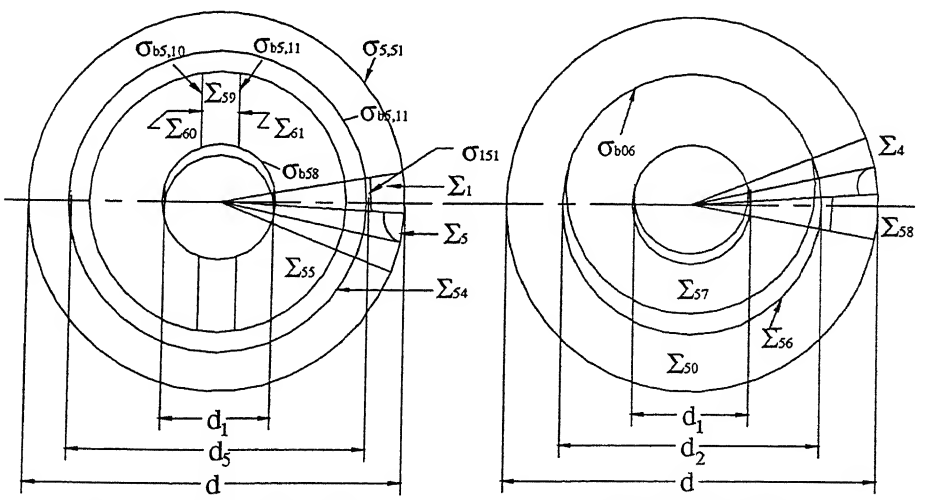

Figure 5.4: Face Mill Blending Surfaces

Blending Surface $\sigma_{1,51}$

This transitional surface blends the surface Σ_1 of the insert seat and the circular disk forming the bottom surface of the collar (Σ_{51}), where axial support rests. It is a conical chamfer surface and presumed to be a 45° chamfer of unit height. Any other

type of chamfered surface can be suitably modeled by altering the relevant data. This surface is formed by rotating an edge given by the vertices ($(\frac{d_4}{2}-0.707)$, 0, $(h-l_1)$) and ($\frac{d_4}{2}$, 0, $(h-l_1-0.707)$) lying on the ZX plane, about global Z axis. The parametric equation for the surface patch $\sigma_{1,51}$ is evolved as

$\mathbf{p}_{1,51}(u_{b1}, \theta_{b1}) = [\ \{\frac{d_4}{2}-0.707(1-u_{b1})\}\cos\theta_{b1} \quad \{\frac{d_4}{2}-0.707(1-u_{b1})\}\sin\theta_{b1}$
$(h-l_1-0.707u_{b1}) \quad 1]$ where $0 \leq u_{b1} \leq 1$ and $\gamma_2 \leq \theta_{b1} \leq \gamma_6$

Blending Surface $\sigma_{5,51}$

It blends the surface Σ_5 of the insert seat and the bottom surface of the collar (Σ_{51}). It is also a conical 45° chamfer of unit length. This surface is formed by rotating an edge formed by joining the vertices given by the coordinates ($(\frac{d}{2}-0.707)$, 0, $(h-l_1)$) and ($\frac{d}{2}$, 0, $(h-l_1-0.707)$) lying on ZX plane about global Z axis.

$\mathbf{p}_{5,51}(u_{b2}, \theta_{b2}) = [\ \{\frac{d}{2}-0.707(1-u_{b2})\}\cos\theta_{b2} \quad \{\frac{d}{2}-0.707(1-u_{b2})\}\sin\theta_{b2}$
$(h-l_1-0.707u_{b2}) \quad 1]$

where $0 \leq u_{b2} \leq 1$ and $\theta_s \leq \theta_{b2} \leq \theta_e$. The angles θ_s and θ_e are designers' prerogative and for a general design of face mill $\theta_s \approx 0.3667\psi$ and $\theta_e \approx 0.6667\psi$

Blending Surface σ_{b45}

This surface blends the surfaces Σ_{54} and Σ_{55} of the core cutter body in the form of a surface of revolution, formed by rotating an edge of unit length at 45° on ZX plane about Z axis. The edge is formed by joining the vertices ($(\frac{d_5}{2}-0.707)$, 0, h) and ($\frac{d_5}{2}$, 0, $(h-0.707)$). The chamfer σ_{b45} as a surface of revolution is represented by

$\mathbf{p}_{b45}(u_{b3}, \theta_{b3}) = [\{\frac{d_5}{2}-0.707(1-u_{b3})\}\cos\theta_{b3} \quad \{\frac{d_5}{2}-0.707(1-u_{b3})\}\sin\theta_{b3} \quad (h-0.707u_{b3}) \quad 1] \qquad (0 \leq u_{b3} \leq 1 \text{ and } 0 \leq \theta_{b3} \leq 2\pi)$

Blending Surface σ_{b58}

This is also a chamfered surface of revolution similar to blending surfaces discussed above and blends Σ_{55} and Σ_{58}. The edge that is rotated to form the blend joins vertices ($\frac{d_1}{2}$, 0, $(h-0.707)$) and ($(\frac{d_1}{2}+0.707)$, 0, h). The blending surface is

$\mathbf{p}_{b58}(u_{b4}, \theta_{b4}) = [(\frac{d_1}{2}+0.707u_{b4})\cos\theta_{b4} \quad (\frac{d_1}{2}+0.707u_{b4})\sin\theta_{b4} \quad \{h-0.707(1-u_{b4})\} \quad 1]$

where $0 \leq u_{b4} \leq 1$ and $\begin{matrix}(\frac{3\pi}{2}+\phi)\\(\frac{\pi}{2}+\phi)\end{matrix} \leq \theta_{b4} \leq \begin{matrix}(\frac{\pi}{2}-\phi)\\(\frac{3\pi}{2}-\phi)\end{matrix}$

Blending Surface σ_{b06}

It is a 45° chamfered surface of revolution of unit width and blends surfaces Σ_{50} and Σ_{56}. The blending surface σ_{b06} is formed by rotating an edge given by the vertices $(\frac{d_2}{2},\ 0,\ 0.707)$ and $(\ (\frac{d_2}{2}+0.707),\ 0,\ 0)$.

$\mathbf{p}_{b06}(u_{b5}, \theta_{b5}) = [(\frac{d_2}{2}+0.707u_{b5})\cos\theta_{b5} \quad (\frac{d_2}{2}+0.707u_{b5})\sin\theta_{b5} \quad 0.707(1-u_{b5}) \quad 1]$

where $0 \leq u_{b5} \leq 1$ and $0 \leq \theta_{b5} \leq 2\pi$

Blending Surface σ_{b78}

This transitional surface blends surfaces Σ_{57} and Σ_{58}. It is also similar to the above defined blending surfaces and is modeled by rotating an edge lying on ZX plane about Z axis, given by joining vertices $(\frac{d_1}{2},\ 0,\ (h-l+0.707)\ )$ and $(\ (\frac{d_1}{2}+0.707),\ 0,\ (h-l)\ )$.

$\mathbf{p}_{b78}(u_{b6}, \theta_{b6}) = [(\frac{d_1}{2}+0.707u_{b6})\cos\theta_{b6} \quad (\frac{d_1}{2}+0.707u_{b6})\sin\theta_{b6} \quad \{h-l+0.707(1-u_{b6})\} \quad 1]$

where $0 \leq u_{b6} \leq 1$ and $0 \leq \theta_{b6} \leq 2\pi$

Blending Surface $\sigma_{b5,10}$

This transitional surface is a planar 45° chamfer surface and is modeled by sweeping linearly an edge of unit width lying on ZX plane and inclined at 45° to X axis, along Y axis. The edge to be swept is defined by vertices given by the coordinates $(-(\frac{b}{2}+0.707),\ 0,\ h)$ and $(-\frac{b}{2},\ 0,\ (h-0.707)\ )$. The surface $\sigma_{b5,10}$ may be defined by the parametric expression

$\mathbf{p}_{b5,10}(u_{b7}, v_{b7}) = [-\{\frac{b}{2}+0.707(1-u_{b7})\} \quad \{\pm\frac{d_1}{2}\cos\phi_1 \pm v_{b7}(\frac{d_5}{2}\cos\phi_2 - \frac{d_1}{2}\cos\phi_1)\}$
$(h-0.707u_{b7}) \quad 1]$

where $0 \leq u_{b7}, v_{b7} \leq 1$, $\phi_1 = \sin^{-1}\left(\frac{b}{d_1}\right)$ and $\phi_2 = \sin^{-1}\left(\frac{b}{d_5}\right)$

Blending Surface $\sigma_{b5,11}$

This is mirror image of blending surface $\sigma_{b5,10}$ about YZ plane and hence is given as

$\mathbf{p}_{b5,11}(u_{b8}, v_{b8}) = [\{\frac{b}{2}+0.707(1-u_{b8})\} \quad \{\pm\frac{d_1}{2}\cos\phi_1 \pm v_{b8}(\frac{d_5}{2}\cos\phi_2 - \frac{d_1}{2}\cos\phi_1)\}$
$(h-0.707u_{b8}) \quad 1]$

where $0 \leq u_{b8}, v_{b8} \leq 1$, $\phi_1 = \sin^{-1}\left(\frac{b}{d_1}\right)$ and $\phi_2 = \sin^{-1}\left(\frac{b}{d_5}\right)$

5.3 Modeling of Inserts

In the case of an insert type cutter, the cutting teeth of the solid type cutter are replaced with the inserts. Here, the body of the cutter is made of one piece of

material and the cutting inserts are of different materials and various types. The actual roughing or finishing operation is performed by mechanically retained, and/or adjustable, solid or hard alloy-tipped tooth or blade [27, 29, 33, 44].

For a inserted-tooth cutter, proper insert selection is an important task. A few key factors responsible for making correct insert selection are [134]:

(i) **Cutter compatability** – indicates the size and shape of insert which a cutter can accommodate

(ii) **Part specifications** – guides whether the insert should have corner radius or chamfer or wiper for finishing

(iii) **Economy**

(iv) **Cutting edge angle** – depth of cut and the number of passes in which the stock is to be removed are influenced by this angle of insert

(v) **Edge preparation** – type of edge - sharp/rounded/chamfered or combination depends on the application and it influences the tool life

The inserts are available in various geometries and sizes as discussed earlier. Each insert type has to be uniquely identifiable. The inserts are classified by a standard code containing nine alphanumeric fields, known as ISO designation [130, 134]. The ISO designation for an indexable insert looks like

Field	1	2	3	4	5	6	7	8	9
Parameter	Type and Shape	Normal Clearance	Tolerance Class	Fixing and/or Chip Breakers	Inscribed circle dia	Thickness	Insert corner configuration	Major cutting edge (optional)	Hand of Insert

Table 5.1: ISO Designation for Indexable Inserts

5.3.1 Geometric Modeling of a Unified Square Insert

The square shaped insert (equilateral and equiangular insert) is the most common of all milling inserts. All the four sides of a square insert can be used for machining. Different variants of a square shape insert exist depending upon other field parameters of the ISO designation.

In this work, geometric model of a unified square insert is developed. The square insert considered here is generic in nature, and includes the geometric features of all available varieties of square inserts. The unified insert, as shown in Figure 5.5 has

both the planishing surfaces (Σ_{I7}, Σ_{I10}, Σ_{I11} and Σ_{I14}) and the surfaces containing auxiliary cutting edges (Σ_{I8}, Σ_{I9}, Σ_{I12} and Σ_{I13}). Besides, these surfaces are also rounded off to form transitional surfaces. Figure 5.6 shows the three-dimensional view of the unified square shaped insert. For the purpose of developing the geometric model of the insert surfaces, the insert is placed in a local right-handed Cartesian coordinate system O_L–$X_LY_LZ_L$. For a unified insert model there are fifteen surface patches identified, while there are six transitional surfaces. Not all surfaces are present in an actual square insert. Depending upon, whether one or more of the parameters, width of planishing surface b_{I1}, width of the auxiliary cutting edge b_{I2}, radius of blend r_I or diameter of cylindrical hole d_{I1}, are equal or not equal to zero, different types of square inserts are generated [134]. For example, if

(i) $r_I = d_{I1} = 0$ and $b_{I1} \neq b_{I2} \neq 0$, then the inserts as per ISO designation are SPAN... or SPKN...

(ii) $b_{I2} = r_I = d_{I1} = 0$ and $b_{I1} \neq 0$, then the insert types may be SEAN.../SFAN...

(iii) the length $l_{I1} > l_I - 2(b_{I1}+b_{I2})\cos 15°$, then the inserts may be SPCX.../SECX...

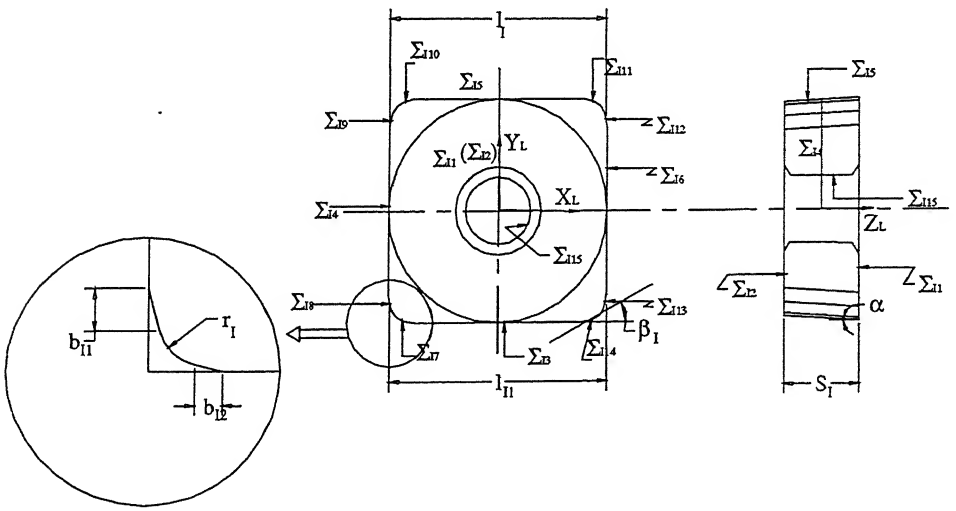

Figure 5.5: Projective Geometry of a Unified Square Insert

All the surfaces of the square insert are planar in geometry, as per Figure 5.5 except the surface patch Σ_{I15}, which is a cylindrical surface. The parametric definition of each of the fifteen surface patches forming the unified square insert, as illustrated in Figure 5.5, is presented herewith.

Surface Patch Σ_{I1}

This surface is formed by translating ($[\mathbf{T}_{z,d_{13}}]$) an X_LY_L plane along Z_L axis by a distance $d_{13} = \frac{S_I}{2}$, where S_{I2} is the thickness of the insert. Therefore,

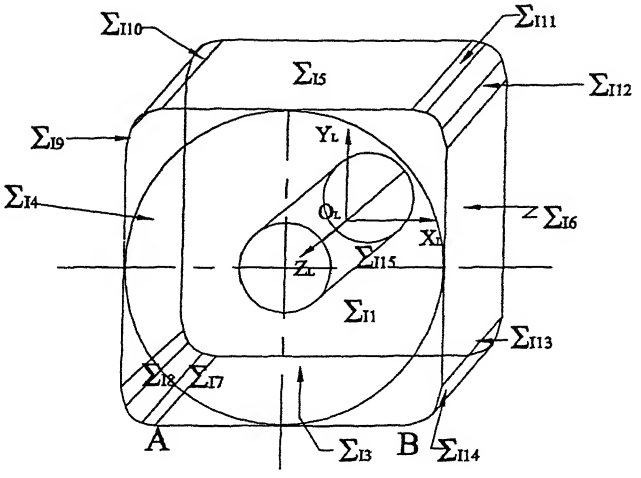

Figure 5.6: A Unified Square Insert

$$\Sigma_{I1} = \mathbf{p}_{I1}(u_1, v_1) = [u_1 \quad v_1 \quad 0 \quad 1].[\mathbf{T}_{z,d_{13}}]$$
$$= [u_1 \quad v_1 \quad d_{13} \quad 1], \quad \text{where } -\infty \leq u_1, v_1 \leq \infty$$

Surface Patch Σ_{I2}

It is formed when the X_LY_L plane is translated along Z_L axis by a distance $d_{23} = -\frac{S_I}{2}$
$\mathbf{p}_{I2}(u_2, v_2) = [u_2 \quad v_2 \quad d_{23} \quad 1]$, where $-\infty \leq u_2, v_2 \leq \infty$

Surface Patch Σ_{I3}

When the Z_LX_L plane is rotated by an angle α_3 about X_L axis ($[\mathbf{R}_{x,\alpha_3}]$) and then translated along Y_L axis by a distance $d_{32} = -(\frac{d_I}{2} - \frac{S_I}{2}\tan\alpha_3)$ ($[\mathbf{T}_{y,d_{32}}]$), surface patch Σ_{I3} of the square insert is formed. The angle α_3 is equal to clearance angle of main cutting edge for insert and depends on designers' discretion. The translation $[\mathbf{T}_{y,d_{32}}]$ positions the front edge of the surface Σ_{I3} (AB) (Figure 5.6) at a distance of $\frac{d_1}{2}$ from the insert axis.

$$\Sigma_{I3} = \mathbf{p}_{I3}(u_3, w_3) = [u_3 \quad 0 \quad w_3 \quad 1].[\mathbf{R}_{x,\alpha_3}].[\mathbf{T}_{y,d_{32}}]$$
$$= [u_3 \quad (-w_3 \sin\alpha_3 + d_{32}) \quad w_3 \cos\alpha_3 \quad 1]$$

where $-\infty \leq u_3, w_3 \leq \infty$ and $\alpha_3 \geq 0$

Surface Patch Σ_{I4}

This is formed by rotating Y_LZ_L plane by an angle $\beta_4 \leq 0$, about Y_L axis ($[\mathbf{R}_{y,\beta_4}]$), followed by translation along X_L axis by $d_{41} = -(\frac{l_I}{2} + \frac{S_I}{2}\tan\beta_4)$ ($[\mathbf{T}_{x,d_{41}}]$). The rotation angle β_4 here, and subsequent rotation angles α_5 and β_6 are meant to provide draft angle to the insert for clearance of its main cutting edge.

$\mathbf{p}_{I4}(v_4, w_4) = [(w_4 \sin\beta_4 + d_{41}) \quad v_4 \quad w_4 \cos\beta_4 \quad 1] \quad (-\infty \leq v_4, w_4 \leq \infty)$

Surface Patch Σ_{I5}

It is formed by transforming a $Z_L X_L$ plane through (i) rotation by an angle α_5 about X_L axis ($[\mathbf{R}_{x,\alpha_5}]$) and (ii) translation along Y_L axis by $d_{52} = (\frac{d_I}{2} + \frac{S_I}{2}\tan\alpha_5)$ ($[\mathbf{T}_{y,d_{52}}]$).
$\mathbf{p}_{I5}(u_5, w_5) = [u_5 \quad (-w_5 \sin\alpha_5 + d_{52}) \quad w_5 \cos\alpha_5 \quad 1](-\infty \leq u_5, w_5 \leq \infty;\ \alpha_5 \leq 0)$

Surface Patch Σ_{I6}

The $Y_L Z_L$ plane rotated by an angle β_6 about Y_L axis ($[\mathbf{R}_{y,\beta_6}]$) and then translated along X_L axis by $d_{61} = (\frac{l_I}{2} - \frac{S_I}{2}\tan\beta_6)$ ($[\mathbf{T}_{x,d_{61}}]$) forms Σ_6.
$\mathbf{p}_{I6}(v_6, w_6) = [(w_6 \sin\beta_6 + d_{61}) \quad v_6 \quad w_6 \cos\beta_6 \quad 1] \quad (-\infty \leq v_6, w_6 \leq \infty)$

Surface Patch Σ_{I7}

A $Z_L X_L$ plane rotated by an angle γ_7 about Z_L axis ($[\mathbf{R}_{z,\gamma_7}]$, $\gamma_7 \leq 0$) and translated by distances $d_{72} = -\frac{d_I}{2}$ along Y_L axis and $d_{71} = -\frac{l_{I1}}{2}$ along X_L axis forms Σ_7. The angle γ_7 gives inclination to planishing surface wrt $Z_L X_L$ plane and is equal to the angle β shown in Figure 5.5.
$\Sigma_{I7} = \mathbf{p}_{I7}(u_7, w_7) = [(u_7 \cos\gamma_7 + d_{71}) \quad (u_7 \sin\gamma_7 + d_{72}) \quad w_7 \quad 1] \quad (-\infty \leq u_7, w_7 \leq \infty)$

Surface Patch Σ_{I8}

It is formed by rotating a $Y_L Z_L$ plane by γ_8 about Z_L axis ($[\mathbf{R}_{z,\gamma_8}]$) and translating it by a distance $d_{81} = -\frac{l_I}{2}$ along X_L axis and $d_{82} = -\frac{l_{I1}}{2}$ along Y_L axis. The angle γ_8 inclines auxiliary cutting surface wrt $Z_L X_L$ plane.
$\mathbf{p}_{I8}(v_8, w_8) = [(-v_8 \sin\gamma_8 + d_{81}) \quad (v_8 \cos\gamma_8 + d_{82}) \quad w_8 \quad 1] \quad (-\infty \leq v_8, w_8 \leq \infty)$

Surface Patch Σ_{I9}

Surface patch Σ_{I9} can also acts as an auxiliary cutting surface and is similar to surface Σ_{I8}. This is formed when $Y_L Z_L$ plane is rotated by an angle γ_9 about Z_L axis ($[\mathbf{R}_{z,\gamma_9}]$) and translated by d_{91} and d_{92} along X_L and Y_L axes respectively, where $d_{91} = -\frac{l_I}{2}$ and $d_{92} = \frac{l_{I1}}{2}$.
$\mathbf{p}_{I9}(v_9, w_9) = [(-v_9 \sin\gamma_9 + d_{91}) \quad (v_9 \cos\gamma_9 + d_{92}) \quad w_9 \quad 1] \quad (-\infty \leq v_9, w_9 \leq \infty)$

Surface Patch Σ_{I10}

Surface patch Σ_{I10} may be used as planishing surface when that side of the insert is used for cutting and is similar in geometry to surface Σ_{I7}. This may be modeled by taking reflection of surface Σ_{I7} about $Z_L X_L$ plane.
$\mathbf{p}_{I10}(u_{10}, w_{10}) = [(u_{10} \cos\gamma_{10} + d_{101}) \quad (u_{10} \sin\gamma_{10} + d_{102}) \quad w_{10} \quad 1] \quad (-\infty \leq u_{10}, w_{10} \leq \infty)$

Surface Patch Σ_{I11}

When a $Z_L X_L$ plane is rotated by γ_{11} about Z_L axis ($[\mathbf{R}_{z,\gamma_{11}}]$, $\gamma_{11} \leq 0$) and translated by distances $d_{112} = \frac{d_I}{2}$ along Y_L axis and $d_{111} = \frac{l_{I1}}{2}$ along X_L axis, it forms Σ_{I11}.
$\mathbf{p}_{I11}(u_{11}, w_{11}) = [(u_{11} \cos\gamma_{11} + d_{111}) \quad (u_{11} \sin\gamma_{11} + d_{112}) \quad w_{11} \quad 1] \quad (-\infty \leq u_{11}, w_{11} \leq \infty)$

Surface Patch Σ_{I12}

Similar to patches Σ_8 and Σ_9, surface Σ_{I12} is modeled when $Y_L Z_L$ plane is rotated by angle γ_{12} about Z_L axis ($[\mathbf{R}_{z,\gamma_{12}}]$) and translated by $d_{121} = \frac{l_I}{2}$ and $d_{122} = \frac{l_{I1}}{2}$ along X_L and Y_L axes respectively.

$\mathbf{p}_{I12}(v_{12}, w_{12}) = [(-v_{12}\sin\gamma_{12}+d_{121}) \quad (v_{12}\cos\gamma_{12}+d_{122}) \quad w_{12} \quad 1] \quad (-\infty \leq v_{12}, w_{12} \leq \infty)$

Surface Patch Σ_{I13}

This is positioned by rotating a $Y_L Z_L$ plane by γ_{13} about Z_L axis ($[\mathbf{R}_{z,\gamma_{13}}]$) and translating by $d_{131} = \frac{l_I}{2}$ along X_L axis and $d_{132} = -\frac{l_{I1}}{2}$ along Y_L axes.

$\mathbf{p}_{I13}(v_{13}, w_{13}) = [(-v_{13}\sin\gamma_{13}+d_{131}) \quad (v_{13}\cos\gamma_{13}+d_{132}) \quad w_{13} \quad 1] \quad (-\infty \leq v_{13}, w_{13} \leq \infty)$

Surface Patch Σ_{I14}

A $Z_L X_L$ plane rotated by γ_{14} about Z_L axis ($[\mathbf{R}_{z,\gamma_{14}}]$) and translated by d_{141} and d_{142} along X_L and Y_L axis respectively, forms Σ_{14}, where $d_{141} = \frac{l_{I1}}{2}$ and $d_{142} = -\frac{d_I}{2}$

$\mathbf{p}_{I14}(u_{14}, w_{14}) = [(u_{14}\cos\gamma_{14}+d_{141}) \quad (u_{14}\sin\gamma_{14}+d_{142}) \quad w_{14} \quad 1] \quad (-\infty \leq u_{14}, w_{14} \leq \infty)$

Surface Patch Σ_{I15}

This is modeled as a surface of revolution when an edge parallel to Z_L axis at a distance of $x = \frac{d_{I1}}{2}$ is revolved about Z_L axis.

$\mathbf{p}_{I15}(v_{15}, \theta_{15}) = [\frac{d_{I1}}{2}\cos\theta_{15} \quad \frac{d_{I1}}{2}\sin\theta_{15} \quad (\frac{S_I}{2} - u_{15}S_I) \quad 1]$

where $0 \leq u_{15} \leq 1$ and $0 \leq \theta_{15} \leq 2\pi$

Figure 5.7 shows the intersecting edges and corner vertices for an indexable insert used for milling. The relations for edges and vertices of intersection due to intersection of a set of surface patches can be developed on lines of Appendix C.

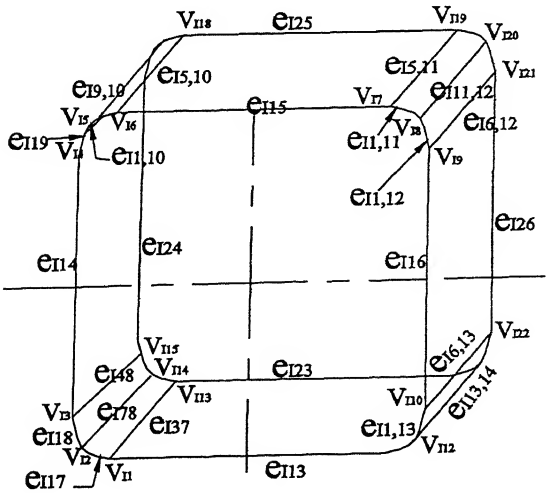

Figure 5.7: Edges and Vertices of intersection for an Indexable Insert

5.3.2 Transitional Surfaces for Square Indexable Inserts

For a unified model of square insert, there are six transitional surfaces. Four blending surfaces are meant to form the nose of radius r_I between planishing surfaces and auxiliary cutting surfaces, as illustrated in Figure 5.6 and two chamfered surfaces, one on each side, at the end of cylindrical hole for fixing. The blending surfaces are labeled as σ_{I78}, $\sigma_{I9,10}$, $\sigma_{I11,12}$ and $\sigma_{I13,14}$ and the chamfered surfaces as $\sigma_{I1,15}$ and $\sigma_{I2,15}$

Blending Surface σ_{I78}

This surface blends the inclined surface patches Σ_{I7} and Σ_{I8}. Edges of intersection of Σ_{I7} and Σ_{I8} are e_{I78},e_{I17}, e_{I18}, e_{I27} and e_{I28} and vertices of intersection are V_{I2} and V_{I14}, and they are known. The radius of blend r_I is also known as it is a manufacturer's prerogative. The blending surface is illustrated in Figure 5.8. The blending surface is geometrically modeled as a bicubic Bézier surface patch $P_{I00}P_{I03}P_{I33}P_{I30}$, with the cubic Bézier curves around vertices V_{I2} ($P_{I00}P_{I03}$) and V_{I14} ($P_{I30}P_{I33}$) in XY plane and straight lines between $\mathbf{p}_{I00}$-$\mathbf{p}_{I30}$ and $\mathbf{p}_{I03}$-$\mathbf{p}_{I33}$ along Z axis [26]. The modeling of blending surface σ_{I78} is as follows

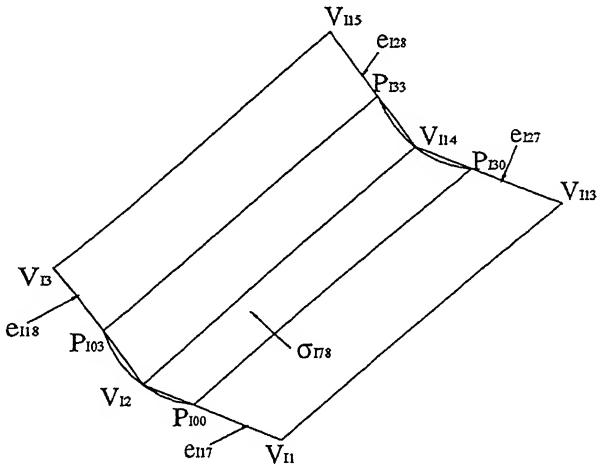

Figure 5.8: Blending for radius of Insert

Unit vector along $V_{I2}V_{I1}$, $\hat{a} = \frac{\mathbf{v}_{I1} - \mathbf{v}_{I2}}{|\mathbf{v}_{I1} - \mathbf{v}_{I2}|}$, and
unit vector along $V_{I2}V_{I3}$, $\hat{b} = \frac{\mathbf{v}_{I3} - \mathbf{v}_{I2}}{|\mathbf{v}_{I3} - \mathbf{v}_{I2}|}$.
Half corner angle $\phi = 0.5\cos^{-1}(\hat{a}.\hat{b})$
Distance between vertex of intersection and the start point of blend is, $\delta_I = \frac{r_I}{\tan\phi}$
The corner vertices of the Bézier curve are: $\mathbf{p}_{I00} = \mathbf{v}_{I2} + \delta_I\hat{a}$, $\mathbf{p}_{I03} = \mathbf{v}_{I2} + \delta_I\hat{b}$, $\mathbf{p}_{I01} = \mathbf{p}_{I00} - \Delta\hat{a}$ and $\mathbf{p}_{I02} = \mathbf{p}_{I03} + \Delta\hat{b}$ where $\Delta = \frac{2|\mathbf{p}_{I03} - \mathbf{p}_{I00}|}{3(1+\sin\phi)}$
Similarly, $\mathbf{p}_{I30} = \mathbf{v}_{I14} + \delta_I\hat{a}$, $\mathbf{p}_{I33} = \mathbf{v}_{I14} + \delta_I\hat{b}$, $\mathbf{p}_{I31} = \mathbf{p}_{I30} - \Delta\hat{a}$ and $\mathbf{p}_{I32} = \mathbf{p}_{I33} + \Delta\hat{b}$

A cubic Bézier curve on X_LY_L plane is plotted with the help of control points $P_{I00}, P_{I01}, P_{I02}, P_{I03}$ and another with $P_{I30}, P_{I31}, P_{I32}, P_{I33}$. Straight lines in the form of cubic Bézier curve are plotted between vertices P_{I00}–P_{I30} and P_{I03}–P_{I33}.

Blending surfaces $\sigma_{I9,10}$ is modeled by taking reflection of σ_{I78} about Z_LX_L plane. Similarly, blending surfaces $\sigma_{I11,12}$ and $\sigma_{I13,14}$ are formed by taking reflection about proper planes.

Chamfered Surface $\sigma_{I1,15}$ of unit width and at 45° is modeled by revolving a line formed by joining vertices $[\frac{d_{I1}}{2} \quad 0 \quad (\frac{S_I}{2} - 0.707) \quad 1]$ and $[(\frac{d_{I1}}{2} + 0.707) \quad 0 \quad \frac{S_I}{2} \quad 1]$. The equation of the chamfered surface is

$\sigma_{I1,15} = [(\frac{d_{I1}}{2} + 0.707u_{Ib5}) \cos\theta_{Ib5} \quad (\frac{d_{I1}}{2} + 0.707u_{Ib5}) \sin\theta_{Ib5} \quad \{\frac{S_I}{2} - 0.707(1 - u_{Ib5})\} \quad 1]$

where $0 \leq u_{Ib5} \leq 1$ and $0 \leq \theta_{Ib5} \leq 2\pi$. Chamfered surface $\sigma_{I2,15}$ is the mirror image of chamfer $\sigma_{I1,15}$ about X_LY_L plane.

5.3.3 Triangular Insert

A unified triangular insert is composed of twelve surface patches and five transition surfaces including three blending surfaces for rounding the insert at the three apexes and two chamfered surfaces at the intersection of cylindrical hole for fixing with the front and back surfaces. Figure 5.9 shows schematically the unified triangular insert. One or more parameters of the unified triangular insert, b_{I1}, b_{I2}, r_I, d_{I1}, α_I or β_I can be equated to zero and different types of triangular inserts as per ISO designation can be obtained [134], for example, if

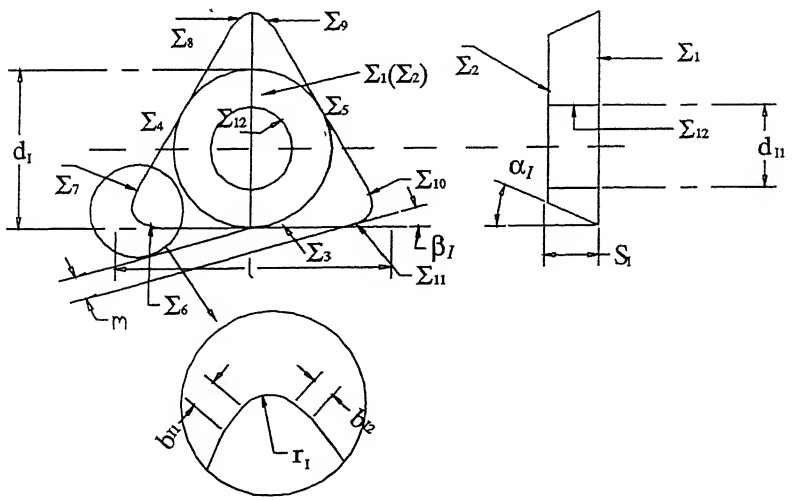

Figure 5.9: Unified Triangular Insert

(i) $r_I = d_{I1} = 0$ and $b_{I1} = b_{I2} \neq 0$, then the inserts may be TPAN/TKAN_PP_

(ii) $r_I = d_{I1} = 0$, $b_{I1} \neq b_{I2} \neq 0$ and $b_{I2} \leq b_{I1} \longrightarrow$ TPAN/TKAN_AE_

(iii) $r_I = d_{I1} = 0$, $b_{I1} \neq b_{I2}$ and $b_{I2} = 0.5b_{I1} \longrightarrow$ TPAN/TKAN_PD_
(iv) $r_I = d_{I1} = b_{I2} = 0$ and $b_{I1} \neq 0 \longrightarrow$ TPCX_AE_
(v) $d_{I1} = b_{I1} = b_{I2} = 0$ and $r_I \neq 0 \longrightarrow$ TPUN
(vi) $d_{I1} = b_{I1} = b_{I2} = \alpha_I = 0$ and $r_I \neq 0 \longrightarrow$ TNUN
(vii) $b_{I1} = b_{I2} = 0$ and $r_I \neq d_{I1} \neq 0 \longrightarrow$ TCMT

5.3.4 Positioning the Insert in the Cutter Body

In the indexable type milling cutters, the inserts are positioned relative to both radial and axial planes. In either plane an insert may be positioned with double positive, double negative or negative-positive rake as illustrated in Tool and Manufacturing Engineers Handbooks [29, 33]. The insert is positioned in the pocket of axial support, where axial support is positioned against the surface patch Σ_1 and Σ_2 of the insert seat of the cutter body. The back of the axial support is positioned with Σ_1 and one of the sides of axial support against Σ_2. The axial support on the other side is clamped with the wedge for axial support.

Three point precision location of insert, as depicted in Figure 5.10, in the pocket of axial support ensures exact seating resulting in greater accuracy and consistent tool life. The axial supports for inserts is firmly supported against a collar, which ensures firm clamping and eliminates cumbersome setting of face run-out. Positive location ensures increased tool life and consistent surface finish. Inserts are clamped from their rear face by a wedge for insert and it eliminates influence of variation in thickness of insert on face run-out [133, 134, 135].

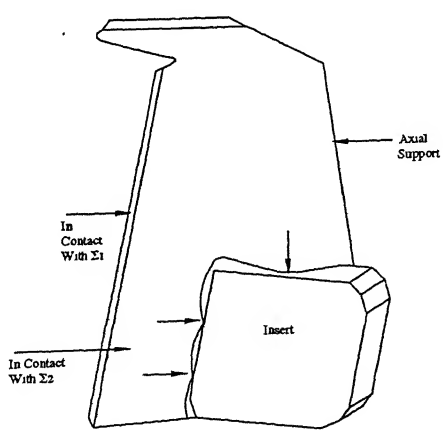

Figure 5.10: 3 Point Location of Insert

Insert is positioned in the cutter body such that the origin of coordinate system O_L-$X_LY_LZ_L$ (C_2) associated with it, is positioned at $[(\frac{D}{2}-\frac{l_I}{2}) \quad \frac{S_I}{2} \quad \frac{d_I}{2} \quad 1]$ with respect

to the global coordinate system O-XYZ (C_1). Before positioning the local origin, the coordinate system C_2 is rotated by 90° about X axis of C_1 such that the X_L axis remains parallel to X axis, while Y_L axis becomes parallel to Z axis and Z_L axis to Y axis. This is highlighted in Figure 5.11.

Once the coordinate system is aligned with respect to global coordinate system, the insert is rotated by angles α_I, β_I and γ_I about local axes X_L, Y_L and Z_L respectively to settle it in its final position in the pocket of inserted axial support. The order of rotation is γ_I about Z_L axis, followed by α_I about X_L axis and angle β_I about Y_L axis. This makes the insert finally oriented and placed in the pocket of axial support for insert and clamped by wedges for the insert and axial support.

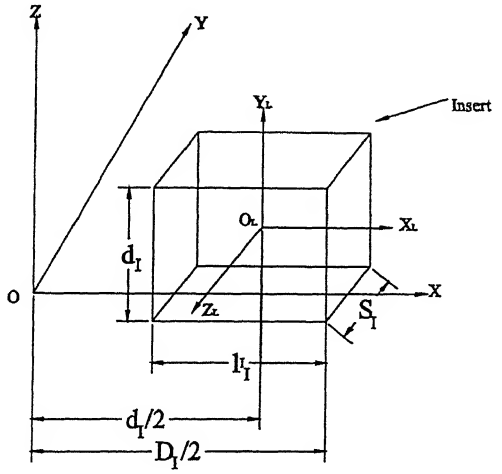

Figure 5.11: Positioning of Insert in the Cutter Body

Relation between Local and Global Coordinate System

If a point on any surface of the insert is known in local coordinate system (C_2) as $^2\mathbf{p}$, then it can be located in the global coordinate system (C_1) as $^1\mathbf{p}$. The relation between $^1\mathbf{p}$ and $^2\mathbf{p}$ depends on positioning and orientation of insert in C_1 and is established by homogenous transformation matrix of a vector from the coordinate system C_2 to the coordinate system C_1 ($[\frac{1}{2}\mathbf{M}]$). Thus

$$^1\mathbf{p} = {}^2\mathbf{p}.[\tfrac{1}{2}\mathbf{M}]$$

The transformation matrix $[\frac{1}{2}\mathbf{M}]$ may be expressed as

$$[\tfrac{1}{2}\mathbf{M}] = [\tfrac{1}{2}\mathbf{R}_x].[\tfrac{1}{2}\mathbf{R}_y].[\tfrac{1}{2}\mathbf{R}_z].[\tfrac{1}{2}\mathbf{T}]$$

where $[\mathbf{R}_x]$, $[\mathbf{R}_y]$, $[\mathbf{R}_z]$ are rotation matrices about X, Y, Z axes respectively and $[\mathbf{T}]$ translation matrix. Here, $[\frac{1}{2}\mathbf{R}_y]$ and $[\frac{1}{2}\mathbf{R}_z]$ are identity matrices, $[\frac{1}{2}\mathbf{T}]$ indicates the

positioning of local origin vis-a-vis global origin (as discussed earlier) and

$$[{}^1_2\mathbf{R}_x] = \begin{bmatrix} 1 & 0 & 0 & 0 \\ 0 & \cos\theta_1 & \sin\theta_1 & 0 \\ 0 & -\sin\theta_1 & \cos\theta_1 & 0 \\ 0 & 0 & 0 & 1 \end{bmatrix}$$

In the present case of positioning of the insert in the face mill, $\theta_1 = 90°$. This gives

$$[{}^1_2\mathbf{M}] = \begin{bmatrix} 1 & 0 & 0 & 0 \\ 0 & 0 & 1 & 0 \\ 0 & -1 & 0 & 0 \\ (\frac{D}{2}-\frac{l_I}{2}) & \frac{S_I}{2} & \frac{d_I}{2} & 1 \end{bmatrix}$$

5.4 Mapping

The set of relations used to associate a set of three-dimensional rotational angles with a set of two-dimensional conventional angles is known as Mapping. For the purpose, sign convention for the two sets of relations is established and shown in Table 5.2. In Figure 5.12 the conventional two-dimensional angles are shown. The procedure of formation of conventional angles employing projective geometry approach is shown in Mapping Guide Table (Table 5.3).

Rotational Angles	Conventional Angles
γ_I = -ve	Insert Face Setting Angle k = +ve
	Face Cutting Edge Angle ϕ_e = +ve
	Peripheral Cutting Edge Angle ϕ_P = +ve
	Nose Angle n_a = +ve
α_I = -ve	Axial Rake Angle, γ_A = +ve
	Face Relief Angle α_f = +ve
	Face Clearance Angle α_{1F} = +ve
	Axial Insert Setting Angle k' = +ve
β_I = -ve	Radial Rake Angle, γ_R = +ve
	Peripheral Relief Angle α_P = +ve
	Peripheral Clearance Angle α_{1P} = +ve

Table 5.2: Sign Convention Table for Face Mill

5.4.1 Forward Mapping

A set of relations specifying conventional two-dimensional angles in terms of three-dimensional rotational angles is known as forward mapping. The equations of surface patches of the insert involved in formulation of these angles are:

$\Sigma_{I1} : \mathbf{p}_{I1}(u_1, v_1) = [u_1 \quad v_1 \quad \frac{S_I}{2} \quad 1]$
$\Sigma_{I3} : \mathbf{p}_{I3}(u_3, w_3) = [u_3 \quad (-w_3 \sin\alpha_3 + d_{32}) \quad w_3 \cos\alpha_3 \quad 1]$
$\Sigma_{I6} : \mathbf{p}_{I6}(v_6, w_6) = [(w_6 \sin\beta_6 + d_{61}) \quad v_6 \quad w_6 \cos\beta_6 \quad 1]$
$\Sigma_{I13} : \mathbf{p}_{I13}(v_{13}, w_{13}) = [(-v_{13} \sin\gamma_{13} + d_{131}) \quad (v_{13} \cos\gamma_{13} + d_{132}) \quad w_{13} \quad 1]$
$\Sigma_{I14} : \mathbf{p}_{I14}(u_{14}, w_{14}) = [(u_{14} \cos\gamma_{14} + d_{141}) \quad (u_{14} \sin\gamma_{14} + d_{142}) \quad w_{14} \quad 1]$

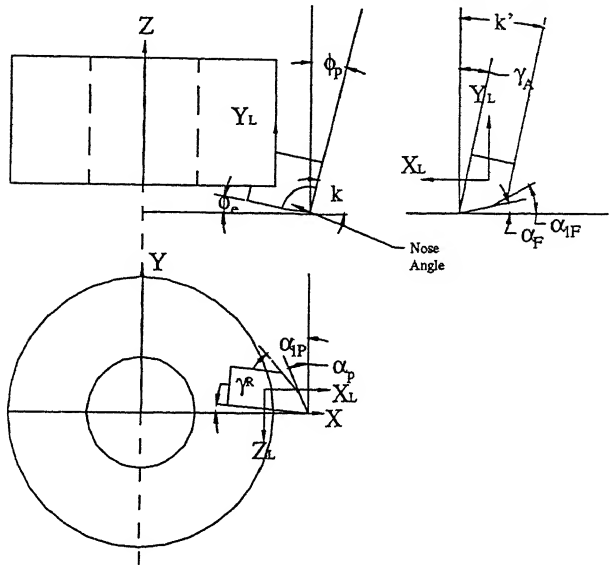

Figure 5.12: Conventional Tool Geometry for Face Mill

The insert is rotated by angle γ_I about Z_L axis, followed by α_I about X_L axis and β_I about Y_L axis. This gives the concatenated rotation matrix as:

$$[\mathbf{R}_{xyz}] = [\mathbf{R}_{z,\gamma_I}].[\mathbf{R}_{x,\alpha_I}].[\mathbf{R}_{y,\beta_I}]$$

Transformed surfaces of interest due to these rotations are:

$\Sigma^*_{I1} = \Sigma_{I1}.[\mathbf{R}_{xyz}]$
$\Sigma^*_{I3} = \Sigma_{I3}.[\mathbf{R}_{xyz}]$
$\Sigma^*_{I6} = \Sigma_{I6}.[\mathbf{R}_{xyz}]$
$\Sigma^*_{I13} = \Sigma_{I13}.[\mathbf{R}_{xyz}]$
$\Sigma^*_{I14} = \Sigma_{I14}.[\mathbf{R}_{xyz}]$

The components of position vector specifying a point lying on the transformed surface Σ^*_{I1} are

$$p^*_{I1x} = u_1(\cos\beta_I \cos\gamma_I + \sin\alpha_I \sin\beta_I \sin\gamma_I) + v_1(\cos\beta_I \sin\gamma_I + \sin\alpha_I \sin\beta_I \cos\gamma_I) + \frac{S_I}{2} \cos\alpha_I \sin\beta_I$$

$$p^*_{I1y} = u_1 \cos\alpha_I \sin\gamma_I + v_1 \cos\alpha_I \cos\gamma_I - \frac{S_I}{2} \sin\alpha_I$$

$$p^*_{I1z} = u_1(-\sin\beta_I \cos\gamma_I + \sin\alpha_I \cos\beta_I \sin\gamma_I) + v_1(\sin\beta_I \sin\gamma_I + \sin\alpha_I \cos\beta_I \cos\gamma_I)$$

Conventional Angles	Formed by Plane	About the Plane	Projected on Plane
Radial Rake Angle, γ_R	Σ_{I1}	X_LY_L	Z_LX_L
Axial Rake Angle, γ_A	Σ_{I1}	X_LY_L	Y_LZ_L
Face Cutting Edge Angle, ϕ_e	Σ_{I3}	Z_LX_L	X_LY_L
Peripheral Cutting Edge Angle, ϕ_P	Σ_{I6}	Y_LZ_L	X_LY_L
Face Relief Angle, α_F	σ_{I13}	Z_LX_L	Y_LZ_L
Face Clearance Angle, α_{1F}	Σ_{I3}	Z_LX_L	Y_LZ_L
Peripheral Relief Angle, α_P	σ_{I16}	Y_LZ_L	Z_LX_L
Peripheral Clearance Angle, α_{1P}	Σ_{I6}	Y_LZ_L	Z_LX_L
Face Setting Angle, k	Σ_{I6}	Z_LX_L	X_LY_L
Axial Setting Angle, k'	Σ_{I2}	X_LY_L	Y_LZ_L

Table 5.3: Mapping Guide Table for Insert-based Face Mill

$$+\frac{S_I}{2}\cos\alpha_I\cos\beta_I$$

The tangents to surface Σ^*_{I1} are

$$\begin{aligned} p^*_{I1u} &= (\cos\beta_I\cos\gamma_I+\sin\alpha_I\sin\beta_I\sin\gamma_I)\hat{\imath}+\cos\alpha_I\sin\gamma_I\hat{\jmath} \\ &\quad +(-\sin\beta_I\cos\gamma_I+\sin\alpha_I\cos\beta_I\sin\gamma_I)\hat{k} \\ p^*_{I1v} &= (-\cos\beta_I\sin\gamma_I+\sin\alpha_I\sin\beta_I\cos\gamma_I)\hat{\imath}+\cos\alpha_I\cos\gamma_I\hat{\jmath} \\ &\quad +(\sin\beta_I\sin\gamma_I+\sin\alpha_I\cos\beta_I\cos\gamma_I)\hat{k} \end{aligned}$$

and the normal to it is

$$\mathbf{n}_{I1}=\cos\alpha_I\sin\beta_I\hat{\imath}-\sin\alpha_I\hat{\jmath}+\cos\alpha_I\cos\beta_I\hat{k}$$

Radial Rake Angle (γ_R)

Radial rake angle is formed by projecting the normal to surface Σ^*_{I1} ($\mathbf{n}_{I1}$) on Z_LX_L plane and taking scalar product of unit projected normal vector ($\hat{n}_{I1p}$) with the normal to X_LY_L plane i.e. unit vector $\hat{k}$. The projection of $\mathbf{n}_{I1}$ on Z_LX_L plane is $\mathbf{n}_{I1p}=\cos\alpha_I\sin\beta_I\hat{\imath}+\cos\alpha_I\cos\beta_I\hat{\jmath}$ and the unit projected normal vector is $\hat{n}_{I1p}=\sin\beta_I\hat{\imath}+\cos\beta_I\hat{k}$. This gives radial rake angle γ_R, by taking scalar product of $\hat{n}_{I1p}$ with $\hat{k}$ as

$$\gamma_R=\beta_I \tag{5.7}$$

Using sign convention as expressed in Table 5.2

$$\gamma_R=-\beta_I$$

Axial Rake Angle (γ_A)

It is formed by Σ_{I1}^* with X_LY_L plane when projected on the Y_LZ_L plane. The projection of $\mathbf{n}_{I1}$ on Y_LZ_L plane is $\mathbf{n}'_{I1p} = -\sin\alpha_I\hat{j} + \cos\alpha_I\cos\beta_I\hat{k}$ and the unit projected normal vector is

$$\hat{n}'_{I1p} = \frac{-\sin\alpha_I\hat{j} + \cos\alpha_I\cos\beta_I\hat{k}}{\sqrt{(\sin^2\alpha_I + \cos^2\alpha_I\cos^2\beta_I)}}$$

Angle formed by Σ_{I1}^* with $X_LY_L$plane gives axial rake angle as

$$\gamma_A = \cos^{-1}\left[\frac{\cos\alpha_I\cos\beta_I}{\sqrt{(\sin^2\alpha_I + \cos^2\alpha_I\cos^2\beta_I)}}\right] \tag{5.8}$$

As per the sign convention expressed in Table 5.2, if α_I is negative, γ_A is positive.

Face Cutting Edge Angle (ϕ_e)

The angle made by transformed surface patch Σ_{I3}^* with the plane Z_LX_L when projected to X_LY_L plane is face cutting edge angle. The surface patch Σ_{I3}^* is defined as

$$\begin{aligned}
p^*_{I3x} &= u_3(\cos\beta_I\cos\gamma_I + \sin\alpha_I\sin\beta_I\sin\gamma_I) + (-w_3\sin\alpha_3 + d_{32})(-\cos\beta_I\sin\gamma_I \\
&\quad + \sin\alpha_I\sin\beta_I\cos\gamma_I) + w_3\cos\alpha_3\cos\alpha_I\sin\beta_I \\
p^*_{I3y} &= u_3\cos\alpha_I\sin\gamma_I + (-w_3\sin\alpha_3 + d_{32})\cos\alpha_I\cos\gamma_I - w_3\cos\alpha_3\sin\alpha_I \\
p^*_{I3z} &= u_3(-\sin\beta_I\cos\gamma_I + \sin\alpha_I\cos\beta_I\sin\gamma_I) - (w_3\sin\alpha_3 - d_{32})(\sin\beta_I\sin\gamma_I \\
&\quad + \sin\alpha_I\cos\beta_I\cos\gamma_I) + w_3\cos\alpha_3\cos\alpha_I\cos\beta_I
\end{aligned}$$

The tangents to surface Σ_{I3}^* are

$$\begin{aligned}
p^*_{I3u} &= (\cos\beta_I\cos\gamma_I + \sin\alpha_I\sin\beta_I\sin\gamma_I)\hat{\imath} + \cos\alpha_I\sin\gamma_I\hat{j} \\
&\quad + (-\sin\beta_I\cos\gamma_I + \sin\alpha_I\cos\beta_I\sin\gamma_I)\hat{k} \\
p^*_{I3w} &= \{\sin\alpha_3(\cos\beta_I\sin\gamma_I - \sin\alpha_I\sin\beta_I\cos\gamma_I) + \cos\alpha_3\cos\alpha_I\sin\beta_I\}\hat{\imath} \\
&\quad - (\sin\alpha_3\cos\alpha_I\cos\gamma_I + \cos\alpha_3\sin\alpha_I)\hat{j} \\
&\quad - (\sin\alpha_3\sin\beta_I\sin\gamma_I + \sin\alpha_3\sin\alpha_I\cos\beta_I\cos\gamma_I - \cos\alpha_3\cos\alpha_I\cos\beta_I)\hat{k}
\end{aligned}$$

and the normal is

$$\begin{aligned}
\mathbf{n}_{I3} &= (-\sin\alpha_3\cos\alpha_I\sin\beta_I + \cos\alpha_3\cos\beta_I\sin\gamma_I - \cos\alpha_3\sin\alpha_I\sin\beta_I\cos\gamma_I)\hat{\imath} \\
&\quad + (\sin\alpha_3\sin\alpha_I - \cos\alpha_3\cos\alpha_I\cos\gamma_I)\hat{j} \\
&\quad - (\sin\alpha_3\cos\alpha_I\cos\beta_I + \cos\alpha_3\sin\beta_I\sin\gamma_I + \cos\alpha_3\sin\alpha_I\cos\beta_I\cos\gamma_I)\hat{k}
\end{aligned}$$

This vector when projected on X_LY_L plane is given as

$$\begin{aligned}\mathbf{n}_{I3p} &= (-\sin\alpha_3\cos\alpha_I\sin\beta_I+\cos\alpha_3\cos\beta_I\sin\gamma_I-\cos\alpha_3\sin\alpha_I\sin\beta_I\cos\gamma_I)\hat{\imath}\\ &\quad+(\sin\alpha_3\sin\alpha_I-\cos\alpha_3\cos\alpha_I\cos\gamma_I)\hat{\jmath}\end{aligned}$$

The scalar product of unit normal projected vector $(\mathbf{n}_{I3p}/|\mathbf{n}_{I3p}|)$ with unit vector $\hat{\jmath}$ gives ϕ_e.

$$\phi_e = \cos^{-1}\left[\frac{\sin\alpha_3\sin\alpha_I-\cos\alpha_3\cos\alpha_I\cos\gamma_I}{|\mathbf{n}_{I3p}|}\right] \tag{5.9}$$

When $\alpha_3 = \alpha_I = \beta_I = 0$, then $\phi_e = \gamma_I$. Sign of ϕ_e is taken care from the sign-convention table.

Peripheral Cutting Edge Angle (ϕ_P)

This angle is formed by surface patch Σ^*_{I6} as explained in the Mapping Guide Table (Table 5.3). The surface patch Σ^*_{I6} satisfies the relations

$$\begin{aligned}p^*_{I6x} &= v_6(-\cos\beta_I\sin\gamma_I+\sin\alpha_I\sin\beta_I\cos\gamma_I)+(w_6\sin\beta_6+d_{61})(\cos\beta_I\cos\gamma_I\\ &\quad+\sin\alpha_I\sin\beta_I\sin\gamma_I)+w_6\cos\beta_6\cos\alpha_I\sin\beta_I\\ p^*_{I6y} &= v_6\cos\alpha_I\cos\gamma_I+(w_6\sin\beta_6+d_{61})\cos\alpha_I\sin\gamma_I-w_6\cos\beta_6\sin\alpha_I\\ p^*_{I6z} &= v_6(\sin\beta_I\sin\gamma_I+\sin\alpha_I\cos\beta_I\cos\gamma_I)+(w_6\sin\beta_6+d_{61})(-\sin\beta_I\cos\gamma_I\\ &\quad+\sin\alpha_I\cos\beta_I\sin\gamma_I)+w_6\cos\beta_6\cos\alpha_I\cos\beta_I\end{aligned}$$

The tangents to surface Σ^*_{I6} are

$$\begin{aligned}p^*_{I6v} &= (-\cos\beta_I\sin\gamma_I+\sin\alpha_I\sin\beta_I\cos\gamma_I)\hat{\imath}+\cos\alpha_I\cos\gamma_I\hat{\jmath}\\ &\quad+(\sin\beta_I\sin\gamma_I+\sin\alpha_I\cos\beta_I\cos\gamma_I)\hat{k}\\ p^*_{I6w} &= \{\sin\beta_6(\cos\beta_I\cos\gamma_I+\sin\alpha_I\sin\beta_I\sin\gamma_I)+\cos\beta_6\cos\alpha_I\sin\beta_I\}\hat{\imath}\\ &\quad+(\sin\beta_6\cos\alpha_I\sin\gamma_I-\cos\beta_6\sin\alpha_I)\hat{\jmath}\\ &\quad+(-\sin\beta_6\sin\beta_I\cos\gamma_I+\sin\beta_6\sin\alpha_I\cos\beta_I\sin\gamma_I+\cos\beta_6\cos\alpha_I\cos\beta_I)\hat{k}\end{aligned}$$

and the normal is

$$\begin{aligned}\mathbf{n}_{I6} &= (-\sin\beta_6\cos\alpha_I\sin\beta_I+\cos\beta_6\cos\beta_I\cos\gamma_I+\cos\beta_6\sin\alpha_I\sin\beta_I\sin\gamma_I)\hat{\imath}\\ &\quad+(\sin\beta_6\sin\alpha_I+\cos\beta_6\cos\alpha_I\sin\gamma_I)\hat{\jmath}\\ &\quad+(-\sin\beta_6\cos\alpha_I\cos\beta_I-\cos\beta_6\sin\beta_I\cos\gamma_I+\cos\beta_6\sin\alpha_I\cos\beta_I\sin\gamma_I)\hat{k}\end{aligned}$$

Projection of $\mathbf{n}_{I6}$ on X_LY_L plane gives

$$\begin{aligned}\mathbf{n}_{I6p} &= (-\sin\beta_6\cos\alpha_I\sin\beta_I+\cos\beta_6\cos\beta_I\cos\gamma_I+\cos\beta_6\sin\alpha_I\sin\beta_I\sin\gamma_I)\hat{\imath}\\ &\quad+(\sin\beta_6\sin\alpha_I+\cos\beta_6\cos\alpha_I\sin\gamma_I)\hat{\jmath}\end{aligned}$$

The scalar product of unit normal projected vector with unit vector $\hat{\imath}$ gives ϕ_P.

$$\phi_P = \cos^{-1}\left[\frac{-\sin\beta_6\cos\alpha_I\sin\beta_I + \cos\beta_6\cos\beta_I\cos\gamma_I + \cos\beta_6\sin\alpha_I\sin\beta_I\sin\gamma_I}{|\mathbf{n}_{I6p}|}\right] \tag{5.10}$$

When $\beta_6 = \alpha_I = \beta_I = 0$, then $\phi_P = \gamma_I$. From sign convention table (Table 5.2), when γ_I is negative, ϕ_P is positive.

Face Relief Angle (α_F)

Face relief angle is formed by blending surface between Σ^*_{I1} and Σ^*_{I3} i.e. σ_{I13}. The slope of the tangent plane to blend surface at the edge of intersection $\mathbf{e}^*_{I13}$ determines the angle α_F. If σ_{I13} is present then the slope of the tangent plane is about 0.5° to 1°, else zero.

Face Clearance Angle (α_{1F})

It is formed by surface Σ^*_{I3} about the plane Z_LX_L when projected on Y_LZ_L plane. Projection of $\mathbf{n}_{I3}$ on Y_LZ_L plane is given by

$$\mathbf{n}'_{I3p} = (\sin\alpha_3\sin\alpha_I - \cos\alpha_3\cos\alpha_I\cos\gamma_I)\hat{\jmath} - (\sin\alpha_3\cos\alpha_I\cos\beta_I + \cos\alpha_3\sin\beta_I\sin\gamma_I + \cos\alpha_3\sin\alpha_I\cos\beta_I\cos\gamma_I)\hat{k}$$

Scalar product of unit projected normal vector $\left(\hat{n}'_{I3p} = \frac{\mathbf{n}'_{I3p}}{|\mathbf{n}'_{I3p}|}\right)$ with unit vector $\hat{\jmath}$ gives face clearance angle as

$$\alpha_{1F} = \cos^{-1}\left[\frac{\sin\alpha_3\sin\alpha_I - \cos\alpha_3\cos\alpha_I\cos\gamma_I}{|\mathbf{n}'_{I3p}|}\right] \tag{5.11}$$

From sign convention table, when α_I is negative, α_{1F} is positive.

Peripheral Relief Angle (α_P)

This angle is formed by blending surface σ_{I16} between Σ^*_{I1} and Σ^*_{I6}. The slope of the tangent plane to σ_{I16} at the edge of intersection $\mathbf{e}^*_{I16}$ influences angle α_P. If σ_{I16} is present then the slope of the tangent plane is about 0.5° to 1°, else zero.

Peripheral Clearance Angle (α_{1P})

It is the angle between the surface Σ^*_{I6} and the plane Y_LZ_L and viewed on projection to Z_LX_L plane. Projection of $\mathbf{n}_{I6}$ on Z_LX_L plane is

$$\mathbf{n}'_{I6p} = (-\sin\beta_6\cos\alpha_I\sin\beta_I + \cos\beta_6\cos\beta_I\cos\gamma_I + \cos\beta_6\sin\alpha_I\sin\beta_I\sin\gamma_I)\hat{\imath} + (-\sin\beta_6\cos\alpha_I\cos\beta_I - \cos\beta_6\sin\beta_I\cos\gamma_I + \cos\beta_6\sin\alpha_I\cos\beta_I\sin\gamma_I)\hat{k}$$

Scalar product of unit projected normal vector ($\hat{n}'_{I6p}$) with unit vector $\hat{\imath}$ gives peripheral clearance angle as

$$\alpha_{1P}=\cos^{-1}\left[\frac{-\sin\beta_6\cos\alpha_I\sin\beta_I+\cos\beta_6\cos\beta_I\cos\gamma_I+\cos\beta_6\sin\alpha_I\sin\beta_I\sin\gamma_I}{|\mathbf{n}'_{I6p}|}\right] \quad (5.12)$$

From sign convention table, when β_I is negative, α_{1P} is positive.

Face Setting Angle (k)

Face setting anle k can be found as $k = \frac{\pi}{2} - \phi_P$

Axial Setting Angle (k')

From the geometry of face mill, axial setting angle k' is equal to axial rake angle γ_A.

5.4.2 Inverse Mapping

The relations to map a set of known conventional two-dimensional angles to unknown three-dimensional angles is labeled in this work as inverse mapping. In the previous section, the relations for radial rake angle, axial rake angle, face cutting edge angle, peripheral cutting edge angle, face clearance angle and peripheral clearance angle are given by Equations (5.7), (5.8), (5.9), (5.10), (5.11) and (5.12) respectively. Solving these equations provides inverse mapping relations. From the relation of radial rake angle

$$\beta_I = \gamma_R$$

while from the relation of axial rake angle

$$\alpha_I = \tan^{-1}\left[\frac{\sqrt{\cos^2\gamma_R - \cos^2\gamma_A\cos^2\gamma_R}}{\cos\gamma_A}\right]$$

On solving the Eq. (5.9) and Eq. (5.11) simultaneously, one gets a relation

$$\sin\alpha_3\sin\alpha_I - \cos\alpha_3\cos\alpha_I\cos\gamma_I = \frac{\cos\phi_e\cos\alpha_{1F}}{\sqrt{(\cos^2\phi_e + \cos^2\alpha_{1F} - \cos^2\phi_e\cos^2\alpha_{1F})}}$$

This relation can be used to evaluate the value of rotation angle γ_I in terms of face cutting edge angle and face clearance angle.

5.5 Grinding Methodology

The insert of indexable insert-based Face Milling cutter can be grinded or, if need be, regrinded on a three-axis universal table. Normally, the insert are not regrinded and when all the four sides of a square insert are worn, they are replaced. The four sides of the insert are used, one at a time, by rotating it around Z_L axis. The surface patches which need to be ground are:

(i) Face (Σ^*_{I1})

(ii) Major Flank (Σ^*_{I6})

(iii) Minor Flank (Σ^*_{I3})

For grinding a particular surface, the grinding principle employed is that the normal to that surface and the normal to the grinding wheel surface should be parallel to each other. The grinding methodology is discussed by Connel [28], Popov et. al. [87] and Rodin [93].

5.5.1 Grinding of Face

To grind the face (Σ^*_{I1}), the cutter is rotated by an angle θ_C about Z axis followed by θ_A about X axis in coordinate system C_1. The face surface Σ^*_{I1} then transforms to

$$\Sigma^{**}_{I1} = \Sigma^*_{I1}.[R_{z,\theta_C}].[R_{x,\theta_A}]$$

such that the unit normal to Σ^{**}_{I1} is given by $\hat{n}^*_{I1} = -\hat{\jmath}$ i.e.Σ^{**}_{I1} is parallel to ZX plane.

Angles θ_A and θ_C are evaluated by finding x, y and z components of $\hat{n}^*_{I1}$ and equating them to (0, -1, 0) respectively. The grinding can be carried out using flaring cup grinding wheel.

5.5.2 Grinding of Major Flank

The cutter is rotated by an angle θ'_C about Z axis, followed by θ'_B about Y axis in global coordinate system C_1. After this rotation, the modified parametric equation of major flank (Σ^*_{I6}) is expressed by

$$\Sigma^{**}_{I6} = \Sigma^*_{I6}.[R_{z,\theta'_C}].[R_{y,\theta'_B}]$$

such that the unit normal to Σ^{**}_{I6} is $\hat{n}^*_{I6} = +\hat{\imath}$ i.e. Σ^{**}_{I6} is parallel to YZ plane.

Angles θ'_C and θ'_B are evaluated by transforming $\mathbf{n}_{I6}$ to $\mathbf{n}^*_{I6}$ ($\mathbf{n}^*_{I6} = \mathbf{n}_{I6}.[R_{z,\theta'_C}].[R_{y,\theta'_B}]$) and equating x, y and z components of $\hat{n}^*_{I6}$ to (+1, 0, 0) respectively. The distance between the axes of the grinding wheel and the cutter is expressed by the vector $[0 \quad \frac{S_I}{2} \quad 0 \quad 1]$.

5.5.3 Grinding of Minor Flank

For the purpose of grinding minor flank (Σ^*_{I3}), the cutter is rotated by an angle θ''_A about X axis, followed by θ''_B about Y axis in C_1. Then, the minor flank is given by

$$\Sigma^{**}_{I3} = \Sigma^*_{I3}.[R_{x,\theta''_A}].[R_{y,\theta''_B}]$$

such that the unit normal to Σ^{**}_{I3} ($\hat{n}^*_{I3}$) is equal to $-\hat{k}$.

Angles θ''_A and θ''_B are evaluated by equating the components of $\hat{n}^*_{I3}$ to (0, 0, -1) respectively. The grinding wheel is at a distance of $\frac{S_I}{2}$ along Y axis i.e. the distance between the cutter axis and the grinding wheel axis is $(0, \frac{S_I}{2}, 0)$.

5.6 Example

This section presents an example of creating an insert-based face mill on the basis of three-dimensional geometric parameters. The three-dimensional parameters used to construct the body of face mill for cutter style : *M40- SP12* (I.S. Code: *M40–SP12 80 542 116*) are shown in Table 5.4 [133, 134]. The resultant cutter body is rendered in OpenGL environment [127, 132, 120, 121] and shown with the help of Figure 5.13. This cutter body uses an insert of ISO designation *SP.N 12 03 ED R/L*.

Input Data for Face Mill	
Dimensional Parameters	Value (mm)
Maximum Machining Diameter(D)	166.0
Nominal Diameter of cutter(d)	160.0
Diameter of Bore(d_1)	40.0
Depth of Bore(l)	29.0
Cutter Height(h)	63.0
Number of Inserts(N)	10.0
Rotational Angles	Relations
γ_2	-0.0667ψ
α_4	$0.85\tan^{-1}\left[\frac{D-d}{h-l_1}\right]$
α_5	$-\alpha_4$
γ_6	0.3333ψ

Table 5.4: Geometric Parameters of Face Mill

A square insert of ISO designation *SPKN 15 04 EDR* and a triangular insert of ISO designation *TPKN 22 04 PDR* are also generated using three-dimensional geometric parameters. The rendered images of these inserts are shown in Figure 5.14.

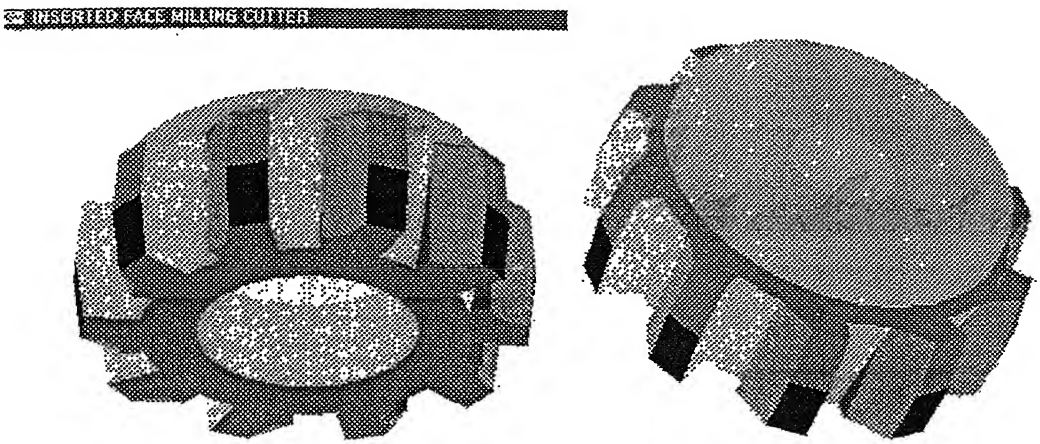

Figure 5.13: Rendering of body of Face Mill

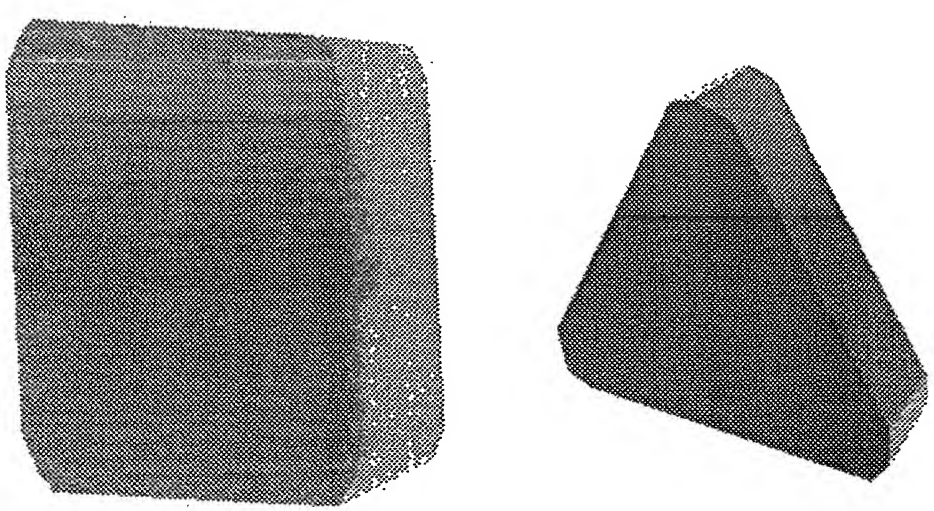

Figure 5.14: Square and Triangle Inserts of Face Mill

5.7 Case Study

The present work develops a comprehensive three-dimensional model of face mill on the basis of three-dimensional geometric parameters. Such a model can be imported into any surface or solid modeling environment and it can be subjected to all feasible down-stream applications. This section presents finite element based engineering analysis (FEA) on the indexable cutting tooth of the face mill. The case-study illustrated hereby is by no means an exhaustive exercise on the analysis of insert during machining but highlights the advantages and utilities unfolded, once a comprehensive 3D definition of the cutter is available. The 3D CAD model of face mill developed on the basis of methodology illustrated in this chapter is imported through ASCII file format in one of the commercial CAD/Analysis software and a wide range of analysis (e.g. static, dynamic, fatigue, thermal etc.) for stress, wear, deflection etc. can be performed on it. One of the exercise among the range of feasible FEA is actually carried out and presented herewith.

A single silicon carbide insert machining a low alloy steel workpiece is considered for analysis. The insert is subjected to static and fatigue analysis in I-DEAS, a CAD package [53]. The purpose of fatigue analysis is to evaluate the response of the structure with respect to loading pattern [118]. From the static analysis, the maximum pressure that the insert can bear without failure comes out to be 50 MPa. For fatigue analysis, this pressure is applied as a cyclic load of magnitude $50 \sin \omega t$ as shown in Figure 5.15 for 10 cycles. After 10 cycles, the pattern repeats, so load is not applied beyond 10 cycles. Figure 5.16 shows the loading of an insert during machining operation. The load duration is evaluated based on cutter RPM and feed rate and it comes out to be 0.0125 seconds. The load is applied in time steps of 0.001 seconds. From fatigue analysis, maximum stress generated on the insert is found to be 27 MPa. First four mode shapes are shown in Figure 5.17 and the stress and displacement distribution at the cutting tip of nose of insert is shown in Figure 5.18.

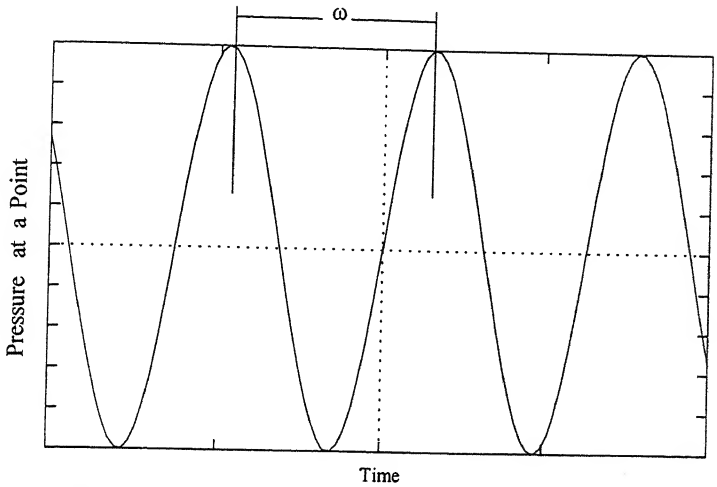

Figure 5.15: Loading Pattern on the Insert Face

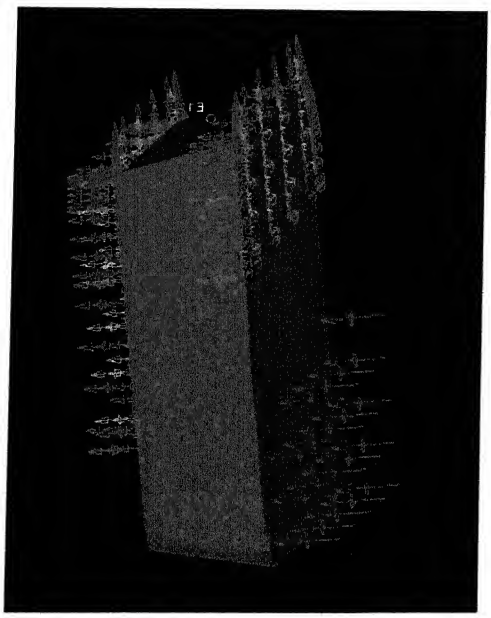

Figure 5.16: Loading of Insert during machining in Face Mill

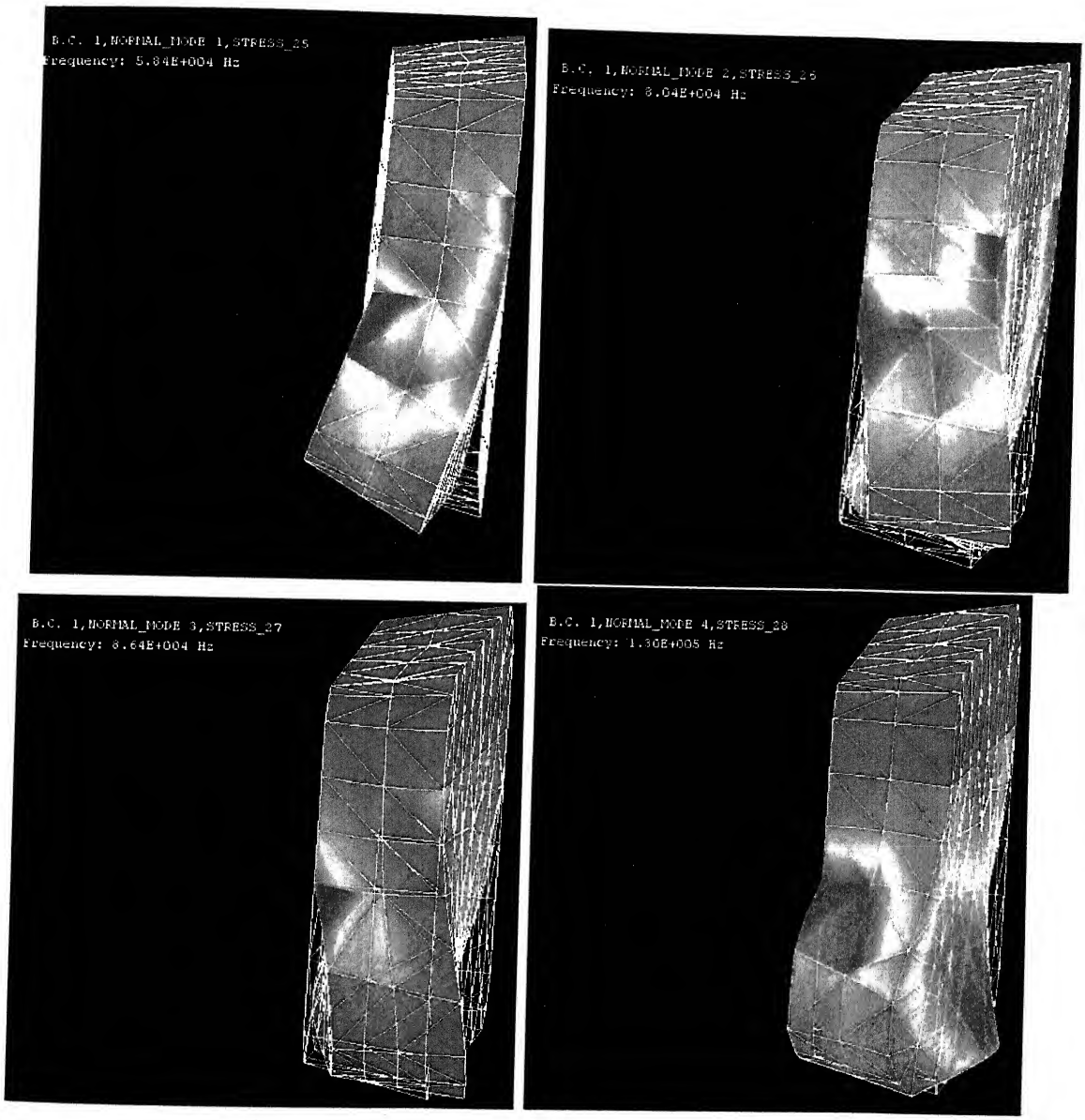

Figure 5.17: First Four Mode Shapes of Insert

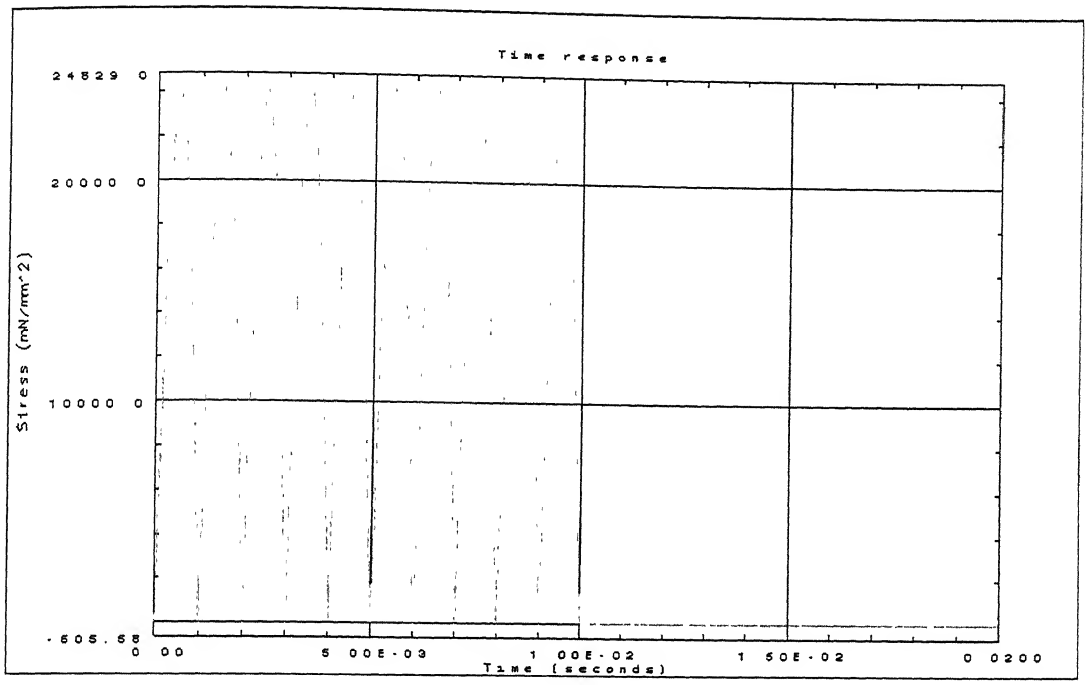

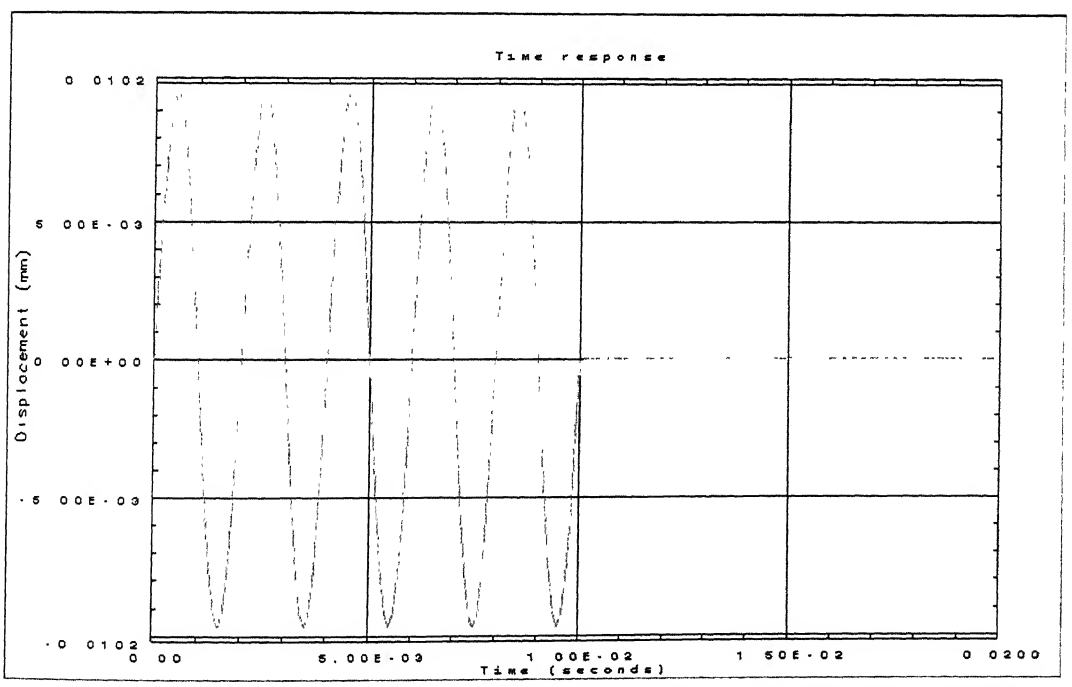

Figure 5.18: Stress and Displacement Distribution at the tip of Insert

Chapter 6

SHELL MILL

These are multiple-teeth cutters, cylindrical in shape with teeth on the periphery and end. They are made without a shank and are designed for mounting on stub arbors, which is driven by keys on the spindle nose [77]. The teeth are generally helical in modern shell mills, also known as shell end mill, with either left or right helix. They may also be straight, parallel to axis of rotation. Shell mills are used to particular advantage in face milling operations requiring the milling of two surfaces at right angles to each other [27]. This chapter presents comprehensive three-dimensional modeling of a solid helical shell mill.

6.1 Surface Modeling of Shell Mill Tooth

The surfaces forming the tooth of a shell mill can be classified into

(i) Peripheral surface patches

(ii) End surface patches

For a generic shell mill, nine surface patches form its tooth. The labeling of these surface patches is shown in Table 6.1. Figure 6.1 and Figure 6.2 show respectively the schematic two-dimensional layout of the shell mill and surface patches forming its tooth. Surface patches $\Sigma_1, \ldots, \Sigma_5$ are peripheral surfaces and modeled as helicoidal surfaces, while surface patches Σ_6 to Σ_9 are end surface patches. The helicoidal surfaces are modeled by sweeping a composite cross-sectional curve in a plane perpendicular to axis, along and about the axis. Figure 6.1 also shows the location of global origin (O) and orientation of global coordinate system C_1.

Label	Surface
Σ_1	Rake Face
Σ_2	Peripheral Land
Σ_3	Major Flank
Σ_4	Tertiary Peripheral Land
Σ_5	Helicoidal Blending Surface
Σ_6	Face Land
Σ_7	Minor Flank
Σ_8	Back of Cutting End
Σ_9	Rake Face Extension

Table 6.1: Surfaces of a Shell Mill Tooth

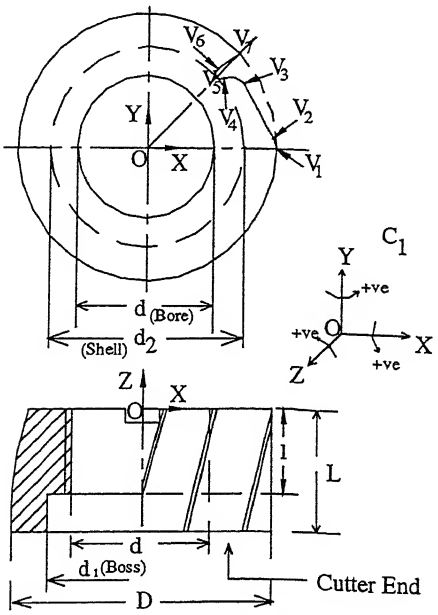

Figure 6.1: Two-dimensional Projective View of Shell Mill

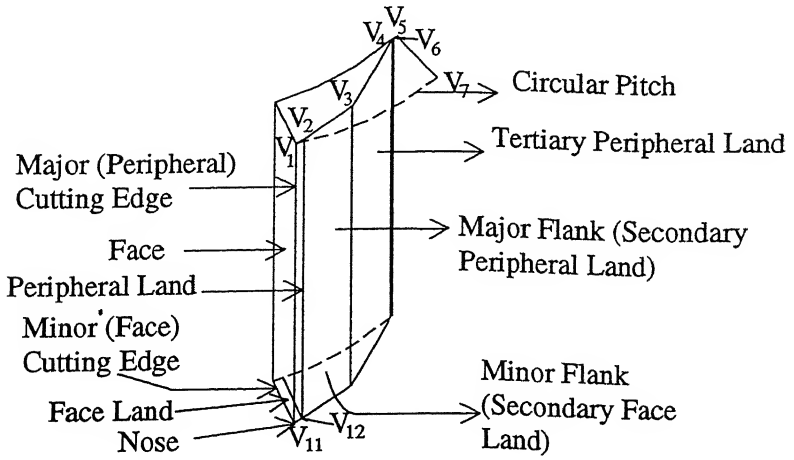

Figure 6.2: Surface Patches of a Tooth of Shell Mill

6.1.1 Cross-Section Profile

The peripheral surfaces of the shell mill are modeled as sweep surfaces. For the purpose a generic composite curve describing tip-to-tip profile of the cutter tooth in XY plane and a sweeping rule are generated [66]. When the sweeping is linear (parallel sweeping) the straight tooth cutter is formed and when the sweep operation is a combination of rotational and parallel sweep about the cutter axis, then the resultant surfaces are helicoidal surfaces and the cutter is helical shell mill. The cross-section profile is formed by vertices $V_1V_2V_3V_4V_5V_6V_7$ and shown for a cutter having negative radial rake angle in Figure 6.3. The composite curve is a tip-to-tip profile, with the projected curve for rake face of N^{th} tooth (V_0V_1) excluded and that for $(N+1)^{th}$ tooth (V_6V_7) included for the convenience of modeling.

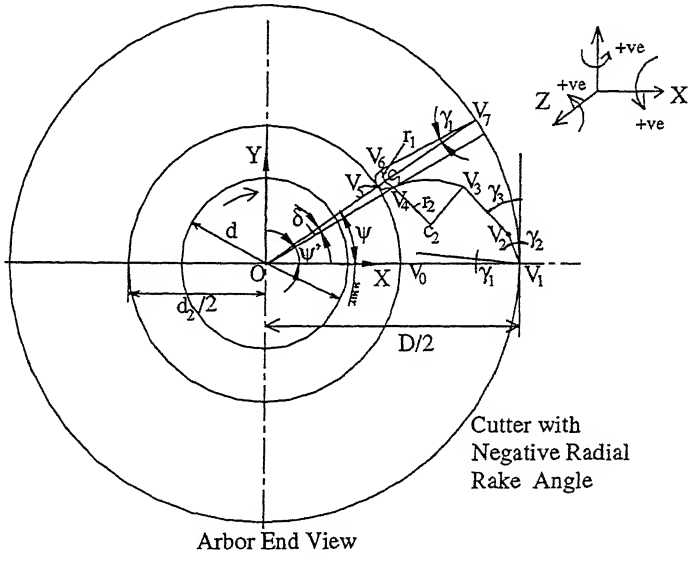

Figure 6.3: Cross-Section Profile of Shell Mill

The composite sectional curve is made up of five segments. Segments V_1V_2, V_2V_3 and V_6V_7 are straight lines and segments V_3V_4 and $V_4V_5V_6$ are circular arcs of fillet radius r_2 and r_1 with centers at c_2 and c_1 respectively. The homogenous coordinates of these vertices are evaluated with the help of Figure 6.3 and Figure 6.4 and given by the following relations:

$$\mathbf{v}_1 = [\frac{D}{2} \quad 0 \quad 0 \quad 1]$$

$$\mathbf{v}_2 = [(\frac{D}{2} - l_1 \sin\gamma_2) \quad l_1 \cos\gamma_2 \quad 0 \quad 1]$$

$$\mathbf{v}_3 = [\{\frac{D}{2} - (l_1 \sin\gamma_2 + l_2 \sin\gamma_3)\} \quad (l_1 \cos\gamma_2 + l_2 \cos\gamma_3) \quad 0 \quad 1]$$

$$
\begin{aligned}
\mathbf{c}_1 &= \left[\left\{(\frac{d_2}{2}+r_1)\cos\psi+\left(\frac{r_1}{\cos\gamma_1}+\left(\frac{D-d_2}{2}-r_1\right)\tan\gamma_1\right)\sin\psi\right\}\right. \\
&\quad \left.\left\{(\frac{d_2}{2}+r_1)\sin\psi-\left(\frac{r_1}{\cos\gamma_1}+\left(\frac{D-d_2}{2}-r_1\right)\tan\gamma_1\right)\cos\psi\right\} \quad 0 \quad 1\right] \\
\mathbf{c}_2 &= [(V_{3x}-r_2\cos\gamma_3) \quad (V_{3y}-r_2\sin\gamma_3) \quad 0 \quad 1] \\
\mathbf{v}_4 &= [(c_{1x}+r_1\sin\phi_1) \quad (c_{1y}-r_1\cos\phi_1) \quad 0 \quad 1] \\
\mathbf{v}_5 &= [\frac{d_2}{2}\cos\psi' \quad \frac{d_2}{2}\sin\psi' \quad 0 \quad 1] \\
\mathbf{v}_6 &= \left[\left\{\frac{D}{2}\cos\psi-\left(\frac{\frac{D-d_2}{2}-r_1}{\cos\gamma_1}+r_1\tan\gamma_1\right)\cos(\psi+\gamma_1)\right\}\right. \\
&\quad \left.\left\{\frac{D}{2}\sin\psi-\left(\frac{\frac{D-d_2}{2}-r_1}{\cos\gamma_1}+r_1\tan\gamma_1\right)\sin(\psi+\gamma_1)\right\} \quad 0 \quad 1\right] \\
\mathbf{v}_7 &= [\frac{D}{2}\cos\psi \quad \frac{D}{2}\sin\psi \quad 0 \quad 1]
\end{aligned}
$$

where $\phi_1 = \tan^{-1}\left[\frac{c_{2x}-c_{1x}}{c_{1y}-c_{2y}}\right]$, $r_2 = \frac{-B\pm\sqrt{B^2-4AC}}{2A}$ and $\psi' = \psi - \delta$.

The parameters A, B and C are given by $A = 4r_1+4l'\cos\phi$, $B = 4{r_1}^2+2r_1l'\cos\phi-2l'^2$ and $C = r_1^3-r_1l'^2$ (for $l' = |\mathbf{c}_1-\mathbf{v}_3|$). The value of δ is obtained by solving the equation

$$\sin\delta + \cos\delta\tan\gamma_1 = \frac{\frac{r_1}{\cos\gamma_1}+\frac{D}{2}\tan\gamma_1}{\frac{d_2}{2}+r_1}$$

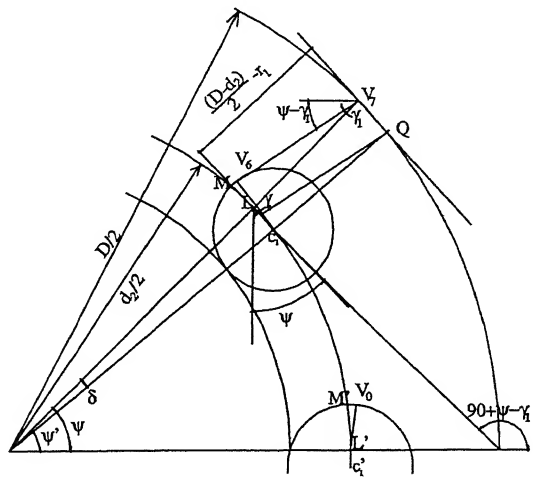

Figure 6.4: Enlarged View of Cross-Section Profile

The cross-section curve V_1V_7 is composed of five parametric curve segments, namely $\mathbf{p}_1(s)$, $\mathbf{p}_2(s)$, $\mathbf{p}_3(s)$, $\mathbf{p}_4(s)$ and $\mathbf{p}_5(s)$. The curve segments $\mathbf{p}_1(s)$, $\mathbf{p}_2(s)$ and $\mathbf{p}_5(s)$ are straight lines between vertices V_1V_2, V_2V_3 and V_6V_7 respectively, while the

curves $\mathbf{p}_3(s)$ and $\mathbf{p}_4(s)$ are circular arcs of radius r_2 and r_1 respectively. The equation of $\mathbf{p}_1(s)$ is evolved as

$$\mathbf{p}_1(s) = V_1 + s(V_2 - V_1), \text{ where } 0 \leq s \leq 1 \tag{6.1}$$

Substituting the values of the x,y and z coordinates of V_1 and V_2, $\mathbf{p}_1(s)$ is given as
$\mathbf{p}_1(s) = [(\frac{D}{2} - s.l_1 \sin\gamma_2) \quad s.l_1 \cos\gamma_2 \quad 0 \quad 1] \quad (0 \leq s \leq 1)$
Similarly, other curve segments are found as

$$\begin{aligned}
\mathbf{p}_2(s) &= [(\frac{D}{2} - l_1 \sin\gamma_2 - s.l_2 \sin\gamma_3) \quad \{l_1 \cos\gamma_2 + s.l_2 \cos\gamma_3)\} \quad 0 \quad 1] \\
\mathbf{p}_3(s) &= [(c_{2x} + r_2 \cos S) \quad (c_{2y} + r_2 \sin S) \quad 0 \quad 1] \quad (S_1 \leq S \leq S_2) \\
\mathbf{p}_4(s) &= [(c_{1x} + r_1 \cos S) \quad (c_{1y} - r_1 \sin S) \quad 0 \quad 1] \quad (S_3 \leq S \leq S_4) \\
\mathbf{p}_5(s) &= [\{\frac{D}{2}\cos\psi - \left(\frac{\frac{D-d_2}{2} - r_1}{\cos\gamma_1} + r_1 \tan\gamma_1\right) \cos(\psi+\gamma_1)(1-s)\} \\
&\quad \{\frac{D}{2}\sin\psi - \left(\frac{\frac{D-d_2}{2} - r_1}{\cos\gamma_1} + r_1 \tan\gamma_1\right) \sin(\psi+\gamma_1)(1-s)\} \quad 0 \quad 1] \quad (6.2)
\end{aligned}$$

where $S_1 = \gamma_3$, $S_2 = \tan^{-1}\left[\frac{V_{4y} - c_{2y}}{V_{4x} - c_{2x}}\right]$, $S_3 = \pi - S_2$ and $S_4 = \frac{3\pi}{2} + \phi'$
$(\phi' = tan^{-1}\left[\frac{V_{6x} - c_{1x}}{V_{6y} - c_{1y}}\right])$.

6.1.2 Peripheral Surface Patches

The peripheral surface patches (Σ_1 - Σ_5) of shell mill are helicoidal in geometry and formed due sweeping cross-section profile according to sweep rule. They are parametrically defined by the vector $\mathbf{p}_i(s, \phi)$ where s is the parameter for section curve in XY plane and ϕ for rotation angle about cutter (Z) axis. The equations for curve segments swept to form peripheral surfaces are defined in the previous section in the form of vector $\mathbf{p}_i(s)$. The sweeping rule is defined with the help of transformation matrix ($[\mathbf{T}_s]$). This rule is responsible for combined rotational and linear sweep.

$$[\mathbf{T}_s] = \begin{bmatrix} \cos\phi & \sin\phi & 0 & 0 \\ -\sin\phi & \cos\phi & 0 & 0 \\ 0 & 0 & 1 & 0 \\ 0 & 0 & -\frac{P\phi}{2\pi} & 0 \end{bmatrix}, \text{ where } 0 \leq \phi \leq \frac{2\pi L}{P}$$

The sweeping operation $\mathbf{p}_1(s).[\mathbf{T}_s]$ models peripheral land (Σ_2). Major flank (Σ_3) is obtained by using relation $\mathbf{p}_2(s).[\mathbf{T}_s]$, while tertiary peripheral land of the tooth (Σ_4) and blending surface (Σ_5) are modeled by performing the operations $\mathbf{p}_3(s).[\mathbf{T}_s]$ and $\mathbf{p}_4(s).[\mathbf{T}_s]$ respectively. The operation $\mathbf{p}_5(s).[\mathbf{T}_s]$ leads to rake face of the 2^{nd} tooth, represented as ${}^2\Sigma_1$.

6.1.3 End Surface Patches

Surface patches Σ_6 to Σ_9 form the end of the tooth of a shell mill. The modeling of these surface patches is described in this subsection.

Face Land Σ_6

Face land is formed when an unbounded XY plane $[u_6\ v_6\ 0\ 1]$ $(-\infty \leq u_6, v_6 \leq \infty)$ undergoes following transformations in order

(i) Rotation by an angle α_6 in positive direction about X axis $[R_{x,\alpha_6}]$
(ii) Rotation by β_6 in positive direction about Y axis $[R_{y,\beta_6}]$
(iii) Rotation by $\phi_c = (\phi_{max} - \gamma_1)$ in negative direction about Z axis $[R_{z,\phi_c}]$
(iv) Translation by d_{61} along X axis and d_{63} along Z axis $[T_{xy}]$

Figure 6.5 shows the orientation and placement of face land in global coordinate system C_1. It is mathematically defined with the expression $\mathbf{p}_6(u_6, v_6) = [u_6\ v_6\ 0\ 1].[R_{x,\alpha_6}].[R_{y,\beta_6}].[R_{z,\phi_c}].[T_{xy}]$. The x, y, z components of $\mathbf{p}_6$ are

$$\begin{aligned} p_{6x} &= u_6 \cos\beta_6 \cos\phi_c + v_6(\sin\alpha_6 \sin\beta_6 \cos\phi_c + \cos\alpha_6 \sin\phi_c) + d_{61} \\ p_{6y} &= -u_6 \cos\beta_6 \sin\phi_c + v_6(-\sin\alpha_6 \sin\beta_6 \sin\phi_c + \cos\alpha_6 \cos\phi_c) \\ p_{6z} &= u_6 \sin\beta_6 + v_6 \sin\alpha_6 \cos\beta_6 + d_{63} \end{aligned} \tag{6.3}$$

Translation distances d_{61} and d_{63} are found to be

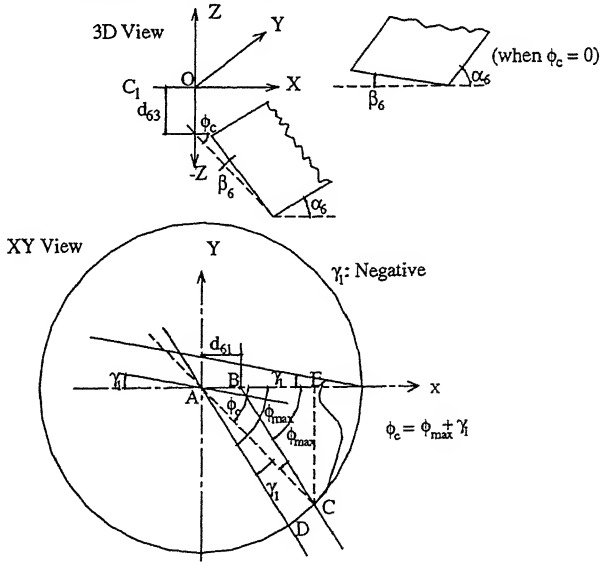

Figure 6.5: Formation of Face Land

$$d_{61} = \frac{D}{2}\left[\cos\phi_{max} - \frac{\sin\phi_{max}}{\tan\phi_c}\right] \text{ and}$$

$$d_{63} = -L + \frac{\frac{D}{2}\sin\phi_{max}}{\sin\phi_c}\tan\beta_6$$

Minor Flank Σ_7

An unbounded XY plane [u_7 v_7 0 1] ($u_7, v_7 \in [-\infty, \infty]$), when rotated by angle α_7 in positive direction about X axis [R_{x,α_7}], followed by ϕ_c in negative direction about Z axis [R_{z,ϕ_c}] and then translated [T_{xy}] by distances d_{71} and d_{73} along X and Z axis respectively forms minor flank.

Figure 6.6 shows the location and orientation of minor flank in C_1. The mathematical definition of $\mathbf{p}_7(u_7, v_7)$ is satisfied by the following relation

$$\mathbf{p}_7 = [(u_7 \cos\phi_c + v_7 \cos\alpha_7 \sin\phi_c + d_{71}) \quad (-u_7 \sin\phi_c + v_7 \cos\alpha_7 \cos\phi_c) \quad (v_7 \sin\alpha_7 + d_{73}) \quad 1] \tag{6.4}$$

where $d_{71} = \frac{D}{2}\left[\cos\phi_{max} - \frac{\sin\phi_{max}}{\tan\phi_c}\right] + \frac{l_3 \cos\alpha_6}{\sin\phi_c}$ and $d_{73} = -L + l_3 \sin\alpha_6$

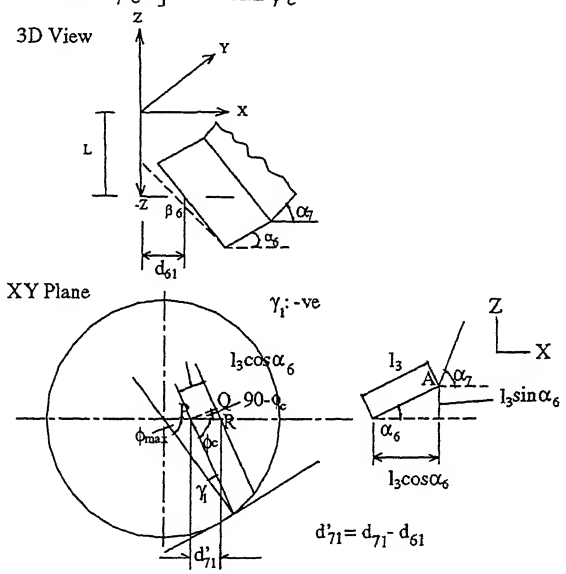

Figure 6.6: Formation of Minor Flank

Back of Cutting Tooth Σ_8

This surface is formed by an XY plane placed at a distance of δ_8 along Z axis and hence given by $\mathbf{p}_8(u_8, v_8) = [u_8 \quad v_8 \quad \delta_8 \quad 1]$ ($-\infty \leq u_8, v_8 \leq \infty$). The value of δ_8 is flexible and depends on designers' discretion.

Rake Face Extension Σ_9

It is formed when an infinite YZ plane [0 v_9 w_9 1] ($-\infty \leq v_9, w_9 \leq \infty$) undergoes following transformations

(i) Rotation by an angle β_9 ($\beta_9 \geq 0$) about Y axis [R_{y,β_9}]. Angle β_9 depends on helix angle λ and is given by $\beta_9 = (90° - \lambda^*)$, where $\lambda^* = \lambda + (15-25)°$, but $\leq 90°$.

(ii) Rotation by α_9 ($\alpha_9 \geq 0$) about X axis $[R_{x,\alpha_9}]$
(iii) Rotation by $(90° - \phi_c)$ in positive sense about Z axis $[R_{z,(90°-\phi_c)}]$
(iv) Translation by d_{91} $(= d_{61})$ along X axis and d_{93} $(= d_{63})$ along Z axis $[T_{xy}]$

The location of rake face extension in a tooth of the shell mill is shown in Figure 6.7. The components of the equation defining Σ_9 expressed by $\mathbf{p}_6(u_9, v_9)$ are

$$\begin{aligned} p_{9x} &= -v_9 \cos\alpha_9 \cos\phi_c + w_9(\sin\beta_9 \sin\phi_c + \sin\alpha_9 \cos\beta_9 \cos\phi_c) + d_{91} \\ p_{9y} &= v_9 \cos\alpha_9 \sin\phi_c + w_9(\sin\beta_9 \cos\phi_c - \sin\alpha_9 \cos\beta_9 \sin\phi_c) \\ p_{9z} &= v_9 \sin\alpha_9 + w_9 \cos\alpha_9 \cos\beta_9 + d_{93} \end{aligned} \tag{6.5}$$

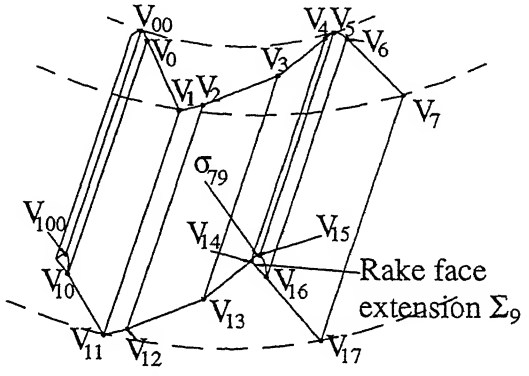

Figure 6.7: Detailed model and the Vertices of a Single Tooth of Shell Mill

6.2 Modeling of Shell Mill Body

The body of shell mill is made up of ten surfaces labeled as $\Sigma_{51} \ldots \Sigma_{60}$. These surfaces are considered to be either planar or cylindrical in geometry. The surfaces in terms of their placement and orientation for one position of the cutter are shown in Figure 6.8 and their geometric modeling for the specified position is described in this section.

Cutter Back Plane Σ_{51}

Surface patch Σ_{51} is the annular plane forming the arbor end of the shell mill as shown in Figure 6.8. It is perpendicular to cutter axis and modeled by displacing an infinite XY plane by an amount $d_{51,3}$ along Z direction. Mathematically it is defined as $\mathbf{p}_{51}(u_{51}, v_{51}) = [u_{51} \quad v_{51} \quad d_{51,3} \quad 1]$ $(-\infty \leq u_{51}, v_{51} \leq \infty)$. The value of $d_{51,3}$ is at the designers' discretion.

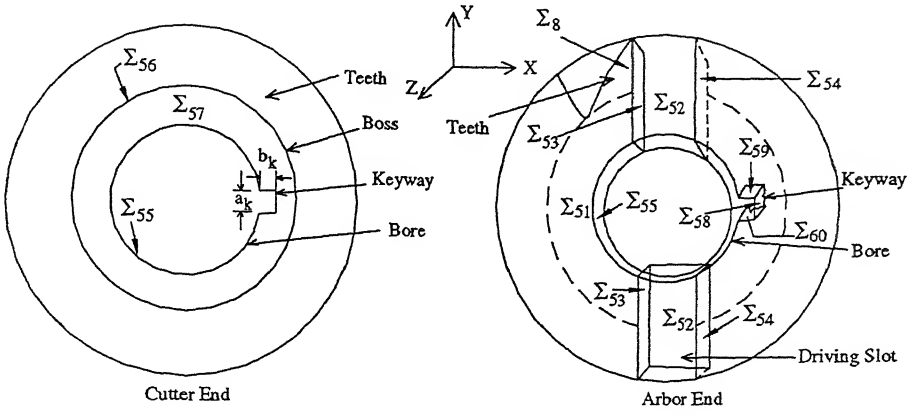

Figure 6.8: Surface Patches of Shell Mill Body

Driving Slot Planes Σ_{52}, Σ_{53} and Σ_{54}

The driving slot of the shell mill is composed of three planes Σ_{52}, Σ_{52} and Σ_{54}. They are formed by suitably positioning appropriate unbounded planes. The plane Σ_{52} is formed by positioning an XY plane at $z = -b$, while the walls of driving slot Σ_{53} and Σ_{54} are formed by placing YZ planes at $x = -\frac{a}{2}$ and $x = \frac{a}{2}$ respectively.

$\mathbf{p}_{52}(u_{52}, v_{52}) = [u_{52} \quad v_{52} \quad -b \quad 1]$

$\mathbf{p}_{53}(v_{53}, w_{53}) = [-\frac{a}{2} \quad v_{53} \quad w_{53} \quad 1]$

$\mathbf{p}_{54}(v_{54}, w_{54}) = [\frac{a}{2} \quad v_{54} \quad w_{54} \quad 1]$

where $-\infty \leq u_{52}, v_{52}, v_{53}, v_{54} \leq \infty$ and $-b \leq w_{53}, w_{54} \leq 0$ for the orientation of the cutter shown in Figure 6.8.

Surface of Bore Σ_{55}

A bore of diameter d and length l with axis normal to XY plane (coinciding with Z axis of C_1) is formed as a cylindrical surface of revolution and defined by the expression $\mathbf{p}_{55}(w_{55}, \phi_{55}) = [\frac{d}{2}\cos\phi_{55} \quad \frac{d}{2}\sin\phi_{55} \quad -l(1-w_{55}) \quad 1]$ for $0 \leq w_{55} \leq 1$ and $0 \leq \phi_{55} \leq 2\pi$

Surface of Boss Σ_{56}

This is also formed as a cylindrical surface of revolution of diameter d_1 and length $(L - l)$. The axis of boss is coincident with the axis of bore (global Z axis). Thus, $\mathbf{p}_{56}(w_{56}, \phi_{56}) = [\frac{d_1}{2}\cos\phi_{56} \quad \frac{d_1}{2}\sin\phi_{56} \quad w_{56} \quad 1]$ for $-L \leq w_{56} \leq -l$ and $0 \leq \phi_{56} \leq 2\pi$

Plane joining Bore and Boss Σ_{57}

This is an XY plane defined as $\mathbf{p}_{57}(u_{57}, v_{57}) = [u_{57} \quad v_{57} \quad -l \quad 1]$ $(u_{57}, v_{57} \in [-\infty, \infty])$.

Keyway Surface Patches Σ_{58}, Σ_{59} and Σ_{60}

Keyway in the body of shell mill is made up of planes $\Sigma_{58} - \Sigma_{60}$. Plane Σ_{58} is formed by suitably transforming a YZ plane while planes Σ_{59} and Σ_{60} are formed due to proper positioning of ZX planes for the orientation of the cutter shown in Figure 6.8. They are expressed with the help of

$\mathbf{p}_{58}(v_{58}, w_{58}) = [(\frac{d}{2} + b_k) \quad v_{58} \quad w_{58} \quad 1]$

$\mathbf{p}_{59}(u_{59}, w_{59}) = [u_{59} \quad \frac{a_k}{2} \quad w_{59} \quad 1]$

$\mathbf{p}_{60}(u_{60}, w_{60}) = [u_{60} \quad -\frac{a_k}{2} \quad w_{60} \quad 1]$

where $-\frac{a_k}{2} \leq v_{58} \leq \frac{a_k}{2}$, $\frac{d}{2} \leq u_{59}, u_{60} \leq (\frac{d}{2} + b_k)$ and $-l \leq w_{58}, w_{59}, w_{60} \leq 0$

6.3 Transitional Surfaces of Shell Mill

A transitional surface is the surface that blends two surfaces to avoid formation of a sharp edge. The transitional surfaces for the design of the shell mill discussed in this chapter are:

(i) Blending surface located on the tooth of shell mill, between surface patches Σ_7 and ${}^2\Sigma_9$, labeled as $\sigma_{7,9}$
(ii) Surface blending tooth with the cutter body, between Σ_8 and $\Sigma_{51} - \sigma_{8,51}$
(iii) Chamfer between Σ_{51} and Σ_{53}, referred as σ_{b13}
(iv) Chamfer between Σ_{51} and $\Sigma_{54} - \sigma_{b14}$
(v) Chamfer between Σ_{51} and $\Sigma_{55} - \sigma_{b15}$
(vi) Chamfer between Σ_{51} and $\Sigma_{58} - \sigma_{b18}$
(vii) Blending surface between Σ_{52} and $\Sigma_{53} - \sigma_{b23}$
(viii) Blending surface between Σ_{52} and $\Sigma_{54} - \sigma_{b24}$
(ix) Chamfer between Σ_{55} and $\Sigma_{57} - \sigma_{b27}$

The last seven transitional surfaces are located on the body of the shell mill. To geometrically model a transitional surface the edge that need to be replaced by blending surface and the vertices defining that edge need to be known a priori. The edges and vertices of intersection of surface patches forming the CAD model of the shell mill are presented in Appendix B. Some of these transitional surfaces are shown with the help of Figure 6.9.

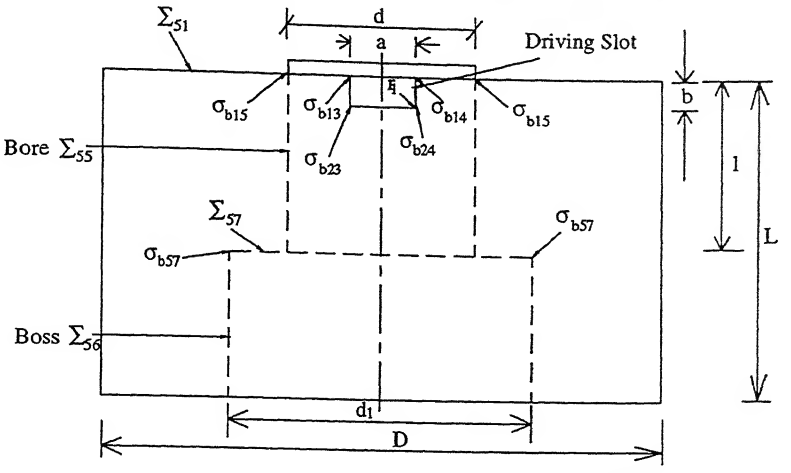

Figure 6.9: Transitional Surfaces of Shell Mill

Blending Surface $\sigma_{7,9}$

This surface blends the minor flank (Σ_7) of one tooth with the rake face extension of next tooth ($^2\Sigma_9$) as shown in Figure 6.7. The vertices V_{15} and V_{23} that form the edge of intersection of Σ_7 and $^2\Sigma_9$ are known a priori and so are other vertices in the neighborhood to these vertices (Appendix B). The blend is modeled as a bicubic Bézier patch, defined with the help of four cubic Bézier boundary curves [80, 94, 125]. Out of these four curves, two approximate circular arcs and two straight lines so as to give proper shape to blend. One of the boundary curves is formed by rounding a pair of edges $V_{14}V_{15}$ and $V_{15}V_{16}$ (Figure 6.7). This round is modeled as a cubic Bézier curve approximating a circular arc with the help of four control points $\mathbf{p}_{00}$, $\mathbf{p}_{01}$, $\mathbf{p}_{02}$ and $\mathbf{p}_{03}$. These control points are evolved as described by Choi[26].

Unit vectors along the directions $V_{15}V_{16}$ and $V_{15}V_{14}$ are
$\hat{a} = \frac{\mathbf{v}_{16} - \mathbf{v}_{15}}{|\mathbf{v}_{16} - \mathbf{v}_{15}|}$ and $\hat{b} = \frac{\mathbf{v}_{14} - \mathbf{v}_{15}}{|\mathbf{v}_{14} - \mathbf{v}_{15}|}$ respectively.
The half corner angle ϕ formed by two line segments is $\phi = \frac{1}{2}\cos^{-1}(\hat{a}.\hat{b})$ $(0 \leq \phi \leq 90°)$, while the distance between the corner point V_{15} and blend end point $\mathbf{p}_{03}$ is
$\delta_{79} = |\mathbf{v}_{14} - \mathbf{v}_{15}|$. The radius of blend can be obtained using the relation
$r_{79} = \delta_{79}.\tan\phi$. Therefore the two end control points are $\mathbf{p}_{00} = \mathbf{v}_{15} + \delta_{79}.\hat{a}$, and $\mathbf{p}_{03} = \mathbf{v}_{14}$. The distance between the mid and end control points is $\Delta = \frac{2|\mathbf{p}_{03} - \mathbf{p}_{00}|}{3(1+\sin\phi)}$.
The middle control points of the Bézier curve are then given as
$\mathbf{p}_{01} = \mathbf{p}_{00} - \Delta.\hat{a}$ and $\mathbf{p}_{02} = \mathbf{p}_{03} - \Delta.\hat{b}$.
Similarly another cubic Bézier curve models a circular arc about vertex V_{23} and is given by $\mathbf{p}_{30}$, $\mathbf{p}_{31}$, $\mathbf{p}_{32}$ and $\mathbf{p}_{33}$. The end control points of this curve are given by
$\mathbf{p}_{30} = \mathbf{v}_{23} + \delta_{79}.\hat{a}'$, and $\mathbf{p}_{33} = \mathbf{v}_{23} + \delta_{79}\hat{b}$ where
$\hat{a}' = \frac{\mathbf{v}_{24} - \mathbf{v}_{23}}{|\mathbf{v}_{24} - \mathbf{v}_{23}|}$

The mid control points are $\mathbf{p}_{31} = \mathbf{p}_{30} - \Delta.\hat{a}'$ and $\mathbf{p}_{32} = \mathbf{p}_{33} - \Delta.\hat{b}$.
The two straight lines formed as cubic Bézier curve are given with the help of control points $\mathbf{p}_{00}\mathbf{p}_{10}\mathbf{p}_{20}\mathbf{p}_{30}$ and $\mathbf{p}_{03}\mathbf{p}_{13}\mathbf{p}_{23}\mathbf{p}_{33}$, where
$\mathbf{p}_{10} = (2\mathbf{p}_{00}+\mathbf{p}_{30})/3$, $\mathbf{p}_{20} = (\mathbf{p}_{00}+2\mathbf{p}_{30})/3$, $\mathbf{p}_{13} = (2\mathbf{p}_{03}+\mathbf{p}_{33})/3$ and $\mathbf{p}_{23} = (\mathbf{p}_{03}+2\mathbf{p}_{33})/3$

Blending surface $\sigma_{8,51}$

This transitional surface blends the back of cutting end (Σ_8) of the tooth and cutter back plane (Σ_{51}). It is modeled by revolving a circular arc in ZX plane about Z axis. The circular arc is modeled as a generalized cubic Bézier curve and defined by control points $\mathbf{p}'_{00}$, $\mathbf{p}'_{01}$, $\mathbf{p}'_{02}$ and $\mathbf{p}'_{03}$. On ZX plane the vertex of intersection of Σ_8 and Σ_{51} is given by $[\frac{d_2}{2}\ \ 0\ \ 0\ \ 1]$. The unit vectors from the intersection point along the direction of $\mathbf{p}'_{00}$ and $\mathbf{p}'_{03}$ are $\hat{a} = \hat{k}$ and $\hat{b} = \hat{\imath}$ respectively and the half corner angle is $\phi = \frac{1}{2}\cos^{-1}(\hat{a}.\hat{b}) = 45°$. This leads to the radius of the circular arc as $r_{8,51} = \delta_{8,51}\tan 45° = d_{51,3}$. The control points of the Bézier curve are
$\mathbf{p}'_{00} = [\frac{d_2}{2}\ \ 0\ \ d_{51,3}\ \ 1]$, $\mathbf{p}'_{03} = [(\frac{d_2}{2}+d_{51,3})\ \ 0\ \ 0\ \ 1]$, $\mathbf{p}'_{01} = [\frac{d_2}{2}\ \ 0\ \ 0.4477d_{51,3}\ \ 1]$ and
$\mathbf{p}'_{02} = [(\frac{d_2}{2} + 0.4477d_{51,3})\ \ 0\ \ 0\ \ 1]$, as $\Delta = \frac{2|\mathbf{p}'_{03} - \mathbf{p}'_{00}|}{3(1+\sin 45°)} = 0.5523d_{51,3}$.
The Bézier curve formed by these control points is expressed as $\mathbf{r}(u) = \sum_{i=0}^{3} B_{i,n}(u)P_{0i}$.
This curve when rotated by an angle ϕ forms the blending surface $\sigma_{8,51}$ which is given by
$\mathbf{p}_{8,51}(u,\phi) = [\mathbf{r}_x(u)\cos\phi\ \ \mathbf{r}_y(u)\sin\phi\ \ \mathbf{r}_z(u)\ \ 1]$

Chamfered Surface σ_{b13}

This transitional surface blends the intersection of driving slot wall Σ_{53} with the cutter back plane Σ_{51}. It is assumed to be a 45° chamfer and modeled by linearly sweeping a straight edge of unit width, inclined at 45° and joining vertices $[\frac{-a}{2}\ \ 0\ \ 0\ \ 1]$ and $[-(\frac{a}{2}+d_{51,3})\ \ 0\ \ d_{51,3}\ \ 1]$. These vertices lie in the neighborhood of vertex of intersection of Σ_{51} and Σ_{53} on ZX plane. The sweep is along Y axis in terms of parameter v. The range of the parameter is specified by $v \in (\pm\frac{d}{2}\cos\theta, \pm\frac{d_2}{2}\cos\theta_1)$, where $\theta = \sin^{-1}(\frac{a}{d})$ and $\theta_1 = \sin^{-1}(\frac{a}{d_2})$. The equation of the chamfer satisfies the relation
$\mathbf{p}_{b13}(u,v) = [(\frac{-a}{2} - ud_{51,3})\ \ \{\pm\frac{d\cos\theta}{2} \pm v(\frac{d_2\cos\theta_1 - d\cos\theta}{2})\}\ \ ud_{51,3}\ \ 1]\ (0 \le u, v \le 1)$

Chamfered Surface σ_{b14}

This being similar to σ_{b13} can be modeled by taking mirror image of σ_{b13} about YZ plane and is expressed as
$\mathbf{p}_{b14}(u,v) = [(\frac{a}{2}+ud_{51,3}) \ \{\pm\frac{d\cos\theta}{2}\pm v(\frac{d_2\cos\theta_1 - d\cos\theta}{2})\} \ ud_{51,3} \ \ 1] \ (0 \le u,v \le 1)$

Chamfered Surface σ_{b15}

This renders a chamfer at the intersection of cutter back plane Σ_{51} and bore Σ_{55}. It is modeled as surface of revolution by rotating an edge of unit length at 45° to X axis on ZX plane about Z axis. The edge is formed by joining the vertices $(\frac{d}{2},\ 0,\ d_{51,3}-0.707)$ and $(\frac{d}{2}+0.707,\ 0,\ d_{51,3})$. The surface of revolution σ_{b15} is defined as
$\mathbf{p}_{b15}(u,\phi) = [(\frac{d}{2}+0.707u)\cos\phi \quad (\frac{d}{2}+0.707u)\sin\phi \quad \{d_{51,3}-0.707(1-u)\} \quad 1]$ with $u \in [0,1]$ and $\phi \in [0,2\pi]$. The range of ϕ is modified to accommodate driving slots and keyway in the chamfer.

Chamfered Surface σ_{b18}

This transitional surface is a planar 45° chamfer defined by sweeping linearly an edge of unit width lying on ZX plane and inclined at 45° to X axis along Y axis. The edge to be swept is defined by vertices $(\frac{d}{2}+b_k,\ 0,\ d_{51,3}-0.707)$ and $(\frac{d}{2}+b_k+0.707,\ 0,\ d_{51,3})$. The surface σ_{b18} is formed by sweeping this edge from $y = -\frac{a_k}{2}$ to $\frac{a_k}{2}$. Therefore,
$\mathbf{p}_{b18}(u,v) = [(\frac{d}{2}+b_k+0.707u) \ \ (\frac{-a_k}{2}+va_k) \ \ \{d_{51,3}-0.707(1-u)\} \ \ 1] \ (0 \le u,v \le 1)$

Blending Surface σ_{b23}

This surface is formed due to rounding of intersection of surface Σ_{52} with Σ_{53}. It is modeled by sweeping linearly a cubic Bézier curve. On $y = 0$ plane, the edge of intersection of Σ_{52} and Σ_{53} is given as $[-\frac{a}{2} \ \ 0 \ \ -b \ \ 1]$. Unit normals from this vertex in the direction of control points $\mathbf{p}_{00}$ and $\mathbf{p}_{03}$ of Bézier curve are $\hat{k}$ and $\hat{\imath}$ respectively. The half corner angle is $\frac{1}{2}\cos^{-1}(\hat{k}.\hat{\imath}) = 45°$. Based on half corner angle and the radius of round forming blend (r_1), four control points of the Bézier curve are
$\mathbf{p}''_{00} = [\frac{-a}{2} \ \ 0 \ \ (-b+r_1) \ \ 1]$, $\mathbf{p}''_{03} = [(\frac{-a}{2}+r_1) \ \ 0 \ \ -b \ \ 1]$,
$\mathbf{p}''_{01} = [\frac{-a}{2} \ \ 0 \ \ (-b+0.4477r_1) \ \ 1]$ and $\mathbf{p}''_{02} = [(\frac{-a}{2}+0.4477r_1) \ \ 0 \ \ -b \ \ 1]$
The curve formed by these four control points is swept along Y axis from $\pm\frac{d}{2}\cos\theta$ to $\pm\frac{d_2}{2}\cos\theta_1$, where θ and θ_1 are as defined for σ_{b13}. The equation of σ_{b23} is given by
$\mathbf{p}_{b23}(u,v) = [\mathbf{r}_x(u) \quad \{\pm\frac{d\cos\theta}{2}\pm v(\frac{d_2\cos\theta_1-d\cos\theta}{2})\} \quad \mathbf{r}_z(u) \quad 1] \ (0 \le u,v \le 1)$

Blending Surface σ_{b24}

This is similar to blending surface σ_{b23}. For the case shown in Figure 6.9, this surface is positioned at $x = +\frac{a}{2}$, while σ_{b23} is placed at $x = -\frac{a}{2}$. Thus,
$\mathbf{p}_{b24}(u,v) = [\mathbf{r'}_x(u) \quad \{\pm\frac{d\cos\theta}{2} \pm v(\frac{d_2\cos\theta_1 - d\cos\theta}{2})\} \quad \mathbf{r}_z(u) \quad 1] \; (0 \leq u, v \leq 1)$

Chamfered Surface σ_{b57}

It is modeled by revolving an unit edge lying on ZX plane and inclined at 45° to X axis about Z axis. The edge is defined by vertices ($\frac{d}{2}$, 0, $-l$+0.707) and ($\frac{d}{2}$+0.707, 0, $-l$). The surface σ_{b57} formed by revolving this edge is given by
$\mathbf{p}_{b57}(u,\phi) = [(\frac{d}{2} + 0.707u)\cos\phi \quad (\frac{d}{2} + 0.707u)\sin\phi \quad \{-l + 0.707(1-u)\} \quad 1]$
with $0 \leq u \leq 1$ and $\alpha_1 \leq \phi \leq (2\pi - \alpha_1)$. Angle $\alpha_1 = \sin^{-1}(\frac{a_k}{d})$ provides width for keyway.

6.4 Mapping

Mapping implies conversion of one set of relations to another. The relations among the angles specified by conventional standards and nomenclature proposed in this work are specified in terms of forward and inverse mapping. Forward mapping means specifying a set of two-dimensional (2D) angles established by conventional nomenclatures in terms of proposed three-dimensional (3D) rotational angles. On the contrary, inverse mapping converts the conventional 2D angles to obtain the relations for 3D angles. The conventional angles for a helicoidal cutter like shell mill are evaluated by projecting on appropriate planes the angles formed by planes tangent to surfaces of its teeth (Figure 6.2) at the nose of the cutter [29, 44, 119]. The nose is formed due to intersection of major and minor cutting edge. This is illustrated with the help of Mapping Guide Table (Table 6.2). The sign convention adopted for 2D and 3D angles is as discussed in the previous chapters.

6.4.1 Forward Mapping

This section develops the relations for conventional 2D angles in terms of 3D rotational angles.

Helical/Axial Rake Angle (γ_H/γ_A)

The mathematical equation of rake face (Σ_1) is derived as $\mathbf{p}_1(s,\phi) = \mathbf{p}_5(s)|_{\psi=0}.[T_s]$
The parametric definition of curve $\mathbf{p}_5(s)$ is specified in Eq. (6.2). Based on it, the

Conventional Angles	Formed by Plane	About the Plane	Projected on Plane
Helical/Axial Rake Angle, γ_H/γ_A	Σ_1	ZX*	YZ*
Radial Rake Angle, γ_R	Σ_1	ZX*	XY
Face Relief Angle, α_F	Σ_6	XY	YZ*
Peripheral Relief Angle, α_P	Σ_2	YZ*	XY
Face Cutting Edge Angle, ϕ_e	Σ_6	XY	ZX*
Peripheral Cutting Edge Angle, ϕ_P	Σ_2	YZ*	ZX*
Face Clearance Angle, α_{1F}	Σ_7	XY	YZ*
Peripheral Clearance Angle, α_{1P}	Σ_3	YZ*	XY

Table 6.2: Mapping Guide Table for Shell Mill

Note: YZ* and ZX* are YZ and ZX planes rotated by $-\phi_{max}$ about Z axis, as the nose is formed when the vertex V_1 is rotated by $-\phi_{max}$ about Z axis

components of $\mathbf{p}_1(s,\phi)$ defining rake face are

$$\begin{aligned} p_{1x}(s,\phi) &= \left\{\frac{D}{2} - A\cos\gamma_1(1-s)\right\}\cos\phi - A\sin\gamma_1(1-s)\sin\phi \\ p_{1y}(s,\phi) &= -\left\{\frac{D}{2} - A\cos\gamma_1(1-s)\right\}\sin\phi - A\sin\gamma_1(1-s)\cos\phi \\ p_{1z}(s,\phi) &= -\frac{P\phi}{2\pi} \end{aligned} \tag{6.6}$$

where $A = \left\{\dfrac{\left(\frac{D-d_2}{2}\right)-r_1}{\cos\gamma_1} + r_1\tan\gamma_1\right\}$

At the nose of the shell mill that is specified by vertex V_{11} and is shown in Figure 6.2 and Figure 6.7, the parameters of $\mathbf{p}_1(s.\phi)$ are $s=1$ and $\phi = \phi_{max} = \frac{2\pi L}{P}$. This gives

$$\begin{aligned} p_{1x}(s,\phi)|_{V_{11}} &= \frac{D}{2}\cos\phi_{max} \\ p_{1y}(s,\phi)|_{V_{11}} &= -\frac{D}{2}\sin\phi_{max} \\ p_{1z}(s,\phi)|_{V_{11}} &= -L \end{aligned}$$

Tangents to rake face are derived as $\frac{\partial \mathbf{p}_1}{\partial s}$ and $\frac{\partial \mathbf{p}_1}{\partial \phi}$ and given by

$$\begin{aligned} \mathbf{p}_{1s}(s,\phi) &= A\cos(\gamma_1-\phi)\hat{\imath} + A\sin(\gamma_1-\phi)\hat{\jmath} \\ \mathbf{p}_{1\phi}(s,\phi) &= \left[-\left\{\frac{D}{2} - A\cos\gamma_1(1-s)\right\}\sin\phi - A\sin\gamma_1(1-s)\cos\phi\right]\hat{\imath} \\ &\quad + \left[-\left\{\frac{D}{2} - A\cos\gamma_1(1-s)\right\}\cos\phi + A\sin\gamma_1(1-s)\sin\phi\right]\hat{\jmath} - \frac{P}{2\pi}\hat{k} \end{aligned}$$

Tangents to Σ_1 at nose are

$$\begin{aligned} \mathbf{p}_{1s}(s,\phi)|_{V_{11}} &= A\cos(\gamma_1-\phi_{max})\hat{\imath} + A\sin(\gamma_1-\phi_{max})\hat{\jmath} \\ \mathbf{p}_{1\phi}(s,\phi)|_{V_{11}} &= -\frac{D}{2}\sin\phi_{max}\hat{\imath} - \frac{D}{2}\cos\phi_{max}\hat{\jmath} - \frac{P}{2\pi}\hat{k} \end{aligned}$$

and the normal to Σ_1 at nose is

$$\mathbf{n}_1|_{V_{11}} = \frac{PA}{2\pi}\sin(\phi_{max} - \gamma_1)\hat{\imath} + \frac{PA}{2\pi}\cos(\phi_{max} - \gamma_1)\hat{\jmath} - \frac{DA}{2}\cos\gamma_1\hat{k} \tag{6.7}$$

Helical rake angle (γ_H) at nose is the angle made by $\mathbf{n}_1|_{V_{11}}$ with ZX plane rotated by $-\phi_{max}$ about Z axis. It is found by projecting the normal $\mathbf{n}_1|_{V_{11}}$ on YZ plane rotated by $-\phi_{max}$ about Z axis. To evaluate γ_H, $\mathbf{n}_1|_{V_{11}}$ is rotated by $+\phi_{max}$ (in inverse direction) about Z axis and then it is projected on YZ plane and angle formed by this projection with ZX plane is found. This angle is equivalent to γ_H at nose.
Normal $\mathbf{n}_1|_{V_{11}}$ when rotated by ϕ_{max} is given as
$\mathbf{n}_{1R}|_{V_{11}} = \frac{PA}{2\pi}\sin(-\gamma_1)\hat{\imath} + \frac{PA}{2\pi}\cos(-\gamma_1)\hat{\jmath} - \frac{DA}{2}\cos\gamma_1\hat{k}$
This normal when projected on YZ plane becomes
$\mathbf{n}_{1Rp}|_{V_{11}} = \frac{PA}{2\pi}\cos(-\gamma_1)\hat{\jmath} - \frac{DA}{2}\cos\gamma_1\hat{k}$
Unit projected normal vector $\hat{n}_{1Rp}|_{V_{11}} = \dfrac{(P/\pi)\hat{\jmath} + D\hat{k}}{\sqrt{(P/\pi)^2 + D^2}}$
Angle γ_H is equivalent to the angle between $\hat{n}'_{1Rp}|_{V_{11}}$ and unit vector normal to ZX plane ($\hat{\jmath}$). Therefore, scalar product of $\hat{n}'_{1Rp}|_{V_{11}}$ with $\hat{\jmath}$ gives

$$\gamma_H = \cos^{-1}\left[\frac{P/\pi}{\sqrt{(P/\pi)^2 + D^2}}\right] \tag{6.8}$$

Radial Rake Angle (γ_R)

To evaluate radial rake angle, the normal to rake face Σ_1 at nose given by Eq. (6.7) is projected on XY plane and expressed as
$\mathbf{n}_{1p}|_{V_{11}} = \frac{PA}{2\pi}\sin(\phi_{max} - \gamma_1)\hat{\imath} + \frac{PA}{2\pi}\cos(\phi_{max} - \gamma_1)\hat{\jmath}$
Unit projected normal vector is $\hat{n}_{1p}|_{V_{11}} = \sin(\phi_{max} - \gamma_1)\hat{\imath} + \cos(\phi_{max} - \gamma_1)\hat{\jmath}$
Radial rake angle at nose is formed by surface Σ_1 with the ZX plane rotated by $-\phi_{max}$ about Z axis. The vector normal to this rotated ZX plane is $(\sin\phi_{max}\hat{\imath} + \cos\phi_{max}\hat{\jmath})$.
Radial rake angle is the angle between $\hat{n}_{1p}|_{V_{11}}$ and the vector normal to rotated ZX plane, given as above, and on solution leads to

$$\gamma_R = -\gamma_1 \tag{6.9}$$

Face Relief Angle (α_F)

Face relief angle is formed by face land (Σ_6) with XY plane and viewed on projection to YZ* plane. Equation (6.3) expresses the mathematical definition of Σ_6. The tangents to Σ_6 are
$\mathbf{p}_{6u} = \cos\beta_6\cos\phi_c\hat{\imath} - \cos\beta_6\sin\phi_c\hat{\jmath} - \sin\beta_6\hat{k}$

$\mathbf{p}_{6v} = (\sin\alpha_6 \sin\beta_6 \cos\phi_c + \cos\alpha_6 \sin\phi_c)\hat{\imath} + (-\sin\alpha_6 \sin\beta_6 \sin\phi_c + \cos\alpha_6 \cos\phi_c)\hat{\jmath} + \sin\alpha_6 \cos\beta_6 \hat{k}$

Vector normal to Σ_6 is $\mathbf{n}_6 = (\cos\alpha_6 \sin\beta_6 \cos\phi_c - \sin\alpha_6 \sin\phi_c)\hat{\imath} - (\cos\alpha_6 \sin\beta_6 \sin\phi_c + \sin\alpha_6 \cos\phi_c)\hat{\jmath} + \cos\alpha_6 \cos\beta_6 \hat{k}$

Instead of finding projection of $\mathbf{n}_6$ on YZ* plane, $\mathbf{n}_6$ is rotated by $+\phi_{max}$ about Z axis and then projected on YZ plane. As $\phi_{max} - \phi_c = \gamma_1$, $\mathbf{n}_6$ on rotation is given as

$$\mathbf{n}_{6R} = (\cos\alpha_6 \sin\beta_6 \cos\gamma_1 + \sin\alpha_6 \sin\gamma_1)\hat{\imath} + (\cos\alpha_6 \sin\beta_6 \sin\gamma_1 - \sin\alpha_6 \cos\gamma_1)\hat{\jmath} + \cos\alpha_6 \cos\beta_6 \hat{k} \tag{6.10}$$

The projection of $\mathbf{n}_{6R}$ on YZ plane is

$\mathbf{n}_{6Rp} = (\cos\alpha_6 \sin\beta_6 \sin\gamma_1 - \sin\alpha_6 \cos\gamma_1)\hat{\jmath} + \cos\alpha_6 \cos\beta_6 \hat{k}$

Unit projected normal vector is

$$\hat{n}_{6Rp} = \frac{(\cos\alpha_6 \sin\beta_6 \sin\gamma_1 - \sin\alpha_6 \cos\gamma_1)\hat{\jmath} + \cos\alpha_6 \cos\beta_6 \hat{k}}{\sqrt{(\cos\alpha_6 \sin\beta_6 \sin\gamma_1 - \sin\alpha_6 \cos\gamma_1)^2 + (\cos\alpha_6 \cos\beta_6)^2}}$$

Scalar product of $\hat{n}_{6Rp}$ with unit vector normal to XY plane provides face relief angle

$$\alpha_F = \cos^{-1}\left[\frac{\cos\alpha_6 \cos\beta_6}{\sqrt{(\cos\alpha_6 \sin\beta_6 \sin\gamma_1 - \sin\alpha_6 \cos\gamma_1)^2 + (\cos\alpha_6 \cos\beta_6)^2}}\right] \tag{6.11}$$

Peripheral Relief Angle (α_P)

This angle is formed by helicoidal surface Σ_2 that is defined as

$\mathbf{p}_2(s,\phi) = [(\frac{D}{2} - s.l_1 \sin\gamma_2)\cos\phi + s.l_1 \cos\gamma_2 \sin\phi]\hat{\imath} + [-(\frac{D}{2} - s.l_1 \sin\gamma_2)\sin\phi + s.l_1 \cos\gamma_2 \cos\phi]\hat{\jmath} - \frac{P\phi}{2\pi}\hat{k}$

At nose, $s = 0$ and $\phi = \phi_{max} = \frac{2\pi L}{P}$. This gives

$\mathbf{p}_2'(s,\phi) = \frac{D}{2}\cos\phi_{max}\hat{\imath} + -\frac{D}{2}\sin\phi_{max}\hat{\jmath} - L\hat{k}$

Tangents to Σ_2 are

$\mathbf{p}_{2s}(s,\phi) = (-l_1 \sin\gamma_2 \cos\phi + l_1 \cos\gamma_2 \sin\phi)\hat{\imath} + (l_1 \sin\gamma_2 \sin\phi + l_1 \cos\gamma_2 \cos\phi)\hat{\jmath}$

$\mathbf{p}_{2\phi}(s,\phi) = [-(\frac{D}{2} - s.l_1 \sin\gamma_2)\sin\phi + s.l_1 \cos\gamma_2 \cos\phi]\hat{\imath} + [-(\frac{D}{2} - s.l_1 \sin\gamma_2)\cos\phi - s.l_1 \cos\gamma_2 \sin\phi]\hat{\jmath} - \frac{P}{2\pi}\hat{k}$

Tangents to Σ_2 at nose ($s = 0$, $\phi = \phi_{max}$) are

$\mathbf{p}_{2s}'(s,\phi) = -l_1 \sin(\gamma_2 - \phi_{max})\hat{\imath} + l_1 \cos(\gamma_2 - \phi_{max})\hat{\jmath}$

$\mathbf{p}_{2\phi}'(s,\phi) = -\frac{D}{2}\sin\phi_{max}\hat{\imath} - \frac{D}{2}\cos\phi_{max}\hat{\jmath} - \frac{P}{2\pi}\hat{k}$

Vector normal to Σ_2 at nose is

$$\mathbf{n}_2 = -\frac{Pl_1}{2\pi}\cos(\phi_{max} - \gamma_2)\hat{\imath} + \frac{Pl_1}{2\pi}\sin(\phi_{max} - \gamma_2)\hat{\jmath} + \frac{Dl_1}{2}\sin\gamma_2\hat{k} \tag{6.12}$$

Projection of $\mathbf{n}_2$ on XY plane is

$\mathbf{n}_{2p} = -\frac{Pl_1}{2\pi}\cos(\phi_{max} - \gamma_2)\hat{\imath} + \frac{Pl_1}{2\pi}\sin(\phi_{max} - \gamma_2)\hat{\jmath}$

Peripheral relief angle is the angle between this projection and the YZ* plane. To fine α_P, $\mathbf{n}_{2p}$ is rotated by $+\phi_{max}$ about Z axis and then the angle is found with YZ plane. The rotated normal vector $\mathbf{n}_{2pR}$ is given as

$\mathbf{n}_{2pR} = -\frac{Pl_1}{2\pi}\cos(-\gamma_2)\hat{\imath} + \frac{Pl_1}{2\pi}\sin(-\gamma_2)\hat{\jmath}$

Unit projected normal vector is then

$\hat{n}_{2pR} = -\cos(-\gamma_2)\hat{\imath} + \sin(-\gamma_2)\hat{\jmath}$

Scalar product of $\hat{n}_{2pR}$ with unit vector $\hat{\imath}$ gives peripheral relief angle as

$$\alpha_P = \gamma_2 \tag{6.13}$$

Face Cutting Edge Angle (ϕ_e)

The angle formed by face land Σ_6 with the XY plane and viewed on projection to ZX* plane is face cutting edge angle. To find ϕ_e, normal to Σ_6 is rotated by $+\phi_{max}$ about Z axis and given by Eq. (6.10). The projection of $\mathbf{n}_{6R}$ on ZX plane is then given by

$\mathbf{n}_{6Rp} = (\cos\alpha_6 \sin\beta_6 \cos\gamma_1 + \sin\alpha_6 \sin\gamma_1)\hat{\imath} + \cos\alpha_6 \cos\beta_6 \hat{k}$

Angle ϕ_e, between Σ_6 and XY plane is equivalent to the angle between unit normal projected vector $\hat{n}_{6Rp} = \frac{\mathbf{n}_{6Rp}}{|\mathbf{n}_{6Rp}|}$ and unit vector $\hat{k}$. This is given as

$$\phi_e = \cos^{-1}\left[\frac{\cos\alpha_6 \cos\beta_6}{\sqrt{(\cos\alpha_6 \sin\beta_6 \cos\gamma_1 + \sin\alpha_6 \sin\gamma_1)^2 + (\cos\alpha_6 \cos\beta_6)^2}}\right] \tag{6.14}$$

Peripheral Cutting Edge Angle (ϕ_P)

This angle is formed when normal to helicoidal surface Σ_2 ($\mathbf{n}_2$ is rotated by $+\phi_{max}$ about Z axis and projected to ZX plane. The angle between the unit projected normal vector, thus found, with the unit vector normal to YZ plane is peripheral cutting edge angle. The normal to surface Σ_2 is given by Eq. (6.12). Rotating $\mathbf{n}_2$ about Z axis by $+\phi_{max}$, we get

$\mathbf{n}_{2R} = -\frac{Pl_1}{2\pi}\cos(-\gamma_2)\hat{\imath} + \frac{Pl_1}{2\pi}\sin(-\gamma_2)\hat{\jmath} + \frac{Dl_1}{2}\sin\gamma_2\hat{k}$

Projection of $\mathbf{n}_{2R}$ on ZX plane gives $\mathbf{n}_{2Rp} = -\frac{Pl_1}{2\pi}\cos(-\gamma_2)\hat{\imath} + \frac{Dl_1}{2}\sin\gamma_2\hat{k}$

Angle formed by unit projected normal vector $\hat{n}_{2Rp}$ $(= \frac{\mathbf{n}_{2R}}{|\mathbf{n}_{2R}|})$ with unit vector $\hat{\imath}$ is equivalent to ϕ_P. This is found by taking scalar product of $\hat{n}_{2Rp}$ with $\hat{\imath}$ and given as

$$\phi_P = \cos^{-1}\left[\frac{\frac{P}{\pi}\cos\gamma_2}{\sqrt{(\frac{P}{\pi})^2\cos^2\gamma_2 + D^2\sin^2\gamma_2}}\right] \tag{6.15}$$

Face Clearance Angle (α_{1F})

This angle is formed by minor flank (Σ_7) with XY plane on projection to YZ* plane. The mathematical expression specifying Σ_7 is given by Eq. (6.4) and the tangents and normal to Σ_7 are given as

$\mathbf{p}_{7u}(u_7, v_7) = \cos\phi_c\hat{\imath} - \sin\phi_c\hat{\jmath}$

$\mathbf{p}_{7v}(u_7, v_7) = \cos\alpha_7 \sin\phi_c\hat{\imath} + \cos\alpha_7\cos\phi_c\hat{\jmath} + \sin\alpha_7\hat{k}$

$\mathbf{n}_7 = -\sin\alpha_7\sin\phi_c\hat{\imath} - \sin\alpha_7\cos\phi_c\hat{\jmath} + \cos\alpha_7\hat{k}$

$\mathbf{n}_7$ when rotated by $+\phi_{max}$ about Z axis is given as

$\mathbf{n}_{7R} = \sin\alpha_7\sin\gamma_1\hat{\imath} - \sin\alpha_7\cos\gamma_1\hat{\jmath} + \cos\alpha_7\hat{k}$

Projection of $\mathbf{n}_{7R}$ on YZ plane is $\mathbf{n}_{7Rp} = -\sin\alpha_7\cos\gamma_1\hat{\jmath} + \cos\alpha_7\hat{k}$

The angle between unit normal projected vector $\hat{n}_{7Rp}$ ($= \mathbf{n}_{7Rp}/|\mathbf{n}_{7Rp}|$) and unit vector normal to XY plane ($\hat{k}$) is face clearance angle satisfying the relation

$$\alpha_{1F} = \cos^{-1}\left[\frac{\cos\alpha_7}{\sqrt{\sin^2\alpha_7\cos^2\gamma_1 + \cos^2\alpha_7}}\right] \tag{6.16}$$

Peripheral Clearance Angle (α_{1P})

Peripheral clearance angle is formed by major flank (Σ_3) with YZ* and viewed on projection to XY plane. The parametric expression of major flank is defined as

$\mathbf{p}_3(s, \phi) = \mathbf{p}_2(s).[T_s]$

Substituting the relation for curve $\mathbf{p}_2(s)$ as given in Eq (6.2), $\mathbf{p}_3(s, \phi)$ becomes

$\mathbf{p}_3(s, \phi) = [(\frac{D}{2} - l_1\sin\gamma_2 - s.l_2\sin\gamma_3)\cos\phi + (l_1\cos\gamma_2 + s.l_2\cos\gamma_3)\sin\phi]\hat{\imath}$

$+ [-(\frac{D}{2} - l_1\sin\gamma_2 - s.l_2\sin\gamma_3)\sin\phi + (l_1\cos\gamma_2 + s.l_2\cos\gamma_3)\cos\phi]\hat{\jmath} - \frac{P\phi}{2\pi}\hat{k}$

Tangents to $\mathbf{p}_3(s, \phi)$ are given by derivatives $\frac{\partial\mathbf{p}_3}{\partial s}$ and $\frac{\partial\mathbf{p}_3}{\partial\phi}$. The parameters of $\mathbf{p}_3$ at the point of intersection of peripheral land, face land, major flank and minor flank (vertex V_{12}) as shown in Figure 6.2 and Figure 6.7 are $s = 0$ and $\phi = \phi' < \phi_{max}$. At this point the tangents to $\mathbf{p}_3(s, \phi)$ are

$\mathbf{p}'_{3s} = l_2\sin(\phi' - \gamma_3)\hat{\imath} + l_2\cos(\phi' - \gamma_3)\hat{\jmath}$

$\mathbf{p}'_{3\phi} = \{-\frac{D}{2} + l_1\cos(\phi' - \gamma_2)\}\hat{\imath} + \{-\frac{D}{2} - l_1\sin(\phi' - \gamma_2)\hat{\jmath}\} - \frac{P}{2\pi}\hat{k}$

where $\phi' = \phi_{max}(1 - \frac{l_3}{L}\sin\alpha_6)$. Normal to Σ_3 is

$\mathbf{n}_3 = -\frac{Pl_2}{2\pi}\cos(\phi' - \gamma_3)\hat{\imath} + \frac{Pl_2}{2\pi}\sin(\phi' - \gamma_3)\hat{\jmath} + \{\frac{Dl_2}{2}\sin\gamma_3 - l_1l_2\cos(\gamma_3 - \gamma_2)\}\hat{k}$

This normal rotated by ϕ_{max} about Z axis and projected on XY plane is given as

$\mathbf{n}_{3Rp} = -\frac{Pl_2}{2\pi}\cos(\Delta\phi + \gamma_3)\hat{\imath} - \frac{Pl_2}{2\pi}\sin(\Delta\phi + \gamma_3)\hat{\jmath}$, where $\Delta\phi = \phi_{max} - \phi'$

Unit projected normal vector is then $\hat{n}_{3Rp} = -\cos(\Delta\phi + \gamma_3)\hat{\imath} - \sin(\Delta\phi + \gamma_3)\hat{\jmath}$

Dot product of $\hat{n}_{3Rp}$ with unit normal to YZ plane help evaluate angle α_{1P} as

$$\alpha_{1p} = \Delta\phi + \gamma_3 \tag{6.17}$$

6.4.2 Inverse Mapping

This section discusses the relations for 3D rotational angles in terms of existing conventional 2D angles. Equations (6.9), (6.13) and (6.17) directly provide the expression for rotational angles γ_1, γ_2 and γ_3. While deriving the mathematical definition of minor flank Σ_7, the values of α_9 and β_9 are obtained as β_6 and $(90° - \lambda^*)$ respectively. Simultaneous solution of Eq. (6.9), (6.11) and (6.14) forms the following relations:

$$\sin^2\alpha_6 - \cos^2\alpha_6 \sin^2\beta_6 - 4\sin\alpha_6\cos\alpha_6\sin\beta_6 \frac{\sin\gamma_R\cos\gamma_R}{(\cos^2\gamma_R - \sin^2\gamma_R)} = \frac{\cos^2\phi_e - \cos^2\alpha_F}{\cos^2\alpha_F + \cos^2\phi_e - \cos^2\alpha_F\cos^2\phi_e}, \text{ and}$$

$$\cos^2\alpha_6\cos^2\beta_6 = \frac{\cos^2\alpha_F\cos^2\phi_e}{\cos^2\alpha_F + \cos^2\phi_e - \cos^2\alpha_F\cos^2\phi_e}$$

Solving these equations iteratively with a seed value of $\beta_6 = \phi_e$ (true for $\gamma_1/\gamma_R = 0$), the relations for α_6 and β_6 are obtained. Equation (6.16) is solved to obtain the relation for α_7. The inverse mapping relations are summarized in Table 6.3.

3D Angles	$\leftarrow$	Relations in terms of Conventional Angles
γ_1	=	$-\gamma_R$
γ_2	=	α_P
γ_3	=	$\alpha_{1P} - \Delta\phi$
α_7	=	$\tan^{-1}\left[\frac{1-\cos^2\alpha_{1F}}{\cos^2\alpha_{1F}\cos^2\gamma_R}\right]$
α_9	=	β_6
β_9	=	$(90° - \lambda^*)$

Table 6.3: Inverse Mapping Relations for Shell Mill

6.5 Example

This section presents the validation of the 3D geometric model of a shell mill. This is illustrated with an example of modeling and rendering of shell mill in terms of 3D geometric parameters. The cutter rendered here bears the cutter designation as referred in *ANSI/ASME B*94.19 – 1985 standards [83], with diameter of the cutter $2\frac{3}{4}''$. The input parameters of the cutter modeled in this section are tabulated in Table 6.4. The resultant cutter body is rendered in OpenGL environment [127, 132, 120, 121] and shown with the help of Figure 6.10.

Input Data for Shell Mill	
Dimensional Parameters	Value (in inches)
Cutter Diameter(D)	$2\frac{3}{4}$
Length of Cutter(L)	$1\frac{5}{8}$
Diameter of Bore(d)	1
Length of Bore(l)	$\frac{3}{4}$
Width of Driving Slot(a)	$\frac{3}{8}$
Depth of Driving Slot(b)	$\frac{7}{32}$
Radius of Driving Slot(r_1)	$\frac{1}{32}$
Diameter of Boss(d_1)	$1\frac{1}{2}$
Pitch(P)	$13\frac{5}{8}$
Number of Teeth(N)	10
Other Dimensional Parameters	Value (in mm)
Width of Primary Land(l_1)	1
Width of Secondary Land(l_2)	7
Width of Face Land(l_3)	2
Diameter of Shell(d_2)	52
Rotational Angles	Value (in degrees)
γ_1	-2.5
γ_2	7.0
γ_3	25.0
α_6	6.0
β_6	0.5
α_7	10.0
α_9	0.5
β_9	6.0
Pitch Angle (λ)	54.58

Table 6.4: Geometric Parameters of Shell Mill

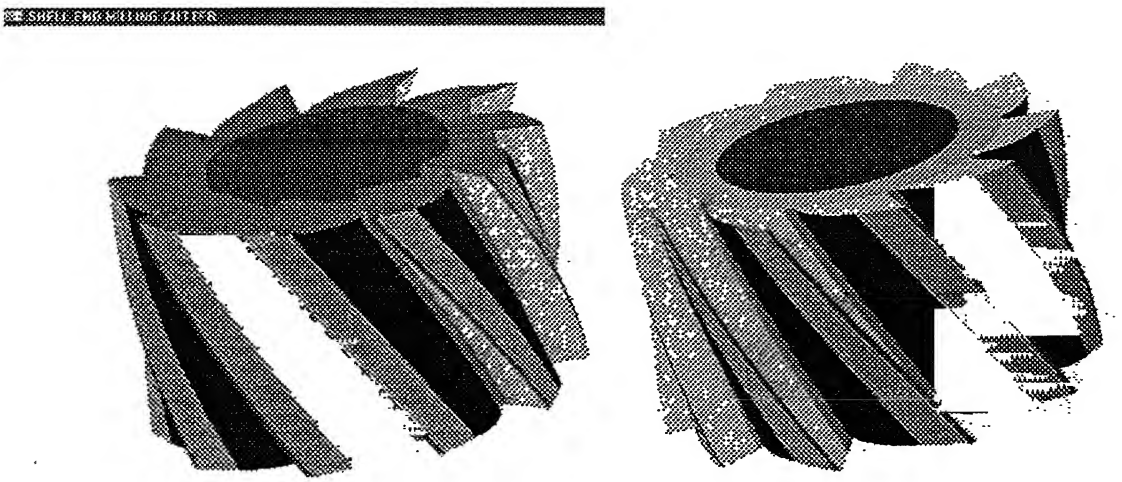

Figure 6.10: Rendering of Shell Mill (Cutter End View and Arbor End View)

6.6 Case Study

This chapter develops the comprehensive 3D model of shell mill on the basis of 3D geometric parameters. A 3D model can be imported into any surface or solid modeling environment and can be subjected to all feasible down-stream applications. This section showcase the utility of 3D model by illustrating the simulation of CNC machining of shell mill. The case study presented here is just an illustration of how a 3D definition of the cutter can be directly used for its manufacturing. This case study makes use of a 3-axis machining software, Delcam's PowerMill [88] that is available at CAD-P Lab, I.I.T. Kanpur. The resultant G-codes obtained can be used for the actual machining of the cutter on a CNC machine. The same model can be imported into a CNC tool and cutter grinding software and can be ground for finishing. Thus, from an appropriate sized block, finished shell mill can be manufactured and the entire operation can be simulated before actual machining of the cutter. The present example is just a case study and not a detailed exercise on machining or refinement of manufacturing methodology of shell mill.

To manufacture a shell mill of diameter $3\frac{3}{8}''$ and length $2''$, an enclosing block of size 88mm×88mm×51mm is taken and then machined in two passes using a three-axis CNC machining software. In the first pass, roughing operations have been carried out with a 6.0 mm end mill with spindle RPM 1500 units/min, cutting speed 500 units/min and rapid traverse rate 3000 units/min. In the second pass, finishing operations have been carried out with 3.0 mm ball end mill. The output of this is cutter location data (cld) file which can be converted to appropriate G-code (tape file) based on the type of post-processor employed. The instances of simulation of CNC machining of shell mill are shown vide Figure 6.11.

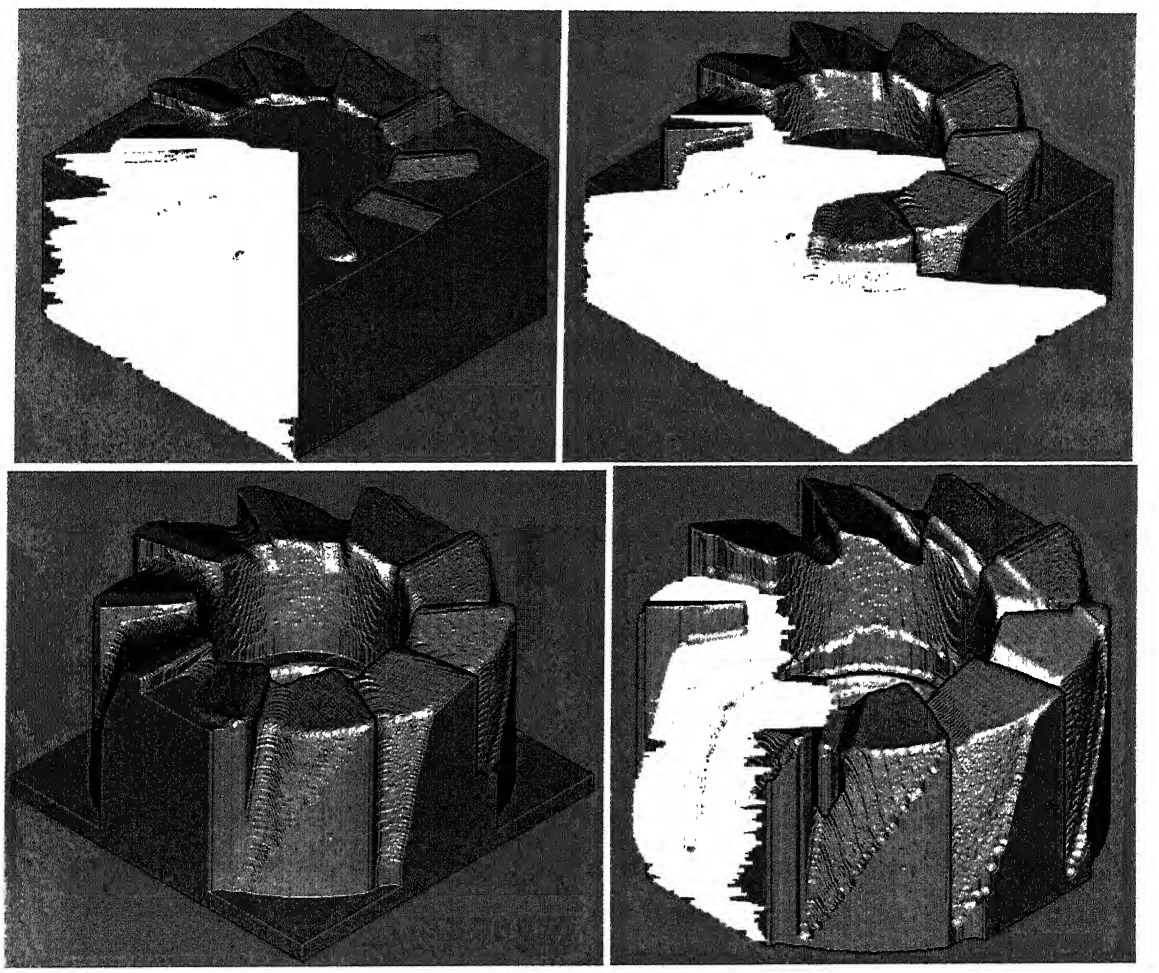

Figure 6.11: Instances of CNC Machining of Shell Mill

The profile produced on the gear is a curve comprising of a number of flats varying with the number of flutes in the hob which pass a given tooth during the generating movement. Every hob tooth, which contacts the gear along the line of action, produces one enveloping cut. Like the straight flank of the hob tooth, the individual cut is straight and in tangent plane to the involute of the tooth flank [33, 77].

The hob is cylindrical in shape with its teeth arranged along a helicoidal thread. A hob can be compared to a worm provided with flutes or gashes and with tooth profile suitably relieved behind the formed cutting edges. It is not to be confused with multi-thread milling cutters, wherein the teeth are not arranged along a helical thread [77]. A number of threads may be provided, but a single start is most common.

The design of the hob is chiefly determined by the job to be cut. The design elements of the hob can be grouped into size, drive, flutes, threads or starts, tooth form, accuracy and material. The general classifications of hobs are based upon the following factors as mentioned in [77]

(i) Construction – Solid hobs, Inserted-blade hobs and Carbide-tipped hobs
(ii) Method of Mounting – Arbor-type hobs and Shank-type hobs
(iii) Hand of Hob – Right hand and Left hand hobs
(iv) Topping Feature – Non-topping hobs, Semi-topping hobs and Topping hobs
(v) Number of Threads – Single thread and multiple thread hobs
(vi) Type of Flute – Straight flute hobs and Helical Flute hobs
(vii) Type of Operation – Finishing, Roughing, Pre-shave and Pre-grind hobs

A gear hob can be geometrically modeled by modeling a tooth of the hob independently and arraying it along and about the axis so as to position the teeth correctly along a helicoidal curve on the cylindrical body of the hob. For the convenience of modeling the geometry, the hob can be segmented into the following three parts:

- Teeth,
- Flutes, and
- Body

The tooth of the hob is modeled with the help of six surface patches labeled as Σ_i ($i \leftarrow 1 \ldots 6$), while three surface patches forming the flute are Σ_{10}, Σ_{11} and Σ_{12}. The body of the hob is composed of six surface patches $\Sigma_{50} \ldots \Sigma_{55}$. The schematic two-dimensional layout of the gear hob and details of it are shown with the help of Figure 7.1, while the cross-sectional view of the gear hob is shown in Figure 7.2. The nomenclature of surface patches of the tooth of hob is illustrated in Table 7.1.

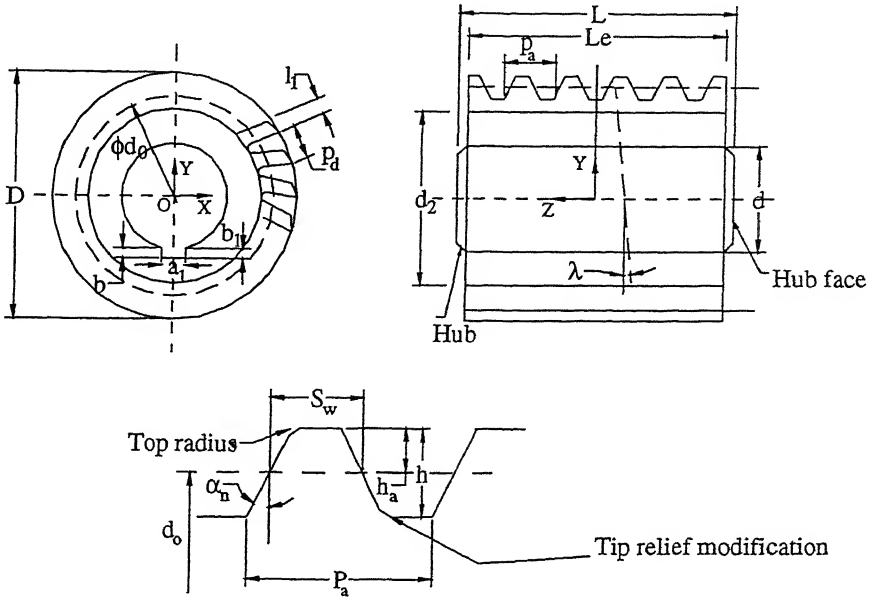

Figure 7.1: Two-dimensional Projected Views of a Right Hand Hob

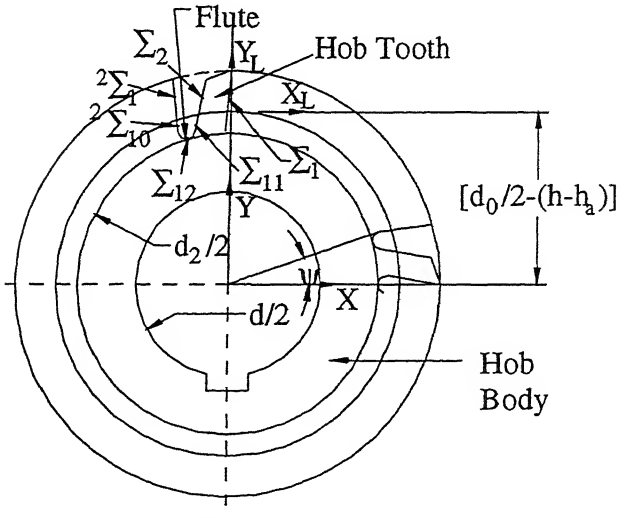

Figure 7.2: Cross-Sectional View of a Gear Hob

Label	Surface
Σ_1	Rake Face
Σ_2	Back of Tooth
Σ_3	Tooth Land
Σ_4	Tooth Flank
Σ_5	Tooth Flank
Σ_6	Root Surface

Table 7.1: Surface Patches of a Hob Tooth

7.1.1 Surface Modeling of Hob Tooth

In this subsection the modeling of the tooth of a right hand, left helix hob in terms of its surface patches, which is shown in Figure 7.3 is discussed.

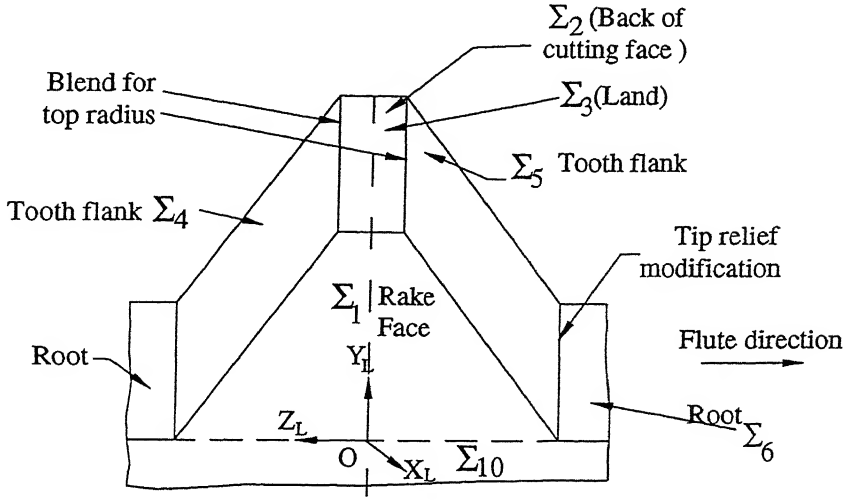

Figure 7.3: Surface Patches forming Tooth of Gear Hob

Rake Face (Σ_1)

All standard hobs and most special hobs are made with radial tooth faces. However, positive or negative rake faces are provided for specific hobbing applications based on jobs. Positive rake is sometimes used for shearing action and negative rake in carbide hobs is used for hobbing hardened gears [77]. Here, rake face is geometrically modeled by rotating a Y_LZ_L plane (YZ plane in local coordinate system C_2) by an angle γ_1 about Z_L axis ($[\mathbf{R}_{z_L,\gamma_1}]$) followed by rotation about Y_L axis by β_1 ($[\mathbf{R}_{y_L,\beta_1}]$) and then translating by a distance d_{12} along Y_L axis ($[\mathbf{T}_{y_L,d_{12}}]$). Displacement d_{12} is given by the relation $d_{12} = h$, where h is the depth of the hob tooth. The generic definition of rake face in terms of parameters v_1, w_1 ($v_1, w_1 \in [-\infty, \infty]$) is developed as
$\mathbf{p}_1(v_1, w_1) = [0 \;\; v_1 \;\; w_1 \;\; 1].[\mathbf{R}_{z_L,\gamma_1}].[\mathbf{R}_{y_L,\beta_1}].[\mathbf{T}_{y_L,d_{12}}]$ and is given by

$$\mathbf{p}_1 = [(-v_1 \sin\gamma_1 \cos\beta_1 + w_1 \sin\beta_1) \;\; (v_1 \cos\gamma_1 + d_{12}) \;\; (v_1 \sin\gamma_1 \sin\beta_1 + w_1 \cos\beta_1) \;\; 1] \quad (7.1)$$

Table 7.2 establishes the relation between the rotational angle γ_1 and rake angle γ_R.

Back of Tooth (Σ_2)

This surface is obtained when a Y_LZ_L plane is rotated by γ_2 ($\gamma_2 < 0$) about Z_L axis ($[\mathbf{R}_{z_L,\gamma_2}]$) followed by an angle β_2 about Y_L axis ($[\mathbf{R}_{y_L,\beta_2}]$) and then translated along Y_L axis by d_{22} ($[\mathbf{T}_{y_L,d_{22}}]$). Displacement d_{22} is given by the relation $d_{22} = h - \frac{l_1'}{\tan\gamma_2}$,

Rotational Angle (γ_1)	Rake Angle (γ_R)
< 0	Positive
$= 0$	Zero
> 0	Negative

Table 7.2: Relation between Rotational Angle γ_1 and Rake Angle γ_R

where $l_1' = \frac{l_1 \cos(\gamma_2 - \gamma_3)}{\cos \gamma_2}$, l_1 stands for width of tooth land (Figure 7.1) and angle β_2 is equivalent to β_1. The definition of Σ_2 in terms of v_2, w_2 is expressed as

$$\mathbf{p}_2 = [(-v_2 \sin\gamma_2 \cos\beta_2 + w_2 \sin\beta_2) \quad (v_2 \cos\gamma_2 + d_{22}) \quad (v_2 \sin\gamma_2 \sin\beta_2 + w_2 \cos\beta_2) \quad 1] \quad (7.2)$$

where $-\infty \leq v_2, w_2 \leq \infty$

Tooth Land (Σ_3)

Surface is obtained by transforming a $Z_L X_L$ plane through successive rotations about Z_L and Y_L axis by angles γ_3 ($[\mathbf{R}_{z_L,\gamma_3}]$) and β_3 ($= \beta_1$) ($[\mathbf{R}_{y_L,\beta_3}]$) followed by translation along Y_L axis by $d_{32} = h$ ($[\mathbf{T}_{y_L,d_{32}}]$) and is known as tooth land. It is defined by vector $\mathbf{p}_3(u_3, w_3)$ where

$$\mathbf{p}_3 = [(u_3 \cos\gamma_3 \cos\beta_3 + w_3 \sin\beta_3) \quad (u_3 \sin\gamma_3 + d_{32}) \quad (-u_3 \cos\gamma_3 \sin\beta_3 + w_3 \cos\beta_3) \quad 1] \quad (7.3)$$

where $-\infty \leq u_3, w_3 \leq \infty$

Tooth Flank (Σ_4)

An $X_L Y_L$ plane when rotated by α_4 ($\alpha_4 < 0$) about X_L axis ($[\mathbf{R}_{x_L,\alpha_4}]$), followed by rotation about Y_L axis by β_4 ($[\mathbf{R}_{y_L,\beta_4}]$) and translation along Z_L axis by d_{43} ($[\mathbf{T}_{z_L,d_{43}}]$) forms tooth flank Σ_4. The displacement d_{43} is given by $d_{43} = [\frac{S_w}{2} - (h - h_a)\tan\alpha_4]$. Position vector of a point on the tooth flank Σ_4 given by $\mathbf{p}_4(u_4, v_4)$ ($u_4, v_4 \in [-\infty, \infty]$) is mathematically defined as

$$\mathbf{p}_4 = [(u_4 \cos\beta_4 + v_4 \sin\alpha_4 \sin\beta_4) \quad v_4 \cos\alpha_4 \quad (-u_4 \sin\beta_4 + v_4 \sin\alpha_4 \cos\beta_4 + d_{43}) \quad 1] \quad (7.4)$$

Tooth Flank (Σ_5)

Flank Σ_5 is formed when an $X_L Y_L$ plane is rotated by α_5 ($\alpha_5 = -\alpha_4$) about X_L axis ($[\mathbf{R}_{x_L,\alpha_5}]$), followed by rotation about Y_L axis by β_5 ($\beta_5 = \beta_4$)($[\mathbf{R}_{y_L,\beta_5}]$) and displacement along Z_L axis by d_{53} ($[\mathbf{T}_{z_L,d_{53}}]$), where $d_{53} = -[\frac{S_w}{2} - (h - h_a)\tan\alpha_5]$. The tooth flank is represented by $\mathbf{p}_5(u_5, v_5)$ ($u_5, v_5 \in [-\infty, \infty]$), which is given by

$$\mathbf{p}_5 = [(u_5 \cos\beta_5 + v_5 \sin\alpha_5 \sin\beta_5) \quad v_5 \cos\alpha_5 \quad (-u_5 \sin\beta_5 + v_5 \sin\alpha_5 \cos\beta_5 + d_{53}) \quad 1] \quad (7.5)$$

Root Surface (Σ_6)

This surface patch is modeled as a $Z_L X_L$ plane place in local coordinate system C_2 and hence is expressed by

$$\mathbf{p}_6(u_6, w_6) = [u_6 \quad 0 \quad w_6 \quad 1] \quad (-\infty \leq u_6, w_6 \leq \infty) \tag{7.6}$$

Width of Σ_6 for the first tooth and location of first set of teeth (center line of land Σ_3) are tool designers' prerogative as depending on length of hob (L) and axial pitch (p_a), hob may have partial teeth also.

7.1.2 Surface Modeling of Hob Flute

Hob flute forms a fillet between back planes (Σ_2) of N^{th} row of teeth and rake faces of $(N+1)^{th}$ row of teeth of hob. It is along the axis of hob and can be straight or helical. The number of flutes and their proportions are more or less established by the depth of form and the diameter of the hob. The proportions provide for free flow of chips and ample clearance for resharpenings [29, 33, 77]. Hob flute is made of three surfaces of which one is an extension of rake faces and another of back planes (Σ_2) of the teeth along the flute.

Surface Patches Σ_{10} and Σ_{11}

Surface patch Σ_{10} is an extension of rake face Σ_1 and connects rake faces of all the teeth placed axially as shown in Figure 7.2. It is defined by the Eq. (7.1). Similarly, surface Σ_{11} is an extension of back of tooth Σ_2 and given by Eq. (7.2).

Fillet Surface (Σ_{12})

This is a cylindrical surface of radius R and modeled by sweeping an arc $\mathbf{a}_1(\phi_{12})$ according to the type of flute. The center of arc in C_2 is evaluated with the help of Figure 7.4 and given by $[-(\frac{d_2}{2}+R)\sin\psi' \quad \{-\frac{d_0}{2}+(h-h_a)+(\frac{d_2}{2}+R)\cos\psi'\} \quad 0 \quad 1]$, where $\psi' = \psi - \delta$, and δ is obtained by solving the equation

$$\sin\delta + \cos\delta \tan\gamma_1 = \frac{\frac{R}{\cos\gamma_1} + \frac{D}{2}\tan\gamma_1}{\frac{d_2}{2} + R}$$

Then, the equation of arc becomes

$$\mathbf{a}_1(\phi_{12}) = [\{-(\frac{d_2}{2}+R)\sin\psi' + R\cos\phi_{12}\} \quad \{-\frac{d_0}{2}+(h-h_a)+(\frac{d_2}{2}+R)\cos\psi' + R\sin\phi_{12}\}\} \quad 0 \quad 1]$$

with $\phi_s \leq \phi_{12} \leq \phi_e$, where $\phi_s = \pi + \psi + \gamma_1$ and $\phi_e = 2\pi + \gamma_2$.

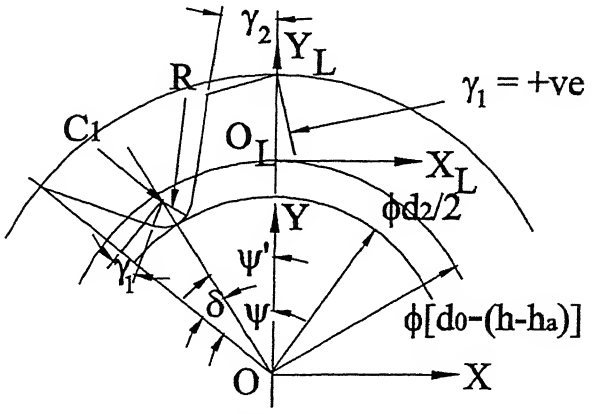

Figure 7.4: Fillet of Gear Hob

When the flute is straight, the equation of Σ_{12} becomes

$$\mathbf{p}_{12,s} = [\{-(\frac{d_2}{2}+R)\sin\psi'+R\cos\phi_{12}\} \quad \{-\frac{d_0}{2}+(h-h_a)+(\frac{d_2}{2}+R)\cos\psi'+R\sin\phi_{12}\} \quad w_{12} \quad 1]$$

The limits of w_{12} are controlled by axial pitch (p_a) and given by $-\frac{p_a}{2} \leq w_{12} \leq \frac{p_a}{2}$
When the flute is helical, then the equation is given as $\mathbf{p}_{12}(w_{12},\phi_{12}) = \mathbf{p}_{12,s}(w_{12},\phi_{12}).[R_{Y,\beta_{12}}]$

$$\begin{aligned} p_{12X} &= \{-(\frac{d_2}{2}+R)\sin\psi' + R\cos\phi_{12}\}\cos\beta_{12} + w_{12}\sin\beta_{12} \\ p_{12Y} &= \{-\frac{d_0}{2}+(h-h_a)+(\frac{d_2}{2}+R)\cos\psi' + R\sin\phi_{12}\} \\ p_{12Z} &= \{(\frac{d_2}{2}+R)\sin\psi' - R\cos\phi_{12}\}\sin\beta_{12} + w_{12}\cos\beta_{12} \end{aligned} \tag{7.7}$$

7.1.3 Surface Modeling of Hob Body

The body of hob is composed of six surface patches that are either planar or cylindrical in nature. The geometric modeling of these patches is described in this subsection.

End Surface Σ_{50}

This is formed by an XY plane placed at $z = \frac{L_e}{2}$ in global coordinate system C_1 and expressed with the help of the relation

$$\mathbf{p}_{50}(u_{50},v_{50}) = [u_{50} \quad v_{50} \quad \frac{L_e}{2} \quad 1] \qquad (-\infty \leq u_{50}, v_{50} \leq \infty)$$

End Surface Σ_{51}

An XY plane when placed at $z = -\frac{L_e}{2}$ forms Σ_{51} and is given by

$$\mathbf{p}_{51}(u_{51},v_{51}) = [u_{51} \quad v_{51} \quad -\frac{L_e}{2} \quad 1] \qquad (-\infty \leq u_{51}, v_{51} \leq \infty)$$

Cylindrical Surface Σ_{52}

This cylindrical surface of diameter d is modeled as a surface of revolution in coordinate system C_1 by revolving an edge parallel to Z axis. The equation of Σ_{52} is

$$\mathbf{p}_{52}(w_{52}, \phi_{52}) = [\frac{d}{2}\cos\phi_{52} \quad \frac{d}{2}\sin\phi_{52} \quad -\frac{L_e}{2}(1-2w_{52}) \quad 1]$$

where $0 \leq w_{52} \leq 1$ and $0 \leq \phi_{52} \leq 2\pi$, with margins for keyway.

Keyway Surface Σ_{53}

It is formed when a ZX plane is placed at $y = -(\frac{d}{2} + b_1) = d_{53,2}$ and expressed by

$$\mathbf{p}_{53}(u_{53}, w_{53}) = [u_{53} \quad d_{53,2} \quad w_{53} \quad 1] \qquad (-\infty \leq u_{53}, w_{53} \leq \infty)$$

Keyway Side Walls Σ_{54} and Σ_{55}

These surfaces are formed by placing YZ planes at $x = -\frac{a_1}{2}$ and $= \frac{a_1}{2}$ respectively and defined with the help of following equations

$$\begin{aligned}\mathbf{p}_{54}(v_{54}, w_{54}) &= [-\frac{a_1}{2} \quad v_{54} \quad w_{54} \quad 1] \\ \mathbf{p}_{55}(v_{55}, w_{55}) &= [\ \frac{a_1}{2} \quad v_{55} \quad w_{55} \quad 1]\end{aligned}$$

with $-\infty \leq v_{54}, w_{54}, v_{55}, w_{55} \leq \infty$

7.1.4 Placement of Hob Teeth on Cutter Body

The relation between tooth coordinate system C_2 and hob coordinate system C_1 is given by the relation $C_1 = C_2[\frac{1}{2}\mathrm{M}]$, where $[\frac{1}{2}\mathrm{M}]$ is homogenous transformation matrix for a vector from the coordinate system C_2 to C_1 and given by the matrix

$$[\tfrac{1}{2}\mathrm{M}] = \begin{bmatrix} 1 & 0 & 0 & 0 \\ 0 & 1 & 0 & 0 \\ 0 & 0 & 1 & 0 \\ 0 & \frac{1}{2}d & 0 & 1 \end{bmatrix}$$

where $\frac{1}{2}d = [d_0 - (h - h_a)]$

For a straight-flute cutter, a tooth is arrayed along the axis at a distance of p_a or by $\frac{L_e}{p_a}$ times and the resultant flute is arrayed along the cylinder by diametral pitch $p_d = \frac{\pi D}{N_f}$ or at an angle $\frac{2\pi}{N_f}$, where N_f is the number of flutes.

For helical-flute hob, the tooth is arrayed along a helix formed by a point rotated about Z axis by an angle $\phi = \frac{2\pi p_a}{P}$ and translated along Z axis by p_a. The resultant flute is arrayed along the circumference by a distance p_d or by an angle $\frac{2\pi}{N_f}$.

7.2 Modeling of Transitional Surfaces

Transitional surfaces are meant to smoothen intersecting surfaces so as to avoid formation of sharp edges. For a hob they can be categorized into following two types

(i) Blending surfaces on a tooth of hob
(ii) Chamfers on the body of hob

The developments of geometric models of transitional surfaces are discussed in this section.

7.2.1 Blending Surfaces of Hob Tooth

On the tooth of a topping gear hob that generates the complete workpiece profile, four blending surfaces are created. Two of them are at the top of tooth and blend land Σ_3 with flanks Σ_4 and Σ_5 respectively. They are called blends for top radius. The former is labeled as σ_{34} and the latter as σ_{35}. The other two are at the bottom of tooth and blend flank Σ_4 with root Σ_6 and Σ_5 with Σ_6. They are known as tip relief modifications and labeled σ_{46} and σ_{56} respectively. Figure 7.3 shows location of these blending surfaces. The mathematical definitions of edges formed due to intersection of surfaces Σ_3, Σ_4, Σ_5 and Σ_6, and vertices forming these edges, V_1 to V_8, are given in Appendix ??. These vertices and edges are required to model the transitional surfaces.

Blend for Top Radius σ_{34}

This surface blends surfaces Σ_3 and Σ_4 at the edge of intersection $\mathbf{e}_{34}$. It is shown in Figure 7.5. The coordinates of vertices V_1 and V_2 forming the edge $\mathbf{e}_{34}$, along with other vertices V_3, V_4, V_5 and V_6 of intersecting patches Σ_3 and Σ_4 are known a priori. The blending surface σ_{34} is modeled as a bicubic Bézier surface with boundary formed by two circular arcs and two linear edges. Unit vector at the vertex V_1 along the direction V_1V_3 on Σ_3 is given by $\hat{a} = \frac{\mathbf{v}_3 - \mathbf{v}_1}{|\mathbf{v}_3 - \mathbf{v}_1|} = -\sin\beta_1\hat{\imath} - \cos\beta_1\hat{k}$
Unit vector along V_1V_5 on Σ_4 is $\hat{b} = \frac{\mathbf{v}_5 - \mathbf{v}_1}{|\mathbf{v}_5 - \mathbf{v}_1|} = \sin\alpha_4\sin\beta_1\hat{\imath} - \cos\alpha_4\hat{\jmath} + \sin\alpha_4\cos\beta_1\hat{k}$
This gives half corner angle as $\phi = \frac{1}{2}\cos^{-1}(\hat{a}.\hat{b}) = \frac{1}{2}\cos^{-1}(-\sin\alpha_4)$
Distance between the blend start point and point of intersection is $\delta_{34} = \frac{r_1}{\tan\phi}$, where r_1 is the radius of the blend. Thus, the control points of the cubic Bézier curve required to approximate the circular arc of the blend are given by

$\mathbf{p}_{00} = \mathbf{v}_1 + \delta_{34}.\hat{a}$, $\mathbf{p}_{01} = \mathbf{p}_{00} - \Delta.\hat{a}$, $\mathbf{p}_{02} = \mathbf{p}_{03} - \Delta.\hat{b}$ and $\mathbf{p}_{03} = \mathbf{v}_1 + \delta_{34}.\hat{b}$.

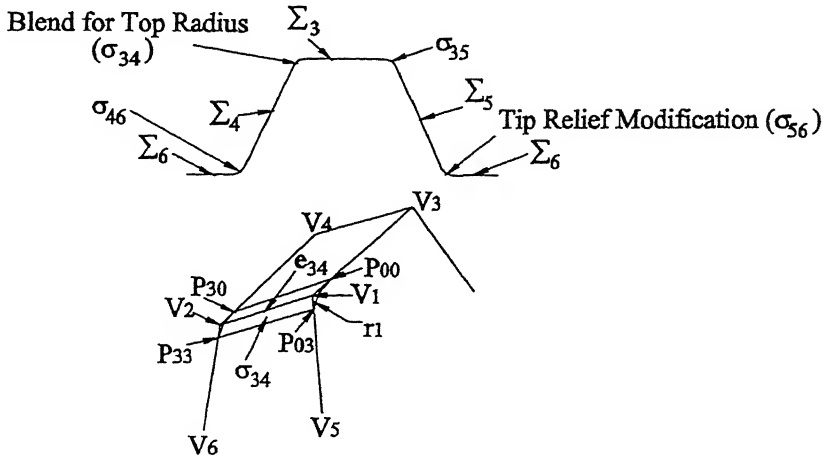

Figure 7.5: Blending Surfaces of Gear Hob

where $\Delta = \frac{2c}{3(1+\sin\phi)}$ and $c = |\mathbf{p}_{03} - \mathbf{p}_{00}|$.

Similarly, second circular arc is formed around vertex V_2 and its control points are

$\mathbf{p}_{30} = \mathbf{v}_2 + \delta_{34}.\hat{a}$, $\mathbf{p}_{33} = \mathbf{v}_2 + \delta_{34}.\hat{b}$, $\mathbf{p}_{31} = \mathbf{p}_{30} - \Delta'.\hat{a}$ and $\mathbf{p}_{32} = \mathbf{p}_{33} - \Delta'.\hat{b}$

where $\Delta' = \frac{2c'}{3(1+\sin\phi)}$ and $c' = |\mathbf{p}_{33} - \mathbf{p}_{30}|$.

The two straight lines formed as cubic Bézier curve are plotted by control points $\mathbf{p}_{00}\mathbf{p}_{10}\mathbf{p}_{20}\mathbf{p}_{30}$ and $\mathbf{p}_{03}\mathbf{p}_{13}\mathbf{p}_{23}\mathbf{p}_{33}$, where

$\mathbf{p}_{10} = (2\mathbf{p}_{00}+\mathbf{p}_{30})/3$, $\mathbf{p}_{20} = (\mathbf{p}_{00}+2\mathbf{p}_{30})/3$, $\mathbf{p}_{13} = (2\mathbf{p}_{03}+\mathbf{p}_{33})/3$ and $\mathbf{p}_{23} = (\mathbf{p}_{03}+2\mathbf{p}_{33})/3$

Blending Surface σ_{35}

The surface blending the intersection of patch Σ_3 with Σ_5 at the edge e_{35} is σ_{35}. The edge is formed by the vertices V_3 and V_4. Unit vectors at V_3 along V_3V_1 and V_3V_7 are $\hat{a} = \sin\beta_1\hat{\imath} + \cos\beta_1\hat{k}$ and $\hat{b} = -\sin\alpha_5\sin\beta_1\hat{\imath} - \cos\alpha_5\hat{\jmath} - \sin\alpha_5\cos\beta_1\hat{k}$ respectively and half corner angle $(\phi) = \frac{1}{2}\cos^{-1}(-\sin\alpha_5)$. The control points $\mathbf{p}'_{00}$, $\mathbf{p}'_{01}$, $\mathbf{p}'_{02}$ and $\mathbf{p}'_{03}$ required to specify cubic Bézier curve approximating circular arc of blend at V_3 are obtained in the same way as for the blend σ_{34}. The control points of other three cubic Bézier boundary curves and hence, boundary curves of the bicubic blending surface σ_{35} are also evolved as discussed earlier. The boundary curves form σ_{35}.

Tip Relief Modification Surfaces σ_{46} and σ_{56}

These blending surfaces depend on the type and size of tip relief on the resultant gear tooth. Tip relief surfaces are usually found in the full depth gear finishing hobs. It can be a blending surface, a chamfered surface or any other special surface, as desired on the tooth of the gear, and hence modeled accordingly.

7.2.2 Chamfered Surfaces on Hob Body

There are four chamfered surfaces on the body of gear hob. Two of them are at the intersection of cylindrical surface for arbor Σ_{52} with the two planar end surfaces Σ_{50} and Σ_{51} of hob. They are circular chamfers and labeled as σ_{b02} and σ_{b12} respectively. The other two are at keyway and formed at the intersection of keyway planar surface Σ_{53} with keyway walls Σ_{54} and Σ_{55}. They are linear chamfers and labeled as σ_{b34} and σ_{b35} respectively.

Chamfer σ_{b02}

This chamfer is assumed to be a 45° chamfer of unit width and formed by rotating an edge obtained by joining the vertices $[(\frac{d}{2}+0.707)\ \ 0\ \ \frac{L_e}{2}\ \ 1]$ and $[\frac{d}{2}\ \ 0\ \ (\frac{L_e}{2}-0.707)\ \ 1]$ by an angle θ. The equation of the surface is given by

$$\left[\{\frac{d}{2}+0.707(1-u)\}\cos\theta \quad \{\frac{d}{2}+0.707(1-u)\}\sin\theta \quad (\frac{L_e}{2}-0.707u) \quad 1\right]$$

$$(0\le u\le 1,\quad 0\le\theta\le 2\pi)$$

Chamfer σ_{b12}

This is also assumed to be 45° chamfer of unit width and is mirror image of σ_{b02} about XY plane. It is expressed by the homogenous vector

$$[\{\frac{d}{2}+0.707(1-u)\}\cos\theta \quad \{\frac{d}{2}+0.707(1-u)\}\sin\theta \quad (\frac{L_e}{2}+0.707u) \quad 1]\ (0\le u\le 1,\ 0\le\theta\le 2\pi)$$

Chamfer σ_{b34}

It is also a 45° linear chamfer of unit width and formed by linearly sweeping the edge joining vertices $[(-\frac{a_1}{2}+0.707)\ \ -\frac{d}{2}\cos\phi\ \ 0\ \ 1]$ and $[-\frac{a_1}{2}\ \ -(\frac{d}{2}\cos\phi+0.707)\ \ 0\ \ 1]$ along Z axis. For the position of keyway as shown in Figure 7.2, it is defined by

$$[\{-\frac{a_1}{2}+0.707(1-u)\} \quad (-\frac{d}{2}\cos\phi-0.707u) \quad \{-\frac{L_e}{2}(1-2v)\} \quad 1] \quad (0\le u,v\le 1)$$

Chamfer σ_{b35}

For the instantiation of the gear hob shown in Figure 7.2, this chamfer is the reflection of σ_{b34} about YZ plane and mathematically expressed with the help of

$$[\{\frac{a_1}{2}-0.707(1-u)\} \quad (-\frac{d}{2}\cos\phi-0.707u) \quad \{-\frac{L_e}{2}(1-2v)\} \quad 1] \quad (0\le u,v\le 1)$$

7.3 Mapping

This section establishes a set of relations among proposed three-dimensional (3D) angles and the conventional projective geometry based two-dimensional (2D) angles in terms of forward and inverse mapping. Forward mapping implies establishing 2D angles if 3D angles are provided, while inverse mapping leads to relations for 3D angles in terms of 2D projected angles. The sign conventions adopted for the 3D and 2D angles are as discussed in Chapter 3. The formation of conventional angles in 3D space and their projection on different planes is summarized with the help of mapping guide given in Table 7.3.

Conventional Angles	Formed by Plane	About the Plane	Projected on Plane
Radial Rake Angle, γ_R	Σ_1	$Y_L Z_L$	$X_L Y_L$
Normal Pressure Angle, α_n	Σ_4 (or Σ_5)	$X_L Y_L$	$Y_L Z_L$
Lead Angle, λ	Σ_4 (or Σ_5)	$X_L Y_L$	$Z_L X_L$

Table 7.3: Mapping Guide Table for Gear Hob

7.3.1 Forward Mapping

This subsection establishes 2D angles defined by conventional nomenclatures to specify the geometry of hob in terms of proposed 3D angles.

Radial Rake Angle (γ_R)

This angle is formed by rake face Σ_1 with $Y_L Z_L$ plane and viewed when projected on $X_L Y_L$ plane as shown in Table 7.3. The rake face is defined by Eq. (7.1) as
$\mathbf{p}_1(v_1, w_1) = [(-v_1 \sin\gamma_1 \cos\beta_1 + w_1 \sin\beta_1) \quad (v_1 \cos\gamma_1 + d_{12}) \quad (v_1 \sin\gamma_1 \sin\beta_1 + w_1 \cos\beta_1) \quad 1]$
Tangents to rake face are expressed by the relations

$$\mathbf{p}_{1v}(v_1, w_1) = \frac{\partial \mathbf{p}_1}{\partial v} = -\sin\gamma_1 \cos\beta_1 \hat{\imath} + \cos\gamma_1 \hat{\jmath} + \sin\gamma_1 \sin\beta_1 \hat{k}$$

$$\mathbf{p}_{1w}(v_1, w_1) = \frac{\partial \mathbf{p}_1}{\partial w} = \sin\beta_1 \hat{\imath} + \cos\beta_1 \hat{k}$$

and the normal to it is $\mathbf{n}_1 = \left[\frac{\partial \mathbf{p}_1}{\partial v} \times \frac{\partial \mathbf{p}_1}{\partial w}\right] = \cos\beta_1 \cos\gamma_1 \hat{\imath} + \sin\gamma_1 \hat{\jmath} - \sin\beta_1 \cos\gamma_1 \hat{k}$
Projection of this normal on $X_L Y_L$ plane is expressed by $\mathbf{n}_{1p} = \cos\beta_1 \cos\gamma_1 \hat{\imath} + \sin\gamma_1 \hat{\jmath}$
Unit projected normal vector to rake face, $\hat{n}_{1p} = \dfrac{\cos\beta_1 \cos\gamma_1 \hat{\imath} + \sin\gamma_1 \hat{\jmath}}{\sqrt{(\cos^2\beta_1 \cos^2\gamma_1 + \sin^2\gamma_1}}$

Radial rake angle γ_R is equivalent to the angle between $\hat{n}_{1p}$ and unit vector $\hat{\imath}$ normal to $Y_L Z_L$ plane. Therefore, scalar product of $\hat{n}_{1p}$ with $\hat{\imath}$ gives

$$\gamma_R = \cos^{-1}\left[\frac{\cos\beta_1 \cos\gamma_1}{\sqrt{\cos^2\beta_1 \cos^2\gamma_1 + \sin^2\gamma_1}}\right] \tag{7.8}$$

From sign conventions as given in Table 7.2, the signs of angles γ_1 and γ_R are opposite. For a straight hob, angle β_1 is zero and Eq. (7.8) provides the relation

$$\pm\gamma_r = \mp\gamma_1$$

Normal Pressure Angle (α_n)

Angle α_n is formed by tooth flank Σ_4 (or Σ_5, as they are symmetric) with $X_L Y_L$ plane and viewed on projection to $Y_L Z_L$ plane. Equation (7.4) expresses the mathematical definition of Σ_4 as

$\mathbf{p}_4(u_4, v_4) = [(u_4 \cos\beta_4 + v_4 \sin\alpha_4 \sin\beta_4) \quad v_4 \cos\alpha_4 \quad (-u_4 \sin\beta_4 + v_4 \sin\alpha_4 \cos\beta_4 + d_{43}) \quad 1]$

The tangents to Σ_4 are

$\mathbf{p}_{4u} = \frac{\partial \mathbf{p}_4}{\partial u} = \cos\beta_4\hat{\imath} - \sin\beta_4\hat{k}$

$\mathbf{p}_{4v} = \frac{\partial \mathbf{p}_4}{\partial v} = \sin\alpha_4 \sin\beta_4\hat{\imath} + \cos\alpha_4\hat{\jmath} + \sin\alpha_4 \cos\beta_4\hat{k}$

and the vector normal to it is $\mathbf{n}_4 = \cos\alpha_4 \sin\beta_4\hat{\imath} - \sin\alpha_4\hat{\jmath} + \cos\alpha_4 \cos\beta_4\hat{k}$

When projected on $Y_L Z_L$ plane, it is given by $\mathbf{n}_{4p} = -\sin\alpha_4\hat{\jmath} + \cos\alpha_4 \cos\beta_4\hat{k}$

and unit projected normal vector to flank σ_4 is $\hat{n}_{4p} = \dfrac{-\sin\alpha_4\hat{\jmath} + \cos\alpha_4 \cos\beta_4\hat{k}}{\sqrt{\sin^2\alpha_4 + \cos^2\alpha_4 \cos^2\beta_4}}$

Scalar product of $\hat{n}_{4p}$ with unit vector normal to $X_L Y_L$ plane ($\hat{k}$) results in normal pressure angle as

$$\alpha_n = \cos^{-1}\left[\frac{\cos\alpha_4 \cos\beta_4}{\sqrt{\sin^2\alpha_4 + \cos^2\alpha_4 \cos^2\beta_4}}\right] \tag{7.9}$$

Lead Angle (λ)

Lead angle is formed by flank Σ_4 (or Σ_5) with $X_L Y_L$ plane and viewed on projection to $Z_L X_L$ plane. Normal to flank Σ_4 ($\mathbf{n_4}$) is expressed above and its projection on $Z_L X_L$ plane is given by $\mathbf{n}'_{4p} = \cos\alpha_4 \sin\beta_4\hat{\imath} + \cos\alpha_4 \cos\beta_4\hat{k}$. Unit vector normal to flank Σ_4 and projected on $Z_L X_L$ plane is expressed as $\hat{n}'_{4p} = \sin\beta_4\hat{\imath} + \cos\beta_4\hat{k}$

Angle λ, between Σ_4 and $X_L Y_L$ plane, is similar to the angle between unit normal projected vector $\hat{n}'_{4p}$ and unit normal vector $\hat{k}$ and given by

$$\lambda = \beta_4 \tag{7.10}$$

7.3.2 Inverse Mapping

When conventional 2D angles are known, values of 3D rotational angles can be obtained by performing inverse mapping. This section develops the inverse mapping relations for gear hob. Equation (7.10) establishes the relation for rotational angle β_4. For helical hobs as $\beta_5 = \beta_4 = \beta_1$, therefore

$$\beta_1 = \beta_4 = \beta_5 = \lambda \tag{7.11}$$

Rearranging Eq. (7.8) and substituting the value of β_1 as given by Eq. (7.11) in it, rotational angle γ_1 may be expressed by the following relation

$$\gamma_1 = \tan^{-1}\left[\tan\gamma_R \cos\lambda\right] \tag{7.12}$$

Similarly, from Eq. (7.9) and Eq. (7.11), rotational angle α_4 can be expressed by

$$\alpha_4 = \tan^{-1}\left[\tan\alpha_n \cos\lambda\right] \tag{7.13}$$

7.4 Gear Shaper

Gear shaping is a generating process. The gear shaper is virtually a gear provided with cutting edges. The tool is rotated at the required velocity ratio relative to the gear and any one gear tooth space is formed by one complete cutter tooth. As cutter rotates with the gear, it forms the tooth space by incremental cuts depending upon the used feed rate, since the tooth are formed by a series of closely spaced individual cuts, and the finely spaced cuts. Certain type of gears can be produced only on gear shaper. Some others that can be produced on a hobber, are best produced by the shaping method. Gear shapers are made in various types and shapes to adapt them to different class of work. The gear shapers are generally classified [77] depending on the following factors:

(i) Construction – Solid cutters and Tipped cutters

(ii) Cutter Blank Design – Arbor type cutters, that includes Disk type, Deep Counter bore type and Hub type cutters and Shank type cutters, including, tapered and straight shank cutters

(iii) Application – Roughing cutters, Pre-Shaving cutters, Pre-Grinding cutters and Finishing cutters

(iv) Tooth Profile Produced – Non-topping cutters, Semi-topping or Chamfering cutters, Topping cutters, Flank Type cutters, Protuberance cutters and Full Fillet type cutters

(v) Helix – Spur type cutters and Helical type cutters

(vi) Type of Sharpening – Circular sharpened cutters, Helical sharpening cutters, Involute sharpened cutters and Vee sharpened cutters

Besides, gear shapers are designed to cut either external or internal gears. This section presents the methodology of geometric modeling for a disk-type cutter for external gears. Figure 7.6 shows one such commercially used gear shaper.

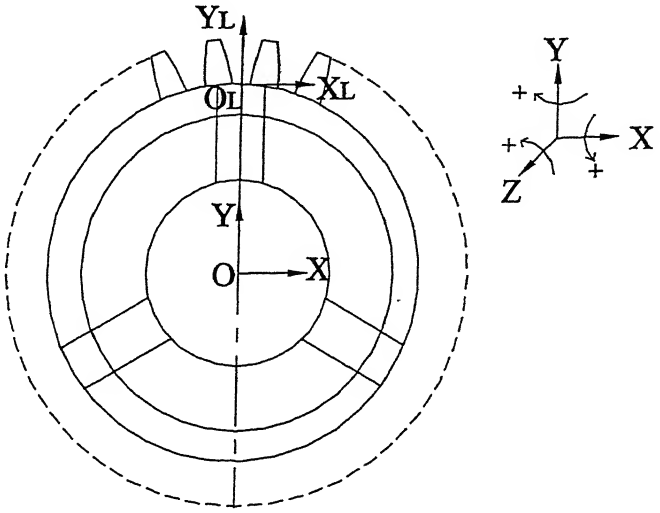

Figure 7.6: Gear Shaper

Shaper Tooth

A tooth of the gear shaper is made up of six surface patches as shown in Figure 7.7. Symmetric surfaces Σ_1 and Σ_2 can be modeled as ruled surfaces, with generatrix as an involute boundary curve and axis X_L as directrix. Surfaces Σ_3, Σ_4, Σ_5 and Σ_6 are planar surfaces and can be geometrically defined appropriately. The surface patches of shaper tooth are developed in a local coordinate system C_2. Once the surface model of shaper tooth is developed, then it is positioned and oriented suitably with respect to global coordinate system C_1.

The relation between C_2 and C_1 for gear shaper is given with the help of transformation matrix $[{}^1_2\mathrm{M}']$, where $[{}^1_2\mathrm{M}']$ consist of following transformational steps:

(i) Rotation about Y_L axis by $-90°$
(ii) Translation about Y axis by $-(\frac{D}{2} - H)$ (i.e along negative Y axis)
(iii) Translation about X axis by $-[p_a - S_w - 2(h - h_a)\tan\alpha_1]$

where p_a is axial pitch, S_w is chordal thickness, h is depth of tooth and h_a is gear tooth addendum.

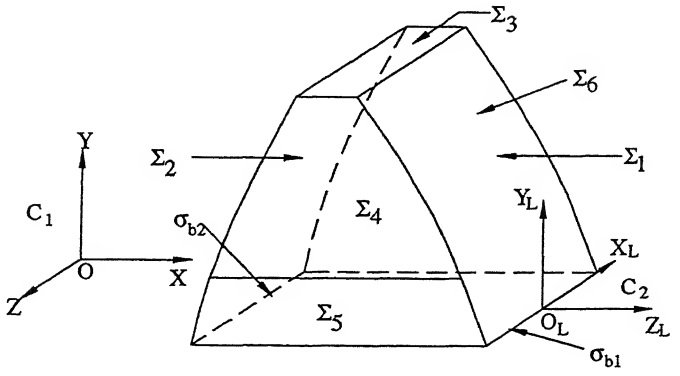

Figure 7.7: Tooth of Gear Shaper

The detailed surface model of the shaper tooth consist of two blending surfaces. These surfaces blend surface patches Σ_1 and Σ_2 with the cutter body and labeled as σ_{b1} and σ_{b2} respectively. Figure 7.7 shows the location of blending surfaces.

7.5 Example

This section presents an example of modeling and rendering in OGL environment [132, 120, 121] a straight-fluted gear hob through 3D geometric parameters. The primary purpose of this is to validate the geometry of hob. The geometric parameters used to model the hob are presented in Table 7.4. Figure 7.8 renders the resultant hob.

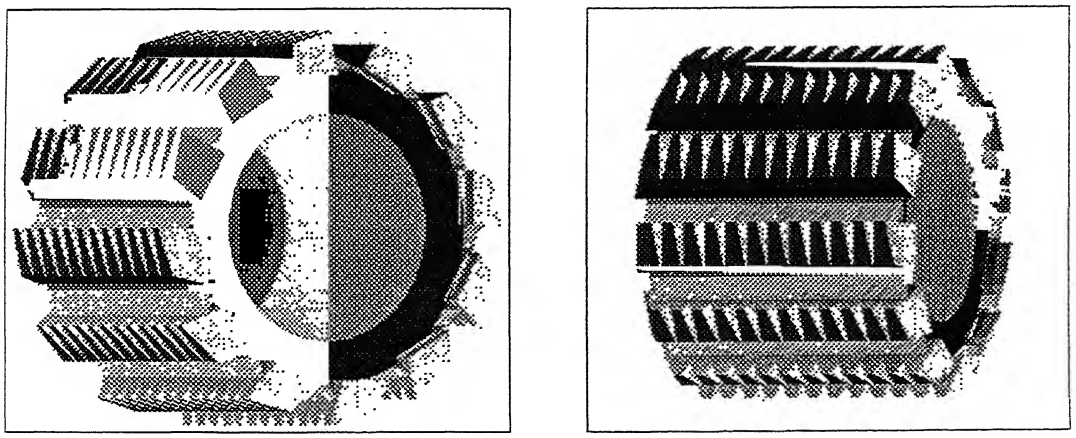

Figure 7.8: Rendering of Gear Hob

Input Data for Gear Hob	
Dimensional Parameters	Value (in mm)
Cutter Diameter(D)	62
Length of Cutter(L)	44
Effective Length of Cutter(L_e)	40
Diameter of Bore(d)	36
Number of flutes(N_f)	12
Other Dimensional Parameters	Value (in mm)
Axial Pitch(P)	4
Tooth Thickness(S_w)	5
Hob Addendum(h_a)	3.5
Tooth depth(h)	7
Width of Land(l_1)	8
Fillet Radius(R)	2
Diameter of Shell(d_2)	50
Rotational Angles	Value (in degrees)
γ_1	-3.0
γ_2	-15.0
γ_3	15.0
α_4	-26.565
β_1	0.0
β_4	0.0

Table 7.4: Geometric Parameters of Gear Hob

7.6 Case Study

This section illustrates the advantages of 3D modeling of cutting tools over conventional approach by showcasing one of the various possible downstream applications that can be performed once a 3D model of the cutter is available. Here, the simulation of CNC machining of gear shaper is presented. This exemplifies how a 3D definition of the shaper can be used for its manufacturing. This exercise makes use of a 3-axis CNC machining software, Delcam's PowerMill [88], available at CAD-P Laboratory, I.I.T. Kanpur. The resultant G-codes obtained can be used for the actual machining of gear shaper on a CNC machine. The same model can also be imported in a CNC tool and cutter grinding package and can be ground for finishing. Thus, from an appropriate sized block, finished shaper can be produced and the entire operation can be simulated before actual machining of the cutter. The present example is just a case study and not a detailed exercise on machining or refinement of manufacturing methodology of gear shaper.

To manufacture a gear shaper of diameter $5\frac{3}{8}''$ and length $\frac{1}{2}''$, an enclosing block of size 137 mm$\times$ 137mm$\times$ 13mm is taken and then machined in two passes using a three-axis CNC machining software. In the first pass roughing operations have been carried out with a 3.0 mm end mill with spindle RPM 1500 units/min, cutting speed 500 units/min and rapid traverse rate 3000 units/min. In the second pass, finishing operations have been carried out with 2.0 mm ball end mill. The output of this is cutter location data (cld) file which can be converted to appropriate G-code (tape file) based on the type of post-processor employed. The instances of simulation of CNC machining of gear shaper are shown with the help of Figure 7.9.

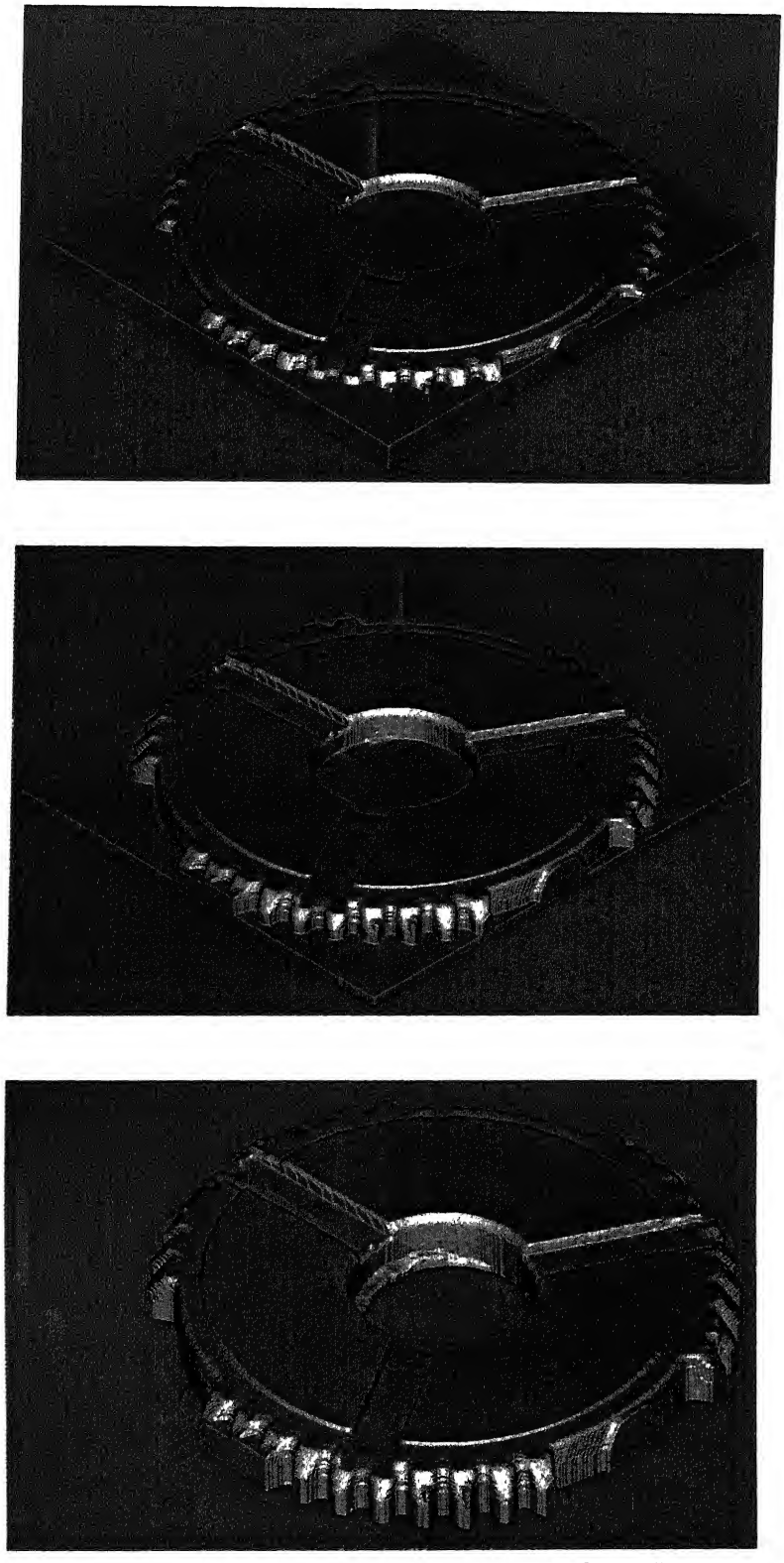

Figure 7.9: Instances of CNC Machining of Gear Shaper

Chapter 8

CONCLUSIONS

This chapter presents the technical summary of the work done in this thesis on three-dimensional geometric modeling of a range of cutting tools. It also presents the scope of work that can be performed further in this direction.

8.1 Summary

The geometric modeling of the cutting tools is an important aspect for the design and manufacturing engineers from the viewpoint of shape realization. The thesis presents the unified geometric models of single-point cutting tools and a class of multi-point cutting tools by mathematically expressing the various surfaces in parametric form. A cutting tool consists of planar as well as curved surface patches. The geometry of an unbounded planar surface patch 'i' is specified a set consisting of three-dimensional (3D) rotational angles α_i, β_i, γ_i about X, Y, Z axes respectively and dimensional parameters, collectively known as geometric parameters. The geometry of a curved surface patch is influenced by the topology of the cutter and is specified by establishing proper bounds to the parameters defining the unbounded surfaces along with ensuring continuity conditions. This parametric design on providing suitable variations to the input data helps to create the family of the cutter of a type for a generic cutting tool.

The work is in the direction of proposing a new nomenclature for defining the geometries of cutting tools and attempts to recast the method of defining a cutting tool in terms of 3D geometric models. The surfaces forming the cutting tool are classified into functional surfaces (cutting elements) and non-critical surfaces (cutter body). The surfaces of the cutting tooth are modeled in a local Cartesian coordinate

frame of reference C_1 and that of the cutter body in a global coordinate system C_2. The orientation and placement of C_2 with respect to C_1 is influenced by the position of cutting tooth on the body of cutter. The edges of intersection that need to be blended or chamfered are located and modeled as transition surfaces. The present modeling methodology is implemented for right-hand cutters only, but left-hand cutters can be modeled by performing suitable transformations.

Forward and inverse mapping relations among proposed tool geometry and conventional specification scheme(s) are established so as to find angles in other nomenclature(s) if known in one nomenclature. The mathematical definitions of the surfaces and the forward mapping have been used to obtain the standard tool angles from the rotational angles. The inverse mapping is used to find 3D rotational angles from the angles proposed in standard nomenclatures. The relations among setting angles of tool and cutter grinder $(\theta_A, \theta_B, \theta_C)$ and the rotational angles are also developed.

Based on the present methodology, a single-point cutting tool is defined in terms of six 3D rotational angles $(\alpha_1, \beta_1, \alpha_2, \beta_2, \alpha_3, \gamma_3)$ along with dimensional parameters. Seven rotational angles, which are $\gamma_1, \gamma_2, \gamma_3, \alpha_4, \beta_4, \gamma_6, \beta_7$, define a side milling cutter. Fluted cutters like slab mill, end mill and drill are defined with the help of four $(\gamma_1, \gamma_2, \gamma_3, \gamma_4)$, four $(\gamma_1, \gamma_2, \gamma_3, \alpha_7)$ and three $(\gamma_2, \beta_4, \gamma_4)$ rotational angles respectively. Eight rotational angles, $\gamma_1, \gamma_2, \gamma_3, \alpha_6, \beta_6, \alpha_7, \alpha_9, \beta_9$ are needed to define a shell mill, while a gear hob can be defined with the help of six $(\gamma_1, \beta_1, \gamma_2, \gamma_3, \alpha_4, \beta_4)$ angles.

These surface-based definitions of cutting tools are verified by rendering the tool designed in terms of 3D geometric parameters in Open Graphics Library (OGL) environment. Three-dimensional geometric parameters not only give identification to the cutting tool but can be used for downstream applications also. To illustrate the effectiveness of these definitions of cutting tools, a few cases on Finite Element Analysis (FEA), geometric assessment of tool wear and defects and CNC machining of different cutting tools are considered. Apart from these, simulation and physical realization of cutting tools through Rapid Prototyping can also be carried out. To show the effectiveness of the approach, the ASCII files of the cutter models are created and imported in a surface modeling environment (Surfacer) and there the watertight surface models of the tools are created. For geometric assessment of tool wear, the surface model and digitized/point-cloud data of a worn/used tool are compared for surface-cloud difference in Surfacer. Three-axis CNC machining of the cutting tool is performed by importing the surface model in a CNC machining environment (Delcam's PowerMILL). Further, the surface models of cutting tools are converted to solid models in a solid modeling environment (I-DEAS) and FEA applications are

performed on them in I-DEAS. Besides, these surface/solid model based definitions of the cutting tools can be post-processed for many other down-stream applications.

8.2 Scope for Future Work

The methodology established in this work can be used to develop a user-friendly menu-driven software or it can be developed as a cutting tool design module of existing commercial CAD packages. Different interfaces like STL, IGES routines can also be conveniently developed during the course of modeling. STL routines can be developed while rendering the model in OGL environment by creating triangular fans of the surface patches. IGES routines for curves and surfaces of the cutting tools can be produced as discussed by Farin [38]. These interfaces act as translators for CAD definitions of cutting tools and enhances the transportability of the geometric models. Once an accurate surface/solid model of a cutting tool is obtained, then a range of down-stream applications on these models can be carried out. This opens up a range of probable areas of research, once an accurate biparametric surface model of a cutting tool is evolved.

The work can be extended for *Form Tools* also. The form tool is normally a piece of high-speed steel ground in form opposite to that desired on the finished workpiece (Figure 8.1). Two styles of form tools are used extensively in industry; the dovetail form tool and the circular form tool. The surface patches making a form tool can be identified and defined geometrically in terms of 3D geometric parameters so as to model comprehensively the form tool.

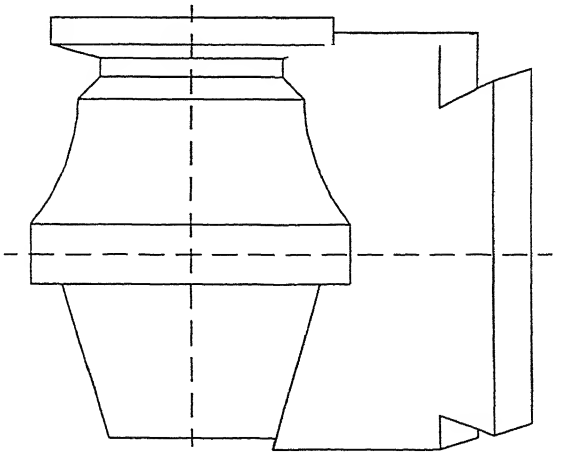

Figure 8.1: A Circular Form Tool

The above concept can also be extended to *custom-made tools.* Currently, such

tools are designed on the basis of users specified parameters that are based on two-dimensional projective geometry approach. With the establishment of this approach, custom-made tools can be designed on the basis of 3D geometric parameters.

Another modification to the present approach of defining the cutting tools in terms of surfaces can be thought to define all the surfaces of the cutting tool as NURBS. The control points of these surfaces can be varied and their effect on design of surfaces and on the machining operation carried out by them can be evaluated.

The surface definitions of the tool faces could be used to model mathematically the grinding process and the effect of grinding parameters on the tool geometry can be studied. The above step would enable the entire grinding or sharpening process of the tool to be simulated in a virtual mode and the results can be verified before any material removal is done.

There is also a need to provide some names to these 3D rotational angles so that they can be standardized and referred properly. An attempt can also be made to evolve a unified representation schemes for milling cutters such that by varying geometric parameters different types of milling cutters can be evolved.

Appendix A

EDGES AND VERTICES OF SIDE MILLING CUTTERS

A.1 Bounding Edges of Cutting Tooth Surfaces

Edges bounding the surface patch Σ_i are located by allowing the infinite surface patch Σ_i to intersect with its neigbouring surface patches Σ_js. Intersection of Σ_i with Σ_j will form an infinite bounding edge $\mathbf{e}_{ij}/\mathbf{e}_{i,j}$ given by parameter $s_{ij}/s_{i,j}$, where $\forall\ s_{ij} \in [-\infty, +\infty]$.

The intersecting edge of surface patch Σ_i is parametrically defined by $\mathbf{p}_i(u_i, v_i)$ with surface patch Σ_j $(\mathbf{p}_j(u_j, v_j))$ is governed by the intersection equation

$$\mathbf{p}_i(u_i, v_i) - \mathbf{p}_j(u_j, v_j) = 0 \tag{A.1}$$

Equation A.1 reveals that there are three equations and four variables. The extra degree of freedom implies that the intersection is an edge (straight or curved) and an additional constraint is required to solve it. The fourth equation is obtained by arbitrarily fixing as constant one of the variables. By incrementing fixed variable by Δ, a series of points sufficient to define the intersection are obtained.

Intersection of Σ_1 & Σ_2 - Edge $\mathbf{e}_{12}$

At the edge of intersection $\mathbf{e}_{12}$, the intersection equation is given as

$$\mathbf{p}_1(v_1, w_1) = \mathbf{p}_2(u_2, w_2) = \mathbf{r}(s_{12})$$

Above equation is solved by equating x, y and z coordinates of Σ_1 and Σ_2 as

$$
\begin{aligned}
-v_1 \sin\gamma_1 &= u_2 \cos\gamma_2 \\
v_1 \cos\gamma_1 + H &= u_2 \sin\gamma_2 + H \\
w_1 &= w_2
\end{aligned}
$$

This helps define $\mathbf{e}_{12}$ parametrically by

$$\mathbf{e}_{12} = [\,0 \;\; H \;\; s_{12} \;\; 1]$$

where $s_{12} \in [-\infty, +\infty]$. Edge $\mathbf{e}_{12}$ and other edges are shown in Figure A.1

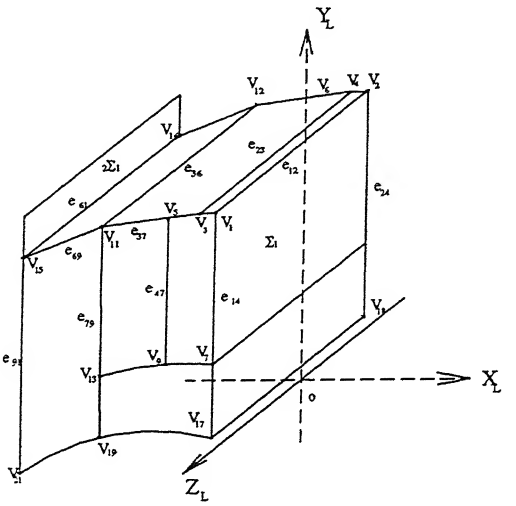

Figure A.1: Bounding Edges and Vertices of Cutter Tooth

Intersection of Σ_1 & Σ_4 - Edge $\mathbf{e}_{14}$

At the edge of intersection $\mathbf{e}_{14}$, the intersection equation is given by $\mathbf{p}_1(v_1, w_1) = \mathbf{p}_4(u_4, v_4) = \mathbf{r}(s_{14})$, which gives the mathematical definition of $\mathbf{e}_{14}$ by

$$
\begin{aligned}
e_{14x} &= -s_{14} \sin\gamma_1 \\
e_{14y} &= H + s_{14} \cos\gamma_1 \\
e_{14z} &= H \tan\alpha_4 \sec\beta_4 + d_{43} + s_{14}(\sin\gamma_1 \tan\beta_4 + \cos\gamma_1 \tan\alpha_4 \sec\beta_4)
\end{aligned}
$$

Intersection of Σ_2 & Σ_4 - Edge $\mathbf{e}_{24}$

At the edge of intersection $\mathbf{e}_{24}$, $\mathbf{p}_2(u_2, w_2) = \mathbf{p}_4(u_4, v_4) = \mathbf{r}(s_{24})$. Solving this defines $\mathbf{e}_{24}$ as

$$
\begin{aligned}
e_{24x} &= s_{24} \cos\gamma_2 \\
e_{24y} &= H + s_{24} \sin\gamma_2 \\
e_{24z} &= H \tan\alpha_4 \sec\beta_4 + d_{43} + s_{24}(-\cos\gamma_2 \tan\beta_4 + \sin\gamma_2 \tan\alpha_4 \sec\beta_4)
\end{aligned}
$$

Intersection of Σ_2 & Σ_3 - Edge e_{23}

Equating the equations of Σ_2 & Σ_3 i.e. $\mathbf{p}_2(u_2, w_2) = \mathbf{p}_3(u_3, w_3) = \mathbf{r}(s_{23})$, e_{23} is defined by

$$e_{23} = [\ -w_{l1}\cos\gamma_2 \quad (H - w_{l1}\sin\gamma_2) \quad s_{23} \quad 1]$$

Intersection of Σ_3 & Σ_6 - Edge e_{36}

From the equations of Σ_3 & Σ_6, intersection equation is obtained as $\mathbf{p}_3(u_3, w_3) = \mathbf{p}_6(u_6, w_6) = \mathbf{r}(s_{36})$. Intersection equations can be solved in terms of u_6. The mathematical definition of e_{36} depends on the design of cutter tooth and specifications of widths of primary and secondary peripheral lands as discussed below.

(i) *Double land cutter* – when both w_{l1} & w_{l2} are specified, then the edge e_{36} is defined as

$$e_{36} = [\ -(w_{l1}\cos\gamma_2 + w_{l2}\cos\gamma_3) \quad \{H - (w_{l1}\sin\gamma_2 + w_{l2}\sin\gamma_3)\} \quad s_{36} \quad 1\ ]$$

(ii) *Double/single land cutter* – When only w_{l1} is known, then the edge e_{36} is

$$e_{36} = [\ u_6\cos\gamma_6 \quad (u_6\sin\gamma_6 + d_{62}) \quad s_{36} \quad 1\ ]$$

$$\text{where } u_6 = \frac{w_{l1}\sin(\gamma_3 - \gamma_2) - (d_{62} - H)\cos\gamma_3}{\sin(\gamma_6 - \gamma_3)}$$

(iii) *Parabolic cutter* – intersection between Σ_3 & Σ_6^p is given as vertex Q_0 on the quadratic curve Q_0Q_1 as defined in Section 3.1.9 and the mathematical definition of e_{36} for parabolic cutter is

$$e_{36} = [\ -(w_{l1}\cos\gamma_2 + w_{l2}\cos\gamma_3) \quad (H - (w_{l1}\sin\gamma_2 + w_{l2}\sin\gamma_3)) \quad s_{36} \quad 1\ ]$$

Intersection of Σ_4 & Σ_7 - Edge e_{47}

In side mills, secondary face land Σ_7 does not actually intersect with the primary face land Σ_4. They are joined by a narrow strip of transition surface (σ_{47}) of width δ_1 along Z_L axis. For the purpose of developing surface models of Σ_4 and Σ_7, the edges bounding these surface patches need to be located. To define the edge of intersection of Σ_4 with Σ_7 (e_{47}), Σ_7 is offsetted along $+Z_L$axis by a distance δ_1. The edge e_{47} marks the boundary of the surface patch Σ_4. The displacement of offset plane Σ_7^o along z axis, such that at e_{47}, $\Sigma_{7z}^o = \Sigma_{4z}$, is given by the relation $d_{73}' = d_{73} + \delta_1$. where δ_1 is given by

$$\delta_1 = \delta_3 - w_f\sin|\beta_4| - w_{l2}\cos\gamma_3\sin|\beta_7| - \delta^*$$

with depression δ^* can be ≥ 0. δ^* is equal to zero, when Σ_7 ends at the surface of cutter body i.e. with value of p_{7z} equal to $w_b/2$. On the other hand, δ^* is greater than zero, when Σ_7 terminates at a plane, where its z value $p_{7z} > w_b/2$.

From the equations of Σ_4 & Σ_7, $\mathbf{e}_{47}$ is given as

$$\begin{aligned} e_{47x} &= \frac{d_{43} - d'_{73}}{\tan\beta_4 - \tan\beta_7} + \frac{s_{47}\sin\alpha_4}{\sin\beta_4 - \cos\beta_4\tan\beta_7} \\ e_{47y} &= s_{47}\cos\alpha_4 \\ e_{47z} &= \frac{d_{43} - d'_{73}}{1 - \tan\beta_4\cot\beta_7} - \frac{s_{47}\sin\alpha_4}{\sin\beta_4\cot\beta_7 - \cos\beta_4} + d'_{73} \end{aligned}$$

Intersection of Σ_7 & Σ_9 - Edge $\mathbf{e}_{79}$

Based on the equations of Σ_7 & Σ_9, $\mathbf{e}_{79}$ is defined as

$$\mathbf{e}_{79} = [\ (d_{73} - d'_{93})\cot\beta_7 \quad s_{79} \quad d'_{93} \quad 1\ ]$$

where $d'_{93} = d_{93} + \delta_2 + \delta^*$, with $\delta^* \geq 0$

Intersection of Σ_1 & Σ_{11} - Edge $\mathbf{e}_{1,11}$

Surface patches Σ_1 & Σ_{11} intersect only at one vertex, labeled V_7 (Figure A.1). To complete the model of the cutter tooth, Σ_1 is virtually extended to the ZX plane, so that it forms edge $\mathbf{e}_{1,11}$ with Σ_{11}. Edge $\mathbf{e}_{1,11}$ is formed by joining projection of vertices V_1 (intersection of edges $\mathbf{e}_{12}$, $\mathbf{e}_{14}$ & $\mathbf{e}_{24}$) and V_7 on Z=$\frac{w_b}{2}$ plane, as Σ_{11z} (or $\mathbf{p}_{11z}$) = $\frac{w_b}{2}$. The mathematical definition of $\mathbf{e}_{1,11}$ is

$$\mathbf{e}_{1,11} = [h\tan\gamma_1(1 - s_{1,11}) \quad \{H - h(1 - s_{1,11})\} \quad \frac{w_b}{2} \quad 1]$$

Intersection of Σ_4 & Σ_{11} - Edge $\mathbf{e}_{4,11}$

Edge $\mathbf{e}_{411}$, formed due to intersection of Σ_4 & Σ_{11} is circular in geometry and is a segment of a virtual circular arc $\mathbf{c}_1$ of radius $(\frac{D}{2} - h)$ (Figure A.1). $\mathbf{c}_1$ is the projection of a circular disk of thickness $\frac{w_b}{2}$, placed with center at O, on $X_L Y_L$plane. Edge $\mathbf{e}_{4,11}$ starts from a vertex with position vector $[h\tan\gamma_1 \quad (H - h) \quad \frac{w_b}{2} \quad 1]$ (projection of vertex V_7 on circular disk and ends at a vertex, which is the intersection of $\mathbf{e}_{47}$ with $\mathbf{c}_1$. Edge $\mathbf{e}_{4,11}$ can be modeled in either of the following two ways:

(i) By mathematically solving the intersection equations, $\mathbf{e}_{4,11}$ can be defined as

$$\mathbf{e}_{4,11} = [-(\frac{D}{2} - h)\sin S \quad \{(\frac{D}{2} - h)\cos S - (\frac{D}{2} - H)\} \quad \frac{w_b}{2} \quad 1]$$

$$\begin{aligned} \text{where } S_1 &\leq S \leq S_2 \text{ and } S_1, S_2 \text{ are given as} \\ S_1 &= \sin^{-1}(\frac{D}{D - 2h}\sin|\gamma_1|) - |\gamma_1| \\ S_2 &\approx \frac{2}{3}.\frac{2\pi}{n} \text{ (For parabolic cutters)} \end{aligned}$$

For double land cutters, S_2 depends on intersection of edge $\mathbf{e}_{79}$ & $\mathbf{c}_1$.

(ii) For the purpose of display, circular arc $\mathbf{c}_1$ with center O_b (projection of global origin on cutter body) can be plotted by finding n^{th} point from the previous point as

$$\begin{aligned} c_{1x_{n+1}} &= O_{b_x} + (c_{1x_n} - O_{b_x})\cos\Delta S - (c_{1y_n} - O_{b_y})\sin\Delta S \\ c_{1y_{n+1}} &= O_{b_y} + (c_{1y_n} - O_{b_y})\cos\Delta S + (c_{1x_n} - O_{b_x})\sin\Delta S \\ c_{1z_{n+1}} &= \frac{w_b}{2} = c_{1z_n}, \end{aligned}$$

where $O_b = [\ 0 \quad 0 \quad \frac{w_b}{2} \quad 1\ ]$, $\Delta S = \frac{S_2 - S_1}{m}$, the seed point, $\mathbf{c}_{1_0} = [h\tan\gamma_1 \quad (H - h) \quad \frac{w_b}{2} \quad 1]$, and $[n \leftarrow 0, 1, ...m]$, with m=total number of points on the edge. S_1 is given above in case (i) and $S_2 = \frac{2\pi}{n}$. $\mathbf{e}_{4,11}$ being a part of arc $\mathbf{c}_1$ can be expressed as

$$\begin{aligned} e_{4,11x_{n+1}} &= e_{4,11x_n}\cos\Delta S - e_{4,11y_n}\sin\Delta S \\ e_{4,11y_{n+1}} &= e_{4,11y_n}\cos\Delta S + e_{4,11x_n}\sin\Delta S \\ e_{4,11z_{n+1}} &= \frac{w_b}{2} \end{aligned}$$

with S_1 and S_2 as given for the case (i) above.

Intersection of Σ_7 & Σ_{11} - Edge $\mathbf{e}_{7,11}$

Circular edge $\mathbf{e}_{7,11}$ being a part of circular arc $\mathbf{c}_1$ from vertices V_9 & V_{13} (Figure A.1) can be given by equation of $\mathbf{c}_1$.

Intersection of Σ_{11} with Cutter Body - Edge $\mathbf{c}_2$

Edge $\mathbf{c}_2$ is also circular in shape, similar to arc $\mathbf{c}_1$, but of radius $(\frac{D}{2} - H)$, with center at projected global origin O_b. $\mathbf{c}_2$ starts at point $[H\tan\gamma_1 \quad 0 \quad \frac{w_b}{2} \quad 1]$. Applying the same methodology as adopted for modeling $\mathbf{c}_1$, $\mathbf{c}_2$ can be modeled as

$$\begin{aligned} c_{2x_{n+1}} &= c_{2x_n}\cos\Delta t - c_{2y_n}\sin\Delta t \\ c_{2y_{n+1}} &= c_{2y_n}\cos\Delta t + c_{2x_n}\sin\Delta t \\ c_{2z_{n+1}} &= \frac{w_b}{2} \end{aligned}$$

$$\begin{aligned} \text{where seed point, } \mathbf{c}_{2_0} &= [H\tan\gamma_1 \quad 0 \quad \frac{w_b}{2} \quad 1], \\ \Delta t &= \frac{t_2 - t_1}{m}, \\ n &\leftarrow 0, 1, ...m \end{aligned}$$

with m = the number of points on $\mathbf{c}_2$, and t_1, t_2 are given as

$$\begin{aligned} t_1 &= \sin^{-1}(\frac{D}{D - 2H}\sin|\gamma_1|) - |\gamma_1| \\ t_2 &= \frac{4\pi}{3n} \text{ (for parabolic cutter)} \end{aligned}$$

For Double Land cutter, t_2 is located by intersection of line l_{79} and curve c_2.

Intersection of Σ_6 & ${}_2\Sigma_1$ - Edge $e_{6,1}$

As tertiary peripheral land Σ_6 has different geometry (straight or parabolic), based on the design of cutter tooth, therefore, edge $e_{6,1}$ is defined differently as per the cutter tooth design as follows:

(i) *Double land cutter*: Equating the respective equations of Σ_6 & ${}_2\Sigma_1$, $e_{6,1}$ for double land cutter is defined as

$$\mathbf{l}_{61} = [\, u_6 \cos\gamma_6 \quad (u_6 \sin\gamma_6 + d_{62}) \quad s_{61} \quad 1\,]$$

$$\text{where } u_6 = \frac{\frac{D}{2}[(\sin\gamma_1 - \sin(\frac{2\pi}{n} + \gamma_1)] + (H - d_{62})\sin(\frac{2\pi}{n} + \gamma_1)}{\cos\{\frac{2\pi}{n} + (\gamma_1 - \gamma_6)\}}$$

(ii) *Parabolic cutter*, as per the definition of Σ_6^p (Section 3.1.9), straight edge joining point $\mathbf{Q}_1$ and its reflection on Σ_{10} about $X_L Y_L$forms edge $e_{6,1}$. The coordinates of vertex $\mathbf{Q}_1$ are given earlier, therefore, for parabolic cutter, edge $\mathbf{e}_{6,1}^p$ is

$$\mathbf{e}_{61}^p = [\{-(\frac{D}{2} - d_1)\sin\frac{2\pi}{n} + d_1 \tan\gamma_1 \cos\frac{2\pi}{n}\} \quad \{(\frac{D}{2} - d_1)\cos\frac{2\pi}{n} + d_1 \tan\gamma_1 \sin\frac{2\pi}{n} - (\frac{D}{2} - H)\} \quad s_{61}^p \quad 1]$$

Intersection of Σ_9 & ${}^2\Sigma_1$ - Edge $e_{9,1}$

From the equations of Σ_9 and ${}^2\Sigma_1$, the definition of edge $e_{9,1}$ can be given as

$$\mathbf{e}_{91} = [\{-\frac{D}{2}\sin\frac{2\pi}{n} - s_{91}\sin(\frac{2\pi}{n} + \gamma_1)\} \quad \{\frac{D}{2}\cos\frac{2\pi}{n} + s_{91}\cos(\frac{2\pi}{n} + \gamma_1) - (\frac{D}{2} - H)\} \quad d_{93} \quad 1]$$

Intersection of Σ_3 & Σ_7 - Edge e_{37}

From the equations of Σ_3 and Σ_7 , edge $\mathbf{e}_{37}$ can be derived as

$$\mathbf{e}_{37} = [(-w_{l1}\cos\gamma_2 + s_{37}\cos\gamma_3) \quad (H - w_{l1}\sin\gamma_2 + s_{37}\sin\gamma_3) \quad \{(w_{l1}\cos\gamma_2 \tan\beta_7 + d_{73}) - s_{37}\cos\gamma_3 \tan\beta_7\} \quad 1]$$

Intersection of Σ_6 & Σ_9 - Edge e_{69}

Edge $\mathbf{e}_{69}$ depends upon the cutter tooth design. For the two types of cutters in question, solving the intersection equation using equations of Σ_6 and Σ_9 (or Σ_9^p), the definition of $\mathbf{e}_{69}$ is given as follows:

(i) *Double land cutter*:

$$\mathbf{e}_{69} = [\, s_{69}\cos\gamma_6 \quad (d_{62} + s_{69}\sin\gamma_6) \quad d_{93} \cdot 1\,]$$

(ii) *Parabolic cutter*: $\mathbf{e}_{69}$ is a part of the quadratic Bézier/PC curve Q_0Q_1. $\mathbf{e}_{69}$ is equivalent to $V_{11}^*Q_1$, where vertex V_{11}^* is the point of intersection of $\mathbf{e}_{79}$ with Q_0Q_1.

Intersection of Σ_9 & Σ_{11} - Edge $\mathbf{e}_{9,11}$

From the equations of Σ_9 and Σ_{11}, two different definitions of edge $\mathbf{e}_{9,11}$ can be obtained based upon the two types of cutters discussed, which are

(i) *Double land cutter*: $\mathbf{e}_{9,11}$ is a straight edge joining the projected global origin O_b and projection of vertex V_{11} (point of intersection of $\mathbf{e}_{36}$ and $\mathbf{e}_{79}$) on z=$\frac{w_b}{2}$ plane. The edge $\mathbf{e}_{9,11}$ and the projection of edge $\mathbf{e}_{79}$ on the plane of $\mathbf{e}_{9,11}$ makes a straight line. Edge $\mathbf{e}_{9,11}$ is terminated by the curve $\mathbf{c}_1$.

(ii) *Parabolic cutter*: Edge $\mathbf{e}_{9,11}$ forms an angle given by $S^* = \frac{4\pi}{3n}$ with the projected global origin O_b. Further, edge $\mathbf{e}_{9,11}$ joins vertex V_{19} (i.e. a point at a distance $(\frac{D}{2} - H)$ from O_b) & V_{13} (i.e. a point at a distance $(\frac{D}{2} - h)$ from O_b). This helps define $\mathbf{e}_{9,11}$ as

$$\mathbf{e}_{9,11} = [-t_{9,11} \sin S^* \quad \{-(\frac{D}{2} - H) + t_{911} \cos S^*\} \quad \frac{w_b}{2} \quad 1]$$

where $[(\frac{D}{2} - H) \leq t_{9,11} \leq (\frac{D}{2} - h)]$

Edges of intersection for Single Land Parabolic Cutter

In a single land parabolic cutter, secondary peripheral land Σ_3 is not manufactured i.e. $w_{l2} = 0$. Based on this property, some edges of double land parabolic cutter need redefinition for single land cutter. These edges are

(i) **Intersection of Σ_6 & Σ_7 - edge $\mathbf{e}^1_{67}$**: Edge $\mathbf{e}^1_{67}$ is a section of parabolic curve Q_0Q_1 and joins vertex Q_0 with V^*_{11}. In the case of single land parabolic cutter, the value of Q_0 given in Eq. 3.12 gets modified and is given as

$$Q^1_0 = [\ -w_{l1} \cos\gamma_2 \quad (H - w_{l1} \sin\gamma_2) \quad (\frac{W}{2} - w_{l1} \cos\gamma_2 \sin\beta_4) \quad 1\ ]$$

Vertex V^*_{11} is found by the intersection of edge $\mathbf{e}_{79}$ & curve Q_0Q_1.

(ii) **Intersection of Σ_6 & Σ_9 - edge $\mathbf{e}^1_{69}$**: Edge $\mathbf{e}^1_{69}$ is also a section of parabolic curve Q_0Q_1, where position vector of vertices Q_0 & $V_1 1$ are modified and both given by equation of Q^1_0 given above.

(iii) **Intersection of Σ_3 & Σ_7 - edge $\mathbf{e}_{37}$**: There is no edge $\mathbf{e}_{37}$ as Σ_3 is not there and it will be converted into the vertex Q_0.

A.2 Vertices of Cutter Tooth

Vertex V_1 & V_2

Vertex V_1 is formed due to intersection of edges $\mathbf{e}_{12}$, $\mathbf{e}_{14}$ & $\mathbf{e}_{24}$ and the intersection equation is given by $\mathbf{e}_{12} = \mathbf{e}_{14} = \mathbf{e}_{24}$. Solving this, by equating the respective equations of intersection equation, the position vector of V_1 is obtained as

$$\mathbf{v}_1 = [\ 0 \quad H \quad (H\tan\alpha_4\sec\beta_4 + d_{43}) \quad 1\ ]$$

where d_{43} is given in the Section 3.1.4.

Vertex V_2 is the reflection of V_1 about $X_LY_L$plane and hence given by

$$\mathbf{v}_2 = [\mathbf{v}_1].[Ref_{z=0}] = [\ 0 \quad H \quad -(H\tan\alpha_4\sec\beta_4 + d_{43}) \quad 1\ ]$$

Vertex V_3 & V_4

Vertex V_3 is formed due to intersection of edges $\mathbf{e}_{23}$ and $\mathbf{e}_{24}$. Solving the intersection equation, equating the equations of $\mathbf{e}_{23}$ & $\mathbf{e}_{24}$, coordinates of V_3 are

$$\mathbf{v}_3 = [\ -w_{l1}\cos\gamma_2 \quad (H - w_{l1}\sin\gamma_2) \quad s_{23} \quad 1\ ]$$

The mirror image of V_3 about $X_LY_L$plane gives the coordinates of V_4 as

$$\mathbf{v}_4 = [-w_{l1}\cos\gamma_2 \quad (H - w_{l1}\sin\gamma_2) \quad -s_{23} \quad 1]$$

where $s_{23} = H\tan\alpha_4\sec\beta_4 - w_{l1}\{-\cos\gamma_2\tan\beta_4 + \sin\gamma_2\tan\alpha_4\sec\beta_4\} + d_{43}$.

Vertex V_5 & V_6

Vertex V_5 is defined by the intersection of edges $\mathbf{e}_{37}$ and $\mathbf{e}_{47}$ by

$V_{5x} = -w_{l1}\cos\gamma_2 + s_{37}\cos\gamma_3$

$V_{5y} = H - w_{l1}\sin\gamma_2 + s_{37}\sin\gamma_3$

$V_{5z} = w_{l1}\cos\gamma_2\tan\beta_7 - s_{37}\cos\gamma_3\tan\beta_7 + d'_{73}$, where d'_{73}=$d_{73} + \delta_1$, and

$$\begin{aligned} s_{37} \;=\; & \frac{(d_{43} - d'_{73})}{(\cos\gamma_3\tan\beta_4 - \cos\gamma_3\tan\beta_7 - \sin\gamma_3\tan\alpha_4\sec\beta_4)} \\ & + \frac{H}{(\cos\gamma_3\cot\alpha_4\sin\beta_4 - \cos\gamma_3\cot\alpha_4\tan\beta_7\cos\beta_4 - \sin\gamma_3)} \\ & - \frac{w_{l1}(\sin\gamma_2\sin\alpha_4\cos\beta_7 - \cos\gamma_2\cos\alpha_4\cos\beta_7\sin\beta_4 + \cos\gamma_2\cos\alpha_4\sin\beta_7\cos\beta_4)}{(\cos\gamma_3\cos\alpha_4\cos\beta_7\sin\beta_4 - \cos\gamma_3\cos\alpha_4\sin\beta_7\cos\beta_4 - \sin\gamma_3\sin\alpha_4\cos\beta_7)} \end{aligned}$$

which gives

$$\begin{aligned} V_{5x} \;=\; & \frac{(d_{43} - d'_{73})}{(\tan\beta_4 - \tan\beta_7 - \tan\gamma_3\tan\alpha_4\sec\beta_4)} \\ & + \frac{H}{(\cot\alpha_4\sin\beta_4 - \cot\alpha_4\tan\beta_7\cos\beta_4 - \tan\gamma_3)} \\ & - \frac{w_{l1}(\sin\gamma_2 - \cos\gamma_2\tan\gamma_3)}{(\cot\alpha_4\sin\beta_4 - \cot\alpha_4\tan\beta_7\cos\beta_4 - \tan\gamma_3)} \\ V_{5y} \;=\; & \frac{(d_{43} - d'_{73})}{(\cot\gamma_3\tan\beta_4 - \cot\gamma_3\tan\beta_7 - \tan\alpha_4\sec\beta_4)} \\ & + \frac{H\sin(\beta_4 - \beta_7)}{\{\sin(\beta_4 - \beta_7) - \tan\gamma_3\tan\alpha_4\cos\beta_7\}} \\ & - \frac{w_{l1}\sin(\gamma_2 - \gamma_3)\sin(\beta_4 - \beta_7)}{\{\cos\gamma_3\sin(\beta_4 - \beta_7) - \sin\gamma_3\tan\alpha_4\cos\beta_7\}} \end{aligned}$$

$$V_{5z} = \frac{w_{l1}\sin(\gamma_2-\gamma_3)}{(\cos\gamma_3\cot\alpha_4\cot\beta_7\sin\beta_4-\cos\gamma_3\cot\alpha_4\cos\beta_4-\sin\gamma_3\cot\beta_7)} - \frac{(d_{43}-d'_{73})\tan\beta_7}{(\tan\beta_4-\tan\beta_7-\tan\gamma_3\tan\alpha_4\sec\beta_4)} - \frac{H\tan\beta_7}{(\cot\alpha_4\sin\beta_4-\cot\alpha_4\tan\beta_7\cos\beta_4-\tan\gamma_3)} + d'_{73}$$

Vertex V_5 and V_6 are defined by $\mathbf{v}_5 = [V_{5x} \quad V_{5y} \quad V_{5z} \quad 1]$, and
$\mathbf{v}_6 = [V_{5x} \quad V_{5y} \quad -V_{5z} \quad 1]$

Vertex V_7 & V_8

The vertex V_7 is formed due to intersection of edge $\mathbf{e}_{14}$ with edge $\mathbf{e}_{4,11}$ (arc $\mathbf{c}_1$). As per the definition of edge $\mathbf{e}_{14}$ as known, at V_7, $s_{14} = \frac{-h}{\cos\gamma_1}$. Therefore, the coordinates of V_7 are given as

$$\mathbf{v}_7 = [h\tan\gamma_1 \quad (H-h) \quad \{(H-h)\tan\alpha_4\sec\beta_4 - h\tan\gamma_1\tan\beta_4 + d_{43}\} \quad 1\,]$$

where d_{43} is given by Section 3.1.4.

Vertex V_8 is the reflection of V_7 about $X_LY_L$plane and given as $[V_{7x} \quad V_{7y} \quad -V_{7z} \quad 1]$

Vertex V_9 & V_{10}

Vertex V_9 is the result of intersection of edge $\mathbf{e}_{47}$ with arc $\mathbf{c}_1$. Solving the equations of edge $\mathbf{e}_{47}$ and $\mathbf{c}_1$, the intersection equation obtained is

$$(\frac{D}{2}-H)\tan\alpha_4\sec\beta_4-(d_{43}-d'_{73}) = (\frac{D}{2}-h)(\sin S\tan\beta_4-\sin S\tan\beta_7+\cos S\tan\alpha_4\sec\beta_4)$$

Solution of this equation gives the value of angle S, which when put in

$$\mathbf{c}_1 = [-(\frac{D}{2}-h)\sin S \quad \{(\frac{D}{2}-h)\cos S-(\frac{D}{2}-H)\} \quad (P_{7z}+w_f\sin\beta_4) \quad 1]$$

gives the coordinates of V_9.

V_{10} is the mirror image of V_9 about $X_LY_L$plane.

Vertex V_{11} & V_{12}

Vertex V_{11} is formed due to intersection of edges $\mathbf{e}_{37}$, $\mathbf{e}_{69}$ & $\mathbf{e}_{36}$. The coordinates of V_{11} are derived as per the following cases:

(i) When both primary peripheral land width w_{l1} & secondary peripheral land width w_{l2} are specified, it is convenient to find V_{11} as intersection of lines $\mathbf{e}_{37}$ and $\mathbf{e}_{36}$. From the equations of $\mathbf{e}_{37}$ and $\mathbf{e}_{36}$, V_9 is given by

$$\mathbf{v}_{11} = [\,-(w_{l1}\cos\gamma_2+w_{l2}\cos\gamma_3) \quad \{H-(w_{l1}\sin\gamma_2+w_{l2}\sin\gamma_3)\} \quad \{w_{l1}\cos\gamma_2\tan\beta_7+w_{l2}\cos\gamma_3\tan\beta_7+d_{73}\} \quad 1\,]$$

(ii) Solving the intersection equation formed by the equations of $\mathbf{e}_{37}$ and $\mathbf{e}_{69}$, the coordinates of V_{11} are given as

$$V_{11x} = \frac{\{w_{l1}\sin(\gamma_2-\gamma_3)+(d_{62}-H)\cos\gamma_3\}\cos\gamma_6}{\sin(\gamma_3-\gamma_6)}$$

$$V_{11y} = \frac{\{w_{l1}\sin(\gamma_2-\gamma_3)-H\cos\gamma_3\}\sin\gamma_6+d_{62}\{\cos\gamma_3\sin\gamma_6+\sin(\gamma_3-\gamma_6)\}}{\sin(\gamma_3-\gamma_6)}$$

$$V_{11z} = w_{l1}\cos\gamma_2\tan\beta_7-\frac{\{w_{l1}\sin(\gamma_2-\gamma_6)+(d_{62}-H)\cos\gamma_6\}\cos\gamma_3\tan\beta_7}{\sin(\gamma_3-\gamma_6)} + d_{73}$$

(iii) For Parabolic cutters, V_{11} is the vertex Q_0 on the quadratic Bézier or PC parabolic curve, which is the bounding curve of Σ_6. Therefore, the coordinates of V_{11} are given by

$$\mathbf{v}_{11} = [\ -(w_{l1}\cos\gamma_2+w_{l2}\cos\gamma_3)\quad \{H-(w_{l1}\sin\gamma_2+w_{l2}\sin\gamma_3)\}\quad w_{l1}\cos\gamma_2\tan\beta_7+w_{l2}\cos\gamma_3\tan\beta_7+d_{73})\quad 1\ ]$$

Further, V_12 being reflection of V_11 about $X_LY_L$plane is given as

$\mathbf{v}_{12} = [V_{11x}\quad V_{11y}\quad -V_{11z}\quad 1]$

Vertex V_{13} & V_{14}

V_{13} is the vertex, which lies on the radial line joining O^p (projection of global origin O at z=V_{11z} plane) with V_{11}. The projection of this radial line on surface patches Σ_7 & Σ_9 acts as boundary curves of Σ_7 and Σ_9 respectively. This helps create Σ_9 as a radial plane for facilitating chip removal. The radial line O^pV_{11} makes an angle S' in CCW direction with the projection of positive Y_L axis on the z=V_{11z} plane. The angle S' for a straight land cutter is given by

$S' = \tan^{-1}[\frac{-\mathbf{v}_{11x}}{(\frac{D}{2}-H)+\mathbf{v}_{11y}}]$ where $\mathbf{v}_{11x}, \mathbf{v}_{11y}, \mathbf{v}_{11z}$ are the x, y, z coordinates of point V_{11}.

For parabolic cutters, angle $S' \approx \frac{4\pi}{3n}$

The coordinates of point V_{13} are then specified as

$$\mathbf{v}_{13} = [\ -(\frac{D}{2}-h)\sin S\quad \{-(\frac{D}{2}-H)+(\frac{D}{2}-h)\cos S\}\quad V_{11z}\quad 1\ ]$$

Further, $V_{14} = [\ V_{13x}\quad V_{13y}\quad -V_{13z}\quad 1\ ]$

Vertex V_{15} & V_{16}

From the equations of edges $\mathbf{e}_{69}$, $\mathbf{e}_{91}$ and $\mathbf{e}_{61}$, the values of the position vector $\mathbf{v}_{15}$ for the straight land cutter and the parabolic cutter is given as

(i) For straight land cutters, the vertex V_{15} is defined as

$$V_{15x} = \frac{\{\frac{D}{2}\sin\gamma_1-(\frac{D}{2}-H+d_{62})\sin(\frac{2\pi}{n}+\gamma_1)\}\cos\gamma_6}{\cos(\frac{2\pi}{n}+\gamma_1-\gamma_6)}$$

$$V_{15y} = \frac{\{\frac{D}{2}\sin\gamma_1 - (\frac{D}{2} - H + d_{62})\sin(\frac{2\pi}{n} + \gamma_1)\}\sin\gamma_6}{\cos(\frac{2\pi}{n} + \gamma_1 - \gamma_6)} + d_{62}$$

$$V_{15z} = d_{93} = \frac{w_b}{2} - \delta_2$$

(ii) For parabolic land cutters, vertex V_{15} is nothing but the point Q_1, used to define the parabolic curve Q_0Q_1.

Similarly, vertex V_{16} is defined by the equation of $\mathbf{v}_{15}$ with $V_{15z} = -Q_{1z}$.

Vertex V_{17} & V_{18}

V_{17} is obtained by rotating a line of length $(\frac{D}{2} - H)$ by an angle t_1, given by $\sin^{-1}[\frac{D}{D-2H}\sin|\gamma_1|] - |\gamma_1|$ about global origin 'O' in CCW direction. This helps define vertex V_{17} & V_{18} as

$$V_{17} = [-(\frac{D}{2} - H)\sin t_1 \quad \{-(\frac{D}{2} - H) + (\frac{D}{2} - H)\cos t_1\} \quad \frac{w_b}{2} \quad 1]$$

$$V_{18} = [V_{17x} \quad V_{17y} \quad -V_{17z} \quad 1]$$

Vertex V_{19} & V_{20}

Radial line O^pP_{11}, discussed in Section A.2 intersects at vertex V_{13} with the curve c_1 and at vertex V_{19} with the curve c_2. Based on this, the coordinates of vertex V_{19} are given as

$$\mathbf{v}_{19} = [-(\frac{D}{2} - H)\sin S \quad \{-(\frac{D}{2} - H) + (\frac{D}{2} - H)\cos S\} \quad \frac{w_b}{2} \quad 1]$$

where the angle S' is the angle made by radial line O^pP_{11} with positive $Y_L$axis as given in Section A.2. For a parabolic cutter, $S' \approx t_2 = \frac{4\pi}{3n}$. Vertex V_{20} is given as

$\mathbf{v}_{20} = [V_{19x} \quad V_{19y} \quad -V_{19z} \quad 1]$

Vertex V_{21} & V_{22}

Vertices V_{21} & V_{22} is obtained by rotating a line of length $(\frac{D}{2} - H)$ by an angle $(\frac{2\pi}{n} + t_1)$ about global origin O in CCW direction. Therefore, coordinates of vertices V_{21} and V_{22} are defined as

$$\mathbf{v}_{21} = [\ \{-(\frac{D}{2} - H)\sin(\frac{2\pi}{n} + t_1)\} \quad (\frac{D}{2} - H)(\cos(\frac{2\pi}{n} + t_1) - 1) \quad \frac{w_b}{2} \quad 1\ ]$$

$$\mathbf{v}_{22} = [\ V_{21x} \quad V_{21y} \quad -V_{21z} \quad 1\ ]$$

Appendix B

EDGES AND VERTICES OF SLAB MILL

The bounding edges of the slab mill are either straight or circular in geometry. The bounding edges of the tooth of the slab mill are obtained by transforming the edges V_0V_1, V_1V_2, V_2V_3, V_3V_4, $V_4V_5V_6$ and V_6V_7 with the help of transformation matrix $[\mathbf{T}_s]$, as per the case of straight tooth cutter or helical mill taking appropriate values of parameters ϕ or t.

The vertices of the tooth of the peripheral milling cutter are obtained by transforming vertices V_0 to V_7 through transformation matrix $[\mathbf{T}_s]$. For example, the vertex V_{L1}, which is equivalent to vertex V_1 at left end surface of the cutter is expressed by

$$V_{L1} = V_1.[\mathbf{T}_s]_{\phi=-\pi L/P \text{ or } t=0}$$

For straight tooth cutter, V_{L1} is given by $[\frac{D}{2} \quad 0 \quad \frac{L}{2} \quad 1]$ and for helical plain milling cutters ($\phi = \phi_{min} = -\frac{\pi L}{P}$), V_{L1} is defined by

$$V_{L1} = [\tfrac{D}{2} \quad 0 \quad 0 \quad 1].\begin{bmatrix} \cos(-\frac{\pi L}{P}) & \sin(-\frac{\pi L}{P}) & 0 & 0 \\ -\sin(-\frac{\pi L}{P}) & \cos(-\frac{\pi L}{P}) & 0 & 0 \\ 0 & 0 & 1 & 0 \\ 0 & 0 & -\frac{P}{2\pi}\frac{-\pi L}{P} & 0 \end{bmatrix}$$

$$= [\tfrac{D}{2}\cos(\tfrac{\pi L}{P}) \quad \tfrac{D}{2}\sin(\tfrac{\pi L}{P}) \quad \tfrac{L}{2} \quad 1]$$

Similarly, V_{R1}, equivalent to vertex V_1 at right end surface is given by $[\frac{D}{2} \quad 0 \quad -\frac{L}{2} \quad 1]$ for straight tooth cutter and for helical milling cutter V_{R1} is

$$V_{R1} = [\tfrac{D}{2}\cos(\tfrac{\pi L}{P}) \quad \tfrac{D}{2}\sin(\tfrac{\pi L}{P}) \quad -\tfrac{L}{2} \quad 1]$$

Similarly other vertices of the fluted cutter may be evaluated.

Appendix C

EDGES AND VERTICES OF INSERT BASED CUTTERS

C.1 Edges bounding the Insert Seat Surfaces

The edges bounding the surface patches of the face mill body are formed by allowing the relevant surface patches to intersect. A bounding edge is also called as edge of intersection and is labeled as e_{ij} (or $e_{i,j}$), when formed due to intersection of surface patches Σ_i and Σ_j. The edge of intersection is found when the x, y and z components of the parametric vector representation of the two intersecting surface patches i and j are equated. The intersection equation may be expressed as $\mathbf{p}_i - \mathbf{p}_j = 0$. As each intersecting surface is defined in terms of two variables so there are in total four variables and three equations. The extra degree of freedom implies that intersection is an edge in terms of variable s_{ij} ($s_{ij} \in [-\infty, \infty]$). The intersecting edges of the insert seat of a face mill can be identified with the help of Figure ??. Homogenous vector representation of various edges of intersection on solution looks like

Edge of intersection of surface patches Σ_1 and Σ_2

$$\mathbf{e}_{12}(s_{12}) = [\{\tfrac{d_3}{2}+s_{12}(\tfrac{d_4-d_3}{2})\}\cos\gamma_2 \quad \{\tfrac{d_3}{2}+s_{12}(\tfrac{d_4-d_3}{2})\}\sin\gamma_2 \quad s_{12}(h-l_1) \quad 1] \; (0 \le s_{12} \le 1)$$

Edge of intersection of Σ_1 and Σ_6

$$\mathbf{e}_{16}(s_{16}) = [\{\tfrac{d_3}{2}+s_{16}(\tfrac{d_4-d_3}{2})\}\cos\gamma_6 \quad \{\tfrac{d_3}{2}+s_{16}(\tfrac{d_4-d_3}{2})\}\sin\gamma_6 \quad s_{16}(h-l_1) \quad 1] \; (0 \le s_{16} \le 1)$$

Edge (circular arc) of intersection of Σ_1 and Σ_{50}

$$\mathbf{e}_{1,50}(\theta_1) = [\tfrac{d_3}{2}\cos\theta_1 \quad \tfrac{d_3}{2}\sin\theta_1 \quad 0 \quad 1] \qquad (\theta_s \le \theta \le \theta_e, \theta_s = \gamma_2, \theta_e = \gamma_6)$$

Edge (circular arc) of intersection of Σ_1 and Σ_{51}

$$e_{1,51}(\theta_1) = [\tfrac{d_4}{2}\cos\theta_1 \quad \tfrac{d_4}{2}\sin\theta_1 \quad (h-l_1) \quad 1] \qquad (\theta_s \le \theta \le \theta_e)$$

Edge of intersection of Σ_2 and Σ_3

$$e_{23}(s_{23}) = [(\tfrac{d}{2}-0.75R_1)\cos\gamma_2 \quad (\tfrac{d}{2}-0.75R_1)\sin\gamma_2 \quad s_{23}(h-l_1) \quad 1] \ (0 \le s_{23} \le 1)$$

Edge of intersection of Σ_2 and Σ_{50}

$$e_{2,50}(s_{2,50}) = [s_{2,50}\cos\gamma_2 \quad s_{2,50}\sin\gamma_2 \quad 0 \quad 1] \qquad (-\infty \le s_{2,50} \le \infty)$$

Edge of intersection of Σ_2 and Σ_{51}

$$e_{2,51}(s_{2,51}) = [s_{2,51}\cos\gamma_2 \quad s_{2,51}\sin\gamma_2 \quad (h-l_1) \quad 1] \qquad (-\infty \le s_{2,51} \le \infty)$$

Edge of intersection of Σ_3 and Σ_4

$$e_{34}(s_{34}) = [\{\tfrac{d}{2}+s_{34}(\tfrac{h-l_1}{2})\tfrac{\tan\alpha_4}{\cos 0.15\psi}\}\cos(\alpha_3+\theta_3') \quad \{\tfrac{d}{2}+s_{34}(\tfrac{h-l_1}{2})\tfrac{\tan\alpha_4}{\cos 0.15\psi}\}\sin(\alpha_3+\theta_3') \quad s_{34}\tfrac{(h-l_1)}{2} \quad 1] \qquad (0 \le s_{34} \le 1)$$

Edge of intersection of Σ_3 and Σ_5

$$e_{35}(s_{35}) = [\{\tfrac{d}{2}+s_{35}(\tfrac{h-l_1}{2})\tfrac{\tan\alpha_5}{\cos 0.15\psi}\}\cos(\alpha_3+\theta_3') \quad \{\tfrac{d}{2}+s_{35}(\tfrac{h-l_1}{2})\tfrac{\tan\alpha_5}{\cos 0.15\psi}\}\sin(\alpha_3+\theta_3') \quad \{(h-l_1)-s_{35}\tfrac{(h-l_1)}{2}\} \quad 1] \qquad (0 \le s_{35} \le 1)$$

Edge (circular arc) of intersection of Σ_3 and Σ_{50}

$$e_{3,50}(\theta_3) = [\{R_1\cos(\theta_3+\theta_3')+(\tfrac{d}{2}+0.25R_1)\cos\theta_3'\} \quad \{R_1\sin(\theta_3+\theta_3')+(\tfrac{d}{2}+0.25R_1)\sin\theta_3'\} \quad 0 \quad 1] \qquad (\pi \le \theta_3 \le \pi+\alpha_2)$$

Edge (circular arc) of intersection of Σ_3 and Σ_{51}

$$e_{3,51}(\theta_3) = [\{R_1\cos(\theta_3+\theta_3')+(\tfrac{d}{2}+0.25R_1)\cos\theta_3'\} \quad \{R_1\sin(\theta_3+\theta_3')+(\tfrac{d}{2}+0.25R_1)\sin\theta_3'\} \quad (h-l_1) \quad 1] \qquad (\pi \le \theta_3 \le \pi+\alpha_2)$$

Edge of intersection of Σ_4 and ${}^2\Sigma_6$

$$e_{4,6nX}(s_{4,6n}) = \tfrac{d}{2}\cos 0.667\psi + s_{4,6n}\{(\tfrac{h-l_1}{2})\tan\alpha_4(\cos\theta - \sin\theta\tan 0.15\psi)\}$$
$$e_{4,6nY}(s_{4,6n}) = -[\tfrac{d}{2}\sin 0.667\psi + s_{4,6n}\{(\tfrac{h-l_1}{2})\tan\alpha_4(\sin\theta + \cos\theta\tan 0.15\psi)\}]$$
$$e_{4,6nZ}(s_{4,6n}) = s_{4,6n}(\tfrac{h-l_1}{2}) \qquad (0 \le s_{4,6n} \le 1)$$

Edge of intersection of Σ_4 and Σ_{50}

$$e_{4,50X}(s_{4,50}) = \tfrac{d}{2}\cos 0.3667\psi + s_{4,50}\tfrac{d}{2}(\cos 0.667\psi - \cos 0.3667\psi)$$
$$e_{4,50Y}(s_{4,50}) = -\tfrac{d}{2}\sin 0.3667\psi + s_{4,50}\tfrac{d}{2}(\sin 0.667\psi - \sin 0.3667\psi)\}$$
$$e_{4,50Z}(s_{4,50}) = 0 \qquad (0 \le s_{4,50} \le 1)$$

Edge of intersection of Σ_4 and Σ_5

$$e_{45X}(s_{45}) = \{\tfrac{d}{2}+(\tfrac{h-l_1}{2})\tfrac{\tan\alpha_4}{\cos 0.15\psi}\}[\cos(\alpha_3+\theta_3')+s_{45}\{\cos 0.667\psi - \cos(\alpha_3+\theta_3')\}]$$
$$e_{45Y}(s_{45}) = \{\tfrac{d}{2}+(\tfrac{h-l_1}{2})\tfrac{\tan\alpha_4}{\cos 0.15\psi}\}[\sin(\alpha_3+\theta_3')+s_{45}\{-\sin 0.667\psi - \sin(\alpha_3+\theta_3')\}]$$
$$e_{45Z}(s_{45}) = \tfrac{h-l_1}{2} \qquad (0 \le s_{45} \le 1)$$

Edge of intersection of Σ_5 and ${}^2\Sigma_6$

$$e_{5,6nX}(s_{5,6n}) = \tfrac{d}{2}\cos 0.667\psi + s_{5,6n}(\tfrac{h-l_1}{2})\tfrac{\tan\alpha_4}{\cos 0.15\psi}\cos 0.667\psi$$
$$e_{5,6nY}(s_{5,6n}) = -\{\tfrac{d}{2}\sin 0.667\psi + s_{5,6n}(\tfrac{h-l_1}{2})\tfrac{\tan\alpha_4}{\cos 0.15\psi}\sin 0.667\psi$$
$$e_{5,6nZ}(s_{5,6n}) = (h-l_1)(1-\tfrac{s_{5,6n}}{2}) \qquad (0 \le s_{5,6n} \le 1)$$

Edge of intersection of Σ_5 and Σ_{51}

$$e_{5,51X}(s_{5,51}) = \tfrac{d}{2}\cos 0.3667\psi + s_{5,51}\tfrac{d}{2}(\cos 0.667\psi - \cos 0.3667\psi)$$
$$e_{5,51Y}(s_{5,51}) = -\tfrac{d}{2}\sin 0.3667\psi + s_{5,51}\tfrac{d}{2}(\sin 0.667\psi - \sin 0.3667\psi)\}$$
$$e_{5,51Z}(s_{5,51}) = (h-l_1) \qquad (0 \le s_{5,51} \le 1)$$

Edge of intersection of Σ_6 and Σ_{50}

$$\mathbf{e}_{6,50}(s_{6,50}) = [s_{6,50}\cos\gamma_6 \quad s_{6,50}\sin\gamma_6 \quad 0 \quad 1] \qquad (-\infty \le s_{6,50} \le \infty)$$

Edge of intersection of Σ_6 and Σ_{51}

$$\mathbf{e}_{6,51}(s_{6,51}) = [s_{6,51}\cos\gamma_6 \quad s_{6,51}\sin\gamma_6 \quad (h-l_1) \quad 1] \qquad (-\infty \le s_{6,51} \le \infty)$$

For a general design of the cutter, $\gamma_2 \approx -0.0667\psi, \gamma_6 \approx 0.333\psi$ and $\theta_3' = \gamma_2$

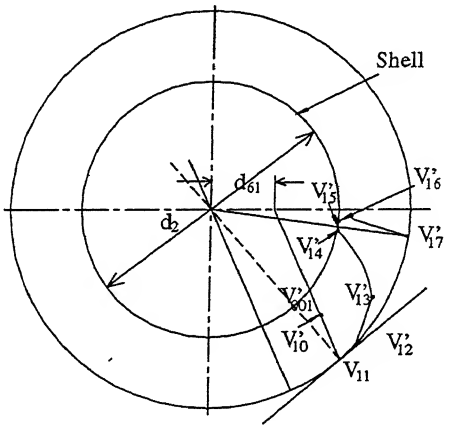

Figure C.1: Projection of Cutting Portion of a Tooth on XY Plane

C.2 Vertices of Insert Seat Surface Patches

The unbounded surface patches forming the insert seat are geometrically located and bounded in the chosen right-handed Cartesian coordinate frame of reference with the help of corner vertices. The unbounded surface patches are bounded by their edges of intersection that too are unbounded. Vertices identified by the intersection of these infinitely-varying and intersecting edges define the range and limit of parameter in which a particular edge varies. Thus, the corner vertices are responsible for defining limits to the unbounded surfaces. When they are known, a biparametric surface patch can be conveniently plotted.

The corner vertices of surface patches are found by equating the components of the parametric equations of the two relevant intersecting edges. There are three equations from the intersection equation $\mathbf{e}_{ij}(s_{ij}) = \mathbf{e}_{kl}(s_{kl})$ and two variables, s_{ij} and s_{kl}. The system being over constrained, can be solved and verified easily for the coordinates of the vertex of intersection referred by V_i. Figure ?? shows all the prominent vertices of the insert seat and their homogenous coordinates on solution to the intersection equations are expressed as

Vertex of intersection of edges $\mathbf{e}_{16}$ and $\mathbf{e}_{1,50}$
(Vertex obtained by the intersection of surface patches Σ_1, Σ_6 and Σ_{50})
$\mathbf{v}_1 = [\frac{d_3}{2}\cos\gamma_6 \quad \frac{d_3}{2}\sin\gamma_6 \quad 0 \quad 1]$

Vertex of intersection of edges $\mathbf{e}_{16}$ and $\mathbf{e}_{1,51}$
(Vertex obtained by the intersection of surface patches Σ_1, Σ_6 and Σ_{51})
$\mathbf{v}_2 = [\frac{d_4}{2}\cos\gamma_6 \quad \frac{d_4}{2}\sin\gamma_6 \quad (h - l_1) \quad 1]$

Vertex of intersection of $\mathbf{e}_{12}$, $\mathbf{e}_{1,50}$ and $\mathbf{e}_{2,50}$
(Vertex obtained by the intersection of Σ_1, Σ_2 and Σ_{50})
$\mathbf{v}_3 = [\frac{d_3}{2}\cos\gamma_2 \quad \frac{d_3}{2}\sin\gamma_2 \quad 0 \quad 1]$

Vertex of intersection of $\mathbf{e}_{12}$, $\mathbf{e}_{1,51}$ and $\mathbf{e}_{2,51}$
(Vertex obtained by the intersection of surface patches Σ_1, Σ_2 and Σ_{51})
$\mathbf{v}_4 = [\frac{d_4}{2}\cos\gamma_2 \quad \frac{d_4}{2}\sin\gamma_2 \quad (h - l_1) \quad 1]$

Vertex of intersection of $\mathbf{e}_{23}$, $\mathbf{e}_{2,50}$ and $\mathbf{e}_{3,50}$
(Vertex obtained by the intersection of Σ_2, Σ_3 and Σ_{50})
$\mathbf{v}_5 = [(\frac{d}{2} - 0.75R_1)\cos\gamma_2 \quad (\frac{d}{2} - 0.75R_1)\sin\gamma_2 \quad 0 \quad 1]$

Vertex of intersection of $\mathbf{e}_{23}$, $\mathbf{e}_{2,51}$ and $\mathbf{e}_{3,51}$
(Vertex obtained by the intersection of Σ_2, Σ_5 and Σ_{51})
$\mathbf{v}_6 = [(\frac{d}{2} - 0.75R_1)\cos\gamma_2 \quad (\frac{d}{2} - 0.75R_1)\sin\gamma_2 \quad (h - l_1) \quad 1]$

Vertex of intersection of $\mathbf{e}_{34}$, $\mathbf{e}_{3,50}$ and $\mathbf{e}_{4,50}$
(Vertex obtained by the intersection of Σ_3, Σ_4 and Σ_{50})
$\mathbf{v}_7 = [\frac{d}{2}\cos(\alpha_3 + \theta_3') \quad \frac{d}{2}\sin(\alpha_3 + \theta_3') \quad 0 \quad 1]$

Vertex of intersection of $\mathbf{e}_{35}$, $\mathbf{e}_{3,51}$ and $\mathbf{e}_{5,51}$
(Vertex obtained by the intersection of surface patches Σ_3, Σ_5 and Σ_{51})
$\mathbf{v}_8 = [\frac{d}{2}\cos(\alpha_3 + \theta_3') \quad \frac{d}{2}\sin(\alpha_3 + \theta_3') \quad (h - l_1) \quad 1]$

Vertex of intersection of $\mathbf{e}_{34}$, $\mathbf{e}_{35}$ and $\mathbf{e}_{45}$
(Vertex obtained by the intersection of surface patches Σ_3, Σ_4 and Σ_5)

$\mathbf{v}_9 = [\{\frac{d}{2}+(\frac{h-l_1}{2})\frac{\tan\alpha_4}{\cos 0.15\psi}\}\cos(\alpha_3+\theta_3') \quad \{\frac{d}{2}+(\frac{h-l_1}{2})\frac{\tan\alpha_4}{\cos 0.15\psi}\}\sin(\alpha_3+\theta_3') \quad (\frac{h-l_1}{2}) \quad 1]$

Vertex of intersection of $e_{4,6n}$ and $e_{4,50}$

(Vertex obtained by the intersection of surface patches Σ_4, Σ_{50} and ${}_2\Sigma_6$)

$\mathbf{v}_{10} = [\frac{d}{2}\cos 0.667\psi \quad -\frac{d}{2}\sin 0.667\psi \quad 0 \quad 1]$

Vertex of intersection of e_{45}, $e_{4,6n}$ and $e_{5,6n}$

(Vertex obtained by the intersection of surface patches Σ_4, Σ_5 and ${}_2\Sigma_6$)

$\mathbf{v}_{11} = [\{\frac{d}{2}+(\frac{h-l_1}{2})\frac{\tan\alpha_4}{\cos 0.15\psi}\}\cos 0.667\psi \quad -\{\frac{d}{2}+(\frac{h-l_1}{2})\frac{\tan\alpha_4}{\cos 0.15\psi}\}\sin 0.667\psi \quad (\frac{h-l_1}{2}) \quad 1]$

Vertex of intersection of $e_{5,6n}$ and $e_{5,51}$

(Vertex obtained by the intersection of surface patches Σ_5, Σ_{51} and ${}_2\Sigma_6$)

$\mathbf{v}_{12} = [\frac{d}{2}\cos 0.667\psi \quad -\frac{d}{2}\sin 0.667\psi \quad (h-l_1) \quad 1]$

Vertex of intersection of $e_{6,50}$ and $e_{6,4p}$

Edge $e_{6,4p}$ is the edge of intersection of surface patch Σ_6 and surface patch Σ_4 for the last (N^{th}) insert seat (i.e. insert seat just preceeding the insert seat in consideration) of the face mill, labeled here as ${}^N\Sigma_4$.

(Vertex obtained by the intersection of surface patches Σ_6, Σ_{50} and ${}^N\Sigma_4$)

$\mathbf{v}_{13} = [\frac{d}{2}\cos\gamma_6 \quad \frac{d}{2}\sin\gamma_6 \quad 0 \quad 1]$

Vertex of intersection of $e_{6,51}$ and $e_{6,5p}$

Like edge $e_{6,4p}$, edge $e_{6,5p}$, is the edge of intersection of surface patch Σ_6 and ${}^N\Sigma_5$, where ${}^N\Sigma_5$ is the surface patch equivalent to Σ_5 for the last (N^{th}) insert seat.

(Vertex obtained by the intersection of Σ_6, Σ_{51} and ${}^N\Sigma_5$)

$\mathbf{v}_{14} = [\frac{d}{2}\cos\gamma_6 \quad \frac{d}{2}\sin\gamma_6 \quad (h-l_1) \quad 1]$

References

[1] Abrari, F. & Elbestawi, M.A., 1997, *Closed Form Formulation of Cutting Forces for Ball and Flat End Mills*, International Journal of Machine Tools & Manufacture, **37**(1), pp. 17–27.

[2] Agullõ-Batlle, J., Cardona-Foix, S. & Viñas-Sanz, C., 1985, *On the Design of Milling Cutters or Grinding Wheels for Twist Drill Manufacture. A CAD Aproach*, Proc. 25^{th} Machine Tool Design & Research Conference, pp. 315–320.

[3] Altintaş, Y., Montgomery, D. & Budak, E., 1992, *Dynamic Peripheral Milling of Flexible Structures*, ASME Journal of Engineering for Industry, **114**(2), pp. 137–145.

[4] Altintaş, Y. & Lee, P., 1996, *A General Mechanics and Dynamics Model for Helical End Mills*, Annals of the CIRP, **45**(1), pp. 59–64.

[5] Altintaş, Y. & Lee, P., 1998, *Mechanics and Dynamics of Ball End Milling*, Transactions ASME - Journal of Manufacturing Science and Engineering, **120**(4), pp. 684–692.

[6] Altintaş, Y. & Engin, S., 2001, *Generalized Modeling of Mechanics and Dynamics of Milling Cutters*, Annals of the CIRP, **50**(1), pp. 25–30.

[7] Armarego, E.J.A. & Kang, D., 1998, *Computer-Aided Modelling of the Fluting Process for Twist Drill Design and Manufacture*, Annals of the CIRP, **47**(1), pp. 259–264.

[8] Arnold, D.B., 2000, *Trends that drive Cutting Tool development*, MMS online, (http://www.mmsonline.com/articles/mtg0003.html).

[9] Au, C.K. & Yuen, M.M.F., 1999, *Feature-based Reverse Engineering of Mannequin for Garment Design*, Computer-Aided Design, **31**, pp. 751–759.

[10] Au, C.K. & Yuen, M.M.F., 2000, *A Semantic Feature Language for Sculptured Object Modelling*, Computer-Aided Design, **32**(1), pp. 63–74.

[11] Baek, D.K., Ko, T.J. & Kim; H.S., 2001, *Optimization of Feedrate in a Face Milling operation using a Surface Roughness Model*, International Journal of Machine Tools & Manufacture, **41**, pp. 451–462.

[12] Bhattacharyya, A., Chatterjee, A.B. & Mullick, B.K., 1973, *Geometry and Performance of Multi-Cone and Curved-Lip Twist Drills*, Annals of the CIRP, **22**(1), pp. 27–28.

[13] Bhattacharyya, A., 1998, *Metal Cutting Theory and Practice*, New Central Book Agency (P) Ltd., Calcutta.

[14] Blackmore, D., Leu, M.C. & Wang, K.K., 1992, *Applications of Flows and Envelopes to NC Machining*, Annals of the CIRP, **41**(1), pp. 493–496.

[15] Boyer, H.E. (editor), 1986, *Atlas of Fatigue Curves*, American Society of Metals, Metals Park, OH.

[16] Carlsson, T. & Stjernstoft, T., 2001, *A Model for Calculation of the Geometric Shape of the Cutting Tool-Workpiece Interface*, Annals of the CIRP, **50**(1), pp. 41–44.

[17] Cavendish, J.C. & Marin, S.P., 1992, *Feature-based Surface Design and Machining*, IEEE Computer Graphics & Applications, (9), pp. 63–74.

[18] Cavendish, J. C. , 1995, *Integrating Feature-based Surface Design with Freeform Deformation*, Computer-Aided Design, **27**(9), pp. 703–711.

[19] Chapman, W.A.J., 1997, *Workshop Technology Part II*, Edward Arnold (Publishers), London.

[20] Chappel, I.T., 1983, *The use of Vectors to simulate material removed by Numerically Controlled Milling*, Computer-Aided Design, **15**(3), pp. 156–158.

[21] Chen, C.-K. & Lin, R.-Y., 2001, *A Study of Manufacturing Models for Ball-End Type Rotating Cutters with Constant Pitch Helical Grooves*, International Journal of Advanced Manufacturing Technology, **18**(3), pp. 157–167.

[22] Chen, W.-F., Lai, H.-Y. & Chen, C.-K., 2001, *A Precision Tool Model for Concave Cone-End Milling Cutters*, International Journal of Advanced Manufacturing Technology, **18**(8), pp. 567–578.

[23] Chen, W.-F., Chen, C.-K. & Lai, H.-Y., 2002, *Design and NC Machining of Concave-Arc Ball-End Milling Cutters*, International Journal of Advanced Manufacturing Technology, **20**(3), pp. 169–179.

[24] Chiu, N.-H. & Malkin, S., 1994, *Computer Simulation for Cree-Feed Form Grinding*, Transactions of NAMRI/SME, **XXII**, pp. 119–126.

[25] Choi, B.K., Lee, C.S., Hwang J.S. & Jun, C.S., 1988, *Compound Surface Modelling and Machining*, Computer-Aided Design, **20**(3), pp. 127–136.

[26] Choi, B.K., 1991, *Surface Modeling for CAD/CAM*, Elsevier, Amsterdam.

[27] Cincinnati Co., 1959, *A Treatise on Milling and Milling Machines*, The Cincinnati Milling Machine Co., Cincinnati, OH.

[28] Connel, R.S., 1955, *Tool and Cutter Grinding*, The Machinery Publishing Co. Ltd., London.

[29] Dallas, D.B., 1976, *Tool and Manufacturing Engineers Handbook, 3rd ed.*, McGraw-Hill, N.Y.

[30] DeGarmo, P.E., 1997, *Materials and Processes in Manufacturing*, Prentice-Hall India, New Delhi.

[31] Deo, Y.V., 1997, *Geometric Modeling of Single Point and Fluted Tool Surfaces*, M.Tech. Thesis, I.I.T. Kanpur.

[32] Dhande, S.G., Karunakaran, K.P. & Misra, B.K., 1995, *Geometric Modeling of Manufacturing Processes using Symbolic and Computational Conjugate Geometry*, ASME Journal of Engineering for Industry, **117**(3), pp. 288–296.

[33] Drodza, T.J. & Wick, C., 1983, *Tool and Manufacturing Engineers Handbook, Volume I – Machining*, Society of Manufacturing Engineers, Dearborn, MI.

[34] Ehmann, K.F., 1990, *Grinding Wheel Profile Definition for the manufacture of Drill Flutes*, Annals of the CIRP, **39**(1), pp. 153–156.

[35] Ehmann, K.F., Kang, S.K. & Lin, C. 1992, *Senstivity Analysis and Tolerance Allocation for Microplanar Drill Point Grinders*, Annals of the CIRP, **41**(1), pp. 361–365.

[36] Ekambaram, B. & Malkin S., 1993, *CAD Software for Helical Flute Grinding of Milling Cutters*, Transactions of NAMRI/SME, **XXI**, pp. 181–188.

[37] Fansteel VR/Wesson-Lexington, 1999, VR/Wesson Cutting Tool Products – *Single Point Brazed Carbide Tools Catalogue*, Fansteel VR/Wesson-Lexington, 203 Lisle Industrial Avenue, P.O.Box 11399, Lexington, KY.

[38] Farin, G., 1990, *Curves and Surfaces for Computer Aided Geometric Design – A Practical Guide*, Academic Press, San Diego.

[39] Faux, I.D., & Pratt, M.J., 1979, *Computational Geometry for Design and Manufacture*, Ellis Horwood Limited, West Sussex, England.

[40] Foley, J.D., van Dam, A., Feiner, S.K., & Hughes, J.F., 1996, *Computer Graphics: Principles and Practice*, Addison Wesley Publishing, Massachusets.

[41] Friedman, M.Y. et. al., 1971, *A Method to determine the Profile of a Disc-Type Cutter when Milling a Helical Slot*, Israel Journal of Technology, **9**(4), pp. 329–332.

[42] Friedman, M.Y. & Meister, I., 1973, *The Profile of a Helical Slot machined by a Form-Milling Cutter*, Annals of the CIRP, **22**(1), pp. 29–30.

[43] Fuji, S., DeVries, M.F. & Wu, S.M., 1972, *Analysis and Design of a Drill Grinder and Evaluation of Grinding Parameters*, ASME Journal of Engineering for Industry, **94**(4), pp. 1157–1163.

[44] *Fundamental of Tool Design, 3rd Ed.*, 1991, Society of Manufacturing Engineers, Dearborn, MI.

[45] Garryson, 2000, *Cutting Tools Catalogue*, Garryson Limited, Spring Road, Ibstock, Leicestershire, LE67 6LR, UK.

[46] Ghosh, A., 1997, *Rapid Prototyping: A Brief Introduction*, Affiliated East West Press Private Limited, New Delhi.

[47] Glaeser, G. & Gröller, E., 1998, *Efficient Volume-Generation during the Simulation of NC-Milling*, Mathematical Visualization: Algorithms, Applications & Numerics, Editors - Hege, H.C. & Polthier K., Springer, pp. 89–106.

[48] Grand, R.L. (editor), 1955, *The New American Machinist Handbook*, McGraw Hill, N.Y.

[49] Grigson, A., 1994, *Model Making*, Manufacturing Engineering, (August), pp. 172–178.

[50] Hogarth, S., 2000, *Are you discarding Profits?*, Manufacturing Engineering, (February), pp. 70–77.

[51] Hsieh, J.-F. & Lin, P.D., 2002, *Mathematical Model of Multiflute Drill Point*, International Journal of Machine Tools & Manufacture, **42**, pp. 1181–1193.

[52] Hui, K.C. & Yadong, L., 1998, *A Feature-based Shape Blending Technique for Industrial Design*, Computer-Aided Design, **30**(10), pp. 823–834.

[53] I-DEAS Master Series 8, 1999, *I-DEAS Students Guide and Training Manual*, SDRC Inc., USA.

[54] Imageware Tutorial and Training Guide, 2000, *Surfacer Version 10.0*, Imageware Inc., USA.

[55] Imani, B.M. & Elbestawi, M.A., 2001, *Geometric Simulation of Ball-End Milling Operations*, Transactions ASME - Journal of Manufacturing Science and Engineering, **123**(2), pp. 177–184.

[56] Kagan, P., Fischer, A. & Shpitaini, M., 1996, *Intuitive Physical-based CAD system for designing of Sculptured Surfaces*, Annals of the CIRP, **45**(1), pp. 121–124.

[57] Kai, C.C., & Fai, L.K., 1997, *Rapid Prototyping: Principles & Applications in Manufacturing*, John Wiley & Sons, Singapore.

[58] Kaldor, S., Moore, K. & Hodgson, T., 1983, *Drill Point Designing by Computer*, Annals of the CIRP, **32**(1), pp. 27–31.

[59] Kaldor, S., Rafael, A.M. & Messinger, D., 1988, *On the CAD of Profiles for Cutters and Helical Flutes — Geometrical Aspects*, Annals of the CIRP, **37**(1), pp. 53–56.

[60] Kaldor, S. & Venuvinod, P.K., 1997, *Macro-level Optimization of Cutting Tool Geometry*, Transactions ASME - Journal of Manufacturing Science and Engineering, **119**(1), pp. 1–9.

[61] Kalpakjian, S., 1992, *Manufacturing Engineeering and Technology, 2^{nd} Ed.*, Addison-Wesley Publishing Company, Reading, MA.

[62] Karunakaran, K.P., 1993, *Geometric Modeling of Manufacturing Processes using Symbolic and Computational Conjugate Geometry*, Ph.D. Thesis, I.I.T. Kanpur.

[63] Karunakaran, K.P. & Dhande S.G., 1998, *Computer-Aided Design of Cutters for Helicoidal Surfaces*, Proc. Institution of Mechanical Engineers, Part B, **212**, pp. 373–382.

[64] Kibbe, R.R., Neely, J.E., Meyer, R.O. & White, W.T., 1999, *Machine Tool Practices, 6^{th} Ed.*, Prentice-Hall, Upper Saddle River, N.J.

[65] Kimura, F., 1997, *Issues in Styling and Engineering Design*, Annals of the CIRP, **46**(2), pp. 527–534.

[66] Kishi, F., 1981, *CAD/CAM for Die Making Industry*, Manufacturing Engineering, **87**(5), pp. 90–92.

[67] Kline, W.A., DeVor, R.E. & Shareef, I.A., 1982, *The Prediction of Surface Accuracy in End Milling*, ASME Journal of Engineering for Industry, **104**(3), pp. 272–278.

[68] Ko, S.-L., 1994, *Geometrical Analysis of Helical Flute Grinding and Application to End Mill*, Transactions of NAMRI/SME, **XXII**, pp. 165–172.

[69] Lacourse, D.E., 1995, *Solid Modeling and Rapid Prototyping – Handbook of Solid Modeling*, McGraw-Hill, N.Y., pp. 19.1–19.20.

[70] Lee, G., 1995, *Virtual Protyping on Personal Computers*, Mechanical Engineering, (July), pp. 70–73.

[71] Lee, P. & Altintaş, Y., 1996, *Predition of Ball-End Milling Forces from Orthogonal Cutting Data*, International Journal of Machine Tools & Manufacture, **36**(9), pp. 1059–1072.

[72] Lee, W.-Y., Kim, K.-W. & Sin, H.-C., 2002, *Design and Analysis of a Milling Cutter with the improved Dynamic Characteristics*, International Journal of Machine Tools & Manufacture, **42**, pp. 961–967.

[73] Li, H.Z., Zhang, W.B. & Li, X.P., 2001, *Modelling of Cutting Forces in Helical End Milling using Predictive Machining Theory*, International Journal of Mechanical Sciences, **43**, pp. 1711–1730.

[74] Lin, C., Kang, S.K. & Ehmann, K.F., 1995, *Helical Micro-Drill Point Design and Grinding*, ASME Journal of Engineering for Industry, **117**(3), pp. 277–287.

[75] Luttervelt, C.A. van et. al., 1998, *Present Situations and Future Trends in Modelling of Machining Operations*- Keynote paper, Annals of the CIRP, **47**(2), pp. 587–626.

[76] Mäntyla, M., 1988, *An Introduction to Solid Modeling*, Computer Science Press, MD.

[77] *Metal Cutting Tool Handbook*, 1965, Metal Cutting Tool Institute, N.Y.

[78] *Metals Handbook – Machining*, 1989, Volume 16, 9^{th} Ed., ASM International, Metals Park, OH.

[79] Mizugaki, Y., Hao, M. & Kikkawa, K., 2001, *Geometric Generating Mechanism of machined surface by Ball-Nosed End Milling*, Annals of the CIRP, **50**(1), pp. 69–72.

[80] Mortenson, M.E., 1985, *Geometric Modeling*, John Wiley & Sons, N.Y.

[81] Mounayri, H.E., Spence, A.D. & Elbestawi, M.A., 1998, "*Milling Process Simulation - A Generic Solid Modeller based Paradigm*", Transactions ASME - Journal of Manufacturing Science and Engineering, **120**(2), pp. 213–221.

[82] Oancea, N. & Oancea, V.G., 1997, *Geometric Modeling of Surface Generation through Wrapping*, Transactions ASME - Journal of Manufacturing Science and Engineering, **119**(4), pp. 829–834.

[83] Oberg, E., Jones, F.D., Horton, H.L. & Ryffel, H.H., 1997, *Machinery's Handbook*, Industrial Press, N.Y.

[84] Owen, J.V., 1997, *CAD/CAM comes of Age*, Manufacturing Engineering, (October), pp. 48–59.

[85] Owen, J.V., 1997, *Virtual Manufacturing*, Manufacturing Engineering, (October), pp. 84–90.

[86] Pham, D.T. & Gault, R.S., 1996, *Solid Ideas*, Manufacturing Engineering, (October), pp. 239–243.

[87] Popov, S., Dibner, L. & Kamankovich, A., 1988, *Sharpening of Cutting Tools*, Mir Publishers, Moscow.

[88] PowerMILL Version 2.4.95, 1999, *Reference Manual*, Delcam International Plc., UK.

[89] Prue, N., 1996, *Virtual Prototyping*, Rapid News, **4**(5), pp. 16–23.

[90] Radzevitch, S.P. & Goodman, E.D., 1997, *About the Orthogonal Parametrization of Sculptured Part Surfaces and Initial Tool Surfaces*, Transactions ASME - Journal of Manufacturing Science and Engineering, **119**(4), pp. 823–828.

[91] Rajpathak, T.S., 1996, *Geometric Modeling of Single Point Cutting Tools for Grinding and Sharpening*, M.Tech. Thesis, I.I.T. Kanpur.

[92] Ren, K. & Ni, J., 1999, *Analysis of Drill Flute and Cutting Angles*, International Journal of Advanced Manufacturing Technology, **15**(8), pp. 546–553.

[93] Rodin, P., 1968, *Design and Production of Metal Cutting Tools*, Mir Publishers, Moscow.

[94] Rogers, D.F., & Adams, J.A., 1990, *Mathematical Elements for Computer Graphics, 2^{nd} ed.*, McGraw-Hill Publishing, N.Y.

[95] Roller, D., 1991, *An Approach to Computer-Aided Parametric Design*, Computer-Aided Design, **23**(5), pp. 385–391.

[96] Sheth, D.S. & Malkin, S., 1990, *CAD/CAM for Geometry and Process Analysis of Helical Groove Machining*, Annals of the CIRP, **39**(1), pp. 129–132.

[97] Shi, H.-M., Zhang, H.-S. & Xiong, L.-S., 1994, *A Study on Curved Edge Drills*, ASME Journal of Engineering for Industry, **116**(2), pp. 267–273.

[98] Sim, C. & Yang, M., 1993, *The Predition of Cutting Force in Ball-End Milling with a Flexible Cutter*, International Journal of Machine Tools & Manufacture, **33**(2), pp. 267–284.

[99] Simon, V., 1993, *Hob for Worm Gear manufacturing with Circular Profile*, International Journal of Machine Tools & Manufacture, **33**(4), pp. 615–625.

[100] Smith, S. & Tlusty, J., 1991, *An Overview of Modeling and Simulation of the Milling Process*, ASME Journal of Engineering for Industry, **113**(2), pp. 169–175.

[101] Spence, A.D. & Altintaş, Y., 1994, *A Solid Modeller based Milling Process Simulation and Planning System*, ASME Journal of Engineering for Industry, **116**(1), pp. 61–69.

[102] Spence, A.D., Abrari, F. & Elbestawi, M.A., 2000, *Integrated Solid Modeller based Solutions for Machining*, Computer-Aided Design, **32**, pp. 553–568.

[103] Tai, C.-C. & Fuh, K.-H., 1994, *A Preditive Force Model in Ball-End Milling including Eccentricity Effects*, International Journal of Machine Tools & Manufacture, **34**(7), pp. 959–979.

[104] Tandon P. et.al., 2001, *Feature Based Design and Rapid Product Development of Saddletree*, International Journal of Agile Manufacturing, **4**(2), pp. 147-161.

[105] Tandon P., Gupta P. & Dhande S.G., 2002, *Geometric Modeling of Single Point Cutting Tool Surfaces*, accepted in International Journal of Advanced Manufacturing Technology.

[106] Tandon P., Gupta P. & Dhande S.G., 2002, *Geometric Modeling of Side Milling Cutting Tool Surfaces*, accepted in International Journal of Engineering Simulation.

[107] Tandon P., Gupta P. & Dhande S.G., 2002, *Virtual Prototyping and Manufacturing of Insert-Based Single-Point Cutting Tool*, accepted in the proceedings of International Conference on e-Manufacturing to be held at Bhopal, India.

[108] Thomas Chatwin Tools, 1999, *Special Tools and Cutters Catalogue*, Thomas Chatwin Tools, Howard Street, Hill Top, West Bromwich, West Midlands, B70 0SN, England.

[109] Timings, R. & May, T., 1997, *Mechanical Engineer's Pocket Book*, Newness, Oxford.

[110] Tönshoff, E.h.H.K. et. al., 1996, *A Unified Approach to Free-form and Regular Feature Modeling*, Annals of the CIRP, **45**(1), pp. 125–128.

[111] Tsai, W.D. & Wu, S.M., 1979, *A Mathematical Model for Drill Point Design and Grinding*, ASME Journal of Engineering for Industry, **101**(3), pp. 333–340.

[112] Tsai, W.D. & Wu, S.M., 1979, *Computer Analysis of Drill Point Geometry*, International Journal of Machine Tools Design & Research, **19**(2), pp. 95–108.

[113] Tsai, W.D. & Wu, S.M., 1979, *Measurement and Control of the Drill Point Grinding Process*, International Journal of Machine Tools Design & Research, **19**(2), pp. 109–120.

[114] Vickers, G.W. & Quan, K.W., 1989, *Ball-Mills versus End-Mills for Curved Surface Machining*, ASME Journal of Engineering for Industry, **111**(1), pp. 22–26.

[115] Voruganti, R.S., Dhande, S.G. & Reinholtz, C.F., 1992, *Symbolic and Computational Conjugate Geometry for the Manufacture of Helically Swept Surfaces*, Transactions of NAMRI/SME, **XX**, pp. 277–282.

[116] Wang, G.-C., Fuh, K.-H. & Yan, B.-H., 2001, *A new mathematical model for Multifacet Drills derived by using Angle-Solid Model*, International Journal of Machine Tools & Manufacture, **41**, pp. 103–132.

[117] Wang, W.P. & Wang, K.K., 1986, *Geometric Modeling of Swept Volume of Moving Solids*, IEEE Computer Graphics & Applications, **6**(2), pp. 8–17.

[118] Wiercigroch, M., 2001, *Nonlinear dynamics of machine tool-cutting process interactions*, Handbook of Machinery Dynamics, Editor - Faulkner, L.L. & Logan, E., Marcell Dekker Inc., N.Y., pp. 139–168.

[119] Wilson, F.W., 1987, *ASTME: Fundamentals of Tool Design*, Prentice Hall, N.J.

[120] Woo, M., Neider, J. & Davis, T., 1998, *OpenGL Programming Guide, 2^{nd} Ed.*, Addison-Wesley, Reading, MA.

[121] Wright Jr., R.S. & Sweet, M., 2000, *OpenGL SuperBible*, Techmedia (Waite Group Press), New Delhi.

[122] Yamaguchi, F., 1988, *Curves and Surfaces in Computer Aided Geometric Design*, Springer-Verlag, Berlin.

[123] Yang, M. & Park, H., 1991, *The Predition of Cutting Force in Ball-End Milling*, International Journal of Machine Tools & Manufacture, **31**(1), pp. 45–54.

[124] Yücesan, G. & Altintaş, Y., 1996, *Prediction of Ball End Milling Forces*, ASME Journal of Engineering for Industry, **118**(1), pp. 95–103.

[125] Zeid, I., 1991, *CAD/CAM Theory and Practice*, McGraw-Hill Publishing, N.Y.

Websites on

[126] *Features and Relations used in Object Oriented Modelling* (Ph.D. Thesis): http://www.opm.wb.utwente.nl/staff/otto/thesis/

[127] *GLUI user interface library*: http://www.cs.unc.edu/~rademach/glui/ 0

[128] *Milling cutter data*: http://www.hanita.com/hanita_protected/techinfo_contents.htm

[129] *Integrating Geometric and Solid Modeling*: http://www.cs.unc.edu/~geom/geom_background.htm

[130] *ISO Designation of the Inserts*: http://www.comaceurope.com/gb/designation_plaq.htm

[131] *NIST – Modeling of Manufacturing Resource Information Project*: http://www.mel.nist.gov/msidlibrary/doc/jurrens95a/resource.htm

[132] *OpenGL*: http://www.starstonesoftware.com/OpenGL/

[133] *Sandvik Coromant*: http://www.coromant.sandvik.com/

[134] *Widia India Limited*: http://www.widiaindia.com/

[135] *Widia Valenite*: http://www.widia.com/en_index.htm